Laboratoire de la construction métallique (ICOM)
INSTITUT DE STRUCTURES
FACULTÉ ENVIRONNEMENT NATUREL, ARCHITECTURAL ET CONSTRUIT
ÉCOLE POLYTECHNIQUE FÉDÉRALE DE LAUSANNE

Rapport

ICOM 489E

FATIGUE DESIGN OF BRIDGES WITH WELDED CIRCULAR HOLLOW SECTIONS

SCHUMACHER Ann
STURM Senta
WALBRIDGE Scott
NUSSBAUMER Alain
HIRT Manfred A.

December 2003

FATIGUE DESIGN OF BRIDGES WITH WELDED CIRCULAR HOLLOW SECTIONS

SCHUMACHER Ann
STURM Senta
WALBRIDGE Scott
NUSSBAUMER Alain
HIRT Manfred A.

Rapport N° ICOM 489E

Ecole polytechnique fédérale de Lausanne (EPFL)
Laboratoire de la construction métallique (ICOM)
CH - 1015 Lausanne
Tél. : + 41-21-693 24 25
Fax : + 41-21-693 28 68

SUMMARY

Circular hollow section (CHS) members are being used in modern bridge applications. In numerous examples CHS members have been cut and welded together directly to form the main load-carrying trusses of steel-concrete composite bridges. The welded connection between brace and chord members forms an intersection characterised by variable stiffness, a non-uniform stress distribution and complex three-dimensional behaviour, all of which can be unfavourable when the joint is subjected to fatigue loading. To date, research on the fatigue of welded tubular joints has been driven primarily by the offshore petroleum industry. The design specifications based on this research seem overly conservative and not entirely applicable when used to design bridges. The main objective of this study was to investigate two specific aspects of welded CHS bridge K-joint fatigue: the joint stresses (**hot-spot stresses**, **stress concentration factors**) at critical fatigue locations and the influence of the so-called **size effect** on the fatigue resistance of these joints.

The fatigue behaviour of welded CHS K-joints typical to bridge applications was investigated through a combination of methods: large-scale fatigue tests, parametric studies using finite element (FE) models and fatigue life predictions based on linear elastic fracture mechanics (LEFM) calculations. Results of the experimental investigation showed that measured hot-spot stresses for typical CHS bridge joints can be considerably lower than the calculated stresses based on existing fatigue design specifications for welded tubular joints. At the same time, however, test results also showed lower fatigue strengths for CHS bridge K-joints in comparison with the $S_{R,hs}$-N design curves presently applicable to these joints. This implies that, although the hot-spot stresses may be lower than what is currently calculated, the fatigue strength of these details is also lower.

Using a validated FE model, stress concentration factors (SCF) were calculated for a range of CHS K-joint geometries and dimensions. These values can be used directly in the determination of hot-spot stresses for the design of welded CHS K-joints typical to bridges and have been synthesised in the form of a modified stress concentration factor, referred to as SCF_{total}. Inherent to SCF_{total} are concepts of load combination and stress partitioning in brace and chord members, which, for the design process, facilitate a more complete overview and comparison between the fatigue behaviour of different joints and critical fatigue locations in the joint.

A LEFM based investigation has allowed for the comparison of fatigue strengths of different welded CHS K-joints. The study has provided indications on the size effect between joints, as influenced by member thickness, geometry and varying load cases. It was seen that the size effect correction factor currently used for this type of structural detail is too penalising and that a more specific correction needs to be developed for the application of CHS members in bridges.

RESUME

Les profilés tubulaires à section circulaire (CHS) sont employés dans la construction des ponts modernes. On trouve de nombreux exemples de ponts mixtes acier-béton dans lesquels les poutres porteuses principales sont constituées de profilés CHS découpés et directement soudés ensemble. L'assemblage soudé des membrures avec les montants et diagonales forme un nœud caractérisé par une rigidité variable, une distribution non uniforme des contraintes et un comportement tridimensionnel complexe, tout ceci pouvant s'avérer défavorable lorsqu'il est soumis à des sollicitations de fatigue. Jusqu'à présent, la recherche dans le domaine de la fatigue des noeuds tubulaires soudés a été menée essentiellement par l'industrie pétrolière offshore. Les prescriptions de dimensionnement basées sur ces recherches semblent trop conservatrices et pas directement applicables au dimensionnement des ponts. L'objectif principal de cette étude était de considérer deux aspects particuliers du phénomène de fatigue dans les noeuds en K de tubes CHS soudés de ponts: les contraintes dans le noeud (**contraintes aux points chauds** (hot-spot stresses), **facteurs de concentration de contrainte**) aux endroits critiques du point de vue de la fatigue, ainsi que l'influence de ce que l'on appelle **l'effet d'échelle** sur la résistance à la fatigue de ces noeuds.

Le comportement à la fatigue des noeuds en K de tubes CHS soudés, de dimensions typiques pour les ponts, a été étudié à travers plusieurs méthodes: essais de fatigue à grande échelle, étude paramétrique à l'aide de modèles numériques (MEF), et estimations de la durée de vie à la fatigue basées sur des calculs par la mécanique de la rupture linéaire élastique. Les résultats de la campagne d'essais ont montré que les contraintes aux points chauds mesurées dans des noeuds tubulaires CHS typiques de ponts peuvent être largement inférieures aux contraintes calculées sur la base des prescriptions existantes pour le dimensionnement à la fatigue de ces assemblages. Dans le même temps, les résultats d'essai ont cependant également montré que la résistance à la fatigue des noeuds en K de profilés CHS dans les ponts était inférieure aux valeurs issues des courbes de dimensionnement $S_{R,hs}$-N actuellement utilisées pour ce type d'assemblage. Cela implique que, bien que les contraintes aux points chauds puissent être inférieures à celles calculées avec les prescriptions actuelles, les courbes de résistance à la fatigue pour ces même contraintes sont également plus basses.

A l'aide d'un modèle aux éléments finis, les facteurs de concentration de contrainte ont été calculés pour différentes géométries et dimensions de noeud en K de profilés CHS. Ces valeurs peuvent être utilisées directement dans la détermination des contraintes aux points chauds pour le dimensionnement des noeuds tubulaires en K typiquement utilisés dans les ponts et ont été synthétisées sous la formes d'un facteur de concentration de contraintes modifié, SCF_{total}. Dans ce facteur sont inclus le concept de combinaison de charges et la répartition des contraintes dans les membrures et diagonales, ce qui, dans le cadre d'un processus de dimensionnement, permet une meilleure vue d'ensemble et comparaison entre le comportement à la fatigue de différents noeuds et des endroits critiques pour la fatigue dans le noeud.

Des recherches basées sur la mécanique de la rupture linéaire élastique ont permis de comparer la résistance à la fatigue de différents nœuds tubulaires soudés an K. L'étude a indiqué que l'effet d'échelle dépend de l'épaisseur des éléments, de la géométrie et des cas de charges variables. On a pu constater que le facteur de correction pour l'effet d'échelle couramment utilisé est trop défavorable et qu'une correction plus spécifique doit être développée pour les applications aux ponts.

ZUSAMMENFASSUNG

Im modernen Brückenbau kommen zunehmend Stahlrohre mit Kreisquerschnitt zur Anwendung. Die Hauptträger zahlreicher Verbundbrücken werden als räumlich aufgelöste Stahlrohrfachwerke ausgebildet, deren Knoten dank präzisem Zuschnitt der Rohre direkt verschweisst werden können. Die veränderliche Steifigkeit, die ungleichmässige Spannungsverteilung und das komplexe, dreidimensionale Verhalten solcher Verbindungen zwischen Gurt und Diagonalen können sich unter Ermüdungsbelastung ungünstig auswirken. Bis heute wurde die Erforschung des Ermüdungsverhaltens von geschweissten Knoten im Wesentlichen von der Offshore-Industrie vorangetrieben. Die Bemessungsempfehlungen, die sich auf diese Forschungsergebnisse abstützen, sind nur bedingt auf den Brückenbau übertragbar und vielfach zu konservativ. Das Hauptziel der vorliegenden Studie war die Untersuchung zweier spezifischer Aspekte des Ermüdungsverhaltens von K-Rohrknoten in Verbundbrücken: die Spannungen an den für einen Ermüdungsriss kritischen Stellen (**Strukturspannungen**, **Spannungskonzentrationsfaktoren**) und der Einfluss des **Massstabseffekts** auf das Ermüdungsverhalten solcher Knoten.

Mit einer Kombination aus grossmassstäblichen Ermüdungsversuchen, Parameterstudien anhand von Finite Elemente (FE) Modellen und Lebensdauerabschätzungen mit der linear elastischen Bruchmechanik (LEFM) wurde das Ermüdungsverhalten von für Verbundbrücken typischen, geschweissten K-Rohrknoten untersucht. Die Versuchsergebnisse haben gezeigt, dass die tatsächlichen Strukturspannungen in solchen Verbindungen deutlich unter den anhand der bestehenden Richtlinien für die Ermüdungsbemessung von geschweissten Rohrknoten berechneten Werten liegen. Gleichzeitig ergaben jedoch die Versuchsergebnisse eine gegenüber den derzeit gültigen $S_{R,hs}$-N Wöhlerkurven niedrigere Ermüdungsfestigkeit.

Anhand eines validierten FE Modells wurden die Spannungskonzentrationsfaktoren (SCF) für verschiedene Knotenabmessungen und -geometrien berechnet. Diese Werte können unmittelbar für die Berechnung der Strukturspannungen, wie sie bei der Bemessung von für Verbundbrücken typischen, geschweissten K-Rohrknoten massgebend sind, verwendet werden. Dazu wurden sie zu einem modifizierten Spannungskonzentrationsfaktor SCF_{total} zusammengefasst, der Lastfallkombinationen und die Spannungsaufteilung zwischen Gurt und Diagonalen implizit mitberücksichtigt. Dies ermöglicht einen besseren Überblick bei der Bemessung und den Vergleich des Ermüdungsverhaltens verschiedener Knoten ebenso wie verschiedener für einen Ermüdungsriss kritischer Stellen innerhalb eines Knotens.

LEFM-Untersuchungen haben den Vergleich der Ermüdungsfestigkeiten verschiedener geschweisster K-Rohrknoten ermöglicht und lassen darauf schliessen, dass der Massstabseffekt von den Wanddicken der Rohre, der Knotengeometrie und den Lastfällen abhängt. Es zeigte sich, dass der derzeitige Korrekturfaktor für den Massstabseffekt für die Bemessung geschweisster Rohrknoten in Verbundbrücken zu konservativ ist und daher ein für diesen speziellen Anwendungsfall optimiertes Konzept entwickelt werden muss.

ACKNOWLEDGEMENTS

The basis for this report is the thesis work of Ann Schumacher, EPFL Thesis n° 2727 (2003). The authors would like to express their gratitude to the Swiss Federal Highway Administration (OFROU), who are the main sponsor of this research (under research grant 88/98). In addition, they would like to thank Vallourec & Mannesmann Tubes, Germany, for providing the tubes for the laboratory tests. The authors also thank S. Demierre, G. Pidoux and H.-J. Reist for their technical assistance during laboratory testing.

NOTATION

FREQUENTLY USED VARIABLES AND SYMBOLS

a	crack depth at the deepest point in crack
a_i	initial crack depth
a_f	final crack depth
A	cross-sectional area
$2c$	crack length
C	material constant
d	brace outside diameter
D	chord outside diameter
e	eccentricity between brace and chord axes intersection
E	modulus of elasticity
f_u	ultimate tensile stress
f_y	tensile yield stress
F	force
F	correction factor
F_f	correction factor for crack shape and the finite dimensions
F_c	geometry correction factor for stress gradient at geometric discontinuity
g	distance between the braces at the chord crown toe
K_t	stress concentration factor due to the local notch effects
K	stress intensity factor
K_{th}	stress intensity factor threshold
L_{chord}	chord length
$L_{r,min}$	minimum extrapolation boundary distance
$L_{r,max}$	maximum extrapolation boundary distance
m	slope of curve
m	material constant
M	moment
n	size effect exponent
N	number of load cycles
N_1	number of cycles at 15% change in strain near point of crack initiation
N_2	number of cycles at detection of a crack
N_3	number of cycles at through thickness cracking
N_4	number of cycles at complete loss of joint strength
Q_{min}	minimum load
Q_{max}	maximum load
ΔQ	load range
R	load ratio
s_N	standard deviation of the dependant variable log$N$
$S_{R,hs}$	hot spot stress range
t	brace wall thickness
T	chord wall thickness
u	displacement component
w	weld length
W	elastic section modulus
x	location on crack path
X_1, X_2	power function exponents
α	chord length slenderness, $2L_{chord} / D$

β	brace-to-chord diameter ratio, d / D
δ	deflection
ε	strain
ε_{nom}	nominal strain
ε_{hs}	hot-spot strain
ε_{ax}	axial strain
ε_{ipb}	strain due to in-plane bending
ε_{opb}	strain due to out-of-plane bending
ε_x	strain perpendicular to y-z plan
ε_y	strain perpendicular to x-z plan
ε_z	strain perpendicular to x-y plan
ϕ	rotational component
ϕ	position around brace-chord intersection
ϕ_{crack}	crack angle
$\Delta\phi$	difference in phase caused by deformation of specimen
γ	chord slenderness, D / $2T$
γ_{fat}	partial safety factor
λ	wave length
ν	Poisson's ratio
θ	angle between brace and chord
θ_{toe}	weld toe angle
ρ	weld notch root radius
σ	stress
σ_{nom}	nominal stress
σ_{hs}	hot-spot stress
σ_{ax}	axial stress
σ_{ipb}	stress due to in-plane bending
σ_{opb}	stress due to out-of-plane bending
σ_b	shell bending stress
σ_m	membrane stress
σ_t	structural stress
σ_x	stress perpendicular to weld toe in chord crown
τ	brace-to-chord wall thickness ratio, t / T
ψ	dihedral angle
ζ	normalized gap parameter, g / D

FREQUENTLY USED INDICES

app	applied
ax	axial
b	bending
br	brace
calc	calculated
ch	chord
comp	compression
eff	effective
hs	hot-spot
i	joint Location i
ipb	in-plane bending
m	membrane
meas	measured

nom	nominal
opb	out-of-plane bending
ref	reference
R	range
t	total

ABBREVIATIONS

BR	backing ring
CHS	circular hollow section
Det. Cat.	detail category
DOB	degree of bending
FEM	finite element method
FP	full penetration weld
LEFM	linear elastic fracture mechanics
MF	magnification factor
RHS	rectangular hollow section
SCF	stress concentration factor
SCF_0	base SCF
SCF_{total}	total SCF
SIF	stress intensity factor
WI	weld improved

1 INTRODUCTION

1.1 MOTIVATION AND STATEMENT OF PROBLEM

In the search for new and innovative bridge designs, engineers and architects are employing structural members in configurations previously considered prohibitively complicated and uneconomical. Circular hollow sections (CHS) are an example of members that are becoming increasingly popular. New cutting, preparation and fabrication techniques are making their use—in particular with respect to the connection between members—more feasible and competitive.

The abundance of circular hollow forms in nature (e.g. plant stems, animal bones) is indelible proof of the structural advantages they offer. Among these, circular hollow sections possess equal bending stiffness, strength and resistance to buckling in all directions, high torsional stiffness and a high strength-to-weight ratio. In bridges these properties allow CHS members to be used in a wide range of configurations, for example: girder bridges with the CHS members acting as girder flanges, arch bridges with concrete filled CHS members as the compression chord or truss bridges (Figure 1.1) with CHS members making up the truss braces and chords.

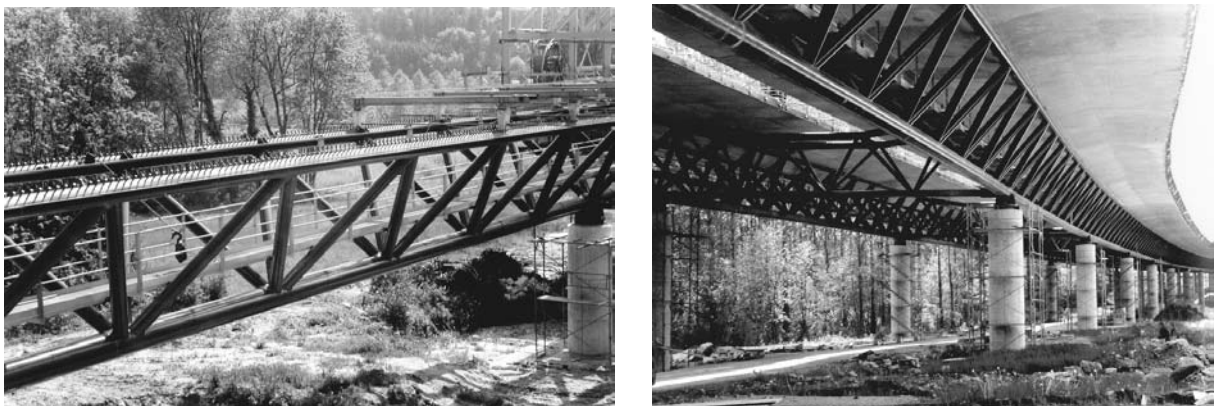

***Figure 1.1** - Lully Viaduct under construction (left) and near completion (right)*

This report concentrates on the use of CHS members in the latter bridge configuration, truss bridges. It is the most classical application as truss bridges have been in use since the earliest development of ferrous materials, in the second half of the 19th century. The substitution of open structural section members with CHS members provides a modern and aesthetic touch to an efficient and proven load carrying system. In addition to conventional all-steel truss bridges typical to rail construction, CHS trusses can also be used in steel-concrete composite bridges. That is, instead of a steel girder or box-girder, the concrete slab is supported by a system of CHS trusses [Dauner 1997, Schumacher and Blanc 1999, Baregg Info 2000, Stahlbau Nachrichten 2002].

Although they mimic forms often found in nature, man-made CHS structures nevertheless pose particular constructive challenges with respect to the connections between members or between members and other elements. The most common connection methods between two or more CHS members include the use of bolts, gusset plates, welds or cast joints, of which the latter two, welding (where the braces are welded directly to the chord) and casting (where the joint is cast and CHS members are welded to the extremities of the cast joint, outside the joint region), have been identified as the most suitable for present-day bridge construction [Schlaich and

Schober 1999, Dauner et al. 1998]. Both methods can result in joints with clean lines, a prerequisite for light, transparent structures.

The work described in this report will concentrate on unstiffened welded CHS joints. For this type of joint, the brace members are cut precisely and welded directly onto a continuous chord. The need for stiffeners is avoided through the choice of appropriate diameter-to-thickness ratios in order to prevent local failure of the joint. In contrast with their relatively simple appearance, however, welded CHS joints exhibit complex three-dimensional behaviour that is difficult to condense into clear, simplified engineering design rules. The stiffness around the brace-chord intersection is variable, resulting in a non-uniform stress distribution that can be unfavourable when the structure is subjected to fatigue loading. In terms of stress flow, the geometric discontinuity at a CHS joint causes a perturbation that can result in a significant increase in the local stress affecting the joint. The definition of local joint stresses and their influence on the fatigue behaviour of the CHS joint is a complex problem for which closed-form solutions do not exist.

One of the first major applications of CHS members was seen in the offshore petroleum industry. With the advantageous properties mentioned above, in addition to low drag coefficients, CHS members have long been used for the construction of offshore tubular space frames used in the drilling and production of oil and gas. Severe loading conditions on the offshore structures, such as oscillating loads from wind and waves, have made fatigue failure of these CHS structures a major concern and therefore an important area of research and a focus of design rule development over the past 40 years.

In comparison with offshore structures, CHS truss bridges exhibit several differences with respect to the welded tubular joints: joint geometries, member dimensions (both absolute and relative), the loads affecting the joint and joint fabrication procedures. For example, offshore tubular trusses comprise members that are often large enough to be accessed from the interior. This implies that welding of the CHS joints can be carried out from the outside and the inside of the joint.

When used in the design of recently constructed CHS truss bridges, current design specifications were found to be incomplete and prohibitively conservative. Tubular bridge member dimensions chosen according to static requirements—as is the procedure most commonly used in bridge design—will often fail the subsequent fatigue verification of the joints. Two main reasons can be identified and are illustrated in Figure 1.2. The fatigue design stress, $\Delta\sigma_{hs}$, calculated for CHS bridge joints using empirical parametric equations found in design specifications is high, typically two to five times higher than the nominal stress, $\Delta\sigma_{nom,i}$, in the truss members. When the design stress is applied to corresponding $S_{R,hs}$-N design lines, a further correction is made depending on the wall thickness, T_i, of the fatigue critical member (chord or brace), which can, in many cases, translate into a further penalty to the fatigue resistance of the joint.

It is possible to design a tubular bridge with joints that adhere to current fatigue design specifications. However, considering the background of the current specifications as well as the apparent need for (structurally and monetarily) economical designs in order to compete with established bridge systems, a re-evaluation of the fatigue behaviour of welded CHS tubular joints specific to bridges appears justified.

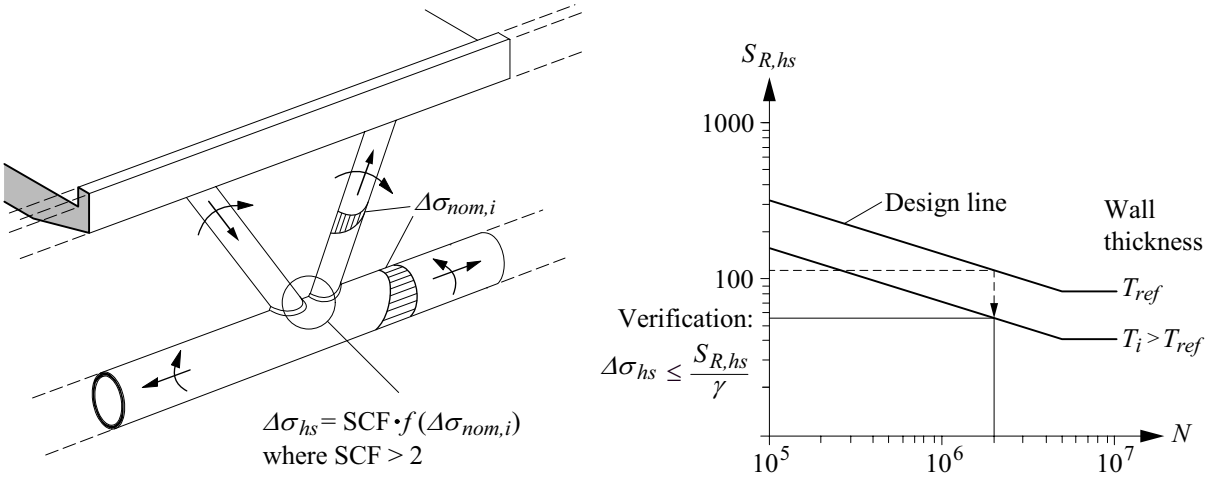

***Figure 1.2** - Fatigue design of welded CHS joints, load effects and resistance*

1.2 SCOPE AND OBJECTIVES

The consequences of dealing with a bridge application on the **scope** of the study presented in this report are the following:

- The dimensions and geometric parameter ranges covered in the study are limited to those most likely to be used in practice. In particular, this is with respect to the chord slenderness parameter, γ (the ratio of the chord diameter to the chord thickness) of the tubular truss. During the design of recently constructed CHS truss bridges, it was found that, based on the static design of the bridge, the required chord slenderness is low (notably $\gamma_{bridges} < 12.0$) as compared with the chord slenderness range covered in the existing design specifications ($\gamma_{specifications} > 12.0$).
- The study concentrates on the fatigue behaviour of welded CHS joints, since this is the critical aspect in the design of these details. For the static design of welded CHS joints the reader is directed to existing design specifications such as the CIDECT design serials (Wardenier et al. 1991, Rondal et al. 1991, Packer et al. 1992) or the new Swiss steel structures design code [SIA 263 2003].

The **objectives** of the present study are:

- To demystify the basic concepts of fatigue and the corresponding rules for welded CHS joints by giving explanations of important concepts such as the hot-spot stress and the effect of joint size and scale.
- To promote a new type of steel-concrete composite bridge.
- To make CHS joints more reliable and economical by gaining knowledge concerning their fatigue strength.
- To supplement current fatigue design specifications by providing information on the fatigue design of bridges with welded CHS joints and to provide the engineer with a calculation method that is a simple, coherent approach to the design of these joints.

1.3 ORGANISATION OF REPORT

This report is based largely on a study carried out by Schumacher [Schumacher 2003]. It summarises this work and puts an emphasis on the practical aspects of the fatigue design of welded CHS truss bridges.

The report is divided into seven chapters and two Appendices. The organisation of the report is shown schematically in Figure 1.3. **The engineer interested in obtaining a rapid overview of the most necessary information required in the fatigue design of welded CHS joints is advised to follow the items in the flowchart highlighted in bold in Figure 1.3.**

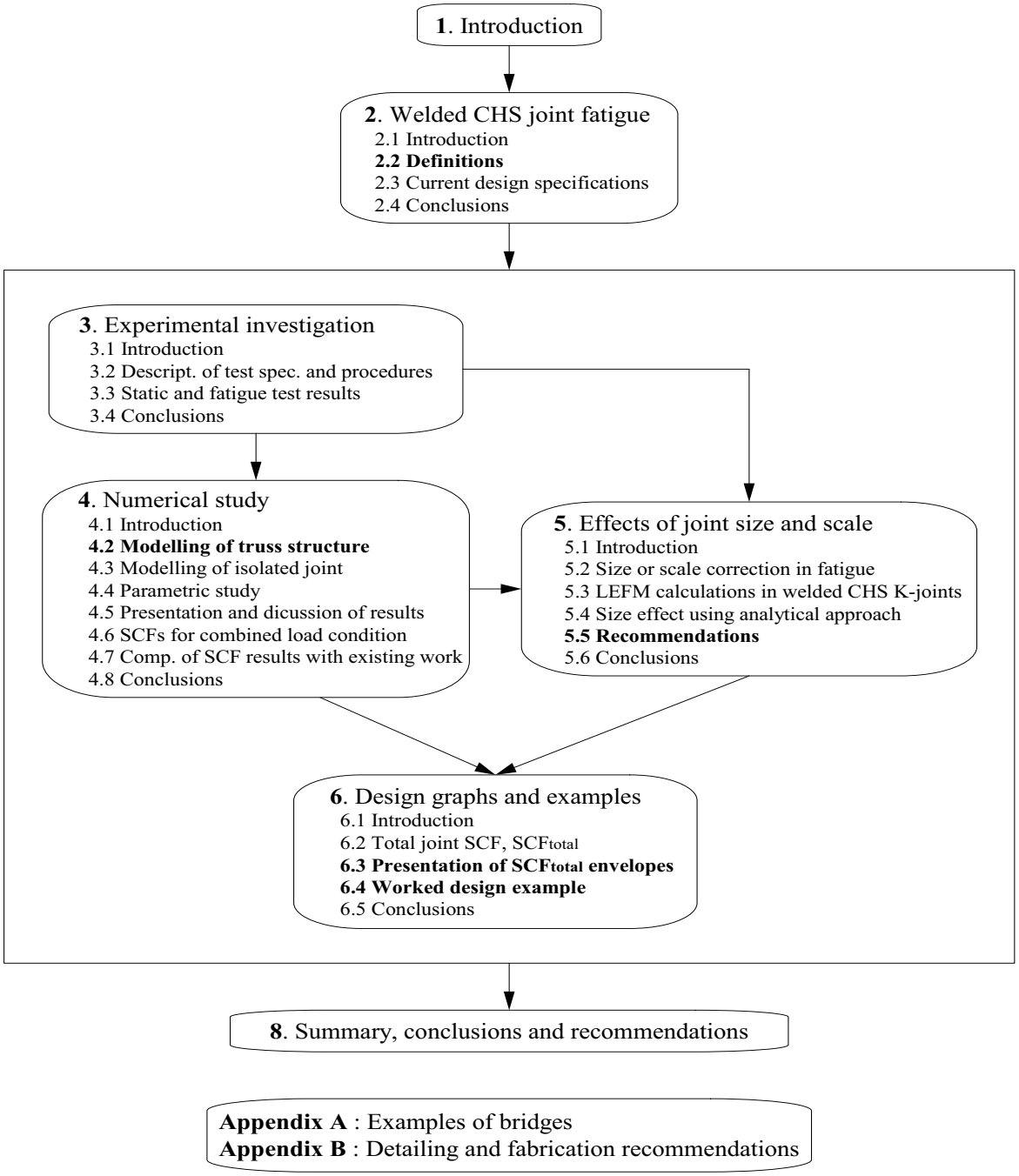

***Figure 1.3** - Organisation of report*

2 WELDED CHS JOINT FATIGUE

2.1 INTRODUCTION

A large amount of work has been carried out over the last 30 years on the fatigue of tubular joints with circular hollow section (CHS) members. As already mentioned in Chapter 1, a majority of this work has been motivated by the petroleum industry, where offshore jacket structures comprising tubular members are subjected to extreme conditions due to severe wind, wave and temperature loads.

As described by Maddox [Maddox 1991], in the context of engineering, fatigue is the process by which a crack can form and then grow under repeated or fluctuating loading. The magnitude of the loading required to produce fatigue cracking in a joint may be much less than that needed to break the joint in a single application of load. The fatigue life of a joint is taken as the number of stress cycles required to grow a crack to a given dimension or to fail the joint, where joint failure can be defined in various ways, depending on the joint and the application. Several methods have been developed to determine the fatigue resistance of welded joints. Three of these are:

- *Classification Method* The most commonly used fatigue design rules for civil engineering structures are based on fatigue strength or $S_{R,nom}$-N curves and detail category tables [ECCS 1985, Eurocode 3 2002]. $S_{R,nom}$-N curves give a relationship between the nominal stress range affecting the joint or detail and the number of stress cycles. The curves are used in conjunction with 'Detail Category Tables', in which different structural details (with limited parameter ranges) of approximately the same fatigue strength are assigned the same category. The so-called Detail Category refers to the nominal stress range under which the joint will fail after $2x10^6$ cycles (assuming a certain probability of failure).
- *Hot-spot Stress Method* Also referred to as the geometric stress method, the hot-spot stress method relates the fatigue life of a joint to the hot-spot stress range in that joint, rather than the nominal stress range [Wardenier 1982, Niemi 1992]. The hot-spot stress includes the effects of joint geometry and the type of load, but excludes local effects due to the weld shape, radius of the weld toe (notch effects), etc. Similar to the Classification Method, the hot-spot stress range for a joint is used in conjunction with design curves, in this case $S_{R,hs}$-N curves. Unlike the Classification Method, however, only one $S_{R,hs}$-N curve is required for the Hot-spot Stress Method, since the effect of different geometries on the fatigue strength is already accounted for in the stress definition.
- *Fracture Mechanics Method* This method is used to estimate the fatigue crack propagation life of a welded joint containing crack-like defects [Maddox 1970, Hirt 1971]. In the application to offshore structures, for example, it is most often used as a tool with which the remaining fatigue life of fatigue damaged structural details is calculated. This method, while proven for simple welded joints, requires a relatively complex calculation procedure and few solutions exists for joints of complicated geometry and loading, e.g. tubular joints.

All three methods can be applied to welded joints in general, but also, more specifically, to welded tubular joints. *This report deals mainly with the hot-spot stress method.* The goal of the present chapter is to give a brief overview of the existing work in the domain of welded tubular joint fatigue (with an emphasis on welded CHS joint fatigue).

Chapter 2 is composed of the following sections:

- **Section 2.2** : *Definitions*, presents some of the most important definitions related to the present work;
- **Section 2.3** : *Current design specifications*, provides an overview of the historical development of research on welded tubular joint fatigue, including a look at the work as it is reflected in current design specifications;
- **Section 2.4** : *Conclusions*.

2.2 DEFINITIONS

The following definitions will be used frequently through-out this document; other more specific definitions will be given at the relevant locations.

K-joint geometry, dimensions and non-dimensional parameters

In Figure 2.1 the general geometry and dimensions of a welded CHS K-joint are given. The non-dimensional parameters associated to the joint dimensions are also listed.

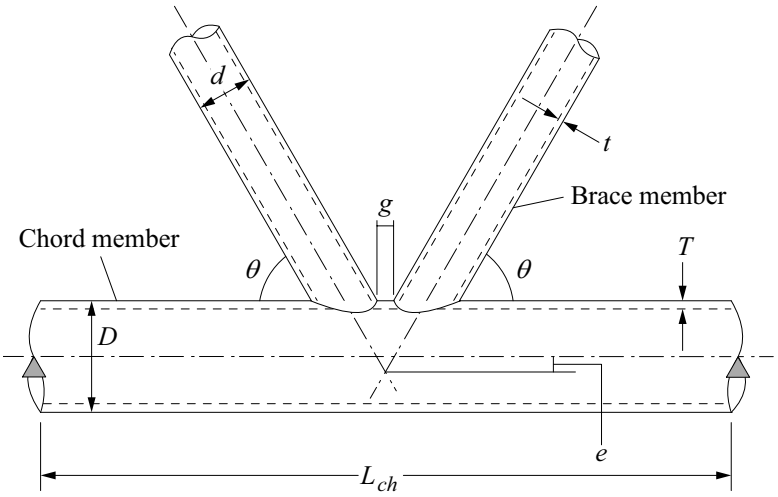

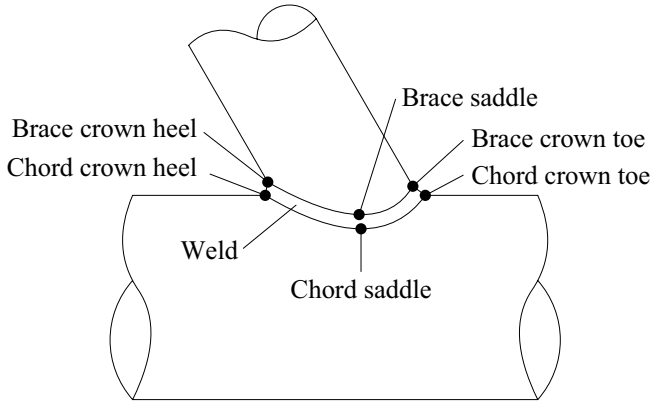

d = outside brace diameter
D = outside chord diameter
t = brace wall thickness
T = chord wall thickness
e = positive eccentricity (negative eccentricity if intersection of brace axes falls above chord axis)
g = gap distance
L_{ch} = chord length between two nodes

$\alpha = 2L_{chord} / D$
$\beta = d / D$
$\gamma = D / 2T$
$\tau = t / T$
θ = brace angle
$\zeta = g / D$

***Figure 2.1** - K-joint geometry, dimensions and non-dimensional parameters*

Types of stresses

Nominal stress

The nominal stress, σ_{nom}, in a CHS joint is the stress away from the joint, in the chord and brace members. It is due to a combination, that is, a superposition of stresses due to both axial load and bending moments (both in-plane and out-of-plane). The nominal stress does not account for

non-uniform stress field distributions due to, for example, shear lag, load introduction, joint geometry, etc.

A stress gradient will most likely be present in the braces or chord due to the bending moments; in order to define the nominal stress in either the braces or chord, the stress gradient is extrapolated to the joint as shown in Figure 2.2. Furthermore, a moment is considered positive if it has the effect of increasing the tensile stresses in the gap region of the joint.

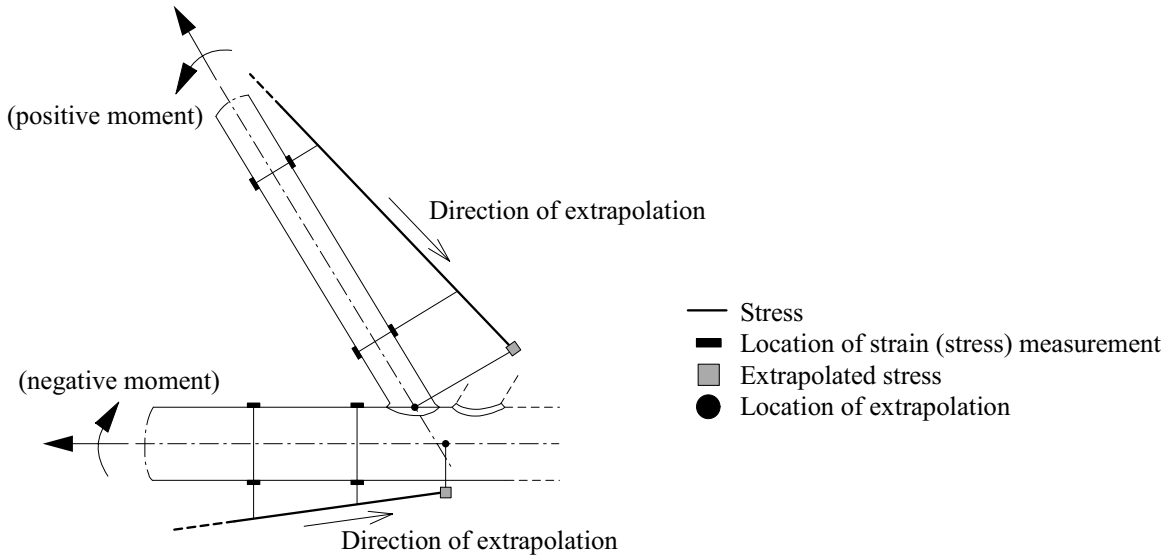

Figure 2.2 - *Extrapolation of stresses in chord and brace due to bending moment*

Hot-spot stress

The hot-spot stress, σ_{hs}, is the stress at the weld toe of a tubular joint, where the fatigue crack is expected and where joint failure will start. It includes the effects of joint geometry and the type of load (global effects), but excludes local effects due to the weld shape, radius of the weld toe (notch effects), etc. According to Marshall [Marshall 1992], the hot-spot stress should have the following attributes:

1. It should place different tubular joint geometries on a common design basis.
2. For repetitive designs, it should be possible to generalise in terms of stress concentration factors (SCF) that are invariant for a given joint geometry, and depend only on the loading pattern.
3. The design reference stress (strain) should be equally derivable from model tests or numerical analysis (e.g. using the finite element method (FEM)).
4. Weld notch effects, residual stresses, etc., which are not amenable to such measurement or calculation, should be implicitly included in the empirical fatigue strength ($S_{R,hs}$-N) design curve.

Since the hot-spot stress is difficult to measure or calculate exactly at the weld toe, a standard procedure for determining the hot-spot stress involves the extrapolation of stresses from a region adjacent to the weld toe, to the weld toe. This concept is illustrated in Figure 2.3. Also shown in Figure 2.3 is the extrapolation region within which the stresses used in the determination of the hot-spot stress should be measured or calculated. The boundaries of the extrapolation region, as defined by Zhao 2000 and IIW 2000, are given in Table 2.1.

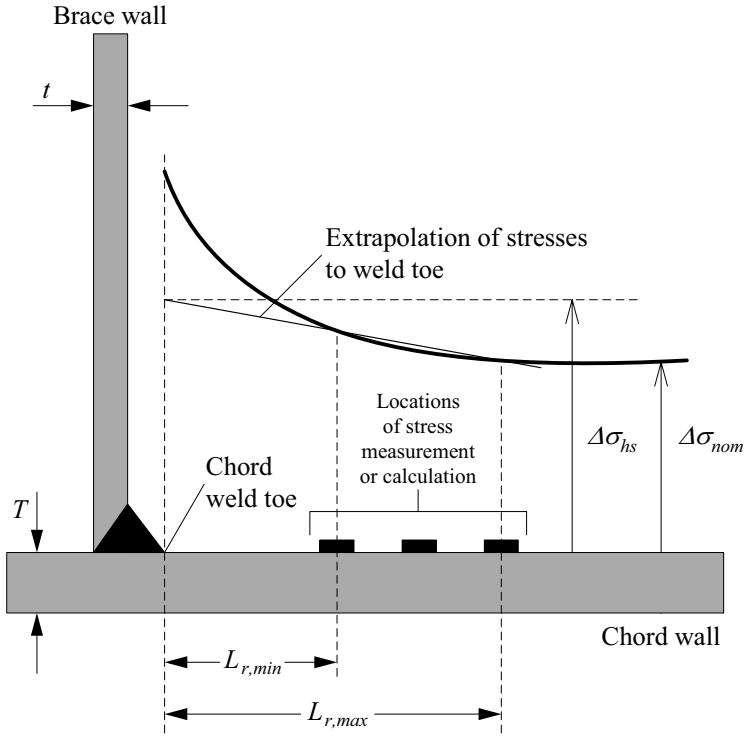

***Figure 2.3** - Extrapolation of stresses to weld toe, extrapolation region*

***Table 2.1** - Boundaries of extrapolation region for CHS joints*

Distances from	Chord		Brace	
weld toe	Saddle	Crown	Saddle	Crown
$L_{r,min}$*	$0.4 \cdot T$		$0.4 \cdot t$	
$L_{r,max}$**	$0.09 \cdot (D/2)$	$0.4 \cdot ((D/2) \cdot T \cdot (d/2) \cdot t)^{0.25}$	$0.65 \cdot ((d/2) \cdot t)^{0.5}$	

*Minimum value for $L_{r,min}$ is 4 mm

**Minimum value for $L_{r,max}$ is $L_{r,min} + 0.6 \cdot t$

Stress concentration factor (SCF)

The stress concentration factor (SCF) is defined as the ratio between the hot-spot stress and the member stress away from the joint, which causes this hot-spot stress:

$$\text{SCF} = \frac{\text{(part of total) hot-spot stress}}{\text{member stress(es) away from joint that causes this hot-spot stress}}$$

For example, the SCF at a joint Location *i* due to an axial load in the brace is expressed as the following:

$$SCF_{i,ax\_br} = \frac{\sigma_{hs,i,ax\_br}}{\sigma_{ax\_br}} \qquad [2.1]$$

or, in terms of hot-spot stress,

$$\sigma_{hs,i,ax\_br} = \sigma_{ax\_br} \cdot SCF_{i,ax\_br} \quad [2.2]$$

where,

σ_{hs,i,ax_br} : hot-spot stress at joint Location *i*, due to axial brace force
σ_{ax_br} : stress in tension brace due to axial brace force
SCF_{i,ax_br} : stress concentration factor at joint Location *i*, due to axial brace force

Since it is assumed that the stresses are elastic, it follows that the **total hot-spot stress**, $\sigma_{hs,i}$, at a particular joint location due to a **combination** of member stresses (both in the brace *and* the chord) can be expressed as follows:

$$\sigma_{hs,i} = \sigma_{ax\_br} \cdot SCF_{i,ax\_br} + \sigma_{ipb\_br} \cdot SCF_{i,ipb\_br} + \sigma_{ax\_ch} \cdot SFC_{i,ax\_ch} + \sigma_{ipb\_ch} \cdot SCF_{i,ipb\_ch} \quad [2.3]$$

where,

$\sigma_{hs,i}$: hot spot stress at joint Location *i*
σ_{ax_br} : stress in tension brace due to axial brace force
SCF_{i,ax_br} : stress concentration factor at joint Location *i* due to axial brace force
σ_{ibp_br} : stress in tension brace due to in-plane bending moment
SCF_{i,ipb_br} : stress concentration factor at joint Location *i* due to moment in brace
σ_{ax_ch} : stress in chord due to chord axial force
SCF_{i,ax_ch} : stress concentration factor at joint Location *i* due to axial chord force
σ_{ipb_ch} : stress in chord due to in-plane bending moment
SCF_{i,ipb_ch} : stress concentr. fact. at joint Location *i* due to in-plane bending moment in chord

and so on...

The stress concentration factor, for a given load case, is determined either through experimental or analytical (using FEM calculations) methods, or found through the application of parametric formulae found in the literature. It is to be noted that the stress concentration factor described here is not equivalent to the geometric stress concentration factor (referred to as K_t or K_f in the literature) as this is a function of the notch radius, e.g. bolt thread, weld toe, groove notches, etc.

$S_{R,hs}$-N design curves

$S_{R,hs}$-*N* design curves relate the fatigue strength (in terms of hot-spot stress) to the fatigue life (in terms of number of cycles to joint failure). The curves are established with a specified probability of failure. Since the effects of joint geometry and loading are included in the definition of hot-spot stress, only one $S_{R,hs}$-*N* curve is required.

The most recently published $S_{R,hs}$-*N* curve for both CHS and RHS (rectangular hollow section) joints is based on the statistical regression of a large database of tubular fatigue test results [van Wingerde et al. 1997]. In order to establish the design curve, a definition for 'cycles to failure' was chosen. Generally, four definitions are recognised:

- N_1 : Number of cycles to a 15% change in strain near the point of crack initiation;
- N_2 : Number of cycles at detection of crack;
- N_3 : Number of cycles to through-thickness cracking of the fatigue damaged member;
- N_4 : Number of cycles to complete loss of static joint strength.

In the $S_{R,hs}$-N curves shown in Figure 2.4 the N_4 definition of joint failure has been used.

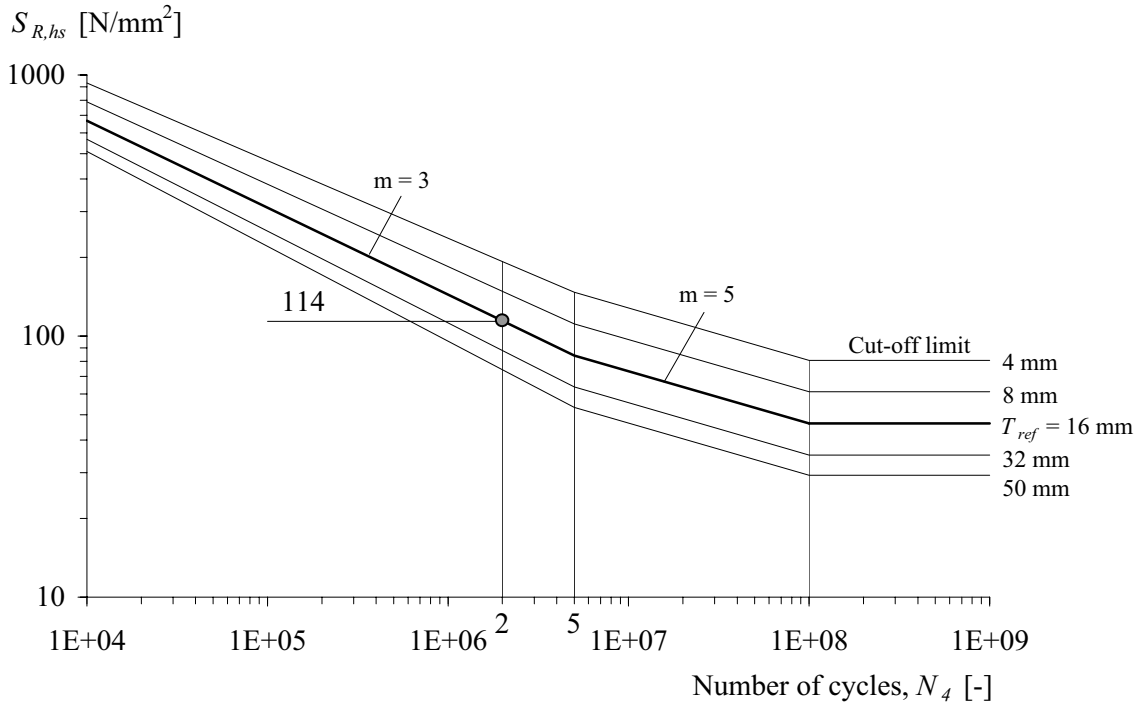

***Figure 2.4** - Hot-spot fatigue strength ($S_{R,hs}$-N) design curves for welded CHS and RHS joints [Zhao et al. 2000, IIW 2000]*

In Figure 2.4, the reference $S_{R,hs}$-N curve is plotted for T_{ref} = 16 mm. This implies that the curve is valid for a joint with a failed member thickness, T (or t), of 16 mm. The reference curve is identified by its $S_{R,hs}$ value at $N = 2\text{x}10^6$ cycles, that is, a co-called Detail Category 114. For joints with wall thicknesses other than 16 mm, size or thickness correction factors are introduced, whereby joints with thinner wall thicknesses are characterised by a higher fatigue strength and joints with a greater wall thickness are characterised by a lower fatigue strength (refer to Figure 2.4). The curves in Figure 2.4 are expressed in equation form as the following:

$$\log(S_{R,hs}) = \frac{1}{3}(12.476 - \log(N_4)) + \left(0.06 \cdot \log(N_4) \cdot \log\left(\frac{16}{T}\right)\right) \quad \text{for } 10^3 < N_4 < 5\text{x}10^6 \quad [2.4]$$

$$\log(S_{R,hs}) = \frac{1}{5}(16.327 - \log(N_4)) + \left(0.402 \cdot \log\left(\frac{16}{T}\right)\right) \quad \text{for } 5\text{x}10^6 < N_4 < 10^8 \quad [2.5]$$

where,

$S_{R,hs}$: hot-spot stress range
N_4 : number of cycles to failure, joint has suffered a complete loss of strength
T : thickness of failed member

2.3 CURRENT DESIGN SPECIFICATIONS

2.3.1 Hot-spot stress method

An accurate prediction of the stress concentration at the weld intersection is of primary importance in the application of the hot-spot stress method in tubular joint design. For this

reason, a large amount of research has been focused on the development of design equations and graphs for the estimation of joint SCFs. The following is a brief chronological overview of some of the most important contributions in terms of research and design specifications for **CHS joints**:

Beale and Toprac

Among the very first, Beale and Toprac 1967 presented a set of parametric equations for axially loaded **T-joints**. Two locations at the brace-chord weld intersection were considered (chord saddle and chord crown) and the proposed SCF values were functions of joint parameters α, β, γ and τ (refer to Figure 2.1). These functions were based on **laboratory test measurements** and their validity ranges were specified as:

$$7.70 \le \alpha \le 15.4$$
$$0.17 \le \beta \le 1.00$$
$$12.3 \le \gamma \le 33.33$$
$$0.40 \le \tau \le 1.00$$

Marshall (AWS, API)

Marshall and his co-researchers have done extensive work on the development of SCF equations: Marshall and Graff 1976, Kinra and Marshall 1979, and Marshall and Luyties 1982. The SCF equations developed and refined by these teams of researchers are based largely on the analytical solution by Kellogg 1956 for cylindrical shells under localised loading. They represent the most compact form of equations for determining stress concentration factors for welded tubular joints and were adopted by the American Welding Society (AWS) and the American Petroleum Institute (API) rules [AWS 2000, API 1993].

Kuang, Potvin and Leick

Kuang et al. 1975 and Kuang et al. 1977 presented parametric equations for T-, Y-, K-, and KT-joints based largely on **FEM analysis**. Since the weld was not modelled in the numerical simulation, however, a certain degree of inaccuracy was expected in the results. Nevertheless, the so-called Kuang or EPR (Exxon Production Research) Equations have been frequently applied in offshore structure design. Their validity ranges are as follows:

$$6.67 \le \alpha \le 40.0$$
$$0.30 \le \beta \le 0.80$$
$$8.33 \le \gamma \le 33.33$$
$$0.34 \le \tau \le 0.80$$
$$0.01 \le \zeta \le 1.00$$
$$0° \le \theta \le 90°$$

Wordsworth and Smedley

Equations by Wordsworth and Smedley [Wordsworth and Smedley 1978, Wordsworth 1981] for T-, X-, Y-, K, and KT-joints were developed as part of the UK Offshore Steels Research Project (UKOSRP) and are based on **acrylic model tests**. The equations have been adopted for various design specifications such as IIW [IIW 1985] and the Canadian Institute of Steel Construction rules [Packer and Henderson 1992]. The IIW specifications provide SCFs for K-joints in graphical form for γ and τ parameter values equal to 12.5 and 0.5, respectively, and variable values of β and θ (referred to as a base SCF, or SCF_0). For other values of γ and τ the SCF_0 is extrapolated using Equation 2.6:

$$SCF_{i,\,Load\ case_n} = SCF0_{i,\,Load\ case_n} \cdot \left(\frac{\gamma}{12}\right)^{X1} \cdot \left(\frac{\tau}{0.5}\right)^{X2} \qquad [2.6]$$

where,

$SCF_{i,Load\ case\ n}$: SCF at Location *i* for Load case *n*
$SCF0_{i,Load\ case\ n}$: base SCF for γ= 12.5 and τ= 0.5, at Location *i* for Load case *n*
X1, *X2* : exponents defined on a per joint location and load case basis

Efthymiou and Durkin

Based on numerical **FEM analysis** using a combination of shell and solid elements, Efthymiou and Durkin 1985 presented a set of SCF equations for the design of T-, Y-, and K-joints under axial load, in-plane bending moment and out-of-plane bending moment. These equations were subsequently extended to KT- and X-joints as well as multi-planar joints [Efthymiou 1988].

Romeijn (IIW 2000, CIDECT [Zhao et al. 2000])

The most extensive study to date for both uni-planar and multi-planar joints, based on both **experimental results** and **FEM analysis** (using solid elements for the entire joint model), has been carried out by Romeijn et al. [de Koning et al. 1992, Romeijn et al. 1992, Romeijn 1994, Karamanos et al. 1997]. A database of SCF results from this work was analysed and used to establish the most **current design specifications** for fatigue in tubular joints [IIW 2000, Zhao et al. 2000]. For simplicity, the new design equations retained the same format as the IIW 1985 design equations (graphs and Equation 2.6), while the actual values in the graphs and equation exponents (*X1* and *X2*) were updated to reflect the new work. For K-joints specifically, the SCF equations cover gap joints without eccentricity, with validity ranges of:

$$0.30 \le \beta \le 0.60$$
$$12.0 \le \gamma \le 30.0$$
$$0.25 \le \tau \le 1.00$$
$$30° \le \theta \le 60°$$

2.3.2 Size and thickness effect in tubular joint fatigue

Stated simply, the size or thickness effect for welded joints is the phenomenon whereby the fatigue strength of a larger or thicker joint is lower than a smaller or thinner joint of the same geometry, subjected to the same magnitude of stresses. Concern over the size or thickness effect in civil engineering structures arose, in particular for offshore structures, from the discrepancy in the plate (or tube) thicknesses and welded joints that were being tested in the laboratory in comparison with the actual, much larger, joints being used in design. In 1979, Gurney [Gurney 1979] showed, on the basis of linear elastic fracture mechanics analysis and experimental evidence, that the effect of the plate thickness in proportionally scaled joints could be significant—the thicker the plate the lower the fatigue strength, assuming the same applied stress.

On the basis of limited *S-N* data for plate and tubular joints, covering plate and member thicknesses of up to 50 mm, Gurney proposed an empirical thickness correction [Gurney 1981]:

$$\frac{S_{R,\,hs,\,T}}{S_{R,\,hs,\,22}} = \left(\frac{22}{T}\right)^n \qquad n = 0.25 \qquad [2.7]$$

where,

$S_{R,hs,T}$: hot-spot stress range for tube wall thickness, T
$S_{R,hs,22}$: hot-spot stress range for reference tube wall thickness, T_{ref} = 22 mm[1]
T : thickness of failed member
n : size effect exponent

The size or thickness correction in Equation 2.7 was subsequently included in the revised 1984 UK Department of Energy Guidance Notes for offshore structures [DEn 1984].

A significant further push on research into the size effect in the 1980s provided more convincing evidence, both experimental and analytical, of a trend for lower fatigue strength in thicker specimens of, for the most part, the same geometry [Noordhoek and de Back 1987]. The research work included various types of joint geometries (plated joints, tubular joints), joint preparation (as-welded, post-weld heat treated), test conditions (in air, in sea water) and load types (tensile load, bending load).

For tubular joints, the size effect correction most recently adopted by current specifications is based on a statistical study on a database of tubular fatigue results carried out by van Wingerde et al. 1997. The correction resulting from this work is significantly more penalising than that suggested by Gurney in 1979. It is expressed as follows:

$$\frac{S_{R,\,hs,\,T}}{S_{R,\,hs,\,16}} = \left(\frac{16}{T}\right)^{n} \qquad n = 0.06 \cdot \log N_4 \qquad \text{for } 10^3 < N_4 < 5\text{x}10^6 \qquad [2.8]$$

$$\frac{S_{R,\,hs,\,T}}{S_{R,\,hs,\,16}} = \left(\frac{16}{T}\right)^{n} \qquad n = 0.402 \qquad \text{for } 5\text{x}10^6 < N_4 < 10^8 \qquad [2.9]$$

where,

$S_{R,hs,T}$: hot-spot stress range for tube wall thickness, T
$S_{R,hs,16}$: hot-spot stress range for reference tube wall thickness, T_{ref} = 16 mm
T : thickness of failed member
n : size effect exponent
N_4 : number of cycles to failure, joint has suffered a complete loss of strength

The effect of the correction presented in Equation 2.8 and Equation 2.9 on the fatigue strength is shown in Figure 2.4 (in terms of $S_{R,hs}$-N plots). In Equation 2.8 and Equation 2.9 it is interesting to note the increase in the correction factor, n, from the correction first proposed by Gurney: n = 0.378 at 2x10^6 cycles as opposed to n = 0.25. A more detailed description and discussion of the statistical analysis carried out by van Wingerde et al. 1997 in finding this size effect correction will be given in Chapter 5.

2.4 CONCLUSIONS

This chapter presents the main definitions related to the work presented in this document, as well as a brief overview of the historical development of research on welded tubular joint fatigue. The following main conclusions have been reached:

- The hot-spot stress method is the only current method for fatigue design of tubular joints that is both scientifically acceptable (in terms of its capacity to explain the physical behavior of a joint) and practical (for use in engineering offices).

1. The reference plate thickness for tubular joints was taken as 32 mm.

- The correction for the so-called size effect applied to the hot-spot fatigue strength ($S_{R,hs}$-N) curves for tubular joints (n = 0.378 at 2x10^6 cycles) is considerably higher than the original correction determined for plated joints (n = 0.25). In design, this correction was seen as relatively penalising, in particular for the joint hot-spot stresses calculated in the chord member. Typical bridge chord member wall thicknesses are substantially greater than the reference thickness of 16 mm and therefore subject to a significant reduction in fatigue strength (due to the size effect correction).

3 EXPERIMENTAL INVESTIGATION

3.1 INTRODUCTION

Large-scale tests were carried out to observe and quantify the behaviour of welded CHS K-joints under static and fatigue loading. The main aims of the experimental investigation were to measure strains in brace and chord members, and strain concentrations in proximity to the brace-chord weld intersection, and to obtain constant amplitude fatigue test results in the form of S-N data and fatigue crack measurements. Results from the tests were then used to validate a numerical (finite element) model and to study the behaviour of the joints as cracking progresses through the wall thickness of the fatigue affected member.

Chapter 3 is composed of the following sections:

- **Section 3.2** : *Description of test specimens and procedures*, describes the test specimens and procedures used in the static and fatigue tests, including the strain measurements carried out at member and joint locations;
- **Section 3.3** : *Static and fatigue test results*, presents and discusses of the main results from the tests including strains measured in the members and joints, the number of fatigue load cycles to crack detection and joint failure. Results in the form of $S_{R,hs}$-N data are compared to $S_{R,hs}$-N design lines using current specifications as well as results from other, similar test programs;
- **Section 3.4** : *Conclusions*.

In addition to the large-scale tests, numerous in-situ measurement campaigns have also been carried out. More information on these studies can be found in Schumacher and Blanc 1999, Schumacher and Edder 2001a and Schumacher and Bays 2002.

3.2 DESCRIPTION OF TEST SPECIMENS AND PROCEDURES

3.2.1 Specimens in truss girder

Eight planar CHS truss girders were tested under static and dynamic load. Each truss comprised four welded CHS K-joints along the bottom chord. Connections between the braces and the top chord, a plate girder, were made using bolted end plates. Figure 3.1 shows the general configuration and dimensions as well as a three-dimensional visualisation of the truss girder. The load was applied at mid-span and the truss was simply supported at the extremities of the top chord.

Due to the location of load application, the two central CHS K-joints were subjected to the highest loads and were thus the critical fatigue details. This central portion comprising two CHS K-joints, four braces and one continuous chord will be referred to as the specimen. Once testing of a particular specimen was completed, it was unbolted, removed and the next specimen was moved into the truss. This means that the two K-joints at the ends of the trusses and the top chord girder remained in place throughout the entire test program. In order to avoid overlapping of the brace members and to facilitate welding in the gap region, a positive eccentricity, e, as defined in Section 2.2 was accepted between the brace and bottom chord axes.

A total of four test series with two specimens each—thus four CHS K-joints per series—were carried out. Table 3.1 lists the test series and gives details for each series: nominal dimensions of the CHS K-joints, non-dimensional joint parameters, weld type (with or without backing

ring) and (with or without) weld improvement (refer to Appendix B). Each test series investigated one parameter, with S1 considered the base series. (With four in each series, joints are numbered in logical order, that is S11, S12, S13 and S14 for series S1, and so on.) The nominal non-dimensional joint parameters were the same for all four test series: $\theta = 60°$, $\beta = 0.51$ (0.53), $\gamma = 6.83$ (6.73) and $\tau = 0.63$ (0.64).

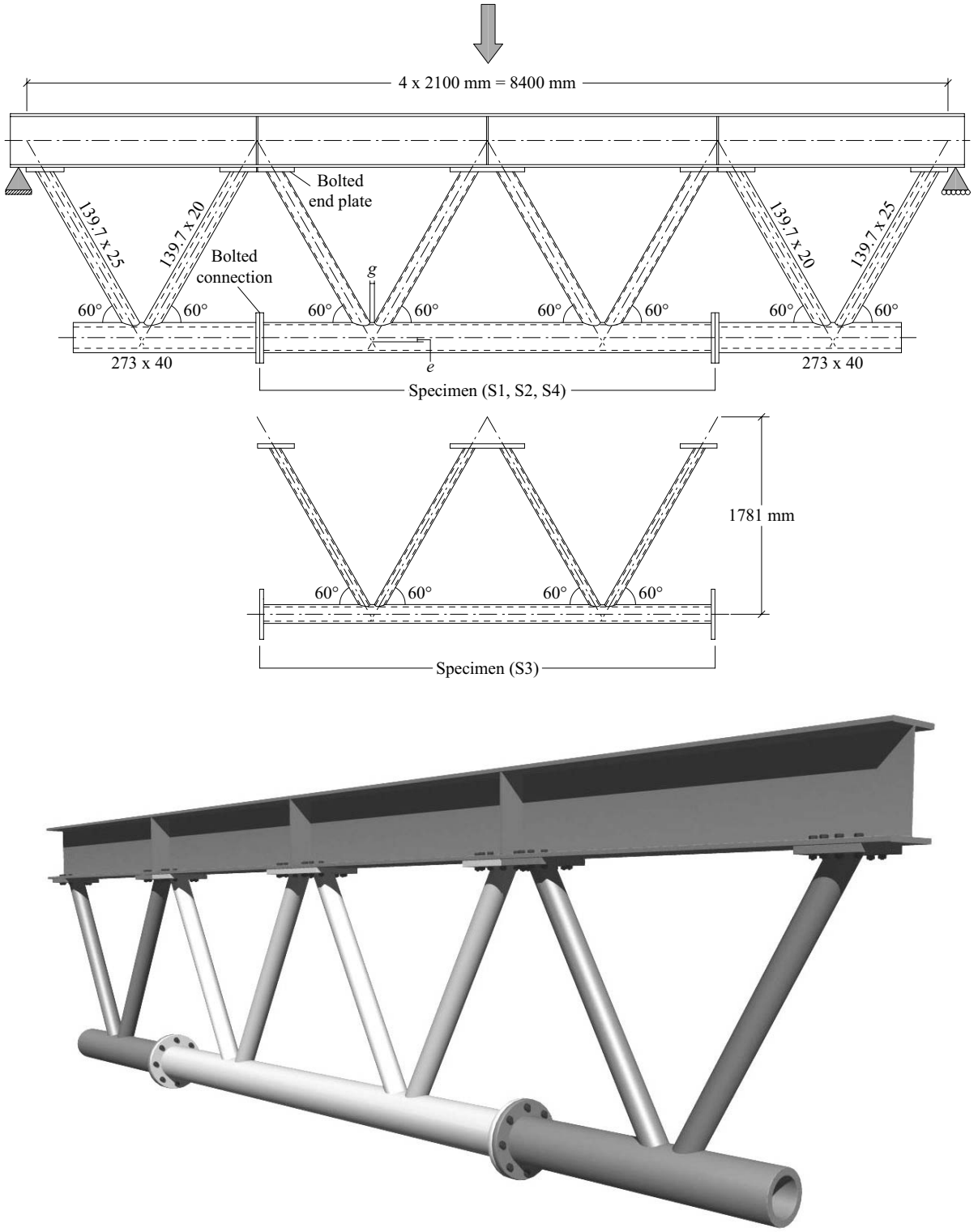

Figure 3.1 *- Truss girder, general configuration and dimensions*

Comparison of Table 3.1 with non-dimensional joint parameters of existing CHS truss bridges, in particular the Lully, Dättwil, Aarwangen and Nesenbachtal bridge (refer to Appendix A), shows similarities between the specimen parameters and those of the bridges. For more information on the fabrication and material properties of the specimen, refer to Schumacher 2003.

***Table 3.1** - Test series, nominal values*

Series	Investig. param.	Nom. Dimensions [mm]		θ [°]	β [-]	γ [-]	τ [-]	Weld [mm]
		Chord	Brace					
S1	Base	273 x 20	139.7 x 12.5	60	0.51	6.83	0.63	FP, BR
S2	Backing ring	273 x 20	139.7 x 12.5	60	0.51	6.83	0.63	FP
S3	Scale	168.3 x 12.5	88.9 x 8	60	0.53	6.73	0.64	FP, BR
S4	Weld impr.	273 x 20	139.7 x 12.5	60	0.51	6.83	0.63	FP, BR, WI

FP : Full penetration weld

BR : Backing ring

WI : Weld improved

3.2.2 Static and fatigue tests

Following the initial static tests, a fatigue test was carried out on each specimen. Load cycles were applied in order to determine the number of cycles to crack initiation and to joint failure. Fatigue loading was applied in the form of a sinusoidal wave at a frequency of about 2 Hz, with a load ratio of $R = 0.1$ ($R = Q_{min} / Q_{max}$). Detailed information on the test procedure can be found in Schumacher 2003.

Joint failure was taken as through-thickness cracking of the chord. In all specimens except for S1(1,2) cracks were present in the second joint by the time the first joint had formed a through thickness crack. For Joint S11 the crack was repaired by gouging and re-welding and testing was continued until cracking in S12 had occurred.

Strain measurements on members

Strain measurements on truss members were taken during the static tests. Brace and chord members were equipped with uni-axial electrical resistance strain gauges (refer to Figure 3.2). Gauges were positioned in pairs, at either two or four points on a cross-section. The orientation of the gauge pairs permitted the measurement of axial strain (ε_{ax}) and either strain due to in-plane bending (ε_{ipb}) or strain due to out-of-plane bending (ε_{opb}), depending on their position on the cross-section.

The locations of the instrumented cross-sections varied with each test joint and series. Generally, two locations per member were instrumented in order to measure the variation in moment over the length of the member and to enable the extrapolation of strains to the test joints. The extrapolation procedure for brace and chord strains to the joint was defined in Figure 2.2. It is recalled that the nominal brace strain, ε_{nom_br}, is taken at the intersection between the brace axes and the top wall of the chord, while the nominal chord strain, ε_{nom_ch}, is taken at the intersection of the brace axes. For the sign convention, moments were considered positive if they increase the tensile strain in the gap region of the joint.

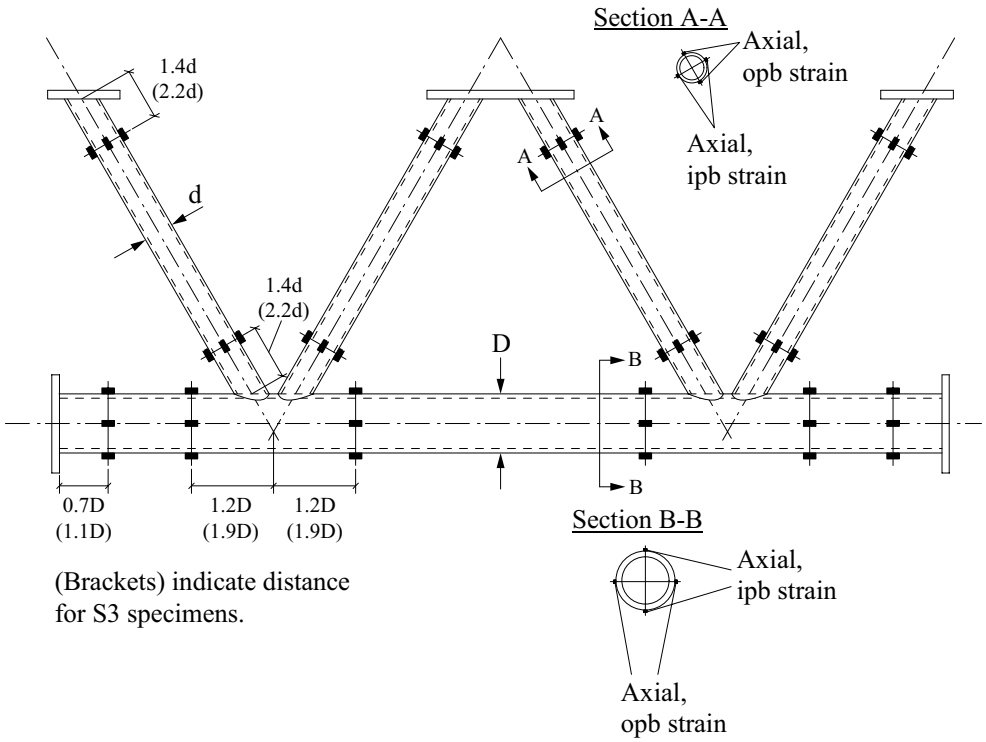

***Figure 3.2** - Position of uni-axial strain gauges on specimen for measuring axial and bending strain in members*

In Figure 3.2, it can be seen that the instrumented cross-sections for series S1, S2 and S4 are located approximately 1.2*D* (for the chord) or 1.4*d* (for the braces) from the joints, that is, considerably less than the 3*D* (3*d*) cited in literature [van Wingerde et al. 1992, Karamanos et al. 1997]. The 3*D* or 3*d* distance is recommended to ensure that the gauges are placed in a region where perturbations due to the joint are no longer present (that is, in the region where the direction of principal stress coincides with the member axis). This smaller distance used in the present tests was investigated in more detail, the results of which are presented in Schumacher 2003.

Strain measurements in joints

Strains in proximity to the brace-chord weld intersection, that is, hot-spot strains, were measured with various types of gauges: uni-axial strain gauges, uni-axial strip gauges, rosettes and strip rosettes. The strains measured with the strip gauges were extrapolated to the weld toe to determine the hot-spot strain at that location.

In general, individual gauges or the first gauge (rosette) in a strip were applied at the larger of 0.4*T* on the chord (0.4*t* on the brace) or 4 mm from the weld toe, as can be seen in Figure 3.3. Also shown in Figure 3.3 are the different locations of interest around the joint (to be referred to later), Locations 1, 11, 2, 3, 31, 4 and 1c. The photo in Figure 3.3 shows joint S31 with strip gauges at Locations 1 and 11. After the first test series, the location of fatigue failure could be anticipated and strain gauges were therefore concentrated at that location (Location 1).

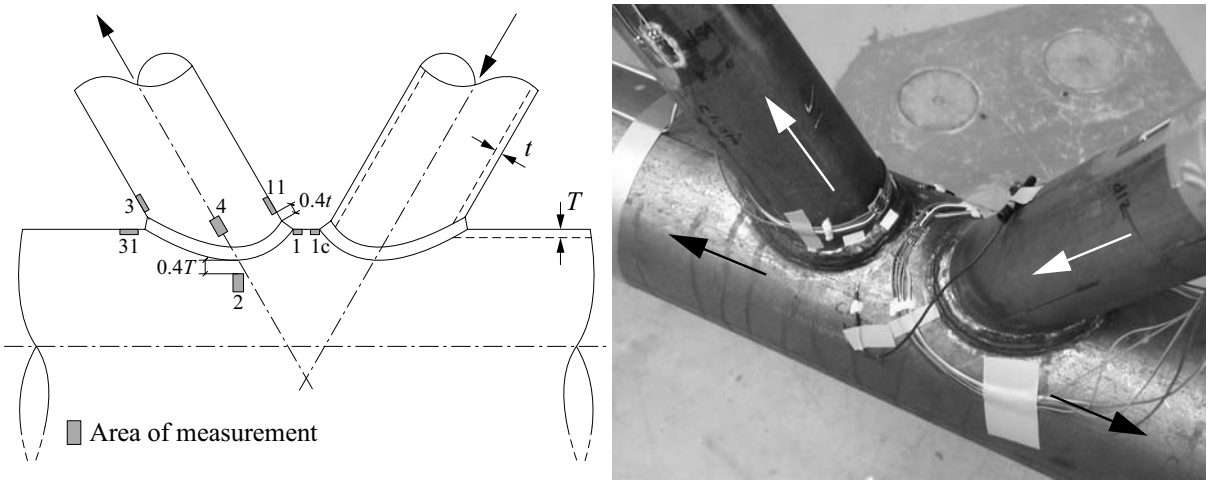

Figure 3.3 - *Gauge locations on joint; gauges on joint S31*

3.3 STATIC AND FATIGUE TEST RESULTS

3.3.1 Static test results

Member strain results

As will be seen in later chapters, decomposition of the strains in a truss member due to different load cases facilitates the understanding of each load type and its effect on the hot-spot strains (stresses) in the joint. From a more global point of view, the member strain measurements also give an indication of the behaviour of the truss and the transfer of the loads from the jacks to the end supports via the various truss members. Table 3.2 shows strain measurement results taken during static loading of the truss. Each strain value reported in the table is an average of six measurements—three taken prior to fatigue testing and three measurements taken once cracking had been detected in one of the joints. Very little difference was seen between measurements. Strains due to the axial force and in-plane bending for the tension and compression braces as well as the chord (on the tension brace side) are given. As would be expected for a planar truss, the out-of-plane strains were small and are therefore not reported here. When possible, bending strains were extrapolated to the CHS K-joint on the bottom chord (refer to Section 2.2 for a description of the extrapolation of strains (stresses) in joint members). Strains that have not been extrapolated are the values that were measured at the instrumented cross-section closest to the joint.

Table 3.3 reports the ratio of total nominal-to-axial member strain for a selection of test joints. The total nominal strain is found through superposition of the axial and extrapolated in-plane bending strains. The ratio gives an indication of the amount of bending present in the members, which depends largely on the rigidity of the truss joints and the eccentricity between member axes. Simulation of the joint rigidity is a difficult task that generally requires three dimensional modelling of the joint. Alternatively, current specifications [Zhao et al. 2000, IIW 2000] recommend the truss to be modelled with simple bar elements and idealised joints. In this case, additional magnification factors must be used to account for the secondary moments not accurately simulated by the model. A more detailed description of truss modelling is given in Section 4.2.

***Table 3.2** - Member strain results*

Joint	Tension brace		Compression brace		Chord	
	ε_{ax_br} [μm/m]	ε_{ipb_br} [μm/m]	ε_{ax_br} [μm/m]	ε_{ipb_br} [μm/m]	ε_{ax_ch} [μm/m]	ε_{ipb_ch} [μm/m]
S11	227	144	-221	-55	109	-57*
S12	229	141	-213	–	109	-53*
S13	203	112	-219	-60*	104	-49*
S14	241	42	-207	–	107	-66*
S21	206	137	-215	-38	122	-50
S22	201	106*	-217	-47*	121	-44*
S23	202	148	-220	-62	101	-43
S24	207	97*	–	–	–	–
S31	239	106	-245	-39	180	-9
S32	231	91*	-237	-29*	182	0*
S33	236	129	-243	-46	185	5
S34	243	97*	-243	-34*	186	0*
S41	206	181	-220	-62	101	-46
S42	207	97*	–	–	–	–
S43	221	142	-212	-75	133	-61*
S44	212	116*	–	–	–	–

– Strains due to this load case not measured

* Not extrapolated to joint, strains at gauge locations

Examining the results presented in Table 3.3, several patterns can be recognised. The proportion of bending in the tension braces is high. In fact, the nominal-to-axial strain ratios in these members are significantly higher (between 1.5 and 1.8) than the 1.3 magnification factor generally called for in specifications. The truss girder used for the tests, however, should not be considered a standard structure. The brace members are bolted on one end and welded on the other—an unusual combination not typical to bridge truss structures.

From a more practical point of view, however, reference is made to the in-situ measurements conducted on CHS truss highway bridges [Schumacher and Edder 2001a, Schumacher and Bays 2002]. In these studies it was also found that the measured nominal-to-axial strain ratios in these existing structures can exceed the magnification factors in specifications. This point, although of importance and requiring additional investigation, is not examined further within the framework of the present study.

The strain ratio also indicates the direction of bending moment with respect to the joint. That is, a ratio of less than unity ($\varepsilon_{nom} / \varepsilon_{ax} < 1.0$) means that the bending moment adds compressive strain to the gap region of the joint, as is seen in almost all of the chord members. It is not possible to account for a reduction of axial strain due to compressive bending moments in the simplified modelling procedure described above, that is, magnification factors given in the specifications to account for bending are *always greater than one*.

***Table 3.3** - Member strain ratios*

Joint	Tension brace		Compression brace		Chord	
	ε_{nom_br} [μm/m]	$\varepsilon_{nom\_br} / \varepsilon_{ax\_br}$	ε_{nom_br} [μm/m]	$\varepsilon_{nom\_br} / \varepsilon_{ax\_br}$	ε_{nom_ch} [μm/m]	$\varepsilon_{nom\_ch} / \varepsilon_{ax\_ch}$
S11	371	1.63	-276	1.25	–	–
S21	343	1.66	-253	1.18	30	0.43
S23	350	1.73	-282	1.28	58	0.57
S31	345	1.44	-284	1.16	171	0.95
S33	365	1.38	-289	1.19	190	1.03
S41	387	1.88	-282	1.28	55	0.54
S43	363	1.64	-287	1.35	–	–

Joint stress results

Joint hot-spot stresses were determined using an appropriate extrapolation method and stress-strain ratio, as described in Schumacher 2003. The hot-spot stress values at the location of cracking were then used in the *S-N* analyses presented below.

The method of extrapolation to find the hot-spot strain has also been thoroughly studied and discussed [Herion 1994, Romeijn 1994, van Wingerde 1992, Panjeh Shahi 1994]. In order to obtain results comparable to existing work, an extrapolation method used by Romeijn 1994 was applied.

The extrapolation limits are based on the rules found in Zhao et al. 2000 and IIW 2000 (refer to Table 2.1). The minimum value for $L_{r,max}$ is used for all of the work herein, both experimental and numerical. In Schumacher 2003 it was seen from the measurements and numerical results that the strain distribution close to the weld toe of the CHS joints can be non-linear and therefore best described by a parabolic function. This observation for CHS joints was also made by Romeijn 1994 and Lee and Bowness 2002. However, as pointed out by Romeijn, simple parabolic extrapolation can be overly sensitive to small changes in data values. A combination of parabolic curve fitting and linear extrapolation is thus more suited.

The extrapolation method is depicted in Figure 3.4. A second order polynomial is fitted to the strain data points in a region close to the weld toe (obtained either from measurements of numerical modelling) and within the limits of extrapolation. A linear extrapolation to the weld toe is then carried from two points: the point on the fitted curve at $L_{r,min}$ and the point on the fitted curve at $L_{r,max}$. The value of extrapolated strain at the weld toe is taken as the hot-spot strain, ε_{hs}.

It should be noted that this method of extrapolation, using both polynomial and linear curve fitting, is advantageous in the sense that it can also be applied to linear or nearly linear strain (stress) distributions. In this case, the quadratic term simply tends towards zero and a first order polynomial (i.e. a straight line) is fitted to the data points.

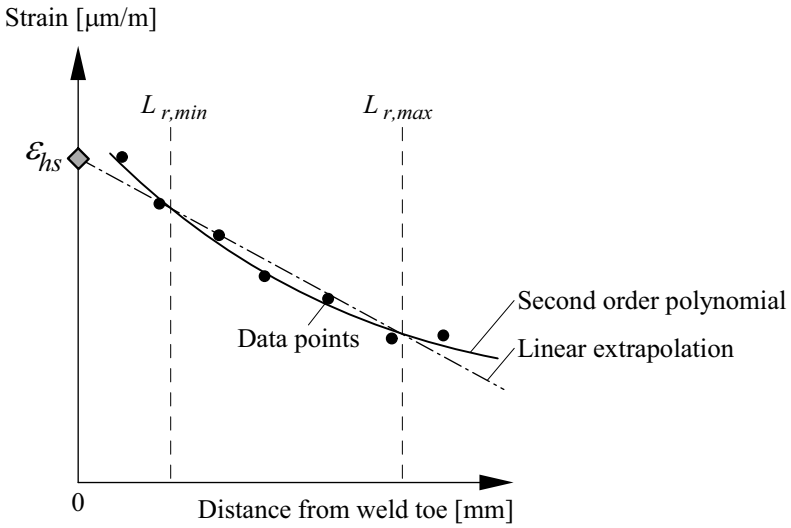

***Figure 3.4** - Extrapolation to determine hot-spot strain at weld toe*

Table 3.4 presents hot-spot stress values for a selection of test joints at Location 1 (the location of cracking in all joints except those from series S4) as well as the nominal stresses in the tension brace and the chord (on the tension brace side).

***Table 3.4** - Nominal and hot-spot stresses for test joints*

Joint	Tension brace	Chord	Location 1	
	σ_{nom_br} [N/mm^2]	σ_{nom_ch} [N/mm^2]	$\sigma_{hs,1}$ [N/mm^2]	$SCF_{total,1}$ [-]
S11	77.9	10.9	114.0[1]	1.28
S21	72.0	15.1	139.6	1.60
S23	73.5	12.2	138.8	1.62
S43	76.2	15.1	148.4	1.62
S31	72.5	35.9	187.0	1.73
S33	76.7	39.9	195.7	1.68

1 Calculated using validated finite element model [Schumacher 2003]

A notion introduced in Table 3.4 and used again in Chapters 4 and 6 is the total stress concentration factor, SCF_{total}. The SCF_{total} is the ratio between the hot-spot stress and the total nominal stress affecting the location in question:

$$SCF_{total,i} = \frac{\sigma_{hs,i}}{\sigma_{nom\_br} + \sigma_{nom\_ch}} \qquad [3.1]$$

where,

$SCF_{total,1}$: total stress concentration factor at joint Location 1
$\sigma_{hs,i}$: hot-spot stress at joint Location 1
σ_{nom_br} : scalar value of nominal stress in brace (due to both axial load and bending)
σ_{nom_ch} : scalar value of nominal stress in chord (due to both axial load and bending)

The SCF_{total} provides a basis for comparison between the different test joints, since at this point not enough information exists to obtain the stress concentration factors due to the different load cases.

One of the most obvious discrepancies in Table 3.4 is the difference in hot-spot stresses and stress concentration factors between joint S11 and the joints of series S2 and S4. Nominally, the joints of series S1, S2 and S4 are dimensionally and geometrically identical and should therefore possess an identical stress response. In reality, however, the joints are not identical. Notably, joint S11 (and the other joints in the S1 series) has a considerably smaller gap size than joints in series S2 and S4. It will be seen in Chapter 4 that gap size influences the stress magnitude at Location 1, more specifically, a smaller gap size can have a lower stress level at that location for a given load.

As was already seen, the nominal stresses between joints (specimens) vary slightly. In all of the joints the brace stress is greater than the chord stress. The hot-spot stress in joints S21 and S23 compare very well. A higher hot-spot stress in joint S43 as compared with joints S21 and S23 can be accounted for by the higher nominal brace stress, σ_{nom_br}, in S43.

The hot-spot stresses for joints S31 and S33 also compare well; a slightly higher hot-spot stress in S33 is due to a higher nominal stress in the brace and chord. The higher stress concentration factors for the series S3 joints as compared with those from series S2 and S4—series that have similar non-dimensional geometric parameters—is caused by the different proportion of brace stress compared with chord stress (the proportion of brace stress in the series S2 and S4 joints is higher).

In general, the good correspondence seen in Table 3.4 between geometrically similar joints, subjected to the same nominal stresses, underlines the validity of the hot-spot stress as a value that can be reproduced in tests and used as a basis for comparison of different joints.

3.3.2 Fatigue test results

Behaviour of weld improved joints

The joints in series S4 were needle peened at and around Location 1. Through this weld improvement method a compressive residual strain is introduced by mechanical plastic deformation of the weld toe region, to a depth of approximately 0.5 to 1.0 mm into the material. The applied tensile strain thus must first overcome the residual strain before it becomes damaging [Haagensen and Maddox 2001].

The fatigue test results for series S4 demonstrate the beneficial influence of needle peening on the fatigue life of the joints. No cracks formed in Location 1 or at any other locations around the tension brace-chord intersection, even at three times the number of load cycles as compared with similar test series (S1 and S2). Cracks were detected, however, at Location 1 on the *compression brace*, denoted as Location 1c (refer to Figure 3.3). The notch at Location 1c is nominally the same as at Location 1. Although the force in the brace is compressive, the chord at that location is in tension and, more importantly, the material adjacent to the weld is also in tension due to tensile residual weld strains. Thus, even if the applied strain range is compressive, the local strain range relevant to fatigue crack initiation and growth may be partly or entirely tensile.

Residual weld strains were not measured as part of this test program. Compared with the cracks in the series S1 and S2 joints, the cracks in series S4 joints at Location 1c were detected later

and propagated at a slower rate suggesting that the effective strain range was only partly tensile. It is interesting to note that at a smaller tensile strain range, Location 1c is still more critical than other locations around the tension brace-chord intersection, including Location 11 where relatively high hot-spot strains were measured. This raises questions about the comparative severity of the notch at different locations around the joint and whether it is justifiable to compare them on the same basis (for example, using the same $S_{R,hs}$-N design line).

More generally, the shift of the critical location in the joint, both in space and time, is an outcome that will require further study in order to appropriately quantify the potential benefit of weld improvement as applied to welded CHS joints. Such a study is not within the scope of the work presented here.

$S_{R,hs}$-N results and comparison with existing data and design lines

The fatigue test results are presented in the form of logarithmically plotted $S_{R,hs}$-N results, where $S_{R,hs}$ the hot-spot stress range and N is the number of load cycles at failure. The hot-spot stress range is taken at Location 1 for all joints. In joints where the hot-spot stress was not measured at Location 1, the hot-spot stress from a similar joint was taken.

In the $S_{R,hs}$-N diagrams, comparisons are made to current $S_{R,hs}$-N design curves (referred to as "IIW design curves") [IIW 2000, Zhao et al. 2001]. The derivation of these curves was carried out based on a different definition of joint failure than the one used in the present investigation. That is, in a study of a large database of fatigue test results for CHS joints [van Wingerde et al. 1997], failure was defined as the point at which the joint suffered a complete loss of strength ($N4$) as opposed to the through-thickness cracking criterion (N_3) used in the present investigation. In the same study by van Wingerde et al., the average ratio between N_4 and N_3 of 329 data points was found to be $N_4 / N_3 = 1.49$. Thus in order to carry out a comparison between the test results and design lines in the following figures, the number of cycles at through-thickness cracking of the test joints has been multiplied by 1.49 (with the exception of Figure 3.10 where the number of cycles at crack detection, N_2, are presented).

In the statistical evaluation of the test results, $S_{R,hs}$-N mean curves were fitted to the data through regression analysis based on a fixed slope of $m = 3.0$ up to the constant amplitude fatigue limit, $N = 5\text{x}10^6$ cycles. At N greater than $N = 5\text{x}10^6$ cycles, a slope of $m = 5.0$ was taken. Fixed slopes were used since all of the specimens were tested at similar hot-spot stress ranges and therefore the experimental determination of a slope was not feasible. Following the determination of a mean curve, *characteristic curves* were established at a certain number of standard deviations (s_N) (of the dependent variable $logN$) below the mean. By taking an appropriate number of standard deviations below the mean—a value which reflects the number of points in the data set, e.g. $3.5s_N$ for 5 data points, $2.7s_N$ for 10 data points, $2.0s_N$ for 50 data points and so on [IIW 1996]—a 95% survival probability with a two-sided 75% confidence level of the mean is achieved.

In the following figures, the characteristic curves are compared to the aforementioned "IIW design curves." The design curves, given by Equation 3.2 and Equation 3.3, are dependent on the thickness of the failed member (T or t). Both the characteristic curves and the design lines are identified by their $S_{R,hs}$ value at $N = 2\text{x}10^6$ cycles (generally referred to as the Detail Category).

$$\log(S_{R,hs}) = \frac{1}{3}(12.476 - \log(N_4)) + \left(0.06 \cdot \log(N_4) \cdot \log\left(\frac{16}{T}\right)\right) \text{ for } 10^3 < N_4 < 5\text{x}10^6 \quad [3.2]$$

$$\log(S_{R,hs}) = \frac{1}{5}(16.327 - \log(N_4)) + \left(0.402 \cdot \log\left(\frac{16}{T}\right)\right) \qquad \text{for } 5\text{x}10^6 < N_4 < 10^8 \quad [3.3]$$

where,

$S_{R,hs}$: hot-spot stress range
N_4 : number of cycles to failure, joint has suffered a complete loss of strength
T : thickness of failed member

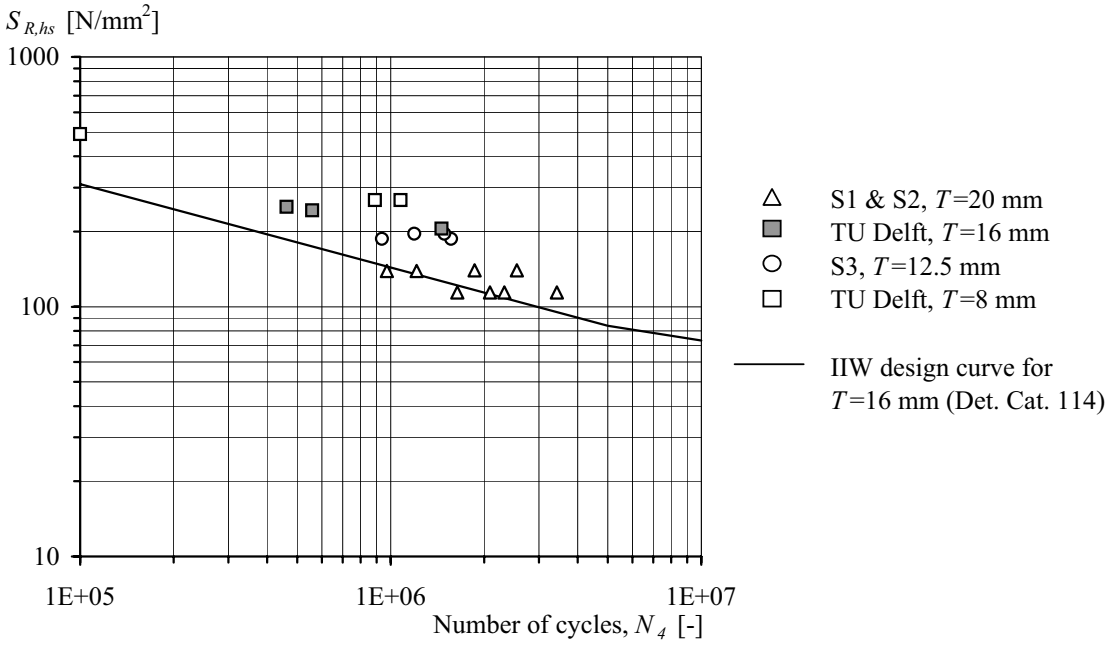

Figure 3.5 - *Results from present study and TU Delft tests on geometrically similar joints*

As a first step, the $S_{R,hs}$-N test results from the series S1, S2 and S3 joints were plotted with results from similar fatigue tests carried out at TU Delft (Figure 3.5). The TU Delft tests [de Koning et al. 1992, Romeijn 1994] were conducted on multi-planar trusses with welded CHS KK-joints.

The non-dimensional parameters for these trusses were the following: $\theta = 45°$, $\beta = 0.40$, $\tau = 0.50$ and $\gamma = 6.0$ and 12.0. For the TU Delft results only data points for failures occurring in the chord are given. Furthermore, as the failure of the TU Delft joints was also defined at N_3, the same adjustment was made as described above whereby the results could be reported in terms of N_4.

Figure 3.5 shows that the two independently carried out test programs produced similar results that fall within the same order of magnitude in terms of fatigue life, over a range of $S_{R,hs}$ (with the exception of one joint in the TU Delft series). Furthermore, the TU Delft results for 16 mm thick specimens seem reasonable when compared to the design curve for this thickness of joint (shown in figure).

In Figure 3.6 the test results from series S1, S2 and S3 are shown as well as design curves corresponding to the thickness of the failed joint members. The horizontal lines represent the calculated hot-spot stress range in the test joints, obtained for two specific joints (S21 and S31, shown by the black points) and based on parametric equations in current design specifications corresponding to the $S_{R,hs}$-N design lines in this figure. Since the goal of the comparison was to evaluate, specifically, the validity of the parametric design equations in the determination of the

hot-spot stress, the *measured* nominal member stresses from the tests were used in the calculation rather than nominal member stresses determined through analysis of a simple bar element model of the truss.

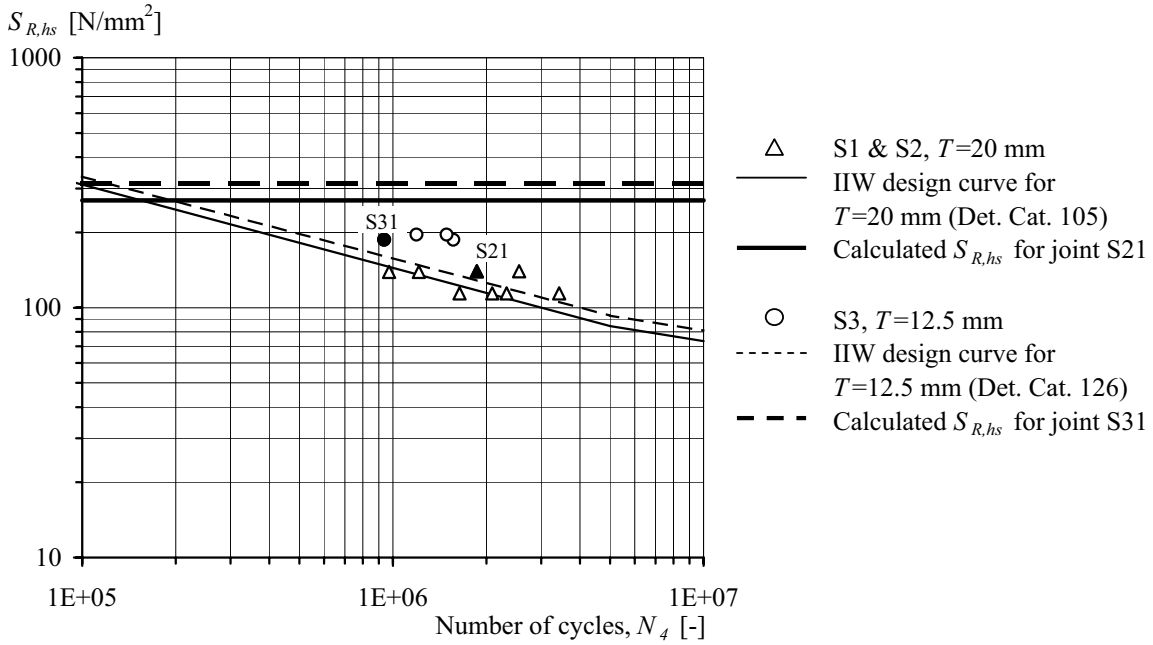

***Figure 3.6** - Comparison between measured and calculated hot-spot stress*

The considerably higher calculated hot-spot stress range as compared with the measured stress ranges confirms the suspicion that current design specifications results in conservative predictions for certain CHS K-joints. Furthermore, considering that the non-dimensional parameter γ for the joints falls outside of the validity range given in the specifications ($\gamma_{test} < 12.0$), it can be assumed that a simple extrapolation of the existing rules (as was done for these calculations) can give inaccurate results.

A. Effect of backing ring

In order to study the effect of the backing ring, a comparison is made between the results from test series S1 and S2 (refer to Table 3.1). In Figure 3.7 regression analysis of the two series is conducted separately. It is seen that the resulting characteristic curves for the two series are very similar, with the curve from series S1 defined as a Detail Category 90 and that for series S2 defined as a Detail Category 87. The similar results were not surprising since failures in the S1 and S2 series joints all occurred at Location 1, at the weld toe and thus were apparently not affected by the presence (or non-presence) of a backing ring.

In other words, although backing rings may help ensure a more fully penetrated weld, failure of the joints was nevertheless dictated by cracking at the surface (and not at the weld root) and thus the presence of backing rings did not effect the fatigue resistance of the joints.

Upon examination of Location 1 in joint S21 [Schumacher 2003], it was seen that the weld was fully penetrated. It is possible, however, that less than full weld penetration can occur, even with bevelled brace ends. Although not observed in the tests, in a partially penetrated weld the strain concentration at the root could exceed the concentration at the weld toe, thus making the root the fatigue critical location in the joint. This is a less desirable failure location than the weld toe since the crack is not readily detectable.

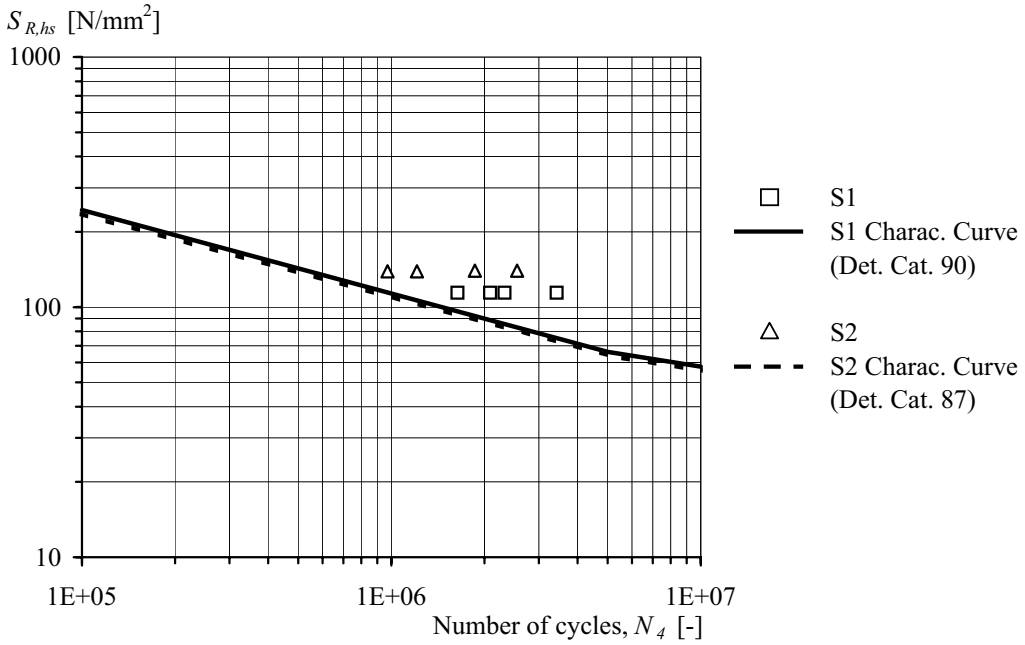

***Figure 3.7** - Fatigue test results for series S1 and S2, separate analysis*

In light of the similar results obtained for series S1 and S2 and to facilitate comparison with other series and existing design lines, the S1 and S2 results will be henceforth considered as one data set, S1 & S2. In Figure 3.8 comparison between the characteristic curve for S1 & S2 and the IIW specified design curve for failure in a 20 mm member (the thickness of the chords in S1 and S2) can be made: the characteristic curve for the test results is lower than the corresponding design curve (Det. Cat. 86 versus Det. Cat. 105). In the IIW specifications the design lines for K-joints specify joints with zero eccentricity, $e = 0$. However, it has been noted here and by Karamanos et al. 1997 that in order to avoid overlap in K-joints with brace-chord angles of 60° and larger β values a small eccentricity must be accepted. The effect of gap and joint eccentricity on K-joints will be examined in more detail in Chapter 4.

B. Effect of size

The effect of size on the fatigue resistance of the welded joints was investigated in test series S3. The dimensions of the joints in S3 were reduced proportionally as compared with S1 & S2 to study the effect of smaller dimensions on the fatigue resistance. Since the reduction was proportional, the non-dimensional parameters, θ, β, γ, τ, did not change. Figure 3.9 plots the results for series S1&S2, and series S3. For each data set the characteristic curve and the IIW curve corresponding to the thickness of the chord is given. In IIW 2000 and Zhao et al. 2001 the correction for the size effect is a function of the thickness of the failed member, with a reference thickness of 16 mm. Thicknesses greater than or less than 16 mm result in a reduction or increase in fatigue strength, respectively, relative to the fatigue strength of the 16 mm joint. In series S1, S2 and S3 failure occurred in the chord thus it stands to reason that the chord thickness, T (20 mm and 12.5 mm), is the relevant dimension.

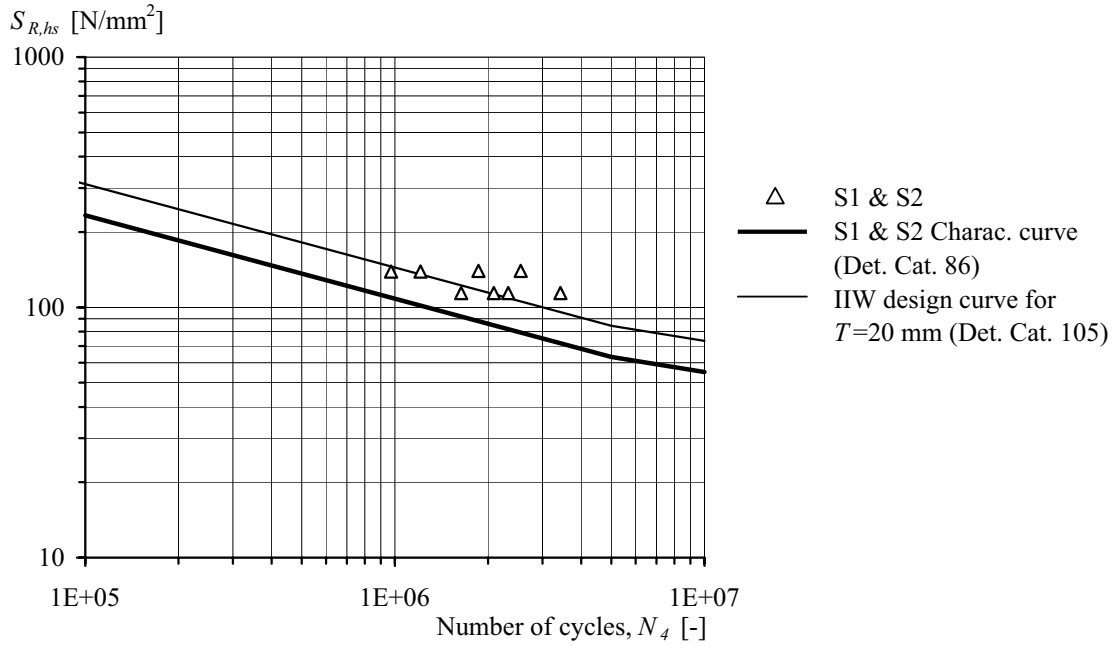

***Figure 3.8** - Fatigue test results for series S1 and S2, combined analysis*

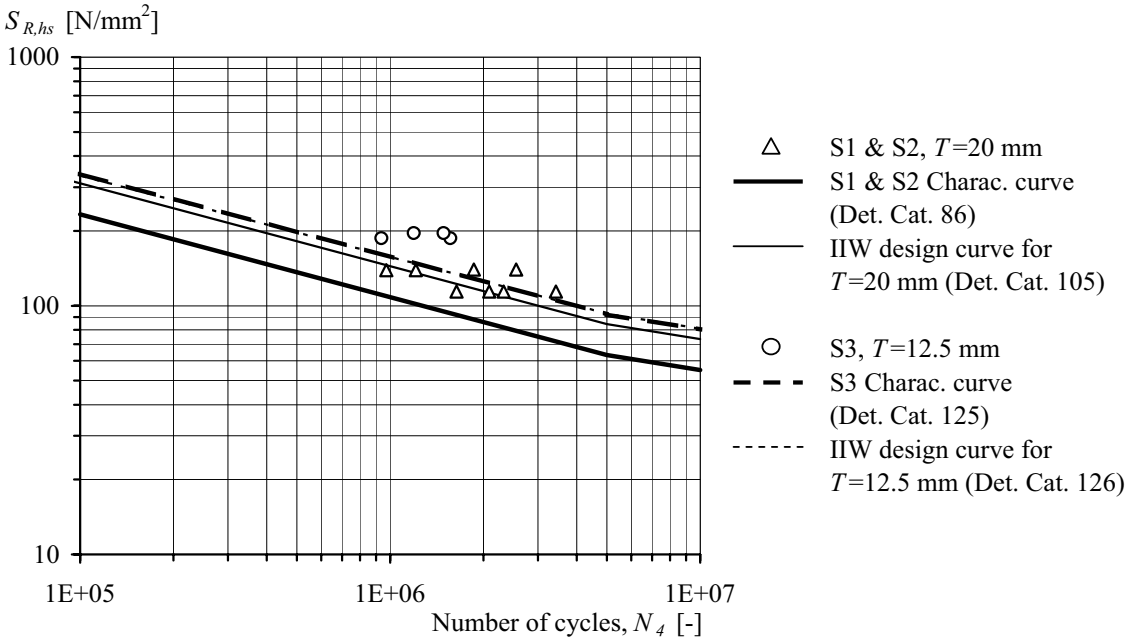

***Figure 3.9** - Fatigue test results (N_4) for series S1 & S2 and S3, effect of size*

The data in Figure 3.9 show the same trend indicated in the specifications: a thicker failed member results in a lower fatigue strength. The characteristic curve for the S3 results falls at the same level as the IIW line for T = 12.5 mm, while, as already seen in Figure 3.8, the characteristic curve for the S1 & S2 results falls below the IIW line T = 20 mm. Based on these results, it can be said that the correction for size inherent to the design lines appears to be unconservative for T > 16 mm. Stated otherwise, the observed size effect for proportionally scaled joints appears to be greater than the size correction included in the design lines. This latter point is a noteworthy result when considering welded CHS bridge joints, since chord members in these structures will, in most cases, have wall thicknesses greater than 16 or even

20 mm. The differences seen between the S1 & S2 and S3 results, as well as the discrepancy between measured and predicted fatigue, are important points in understanding and defining the fatigue strength of welded CHS joints and will be discussed in more detail in Chapter 5.

When the fatigue data for series S1 & S2 and S3 are plotted in terms of the hot-spot stress versus the number of cycles at crack detection, $S_{R,hs}$-N_2 (Figure 3.10) a similar trend is seen between the series: the smaller joints display a higher fatigue strength.

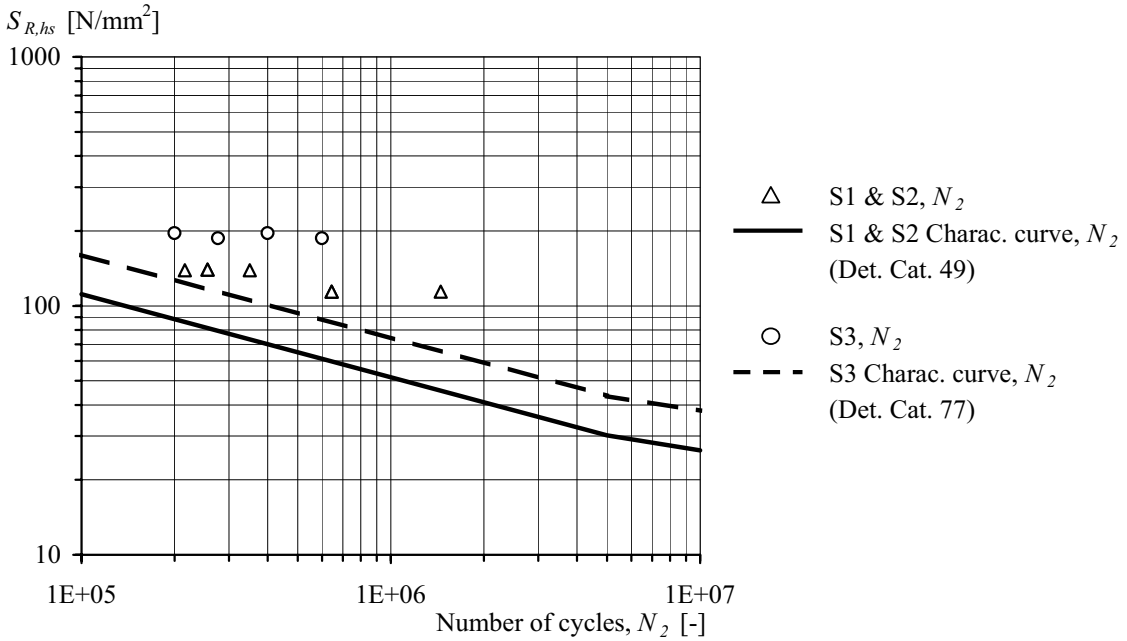

***Figure 3.10** - Fatigue test results (N_2) at crack detection for S1 & S2 and S3, effect of size*

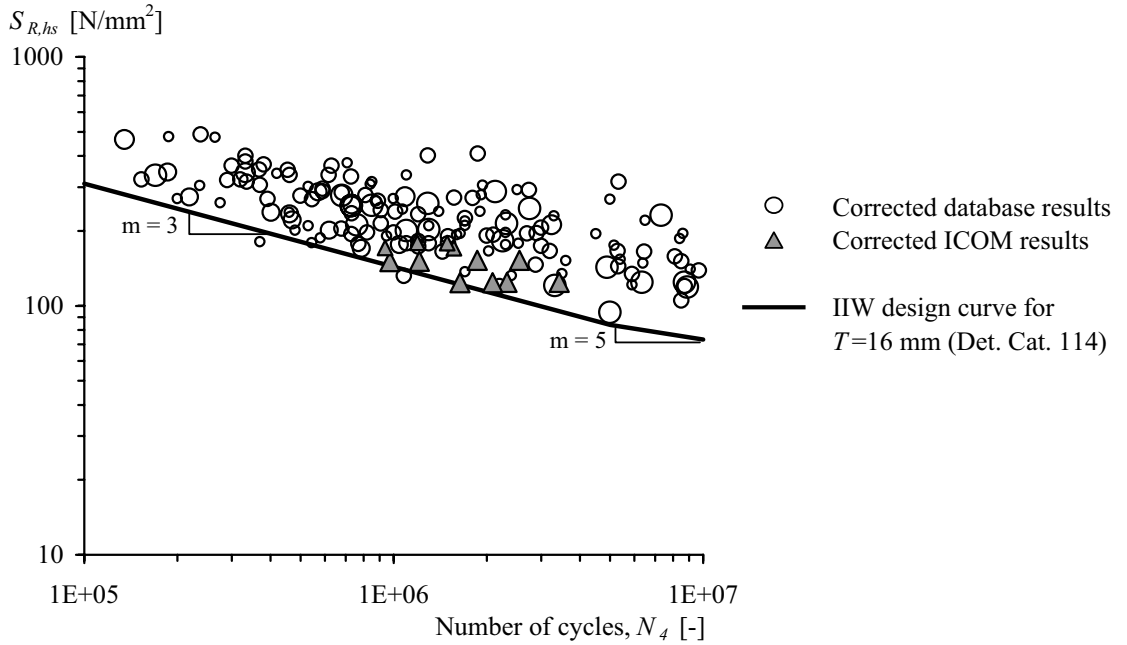

***Figure 3.11** - Comparison of test result to CHS joint database*

For reasons that will become clearer in Chapter 5, the fatigue test results for series S1, S2 and S3 are plotted in Figure 3.11 along with a large database of welded CHS joint fatigue data. As

explained above, the database was used by van Wingerde et al. [van Wingerde et al. 1997] in the derivation of the $S_{R,hs}$-N design curves in current design specifications. In the figure, the size of the data points is approximately representative of the thickness of the failed member, i.e. the larger the data point, the greater the thickness of the failed member. A visual inspection of the data seems to indicate a generally lower fatigue strength for joints with thicker members.

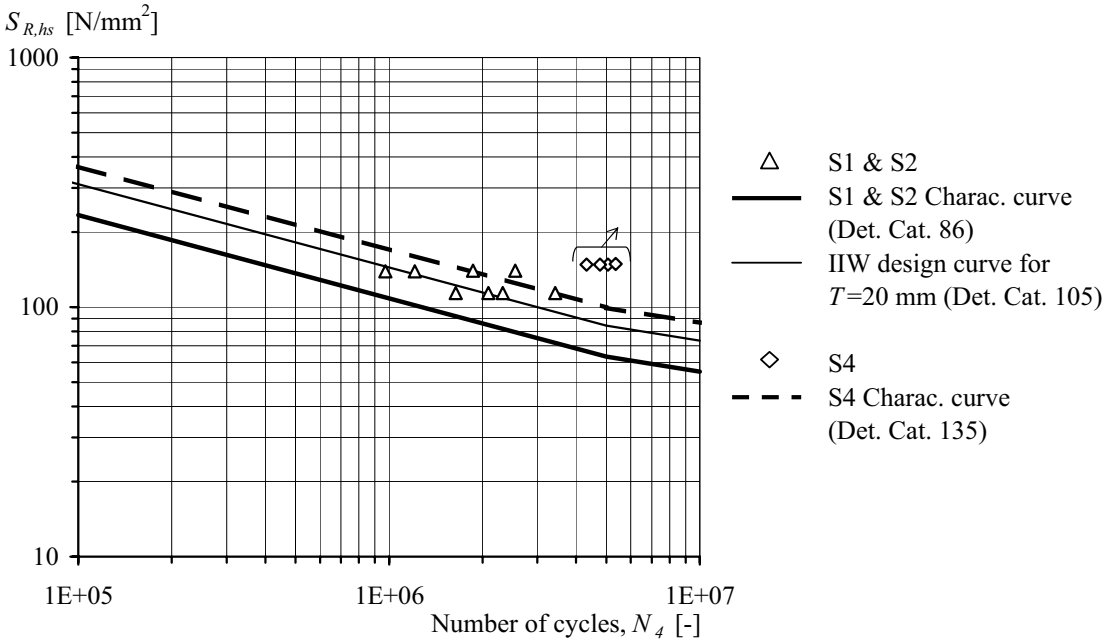

***Figure 3.12** - As-welded joints, S1 & S2 versus weld improved joints, S4*

C. Effect of weld improvement

Figure 3.12 shows the results for series S4 along with results from series S1 & S2. Testing of S4 the joints was stopped at approximately 3x10^6 cycles (Figure 3.12 shows the number of cycles multiplied by 1.49). At this point, none of the joints in the series had failed, however, small fatigue cracks had been detected at Location 1c (in the gap, adjacent to the compression brace weld toe).

Since the tests were stopped prior to failure, a standard deviation for the S4 data points cannot be determined, however, when the standard deviation found for the S1 & S2 data is applied to the S4 data, a comparison between the characteristic curves of the two data sets can be made. The increase in fatigue category from Cat. 86 to Cat. 135—a more than 50% increase in fatigue strength and a 3 fold increase in fatigue life—is a very positive result in terms of the potential of needle peening as a method for improving the fatigue behaviour of welded tubular joints. This result is in line with results of other studies where weld improvement techniques have been found to lengthen the fatigue life of welded steel and aluminium details [Haagensen and Maddox 2001, Dubois 1994, Bremen 1989].

3.4 CONCLUSIONS

This chapter presents the test program description and results from an experimental investigation on the fatigue behaviour of welded CHS bridge K-joints. Conclusions of this investigation are presented in two parts:

Conclusions from the static tests

- ε_{nom} / ε_{ax} ratios less than 1.0 were seen for some truss members. This means that the moment in the member adds compressive strain to the gap region of the joint. It is not possible to account for such a reduction in axial strain due to a compressive bending moment in the simplified modelling procedure described above, as the magnification factors given to account for bending moments are always greater than one.
- For some of the locations on the joint, a non-linear strain distribution was observed; the choice of a combined second-order polynomial / linear function for the extrapolation method is deemed appropriate, since it can accommodate both linear and polynomial distributions.

Conclusions from the fatigue tests

- Cracking in series S1, S2 and S3 all occurred at Location 1, at the location of highest measured strain.
- Comparison between results from the present study with results from similar tests carried out independently at the TU Delft, show comparable data that fall within the same order of magnitude in terms of fatigue life, over a range of stress, $S_{R,hs}$.
- The hot-spot stress ranges calculated for the test joints, based on current design specifications (using the nominal member stresses measured in the tests), is considerably higher than the measured hot-spot stress ranges. This confirms the postulation made in Chapter 2: that current design specifications result in conservative predictions for certain CHS K-joints. Considering that the non-dimensional parameter γ of the test joints falls outside of the validity range given in the specifications ($\gamma_{test} < 12.0$), it can thus be concluded that a simple extrapolation of the existing rules (as was done for the calculations) can give misleading results.
- Although backing rings may help ensure a more fully penetrated weld, failure of the joints is dictated by cracking at the surface (and not from the weld root) and thus the backing rings do not affect fatigue resistance. Therefore, the inclusion of the backing ring is a decision that should be left to the engineer, based on the engineer's confidence that a backing ring is or is not needed to ensure a successful, fully penetrated weld.
- $S_{R,hs}$-N results from a data set of eight joints, where failure occurred in the 20 mm thick chord member (the thickness of the chords in series S1 and S2) have indicated a characteristic curve that is lower than the corresponding $S_{R,hs}$-N design curve: Detail Category 86 versus Detail Category 105.
- Investigation of the size effect through comparison of fatigue $S_{R,hs}$-N results from smaller and larger welded CHS joints shows the same trend indicated in design specifications: a thicker failed member results in a lower fatigue strength. The characteristic curve for the smaller joints falls at the same level as the current design curve for T = 12.5 mm, while the characteristic curve for the larger joints falls below the current design curve for T = 20 mm (see previous conclusion). Based on these results, the correction for size inherent to the design curves appears unconservative for T > 16 mm (T = 16 mm being the reference thickness used in the design specifications). Furthermore, although the results for 12.5 mm chord joints seem to correspond with the design curve for this thickness, the number of data points used in the statistical analysis of these results (4) must be kept in perspective.

- The fatigue test results from series S4 demonstrate the beneficial influence of needle peening on the fatigue life of the joints. No cracks formed in Location 1 or at any other locations around the tension brace-chord intersection, even after three times the number of load cycles as compared with other similar test series. The shift of the critical location in the joint, both in space and time, is an outcome that will require further study in order to appropriately quantify the potential benefit of weld improvement as applied to welded CHS joints.

4 NUMERICAL STUDY

4.1 INTRODUCTION

The experimental investigation described in the previous chapter has resulted in the determination of strain and stress distributions in CHS truss members and welded CHS K-joints. It was seen that the point of highest strain in a joint corresponds to the location of fatigue cracking. The information obtained from the tests is, however, restricted to the dimensions and geometric parameters of the test specimens. Therefore, to broaden the range of study, a numerical model using finite elements was established based on previous finite element (FE) studies of similar joints and validated through comparison to the measured behaviour of the test joints. A well-functioning model will then be used to simulate the behaviour of a series of K-joints with varying dimensions and geometries within the context of a parametric study.

Chapter 4 includes the following sections:

- **Section 4.2** : *Modelling of complete tubular structure*, describes truss modelling using beam type finite elements in order to extract truss member forces and member nominal stresses;
- **Section 4.3** : *Modelling of isolated joint*, presents the important aspects in the finite element modelling of an isolated joint—weld size and shape, boundary conditions, loading—and a description of a standardised model used in the subsequent parametric study;
- **Section 4.4** : *Parametric study*, describes the goals and scope of a parametric study that uses a standardised finite element model;
- **Section 4.5** : *Presentation and discussion of results*, presents the results of this parametric study for a range of joints and load cases;
- **Section 4.6** : *SCFs for combined load condition*, proposes a method for combining results of the parametric study from individual load cases in order to obtain hot-spot stresses due to a combined load condition;
- **Section 4.7** : *Comparison of SCF results with existing work*, compares the results from the present parametric study with existing work (e.g. work described in Section 2.3);
- **Section 4.8** : *Conclusions*.

4.2 MODELLING OF TRUSS STRUCTURE [ZHAO ET AL. 2000, IIW 2000]

The following sections (Section 4.2.1 and Section 4.2.2) are taken from Zhao et al. 2000 and IIW 2000.

4.2.1 Member forces

For welded hollow section structures, member forces must be obtained by analysis of the complete structure, in which noding eccentricity of the member centre lines at the joint as well as local joint flexibility is taken into account [Romeijn 1997 and Herion and Puthli 1998]. This can be achieved by the following methods:

- *Sophisticated three dimensional finite element modelling* where plate, shell and solid elements are used at the joints (appropriate for experienced analysts), or

- *Simplified structural analysis* using frame analysis for triangulated trusses or lattice girders. Axial forces and bending moments in the members can be determined using a structural analysis assuming a continuous chord and pin-ended braces (refer to Figure 4.1). This produces axial forces in the braces, and both axial forces and bending moments in the chord. This modelling assumption is particularly appropriate for moving loads along the chord members in structures such as cranes and bridges.

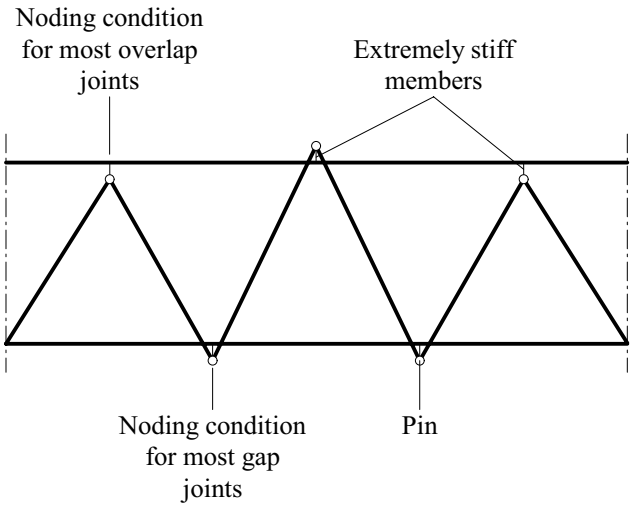

***Figure 4.1** - Plane frame joint modelling assumptions*

4.2.2 Nominal stress ranges

The determination of nominal stress ranges depends on the method used to determine member forces.

For analysis undertaken using the *sophisticated three dimensional finite element modelling*, the nominal stress range in any member can be determined by:

$$\Delta\sigma_{ax} = \frac{\Delta F_{ax}}{A} \qquad \Delta\sigma_{ipb} = \frac{\Delta M_{ipb}}{W_{ipb}} \qquad [4.1]$$

where,

$\Delta\sigma_{ax}$: stress range due to axial force
ΔF_{ax} : axial force range
A : cross-sectional area
$\Delta\sigma_{ipb}$: stress range due to in-plane bending moment
ΔM_{ipb} : in-plane bending moment range
W_{ipb} : elastic section modulus for in-plane bending

For analysis undertaken for *simplified structural analysis*, the nominal stress range in any member can be determined by:

$$\Delta\sigma_{ax} = MF \cdot \frac{\Delta F_{ax}}{A} \qquad \Delta\sigma_{ipb} = \frac{\Delta M_{ipb}}{W_{ipb}} \qquad [4.2]$$

where,

$\Delta\sigma_{ax}$: stress range due to axial force
MF : magnification factor (refer to Table 4.1)
ΔF_{ax} : axial force range
A : cross-sectional area
$\Delta\sigma_{ipb}$: stress range due to in-plane bending moment
ΔM_{ipb} : in-plane bending moment range
W_{ipb} : elastic section modulus for in-plane bending

***Table 4.1** - Magnification factors to account for secondary bending moments in CHS joints*

Type of joint		Chords	Braces (vertical members)	Braces (diagonal members)
Gap joints	K	1.5	-	1.3
	N		1.8	1.4
Overlap joints	K		-	1.2
	N		1.65	1.25

Once $\Delta\sigma_{ax}$ and $\Delta\sigma_{ipb}$ have been determined, fatigue design based on the hot-spot stress method (such as the method presented in Chapter 6) can be applied.

4.3 MODELLING OF ISOLATED K-JOINT

4.3.1 Description

Commercial finite element programs offer a broad range of element types and integration schemes. The choice of element is based on consideration for the type of structure or detail being modelled, the output and accuracy required and the computational capacity available. In order to model the complex stress distribution of welded CHS joints, three-dimensional, second-order shell or continuum (solid) elements are generally recognised as the most suitable. An appropriate integration scheme for the elements must also be selected and can also influence the computational efficiency and the accuracy of the results. For 20-node continuum elements, a 2x2x2 reduced integration scheme versus a 3x3x3 integration scheme will also translate to significant computational savings. When reduced integration schemes are used, however, an adequate number of element layers must be included through the wall thickness in order for the bending response to be modelled accurately.

The finite element model of the isolated K-joint was built in two phases. First, the chord was modelled and meshed in the commercial finite element program I-Deas [SDRC 1999]. In the second phase of model building, the elements that form the brace and weld were built up from the brace-chord intersection (already defined in the chord mesh) using a Microsoft Excel spreadsheet [Microsoft 2000]. Finite element calculations were carried out using the commercial finite element code ABAQUS [Hibbitt et al. 2000].

The ABAQUS element C3D20R was used to model the chord, brace and bottom layer of the weld. C3D15 elements were used for the top layer of the weld model. Since the analysis carried out was elastic, only the modulus of elasticity and Poisson's ratio were required as input for the material model. These values were taken as: E = 210'000 MPa and ν = 0.3. Two layers of elements were used in both the brace and chord thickness directions.

An accurate weld model is important in simulating the real rigidity and stress distribution in a tubular joint. Modelling the weld at the intersection of two CHS members is complicated by the changing dihedral angle, ψ, that is the angle between the chord tangent perpendicular to the brace-chord intersection and the brace. The dihedral angle changes with changing position around the intersection and depends on the angle between the brace and chord and the brace-chord diameter ratio, β. With modern preparation techniques, the brace ends may also be bevelled, which will also effect the shape and size of the weld and thus further complicate FE modelling. A detailed description of the creation of the weld model for the isolated K-joint is given in Schumacher 2003. Figure 4.2 shows a meshed model of test joint S21 including the weld. It can be seen that elements were concentrated at the brace-chord intersection; farther out from the joint element sizes were increased.

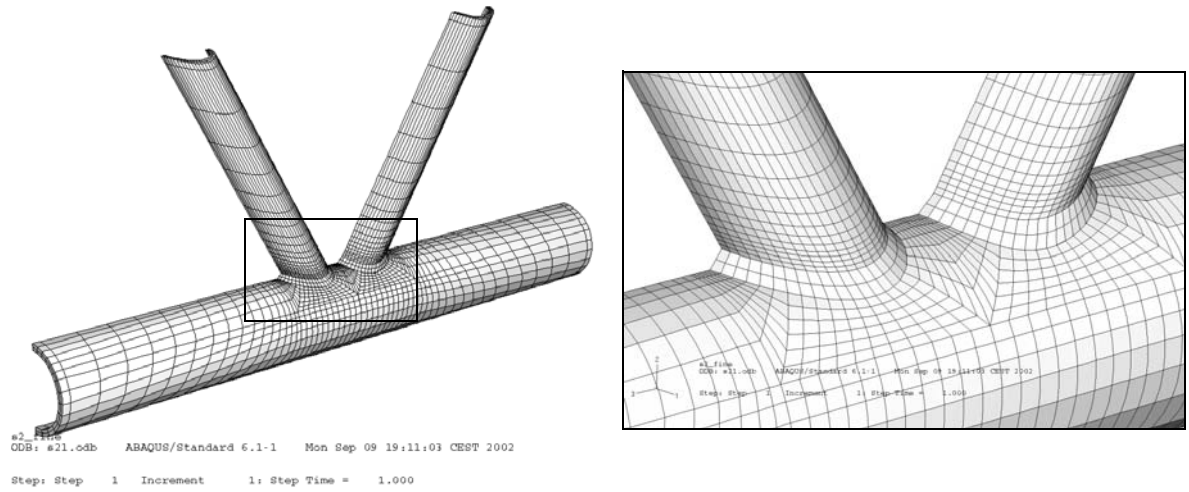

Figure 4.2 *- Joint model S21, weld at brace-chord intersection*

4.3.2 Boundary conditions and loading of isolated K-joint

An isolated FE K-joint model can be loaded as part of a larger truss model, which implies a real loading situation with combined axial and bending loads in the members. A principal goal of the parametric study in Section 4.4 and Section 4.5, however, is to analyse the effects of different, individual types of load cases on the behaviour of CHS welded K-joints, and to determine load case specific stress concentration factors. For this reason, a different loading approach will be used for the parametric study.

From a design point of view, the determination of hot-spot stress under combined loading, for a wide range of joints, is impossible. It is recalled, however, that stress concentration factors for *specific load cases* facilitate the determination of hot-spot stresses. That is, when the nominal stresses due to a certain load case are known, multiplication of these individual nominal stresses by the appropriate stress concentration factor will result in the hot-spot stress due to these nominal stresses. Subsequent superposition of the hot-spot stresses at a particular joint location, due to different load cases, results in the total hot-spot stress.

To separate the effect of different loads, the isolated FE joint model was subjected to individual load cases. The challenge posed by an isolated joint was the determination of boundary conditions that give the same or similar conditions as those present in a truss. Towards this end, an investigation was carried out wherein the isolated joint was subjected to various individual load cases and different boundary conditions. It was found that the joint supported as a

cantilever—the chord clamped on the compression brace side and free on the tension brace side (see Table 4.2 below)—gave stress distributions that were very similar to the stresses obtained from the truss model (i.e. a K-joint model loaded as part of a larger truss model).

Table 4.2 illustrates the different load cases and boundary conditions required to simulate loading in a truss. The following remarks are made concerning the selected method of load decomposition:

- Only a balanced axial brace load case is treated. It is obvious that other axial brace load combinations are possible, however, it has been shown that the difference in axial brace loads in K-joints of truss structures such as those common to bridge construction can be expected to be less than 10% [Romeijn et al. 1997]. Another study has shown that brace loads can be considered balanced if they differ by less than 15% [Efthymiou and Durkin 1985]. Stated otherwise, joint stresses remain fairly unaffected up to a 15% difference in the loads between the two braces of a K-joint.
- For the balanced axial brace load case, the cantilever boundary conditions generate additional axial and bending moment loads in the chord member between the clamped end and the joint. It has been observed, however, that the influence of additional axial and bending moment stresses (in that part of the chord) on the region around the tension brace-to-chord intersection is very small and can be neglected. Furthermore, only the tension brace-to-chord region of the joint will be considered in the parametric study.

***Table 4.2** - Isolated joint model, individual load cases and boundary conditions*

Load case		Schematic	Nominal stress
Balanced axial brace	F_{ax_br}	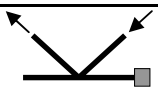	σ_{ax_br}
Un-balanced in-plane bending brace	M_{ipb1_br}	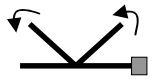	σ_{ipb1_br}
Balanced in-plane bending brace	M_{ipb2_br}	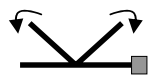	σ_{ipb2_br}
Axial chord	F_{ax_ch}		σ_{ax_ch}
In-plane bending chord	M_{ipb_ch}		σ_{ipb_ch}

- Two brace moment load cases are included that have different consequences on joint stresses. A third and a fourth case could also be introduced (the mirror case of both M_{ipb1_br} and M_{ipb2_br}) that result in stresses and stress concentration factors with the same magnitude as M_{ipb1_br} and M_{ipb2_br}, but opposite sign. To include the possible effects of the two mirror bending load cases, absolute stresses and stress concentration factors are taken from load cases M_{ipb1_br} and M_{ipb2_br}.
- For load cases M_{ipb1_br} (M_{ipb2_br}) and M_{ipb_ch} a constant moment is applied to the free brace and chord ends, respectively. These load cases have the effect of creating a constant bending moment stress along the length of the member. In a truss structure the bending moment stresses are provoked through a transverse (shear) load that creates a stress gradient. It is

possible to simulate the stress gradient using isolated joints by applying a shear load at the free end of a member, however, a new variable is introduced on which the moment stresses and the gradient are dependent: the member length. As done in similar studies [Romeijn 1994, Karamanos et al. 1997, Herion 1994, van Wingerde 1992] the inconsistency caused when applying a constant moment is recognised and accepted in the present study.

4.3.3 Standard model

It was seen briefly above and in more detail in Schumacher 2003 that even when specific dimensions of a joint are chosen, a certain number of choices must nevertheless be made, notably concerning the weld shape and gap size of the joint. For a parametric study, however, a standardised geometry is required, which implies that joints with different dimensions will respect the same basic geometric rules.

The consequences of the choices made for the isolated K-joint above and in Schumacher 2003 concerning weld shape, gap size and loading have been examined. This was done through comparisons between a so-called standard model and test joints models S21 and S31 (validated in Schumacher 2003). As seen in Table 4.3, the standard model, designated b5_76, is characterised by similar non-dimensional parameters as the test joints. It is recalled that ζ is the normalised gap parameter equal to the gap size divided by the chord diameter, g / D.

***Table 4.3** - Dimensions and non-dimensional parameters of standard model and test models*

Model	D	T	d	t	θ	β	γ	τ	ζ	e/D
	[mm]				[-]				[-]	[-]
b5_76	508	37	260	22.2	60°	0.51	6.9	0.60	0.18	0.16
S21	273	20	139.7	12.5	60°	0.51	6.8	0.63	0.22	0.20
S31	168.3	12.5	88.9	8	60°	0.53	6.7	0.64	0.21	0.21

The similar ζ parameter and e / D ratio for the models in Table 4.3 indicate that the gap size rules (refer to Schumacher 2003), in this case, resulted in realistic spacing and eccentricities between the two braces.

In theory, the stress response in the three parametrically “identical” models should be the same. Alone a comparison between the two test joint models, S21 and S31, shows small differences due to the non-proportional scaling of the welds. It therefore follows that the stresses in the standard model (with proportionally scaled welds), as compared with the S21 and S31 models, also differ slightly. For the standard model, it was generally found that the smaller weld angle on the chord side, due to the smaller chord weld leg length, causes the stresses to increase with respect to the S21 and S31 models. At the same time, this resulted in smaller (less abrupt) angles on the brace side and an accompanying decrease in stresses. It is interesting to note that these effects on the stresses, in particular the brace stresses, are contrary to the assumption often made for finite element models when the weld is ignored (e.g. Kuhlmann et al. 2002). For these models it is assumed that the omission of the weld will result in conservative predictions of stress, due to the sharper transition at the brace-chord intersection. Although this may be reasonable for the stresses in the chord, the opposite may be true for brace stresses: without a weld model the predicted brace stresses may *decrease*.

From the comparisons above, it is clear that any model will contain the effects of the chosen weld model. It is therefore all the more important that the weld chosen for the standard model,

to be used in the investigation of a wide range of joints, be, on the one hand, reproducible for all models and, on the other hand, based on widely recognised rules.

Lastly, the overall response of the standard model was compared with the response of the S21 and S31 models under combined loading. Figure 4.3 compares the stress distribution between model S31 and model b5_76 at Locations 1 and 11. The test joint model was loaded as part of a truss configuration [Schumacher 2003]. The b5_76 model results are taken from a superposition of stresses due to the effects of individual load cases on the isolated joint. A good correspondence of stresses at Locations 1 and 11 between the standard model and the test model, as well as similar results seen for other joint locations and comparisons with joint model S21, confirms the method of loading and corresponding boundary conditions. Thus, the isolated standard model is deemed acceptable for use in further numerical investigations.

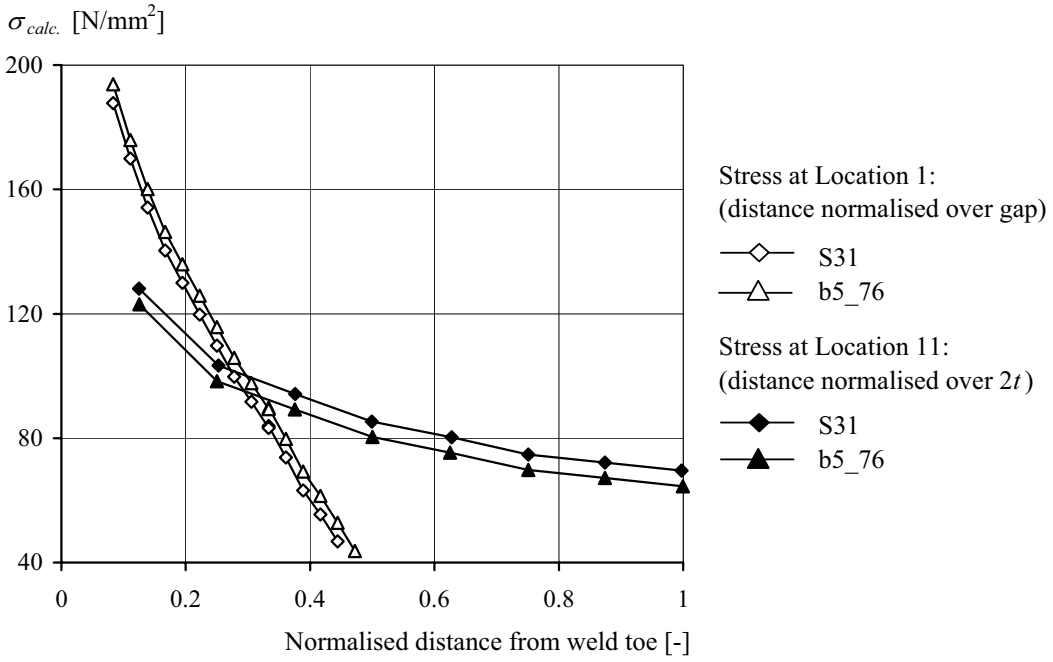

***Figure 4.3** - Comparison between standard model and joint model S31 under truss loading*

4.4 PARAMETRIC STUDY

4.4.1 Introduction

The validated and standardised finite element model is used to study the stress response in a range of welded CHS K-joints, specifically, a set of joint models including a range of smaller chord slenderness values, γ. Through comparisons between the joint models, the influences of different parameters, geometries and load cases on the behaviour of the joints can be examined. In addition, comparisons between the results of this parametric study and other similar studies—notably, those on which the current design specifications are based—will allow the present work to be situated and judged with respect to the body of existing work concerning fatigue in welded CHS K-joints.

The work in the remainder of this chapter will deal mainly with stresses on the joint surface as well as **stress concentration factors** (SCF). The general definition for a stress concentration factor is recalled from Chapter 2 as:

$$\text{SCF} = \frac{\text{(part of total) hot-spot stress}}{\text{member stress(es) away from joint that causes this hot-spot stress}}$$

For the most part, the stress concentration factors will be examined for a particular location on the joint and on a per load case basis.

4.4.2 Scope of study

Geometry and parameters

The parametric study covers a range of K-joint geometries common to bridge applications. The main geometric parameters that were varied are: θ, β, γ and τ. These parameters were defined in Section 2.2. Their definitions are repeated here for practical purposes along with the definitions for two other joint parameters, α and ζ:

$$\beta = \frac{d}{D} \qquad \gamma = \frac{D}{2T} \qquad \tau = \frac{t}{T} \qquad \alpha = \frac{2L_{ch}}{D} \qquad \zeta = \frac{g}{D} \qquad [4.3]$$

where,

d : outside diameter of brace
D : outside diameter of chord
t : brace wall thickness
T : chord wall thickness
L_{ch} : chord length between two nodes
g : gap size (between outer walls of two braces)

Table 4.4 lists the 36 FE models created for the parametric study. The joint models are based on the *standard model* developed in Section 4.3 and therefore all use weld profiles defined in the AWS guidelines [AWS 2000]. The parametric study only covers K-joints with dimensionally identical tension and compression braces. The designations given to the joint models in Table 4.4 are based on the following: the letter refers to the brace angle (a=45° and b=60°), the first, second and third numbers refer to the β, γ and τ values, respectively. For example, b5_75 designates a joint with θ = 60°, β = 0.51, γ = 6.9 and τ = 0.50. The models closest in geometry to the CHS K-joint tested in the laboratory are models b5_75 and b5_77, shown in grey in Table 4.4.

***Table 4.4** - Dimensions and parameters of joint model database*

Model	D	T	d	t	θ	β	γ	τ	α	ζ	g	e/D
	[mm]				[-]						[mm]	[-]
a5_43	508	60	260	18	45°	0.51	4.2	0.30	15.4	0.21	106	-0.03
a5_45	508	60	260	30	45°	0.51	4.2	0.50	15.4	0.24	120	-0.02
a5_47	508	60	260	42	45°	0.51	4.2	0.70	15.4	0.33	168	0.03
a5_73	508	37	260	11	45°	0.51	6.9	0.30	15.4	0.13	65	-0.07
a5_75	508	37	260	18.5	45°	0.51	6.9	0.50	15.4	0.15	74	-0.07
a5_77	508	37	260	26	45°	0.51	6.9	0.70	15.4	0.20	104	-0.04
a5_123	508	20	260	6	45°	0.51	12.7	0.30	15.4	0.07	35	-0.10
a5_125	508	20	260	10	45°	0.51	12.7	0.50	15.4	0.08	40	-0.10
a5_127	508	20	260	14	45°	0.51	12.7	0.70	15.4	0.11	56	-0.08
a6_43	508	60	325	18	45°	0.64	4.2	0.30	15.4	0.21	106	0.06
a6_45	508	60	325	30	45°	0.64	4.2	0.50	15.4	0.24	120	0.07
a6_47	508	60	325	42	45°	0.64	4.2	0.70	15.4	0.33	168	0.12
a6_73	508	37	325	11	45°	0.64	6.9	0.30	15.4	0.13	65	0.02
a6_75	508	37	325	18.5	45°	0.64	6.9	0.50	15.4	0.15	74	0.03
a6_77	508	37	325	26	45°	0.64	6.9	0.70	15.4	0.20	104	0.05
a6_123	508	20	325	6	45°	0.64	12.7	0.30	15.4	0.07	35	-0.01
a6_125	508	20	325	10	45°	0.64	12.7	0.50	15.4	0.08	40	-0.01
a6_127	508	20	325	14	45°	0.64	12.7	0.70	15.4	0.11	56	0.01
b5_43	508	60	260	18	60°	0.51	4.2	0.30	15.4	0.21	109	0.20
b5_45	508	60	260	30	60°	0.51	4.2	0.50	15.4	0.24	120	0.22
b5_47	508	60	260	42	60°	0.51	4.2	0.70	15.4	0.33	168	0.30
b5_73	508	37	260	11	60°	0.51	6.9	0.30	15.4	0.13	67	0.13
b5_75	508	37	260	18.5	60°	0.51	6.9	0.50	15.4	0.15	74	0.14
b5_77	508	37	260	26	60°	0.51	6.9	0.70	15.4	0.20	104	0.19
b5_123	508	20	260	6	60°	0.51	12.7	0.30	15.4	0.07	36	0.07
b5_125	508	20	260	10	60°	0.51	12.7	0.50	15.4	0.08	40	0.08
b5_127	508	20	260	14	60°	0.51	12.7	0.70	15.4	0.11	56	0.11
b6_43	508	60	325	18	60°	0.64	4.2	0.30	15.4	0.21	109	0.33
b6_45	508	60	325	30	60°	0.64	4.2	0.50	15.4	0.24	120	0.34
b6_47	508	60	325	42	60°	0.64	4.2	0.70	15.4	0.33	168	0.43
b6_73	508	37	325	11	60°	0.64	6.9	0.30	15.4	0.13	67	0.25
b6_75	508	37	325	18.5	60°	0.64	6.9	0.50	15.4	0.15	74	0.27
b6_77	508	37	325	26	60°	0.64	6.9	0.70	15.4	0.20	104	0.32
b6_123	508	20	325	6	60°	0.64	12.7	0.30	15.4	0.07	36	0.20
b6_125	508	20	325	10	60°	0.64	12.7	0.50	15.4	0.08	40	0.21
b6_127	508	20	325	14	60°	0.64	12.7	0.70	15.4	0.11	56	0.24

Load cases

Five load cases are considered in the parametric study. Each load case relates to a particular nominal stress and stress concentration factor at Location *i* on the joint (refer to Table 4.5). The brace loaded in tension in the F_{ax_br} load case (the left-hand brace in Table 4.5) is referred to as the reference brace, while the compression brace is referred to as the carry-over brace.

For joint models with 45° braces subjected to balanced axial loading, the stresses in the gap region indicated an additional, undesirable influence from the horizontal tensile force resultant in the chord member (between the joint and the fixed end). For all joints with $\theta = 45°$, a

compensating horizontal compressive force was therefore applied to the free end of the chord in order to counteract this effect (as seen in Table 4.5). As explained in Section 4.5.6 this effect was not present in joint models with braces inclined at 60° and therefore no compensating force was required.

***Table 4.5** - Load cases and corresponding nominal stresses and SCFs*

Load case		Schematic	Nominal stress	*SCF* at Location *i* of joint
Balanced axial brace	F_{ax_br}	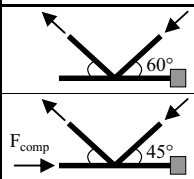	σ_{ax_br}	SCF_{i,ax_br}
Un-balanced in-plane bending brace	M_{ipb1_br}	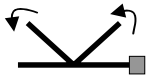	σ_{ipb1_br}	$SCF_{i,ipb1\_br}$
Balanced in-plane bending brace	M_{ipb2_br}	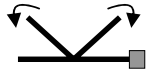	σ_{ipb2_br}	$SCF_{i,ipb2\_br}$
Axial chord	F_{ax_ch}		σ_{ax_ch}	SCF_{i,ax_ch}
In-plane bending chord	M_{ipb_ch}		σ_{ipb_ch}	SCF_{i,ipb_ch}

4.4.3 Procedure

The K-joint finite element models for the parametric study were created using the two phase procedure described in Section 4.3.1: the chord was modelled and meshed using the commercial finite element program and preprocessor I-Deas [SDRC 1999], while elements that formed the brace and weld were built up from the brace-chord intersection already defined in the chord mesh using a Microsoft Excel spreadsheet. Finite element calculations were carried out using the commercial finite element code ABAQUS [Hibbitt et al. 2000].

Each model was subjected to five different load cases. The load applied for each case was equal to the load required to provoke a nominal stress of 1 N/mm^2 in the member (in the extreme fibre for bending load cases). Stress concentration factors were determined at six locations around the reference brace of the joint models: Locations 1, 11, 2, 3, 31 and 4 (refer to Figure 4.4). SCFs were determined through the extrapolation of primary stresses (in the determination of the hot-spot stress) in the vicinity of the weld using the extrapolation procedure described in Chapter 3 (refer to Figure 3.4). High stress concentrations can also occur at so-called in-between locations, that is, at locations in-between the six locations defined above. For the present study it was found, however, that the in-between locations were only more critical in models with high γvalues, γ= 12.7, and restricted to a region in-between Locations 2 and 31 on the chord. For these models, the stress concentration factor was determined at the peak stress location in-between the two standard locations and then designated as the SCF at either Location 2 or Location 31 (the closer of the two).

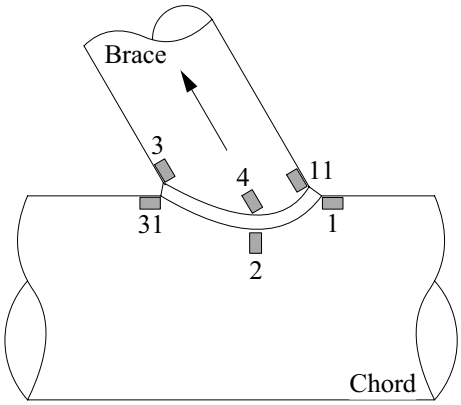

Figure 4.4 - *Locations on joint for determination of SCF*

4.5 PRESENTATION AND DISCUSSION OF RESULTS

A comparison of the maximum principal stress distribution around the brace-chord intersection is carried out to study the relative effect of individual parameters and to obtain a more general, qualitative impression of the joint behaviour. To do this, a base model is chosen to which four models are compared: for each of the four models one parameter is changed with respect to the base model.

The principal stress is taken at 24 points around the half-joint intersection (between the crown toe, 0°, and the crown heel, 180°, with the saddle at 90°), on both the chord and the tension brace at a distance of approximately $0.12T$ from the chord weld toe and $0.5t$ from the brace weld toe. Clearly, a change in parameters between joints will also cause the direction of the principal stresses to change. Nevertheless, a comparison between principal stress magnitudes can give indications about the relative effect on the joint behaviour of changing one parameter over another. It is important to note that the parameters were changed as much as possible, but within the limits of the parameter range being studied. For this reason, it is more the trend caused by the change in parameter (do the stresses increase, decrease, stay more or less the same?...) rather than the actual magnitude of increase or decrease that is the focus of the comparisons.

The maximum principal stresses are not to be compared directly with the SCF values, as the latter are based on primary stress.

4.5.1 Joint behaviour under balanced axial brace loading

Distribution of stresses around brace-chord intersection

The following major observations on the maximum principal stress distribution in the chord (Figure 4.5) and brace (Figure 4.6) due to a balanced axial brace load, F_{ax_br}, can be made:

- In the chord, increases in γ or τ have the effect of increasing the stresses in the chord. An increase in β or a decrease in θ seem to have only a minor effect on the chord stresses and their distribution, although at the chord saddle, a higher β decreases the stresses at that location with respect to the base model.

- In the brace, an increase in γ also increases the stresses in the brace and causes a less uniform distribution around the intersection. The chord can be compared to a support for the braces. By increasing γ the support becomes more flexible thus causing more secondary bending in the brace and a less uniform stress distribution around the intersection. The effect

of changing the β, γ, τ and θ seems to have only a minor effect on the stresses and their distribution.

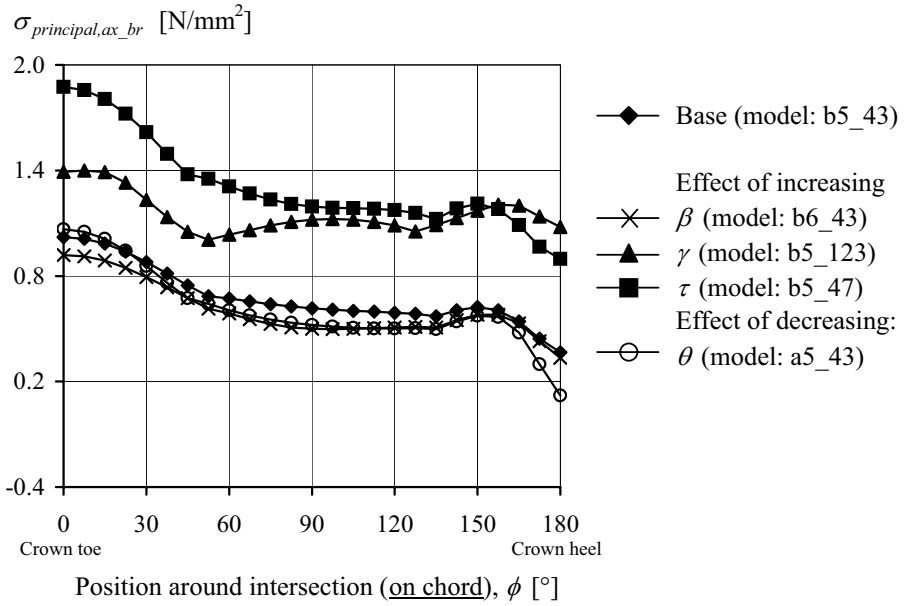

***Figure 4.5** - Principal stresses in the chord due to balanced axial brace load*

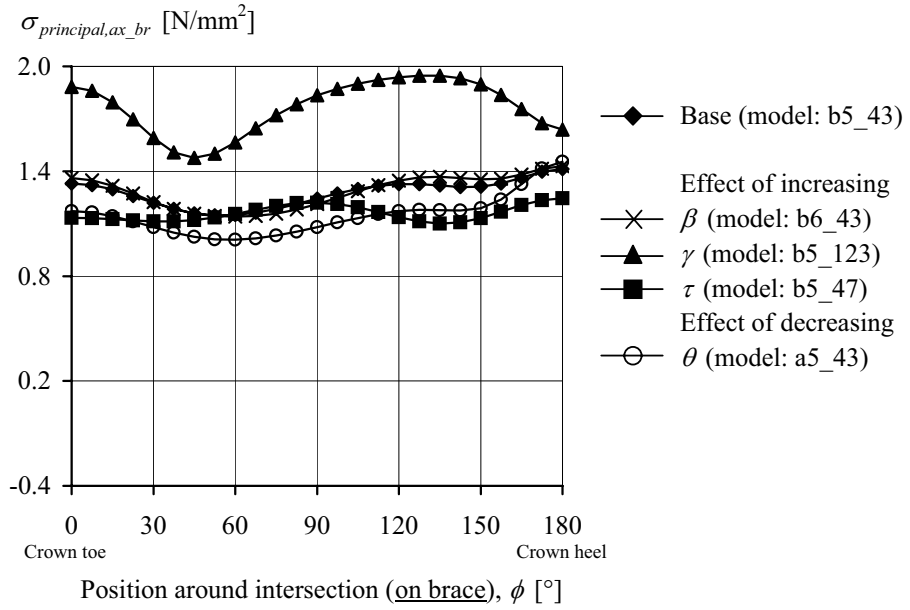

***Figure 4.6** - Principal stresses in the brace due to balanced axial brace load*

SCF results and trends

The general SCF trends due to variations in each of the studied joint parameters are summarised in Table 4.6, while Table 4.7 presents SCF results at six different joint locations for each joint model. In Table 4.7 the maximum SCF per joint, for the load case under examination, is highlighted in grey. Again, it is recalled that *primary* stresses have been used to calculate SCFs. Regarding SCF trends and values, the following comments can be made:

- The highest SCF value is **3.52** at Location 1 of model b5_127.

- Maximum SCF values occur predominantly at Locations 1, 11 and 3, with two maximum SCFs seen at Location 2 for joints with high γ values.
- An increase in τ generally shifts the location of highest SCF from the brace (Location 11 or 3) to the chord (Location 1).
- An increase in θ results in higher SCF values at all locations. In general, a larger brace angle translates into a smaller area in the vicinity of the brace-chord intersection in which the load transfer occurs, thus resulting in higher stresses.
- An increase in β results mainly in lower SCFs at Location 2.
- Increases in γ or τ results in higher SCF values at all locations with the exception of Location 3, where an increase in τ decreases the SCF.

***Table 4.6** - SCF trends due to balanced axial brace load*

Change in parameter	Corresponding change in SCF_{i,ax_br} at Locations:					
	1	11	2	3	31	4
$\theta \Uparrow$	⇑	⇑	⇑	↑	⇑	⇑
$\beta \Uparrow$	↓	↓	⇓	↓	↑	↓
$\gamma \Uparrow$	⇑	⇑	⇑	↑	⇑	⇑
$\tau \Uparrow$	⇑	↑	⇑	⇓	⇑	⇑

⇑,⇓ : Solid trend (increasing or decreasing)

↑,↓ : Weak trend or small differences

***Table 4.7** - SCF values due to balanced axial brace load*

Model	θ	β	γ	τ	SCF_{i,ax_br} at Locations: 1	11	2	3	31	4
a5_43				0.30	0.79	1.31	0.39	1.61	0.13	1.08
a5_45	45°	0.51	4.2	0.50	1.20	1.28	0.61	1.53	-	1.22
a5_47				0.70	1.65	1.27	0.86	1.45	-	1.29
a5_73				0.30	0.92	1.51	0.75	1.61	0.17	1.10
a5_75	45°	0.51	6.9	0.50	1.48	1.54	1.27	1.56	0.40	1.39
a5_77				0.70	2.21	1.56	1.72	1.48	0.67	1.57
a5_123				0.30	1.08	1.79	1.08	1.69	0.67	1.25
a5_125	45°	0.51	12.7	0.50	1.83	1.98	1.88	1.60	1.15	1.66
a5_127				0.70	2.88	2.11	2.73	1.43	1.54	1.97
a6_43				0.30	0.81	1.35	0.34	1.59	0.11	0.95
a6_45	45°	0.64	4.2	0.50	1.23	1.30	0.54	1.58	-	1.15
a6_47				0.70	1.72	1.29	0.73	1.50	-	1.31
a6_73				0.30	0.91	1.50	0.70	1.59	0.21	0.97
a6_75	45°	0.64	6.9	0.50	1.44	1.59	1.16	1.53	0.43	1.29
a6_77				0.70	2.15	1.50	1.54	1.50	0.69	1.50
a6_123				0.30	1.03	1.63	1.04	1.65	0.71	1.11
a6_125	45°	0.64	12.7	0.50	1.74	1.84	1.83	1.51	0.56	1.57
a6_127				0.70	2.75	1.96	2.67	1.34	1.60	1.94
b5_43				0.30	0.89	1.57	0.61	1.63	0.19	1.36
b5_45	60°	0.51	4.2	0.50	1.37	1.44	0.94	1.54	0.38	1.37
b5_47				0.70	1.82	1.40	1.25	1.46	0.53	1.42
b5_73				0.30	1.07	1.78	1.14	1.73	0.55	1.54
b5_75	60°	0.51	6.9	0.50	1.75	1.82	1.81	1.64	0.95	1.75
b5_77				0.70	2.58	1.84	2.07	1.51	1.34	1.94
b5_123				0.30	1.25	2.13	1.61	1.94	1.03	2.00
b5_125	60°	0.51	12.7	0.50	2.21	2.54	2.78	1.81	1.75	2.46
b5_127				0.70	3.52	2.66	2.86	1.60	2.41	2.74
b6_43				0.30	0.81	1.51	0.51	1.63	0.21	1.24
b6_45	60°	0.64	4.2	0.50	1.20	1.48	0.78	1.59	0.38	1.40
b6_47				0.70	1.65	1.47	1.00	1.52	0.56	1.54
b6_73				0.30	0.99	1.73	1.02	1.69	0.58	1.43
b6_75	60°	0.64	6.9	0.50	1.59	1.86	1.69	1.61	0.96	1.74
b6_77				0.70	2.35	1.90	2.03	1.51	1.33	2.02
b6_123				0.30	1.22	1.92	1.53	1.85	1.07	1.77
b6_125	60°	0.64	12.7	0.50	2.01	2.23	2.66	1.67	1.66	2.35
b6_127				0.70	3.22	2.49	2.80	1.49	2.26	2.83

: Maximum SCF for model

- : SCF less than 0.10

Shaded (grey) : SCF less than 1.00

4.5.2 Joint behaviour under in-plane brace bending

Two types of in-plane bending were applied to the joint models: un-balanced in-plane bending, M_{ipb1_br}, and balanced in-plane bending, M_{ipb2_br}. Two more in-plane load cases with bending in both braces are possible; they are the mirror cases of the two load cases examined here and produce the same SCFs, however, with the opposite sign. To account for the possibility of these load cases the absolute SCF values around the reference brace-chord intersection are reported below.

Distribution of stresses around brace-chord intersection

The following major observations on the maximum principal stress distribution in the chord (Figure 4.7) and brace (Figure 4.8) due to a un-balanced in-plane bending, M_{ipb1_br}, can be made:

- The maximum principal stress in both the chord and the brace goes from a maximum value at the crown toe to a minimum value at the crown heel, indicating a concentration of the load transfer in the gap region of the joint. Due to the direction of bending, compressive stresses are present at the crown heel.
- As expected, the stress at the saddle on both the brace and chord is nearly or equal to zero.
- In some of the models the peak principal stress is less than 1 N/mm^2 (the magnitude of the nominal stress) at the crown toe in both the chord and brace. This is due to the in-plane bending effect from the carry-over brace, which causes negative stresses in the gap region and thus has the effect of reducing the tension stresses in the reference brace area.
- In the chord, an increase in θ, β, γ and τ will increase the stresses between the crown toe and saddle. In particular, an increase in γ implies a less rigid and more deformable chord member that will result in higher stresses.

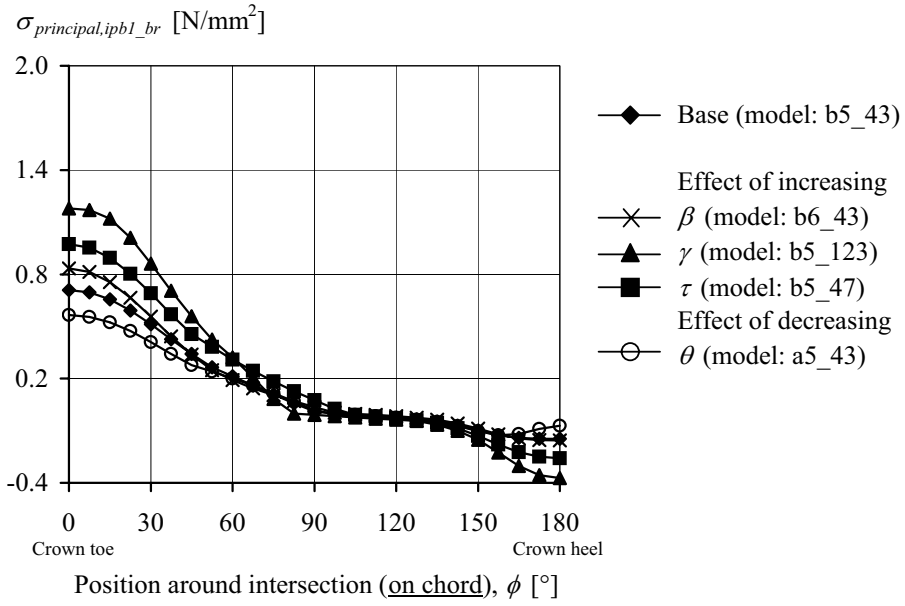

***Figure 4.7** - Principal stresses in the chord due to balanced in-plane brace bending*

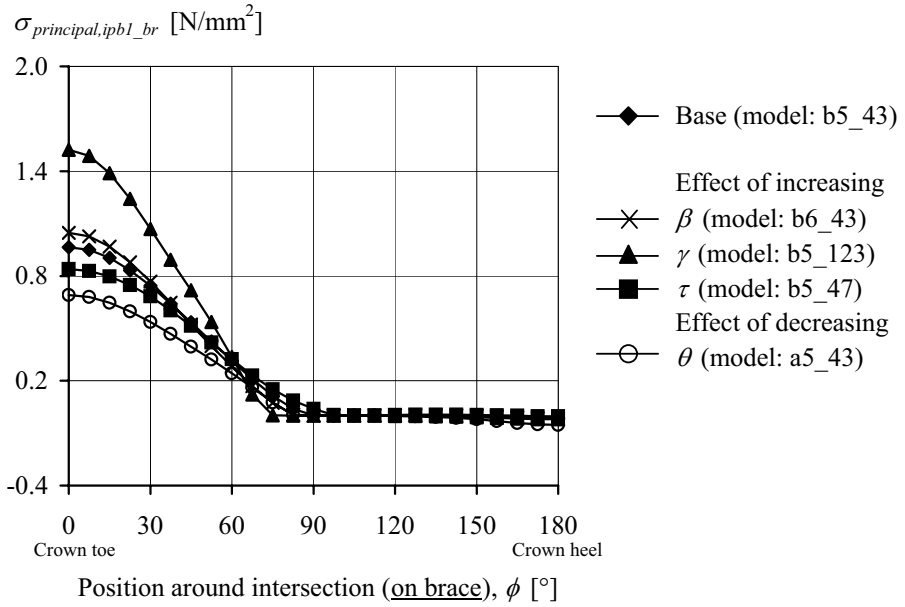

***Figure 4.8** - Principal stresses in the brace due to balanced in-plane brace bending*

SCF results and trends

The general SCF trends due to variations in each of the studied joint parameters are summarised in Table 4.8. Table 4.9 and Table 4.10 present SCF results for load cases M_{ipb1_br} and M_{ipb2_br}, respectively. Regarding SCF trends and values for both load cases, the following comments can be made:

- The highest absolute SCF value at Location 1 (due to balanced in-plane bending) is **3.09** in model b6_127.
- Maximum SCF values occur either at Location 1 or Location 3.
- At Locations 1 and 3 the SCFs due to load case M_{ipb2_br} are greater than the SCFs due to M_{ipb1_br}.
- At higher values of γ, an increase in τ generally shifts the location of highest SCF from the brace (Location 3) to the chord (Location 1).
- An increase in γ increases SCF values at Locations 1, 11, 3 and 31, with the largest influence seen at Location 1.
- All SCFs at Location 2 and most SCFs at Location 4 are less than 1.00.

***Table 4.8** - SCF trends due to in-plane bending moment brace load*

Change in parameter	Corresponding change in SCF_{i,ipb_br} at Locations:					
	1	11	2	3	31	4
$\theta \Uparrow$	$\Uparrow$	$\Uparrow$	–	$\downarrow$	$\Uparrow$	–
$\beta \Uparrow$	$\Uparrow$	$\Uparrow$	–	$\downarrow$	$\uparrow$	–
$\gamma \Uparrow$	$\Uparrow$	$\Uparrow$	–	$\Uparrow$	$\Uparrow$	–
$\tau \Uparrow$	$\Uparrow$	$\Downarrow$	–	$\Downarrow$	$\Uparrow$	–

– : Majority of SCF values below 1.00
$\Uparrow$,$\Downarrow$: Solid trend (increasing or decreasing)
$\uparrow$,$\downarrow$: Weak trend (exceptions possible) or small differences

***Table 4.9** - SCF values due to un-balanced in-plane bending moment brace load*

Model	θ	β	γ	τ	$SCF_{i,ipb1\_br}$ at Locations: 1	11	2	3	31	4
a5_43				0.30	0.50	0.72	-	2.19	-	0.19
a5_45	45°	0.51	4.2	0.50	0.63	0.62	-	1.87	0.25	0.19
a5_47				0.70	0.71	0.59	-	1.62	0.40	0.18
a5_73				0.30	0.66	0.90	-	2.28	0.27	0.29
a5_75	45°	0.51	6.9	0.50	0.93	0.82	-	2.03	0.62	0.37
a5_77				0.70	1.17	0.74	-	1.80	0.96	0.40
a5_123				0.30	0.86	1.19	0.12	2.29	0.71	0.50
a5_125	45°	0.51	12.7	0.50	1.37	1.18	0.31	2.10	1.25	0.70
a5_127				0.70	1.95	1.13	0.49	1.82	1.64	0.81
a6_43				0.30	0.62	0.81	-	2.24	-	0.21
a6_45	45°	0.64	4.2	0.50	0.83	0.69	-	2.00	0.25	0.25
a6_47				0.70	0.97	0.65	-	1.75	0.44	0.27
a6_73				0.30	0.75	0.97	-	2.27	0.28	0.32
a6_75	45°	0.64	6.9	0.50	1.13	0.91	-	2.12	0.65	0.45
a6_77				0.70	1.41	0.77	-	1.87	0.97	0.47
a6_123				0.30	0.90	1.16	0.12	2.26	0.73	0.50
a6_125	45°	0.64	12.7	0.50	1.48	1.19	0.36	2.05	0.43	0.76
a6_127				0.70	2.13	1.15	0.61	1.77	1.72	0.93
b5_43				0.30	0.61	1.06	-	2.05	0.24	0.25
b5_45	60°	0.51	4.2	0.50	0.80	0.92	-	1.82	0.45	0.13
b5_47				0.70	0.91	0.75	0.12	1.73	0.62	0.11
b5_73				0.30	0.82	1.28	-	2.09	0.53	0.38
b5_75	60°	0.51	6.9	0.50	1.21	1.21	0.15	1.92	0.89	0.47
b5_77				0.70	1.55	1.14	0.19	1.78	1.21	0.50
b5_123				0.30	1.10	1.70	0.24	2.26	0.96	0.64
b5_125	60°	0.51	12.7	0.50	1.85	1.92	0.39	2.01	1.49	0.98
b5_127				0.70	2.67	1.87	0.78	1.83	2.06	1.10
b6_43				0.30	0.73	1.12	-	2.07	0.25	0.27
b6_45	60°	0.64	4.2	0.50	1.01	1.02	-	1.90	0.47	0.33
b6_47				0.70	1.21	0.97	-	1.77	0.66	0.33
b6_73				0.30	0.91	1.34	-	2.08	0.55	0.40
b6_75	60°	0.64	6.9	0.50	1.39	1.31	0.17	1.93	0.92	0.54
b6_77				0.70	1.84	1.24	0.19	1.80	1.24	0.61
b6_123				0.30	1.15	1.61	0.24	2.20	0.96	0.64
b6_125	60°	0.64	12.7	0.50	1.89	1.85	0.57	1.97	1.46	0.94
b6_127				0.70	2.87	1.93	0.89	1.77	1.97	1.16

: Maximum SCF for model

- : SCF less than 0.10

Shaded (grey) : SCF less than 1.00

***Table 4.10** - SCF values due to balanced in-plane bending moment in brace load*

Model	θ	β	γ	τ	$SCF_{i,ipb2\_br}$ at Locations: 1	11	2	3	31	4
a5_43				0.30	0.61	0.66	-	2.24	-	0.13
a5_45	45°	0.51	4.2	0.50	0.72	0.52	0.11	1.90	0.25	0.12
a5_47				0.70	0.74	0.51	0.15	1.64	0.42	0.12
a5_73				0.30	0.95	0.88	-	2.35	0.22	0.18
a5_75	45°	0.51	6.9	0.50	1.24	0.68	0.15	2.13	0.57	0.19
a5_77				0.70	1.37	0.56	0.24	1.89	0.93	0.21
a5_123				0.30	1.49	1.38	-	2.34	0.61	0.29
a5_125	45°	0.51	12.7	0.50	2.16	1.09	-	2.27	1.10	0.34
a5_127				0.70	2.48	0.85	0.11	2.04	1.51	0.36
a6_43				0.30	0.74	0.76	-	2.29	-	0.16
a6_45	45°	0.64	4.2	0.50	0.93	0.58	0.11	2.05	0.27	0.17
a6_47				0.70	1.01	0.54	0.14	1.78	0.48	0.19
a6_73				0.30	1.08	0.98	-	2.32	0.24	0.23
a6_75	45°	0.64	6.9	0.50	1.55	0.82	0.10	2.28	0.62	0.26
a6_77				0.70	1.65	0.58	0.17	1.99	0.96	0.26
a6_123				0.30	1.59	1.39	-	2.27	0.64	0.34
a6_125	45°	0.64	12.7	0.50	2.34	1.19	-	2.19	0.39	0.43
a6_127				0.70	2.74	0.98	-	1.98	1.61	0.47
b5_43				0.30	0.70	0.95	-	2.12	0.23	0.16
b5_45	60°	0.51	4.2	0.50	0.88	0.75	-	1.90	0.46	0.13
b5_47				0.70	0.91	0.75	0.12	1.73	0.62	0.11
b5_73				0.30	1.08	1.14	-	2.19	0.48	0.21
b5_75	60°	0.51	6.9	0.50	1.49	0.88	0.13	2.09	0.85	0.21
b5_77				0.70	1.64	0.79	0.23	1.96	1.20	0.22
b5_123				0.30	1.63	1.68	-	2.33	0.90	0.32
b5_125	60°	0.51	12.7	0.50	2.46	1.48	0.13	2.26	1.49	0.37
b5_127				0.70	2.88	1.13	0.16	2.12	2.06	0.38
b6_43				0.30	0.83	0.99	-	2.14	0.25	0.19
b6_45	60°	0.64	4.2	0.50	1.09	0.81	-	2.00	0.49	0.20
b6_47				0.70	1.20	0.78	0.11	1.85	0.71	0.20
b6_73				0.30	1.18	1.22	-	2.14	0.51	0.24
b6_75	60°	0.64	6.9	0.50	1.69	0.98	-	2.09	0.89	0.26
b6_77				0.70	1.93	0.85	0.16	1.98	1.26	0.27
b6_123				0.30	1.70	1.64	-	2.22	0.92	0.36
b6_125	60°	0.64	12.7	0.50	2.57	1.47	-	2.12	1.45	0.45
b6_127				0.70	3.09	1.27	-	2.00	1.99	0.49

: Maximum SCF for model

- : SCF less than 0.10

Shaded (grey) : SCF less than 1.00

4.5.3 Joint behaviour under axial chord loading

Distribution of stresses around brace-chord intersection

The following major observations on the maximum principal stress distribution in the chord (Figure 4.9) due to an axial chord load, F_{ax_ch}, can be made. The stresses in the brace due to this load case are, in most cases, very small, and can therefore be neglected:

- In all models the principal stress goes from a peak at the crown toe to a minimum at the saddle and peaks again at the crown heel.
- At the saddle location, the *primary* stresses due to an axial chord load are assumed to be zero. It is seen that even the maximum principal stress at this location due to the same load case results in a principal stress equal to or less than 1.0 N/mm^2.

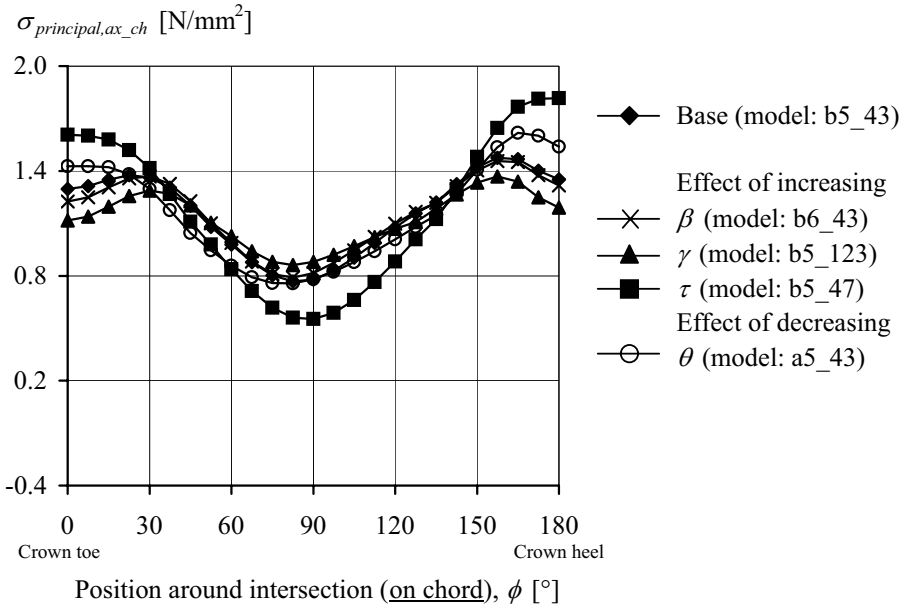

***Figure 4.9** - Principal stresses in the chord due to axial chord load*

- Stresses are generally higher at the crown heel than at the crown toe.
- An increase in γ decreases the stresses near the crowns. In contrast, an increase in τ results in an increase in the stresses at these locations. A larger τ (a larger t with respect to T) can be seen as a larger perturbation to the stress flow in the chord, which results in higher stresses, in particular, near the crowns.
- An example of higher stress in the in-between region is seen, most notably, for joint model b5_123, where the stresses immediately adjacent to the crown are higher than the stress exactly at the crown.

SCF results and trends

The general SCF trends due to variations in each of the studied joint parameters are summarised in Table 4.11. Table 4.12 presents SCF results for load case F_{ax_ch}. The following comments about SCF trends and values can be made:

- The highest SCF value at Location 31 is **1.66** in model a5_47.
- Maximum SCF values are seen at Locations 1 and 31.

- At higher β, γ and τ values the maximum SCF generally shifts from Location 1 to Location 31.
- SCFs at Locations 11, 2 and 3 are very small; SCFs at Location 4 are always less than 1.00.
- An increase in θ, β or γ results in a decrease in SCF values. As already seen in Figure 4.9, an increase in τ results in an increase in SCF values.

***Table 4.11** - SCF trends due to axial load in chord*

Change in parameter	Corresponding change in SCF_{i,ax_ch} at Locations:					
	1	11	2	3	31	4
$\theta \Uparrow$	$\Downarrow$	–	–	–	$\Downarrow$	–
$\beta \Uparrow$	$\Downarrow$	–	–	–	$\downarrow$	–
$\gamma \Uparrow$	$\Downarrow$	–	–	–	$\Downarrow$	–
$\tau \Uparrow$	$\Uparrow$	–	–	–	$\Uparrow$	–

– : Majority of SCF values below 1.00
$\Uparrow$,$\Downarrow$: Solid trend (increasing or decreasing)
$\uparrow$,$\downarrow$: Weak trend or small differences

Table 4.12 - *SCF values due to axial load in chord*

					SCF_{i,ax_ch} at Locations:					
Model	θ	β	γ	τ	1	11	2	3	31	4
a5_43				0.30	1.32	0.24	-	-	1.29	0.34
a5_45	45°	0.51	4.2	0.50	1.49	0.17	-	0.15	1.51	-
a5_47				0.70	1.56	-	0.14	0.19	1.66	-
a5_73				0.30	1.25	0.13	-	-	1.23	0.61
a5_75	45°	0.51	6.9	0.50	1.47	0.16	-	-	1.46	0.30
a5_77				0.70	1.59	0.10	0.14	0.17	1.65	0.13
a5_123				0.30	1.12	-	-	0.11	1.15	0.91
a5_125	45°	0.51	12.7	0.50	1.31	-	-	-	1.32	0.59
a5_127				0.70	1.44	-	-	-	1.44	0.39
a6_43				0.30	1.24	0.17	-	-	1.26	0.54
a6_45	45°	0.64	4.2	0.50	1.43	0.17	-	0.11	1.48	0.22
a6_47				0.70	1.52	0.11	0.11	0.19	1.65	-
a6_73				0.30	1.14	-	-	0.12	1.20	0.78
a6_75	45°	0.64	6.9	0.50	1.34	0.12	-	-	1.40	0.48
a6_77				0.70	1.48	0.10	0.11	0.14	1.60	0.27
a6_123				0.30	1.01	0.17	-	0.10	1.12	0.99
a6_125	45°	0.64	12.7	0.50	1.13	-	-	-	1.30	0.73
a6_127				0.70	1.25	-	-	-	1.44	0.54
b5_43				0.30	1.21	0.15	-	0.11	1.20	0.17
b5_45	60°	0.51	4.2	0.50	1.39	0.10	-	-	1.39	0.10
b5_47				0.70	1.48	-	0.14	0.16	1.53	0.12
b5_73				0.30	1.16	-	-	0.11	1.15	0.44
b5_75	60°	0.51	6.9	0.50	1.33	-	-	-	1.31	0.11
b5_77				0.70	1.44	-	0.12	-	1.48	-
b5_123				0.30	1.07	-	-	-	1.09	0.80
b5_125	60°	0.51	12.7	0.50	1.17	-	-	-	1.20	0.44
b5_127				0.70	1.27	-	-	-	1.32	0.20
b6_43				0.30	1.15	-	-	0.13	1.18	0.36
b6_45	60°	0.64	4.2	0.50	1.32	0.11	-	-	1.35	-
b6_47				0.70	1.43	-	0.11	0.12	1.50	-
b6_73				0.30	1.08	-	-	0.12	1.12	0.65
b6_75	60°	0.64	6.9	0.50	1.22	-	-	-	1.27	0.30
b6_77				0.70	1.33	-	-	-	1.42	0.11
b6_123				0.30	1.01	0.14	-	-	1.07	0.92
b6_125	60°	0.64	12.7	0.50	1.06	-	-	-	1.15	0.58
b6_127				0.70	1.13	-	-	-	1.27	0.37

: Maximum SCF for model

- : SCF less than 0.10

Shaded (grey) : SCF less than 1.00

4.5.4 Joint behaviour under in-plane chord bending

Distribution of stresses around brace-chord intersection

The maximum principal stress distribution in the chord resulting from an in-plane bending moment load on the chord, M_{ipb_ch}, is shown in Figure 4.10. Through comparison of the results plotted in Figure 4.10 with those plotted in Figure 4.9 it can be seen that the stress response in the joints due to M_{ipb_ch} is very similar to the stress response due to F_{ax_ch}. For this reason, the same observations regarding the stress distribution apply here as were made in Section 4.5.3. Worth noting is that the stresses at the crown locations are slightly higher due to in-plane bending as opposed to axial loading.

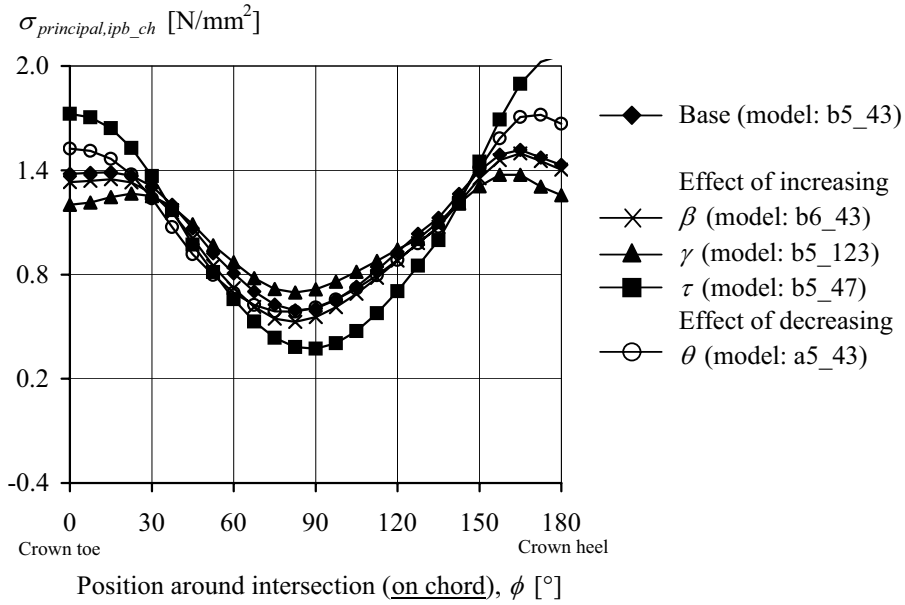

***Figure 4.10** - Principal stresses in the chord due to in-plane chord bending*

SCF results and trends

The general SCF trends due to variations in each of the studied joint parameters are summarised in Table 4.13. Table 4.14 presents SCF results for load case M_{ipb_ch}. The following comments about SCF trends and values can be made:

- The highest absolute SCF value at Location 31 is **1.81** in model a6_47.

***Table 4.13** - SCF trends due to in-plane bending moment in chord*

Change in parameter	Corresponding change in SCF_{i,ipb_ch} at Locations:					
	1	11	2	3	31	4
$\theta \Uparrow$	$\Downarrow$	–	–	–	$\Downarrow$	–
$\beta \Uparrow$	$\downarrow$	–	–	–	$\downarrow$	–
$\gamma \Uparrow$	$\downarrow$	–	–	–	$\downarrow$	–
$\tau \Uparrow$	$\Uparrow$	–	–	–	$\Uparrow$	–

– : Majority of SCF values below 1.00
$\Uparrow$,$\Downarrow$: Solid trend (increasing or decreasing)
$\uparrow$,$\downarrow$: Weak trend (exceptions possible) or small differences

- Maximum SCF values are seen at Location 1 and 31.

- At higher γ and τ values the maximum SCF generally shifts from Location 1 to Location 31.
- SCFs at Locations 11, 2, 3 and 4 are small; all values are less than 1.00.

***Table 4.14** - SCF values due to in-plane-bending moment in chord*

					SCF_{i,ipb_ch} at Locations:					
Model	θ	β	γ	τ	1	11	2	3	31	4
a5_43				0.30	1.40	0.40	-	0.30	1.32	0.26
a5_45	45°	0.51	4.2	0.50	1.58	0.33	0.15	-	1.59	-
a5_47				0.70	1.66	0.26	0.20	-	1.77	-
a5_73				0.30	1.34	0.26	-	0.34	1.27	0.52
a5_75	45°	0.51	6.9	0.50	1.59	0.29	0.17	0.14	1.55	0.23
a5_77				0.70	1.73	0.23	0.24	-	1.80	-
a5_123				0.30	1.21	-	-	0.30	1.20	0.82
a5_125	45°	0.51	12.7	0.50	1.44	0.20	0.13	0.22	1.42	0.52
a5_127				0.70	1.58	0.18	0.18	-	1.57	0.33
a6_43				0.30	1.34	0.35	0.10	0.42	1.29	0.42
a6_45	45°	0.64	4.2	0.50	1.56	0.35	0.15	0.14	1.59	0.12
a6_47				0.70	1.66	0.30	0.19	-	1.81	-
a6_73				0.30	1.26	0.18	0.10	0.42	1.24	0.64
a6_75	45°	0.64	6.9	0.50	1.50	0.28	0.18	0.26	1.51	0.38
a6_77				0.70	1.65	0.24	0.23	-	1.78	0.19
a6_123				0.30	1.12	-	0.10	0.34	1.18	0.84
a6_125	45°	0.64	12.7	0.50	1.29	0.16	0.15	0.30	1.33	0.61
a6_127				0.70	1.43	0.19	0.19	0.18	1.61	0.45
b5_43				0.30	1.27	0.30	-	0.36	1.24	0.11
b5_45	60°	0.51	4.2	0.50	1.47	0.25	0.14	0.13	1.46	0.16
b5_47				0.70	1.58	0.18	0.20	-	1.63	0.19
b5_73				0.30	1.23	0.17	-	0.32	1.20	0.38
b5_75	60°	0.51	6.9	0.50	1.43	0.20	0.13	0.21	1.40	-
b5_77				0.70	1.56	0.17	0.22	-	1.60	-
b5_123				0.30	1.14	-	-	0.24	1.14	0.71
b5_125	60°	0.51	12.7	0.50	1.28	0.13	-	0.23	1.28	0.39
b5_127				0.70	1.39	0.13	0.13	0.15	1.44	0.17
b6_43				0.30	1.24	0.26	-	0.43	1.21	0.27
b6_45	60°	0.64	4.2	0.50	1.43	0.28	0.14	0.25	1.44	-
b6_47				0.70	1.56	0.24	0.18	-	1.64	0.15
b6_73				0.30	1.18	0.13	-	0.37	1.17	0.53
b6_75	60°	0.64	6.9	0.50	1.35	0.20	0.15	0.30	1.37	0.23
b6_77				0.70	1.48	0.20	0.19	0.17	1.57	-
b6_123				0.30	1.09	-	-	0.25	1.13	0.77
b6_125	60°	0.64	12.7	0.50	1.18	0.11	0.12	0.28	1.25	0.49
b6_127				0.70	1.27	0.15	0.15	0.22	1.40	0.31

: Maximum SCF for model

- : SCF less than 0.10

Shaded (grey) : SCF less than 1.00

4.5.5 Axial force versus in-plane bending moment effects

The SCFs due to axial forces and in-plane bending moments, both in the brace and chord, have been examined. In current design specifications [Zhao et al. 2000, IIW 2000] no differentiation is made between these two load cases—for simplicity, the same SCF (based on axial loading) is used for both types of load. Comparing SCF values in Table 4.7 with those in Table 4.9 (or Table 4.10), and Table 4.12 and Table 4.14 it is seen that for certain joint locations and, in some cases, depending on the combination of joint parameters, the SCFs due to in-plane bending will be higher. Figure 4.11 and Figure 4.12 confirm this observation showing that, for the same joint, SCFs can not only differ due to axial force versus in-plane bending, but that the *distribution* of stresses in the vicinity of the weld toe can also be affected (e.g. left graphic in Figure 4.11). The latter point calls into question the feasibility of superpostion between the two types of loads, which is implied by the aforementioned simplification in the specifications.

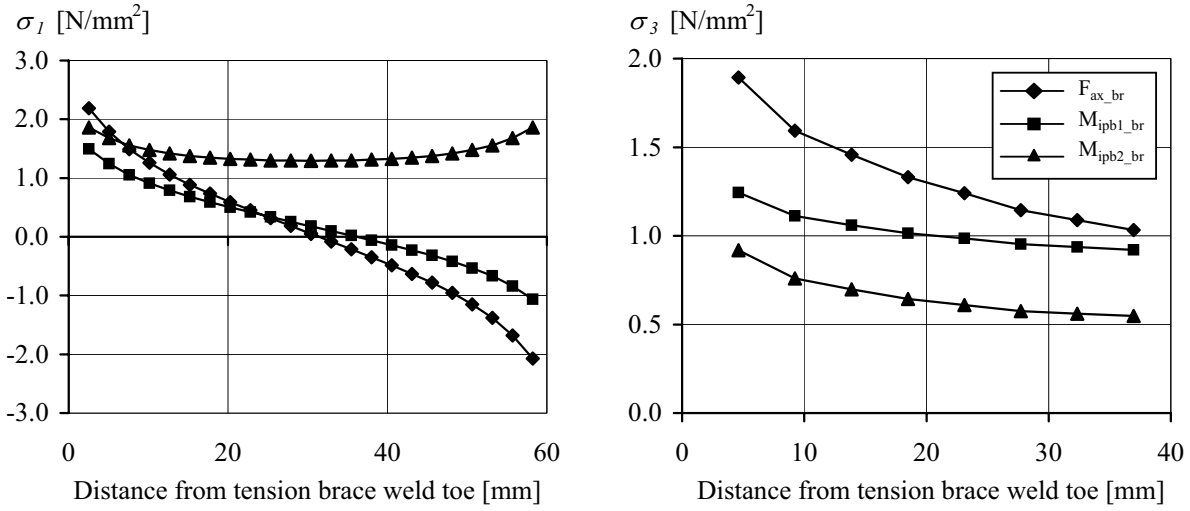

***Figure 4.11** - Primary stresses in joint model b5_75 due to balanced axial brace force and brace in-plane bending moment effects at Location 1 (left) and Location 3 (right)*

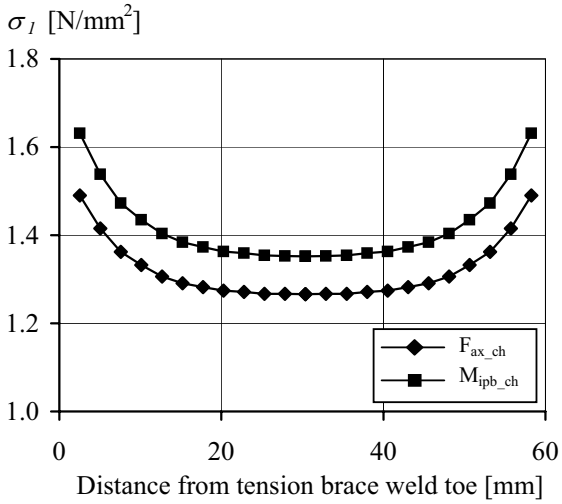

***Figure 4.12** - Primary stresses in joint model b5_75 due to axial chord force and chord in-plane bending moment effects at Location 1*

4.5.6 Commentary

With the many trends and magnitudes of SCF values that have been described and examined—the shifting locations of the maximum SCFs, the influence of one load case over the other—a clear, synthesised overview of the most important aspects is difficult to maintain. Nevertheless, two (related) observations that apply globally to the parametric study and that seem particularly pertinent to the present investigation are summarised here:

1. For the brace axial force and in-plane bending moment load cases there is a strong tendency for the SCF values to decrease with decreasing γ, especially at locations of maximum SCF. A low γ value, such as the low γ joints ($\gamma < 12.0$) seen in existing bridges, is therefore a desirable geometric characteristic. For chord load cases, the opposite is seen with respect to γ: SCF values increase with a decrease in γ. SCF values due to chord load, however, are generally lower than brace load SCFs and the influence of γ on the chord load SCFs is also less pronounced.
2. SCF values were found to be relatively low. For brace loads, the SCF values lie mainly between 1.5 and 2.5, while for chord loading the SCF values fall principally between 1.0 and 1.5. In the current design specification for the determination of SCFs for tubular joints [Zhao et al. 2000, IIW 2000] a general recommendation is given (for all welded tubular joints, CHS and RHS) that a minimum SCF of 2.0 be employed for all load cases and locations, except in cases where the SCF is negligible. The basis for the minimum SCF values are given as the following:
   - *The SCFs are determined along limited fixed lines or locations of interest. The hot-spot stresses found may underestimate the 'true' hot-spot stress if the direction of the principal stresses deviates from these lines, especially if the stress concentration is less pronounced.*
   - *Difficulties in FE modelling, such as the case where $\beta = 1.0$ and the case where weld shapes have a strong influence on SCFs.*
   - *Crack initiation from the root of the weld for low SCFs.*

The first reason given in the specifications has been addressed in this work, whereby it was seen that, for a few models with higher γ values ($\gamma = 12.7$), a higher principal stresses may occur away from the standard locations (refer to Figure 4.9). For these cases, the SCF was determined specifically at the locations of higher stress, however, it is relevant to note that the SCFs at these more critical locations were only between 10% and 20% higher than at the standard location.

Although the difficulty of modelling joints with $\beta = 1.0$, in particular, with respect to the weld model at the saddle (CHS) or chord edge (RHS), is recognised, this does not apply to the range of parameters covered in the present work. Furthermore, although it was seen that the weld shape and volume plays an important role in defining the stress response of the joints, it is thought that the influence of the weld was relatively constant for all models at all joint locations.

The third reason given in the recommendations for a minimum SCF is a plausible scenario, in particular for joints with welds that are less than fully penetrated. For fully penetrated welds, however, the recommendation seems penalising, especially in light of the test results reported in Chapter 3. For the joints tested as part of the present study, it was seen that the location of fatigue cracking—the location of highest stress, but nevertheless with a SCF below 2.0 (refer to Table 3.4)—always occurred at the weld toe, never at the weld root. Even for post-weld treated

joints, whereby the weld toe was improved, further reducing the effective stresses at that location, cracking at the weld root was not an issue.

In summary, while it is clear that a *safe* fatigue design of welded tubular joints must remain a priority, the recommended minimum SCF in the design specifications would be very penalising if maintained for the welded CHS K-joints studied here. A more realistic, less conservative approach might involve similar recommendations to those listed above, however, with more specific reference to the types of joints to which they should be applied. In the case of bridges, for example, the application of a $SCF_{min} = 1.0$ be applied in the presence of fully penetrated welds and a maximum brace-to-chord diameter ratio, β, of 0.7.

4.6 SCFS FOR COMBINED LOAD CONDITION

The investigation of SCFs for individual load cases has facilitated the understanding of a problem characterised by a large number of parameters and variables. In reality, however, it is the ensemble of all the parameters and variables that must be considered and that will facilitate the determination of the most susceptible fatigue location in the joint. A simple bridge example with two load scenarios is used to illustrate this point.

First, however, the calculation of hot-spot stresses at joint locations for given joint geometries is recalled. The calculation employs the SCF values presented in the Section 4.5 and is based on the superposition principle introduced in Equation 2.3:

$$\sigma_{hs,i} = \sigma_{ax\_br} \cdot SCF_{i,ax\_br} + \sigma_{ipb\_br} \cdot SCF_{i,ipb\_br} + \sigma_{ax\_ch} \cdot SFC_{i,ax\_ch} + \sigma_{ipb\_ch} \cdot SCF_{i,ipb\_ch} \quad [4.4]$$

where,

$\sigma_{hs,i}$: hot spot stress at joint Location *i*
σ_{ax_br} : stress in tension brace due to balanced brace axial force
SCF_{i,ax_br} : SCF at joint Location *i* due to balanced axial brace force (Table 4.7)
σ_{ibp_br} : stress in tension brace due to in-plane bending moment
SCF_{i,ipb_br} : SCF at joint Location *i* due to moment in brace (Table 4.9 or Table 4.10)
σ_{ax_ch} : stress in chord due to chord axial force
SCF_{i,ax_ch} : SCF at joint Location *i* due to axial chord force (Table 4.12)
σ_{ipb_ch} : stress in chord due to in-plane bending moment
SCF_{i,ipb_ch} : SCF at joint Location *i* due to moment in chord (Table 4.14)

In Figure 4.13 a continuous, steel-concrete composite tubular truss bridge span is shown. The concrete deck is supported by uni-planar trusses comprising welded CHS K-joints. Two load scenarios are chosen to represent two areas on the span: Load scenario 1 describes the stresses that can be expected in the vicinity of a support with higher stresses in the brace members, while Load scenario 2 describes a scenario at mid-span, where higher stresses might occur in the chord. The table in Figure 4.13 gives a description of the stresses affecting the joint in terms of percentages (Column A). For example, in Load scenario 1, it can be said that 80% of the total nominal stress, $\sigma_{total\ nom}$, affecting the joint is due to the tension brace load, while the other 20% is due to the chord load.

A further partitioning of the stresses is possible on a member basis when the division between axial load effects and in-plane bending moment effects is considered. Here, the partitioning is based on the assumption that a simple static analysis has been carried out and the bending

moment in the members has been accounted for through magnification factors found in the current specifications [Zhao et al. 2000, IIW 2000] (refer to Section 3.3 and Section 4.2). For example, again for Load scenario 1, it is seen that 75% of the nominal stress in the brace is due to an axial force, while 25% is due to an in-plane bending moment (Column B). A slightly higher percentage of stress, 35%, due to in-plane bending has been assigned to the chord member. With the percentage of total nominal joint stress and the percentage of member stress (axial versus in-plane bending) known, the so-called member stress percentages are also known (Column C). The actual stresses per load case are thus obtained through a multiplication of the member stress percentages with the total nominal stress, $\sigma_{total\ nom}$, affecting the joint (shown for Load scenario 1 and 2 in Figure 4.13).

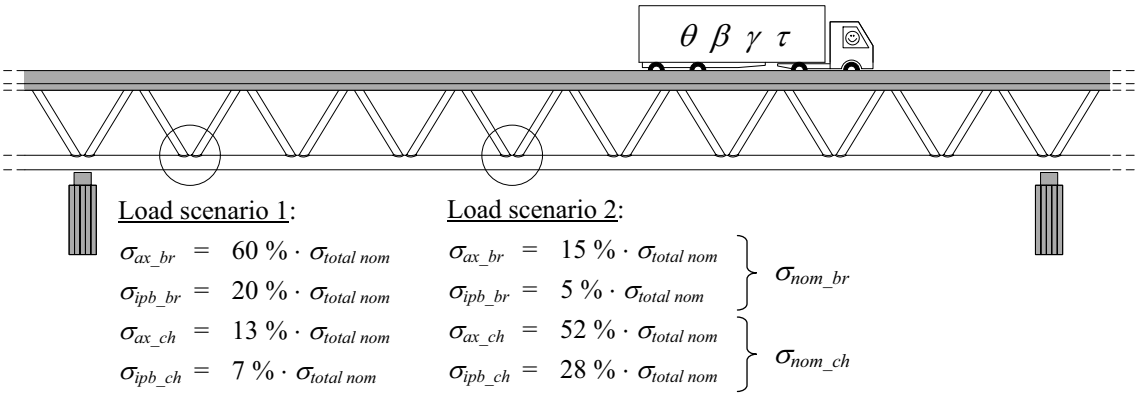

		A Stress partition, of total, [%]	B Stress partition in members, [%]		C = A · B Member stresses as a percentage of total, [%]	
		$\sigma_{total\ nom}$	σ_{ax}	σ_{ipb}	σ_{ax}	σ_{ipb}
Load scenario 1	Brace	80	75	25	60	20
	Chord	20	65	35	13	7
Load scenario 2	Brace	20	75	25	15	5
	Chord	80	65	35	52	28

***Figure 4.13** - Load scenarios for welded CHS K-joints in a bridge*

Continuing with Load scenario 1, the member stresses in Equation 4.4 can be replaced by a percentage of the total nominal stress:

$$\sigma_{hs,i} = 0.60\sigma_{total\ nom} \cdot SCF_{i,ax\_br} + 0.20\sigma_{total\ nom} \cdot SCF_{i,ipb\_br} + 0.13\sigma_{total\ nom} \cdot SFC_{i,ax\_ch} + 0.07\sigma_{total\ nom} \cdot SCF_{i,ipb\_ch} \quad [4.5]$$

which simplifies to,

$$\sigma_{hs,i} = \sigma_{total\ nom} \cdot (0.60SCF_{i,ax\_br} + 0.20SCF_{i,ipb\_br} + 0.13SCF_{i,ax\_ch} + 0.07SCF_{i,ipb\_ch}) \quad [4.6]$$

where the term in brackets can be considered as the total stress concentration factor, SCF_{total},

$$\sigma_{hs,i} = \sigma_{total\ nom} \cdot SCF_{total,\,i} \qquad [4.7]$$

where,

$\sigma_{total\ nom}$: total nominal stress affecting the joint
$SCF_{total,i}$: SCF at joint Location *i* due to combined loading

The sequence of equations, Equation 4.5 to Equation 4.7, presents a simplified method of expressing the stress concentration factor. The fact that the equations imply a scalar superposition of member stresses that act in different directions is accounted for by the SCFs.

To illustrate further this concept, SCF_{total} values have been calculated for a set of joint geometries ($\theta = 45°$, $\beta = 0.5$). The results are presented in Table 4.15 and Table 4.16; the maximum SCF between the two cases of in-plane bending moment (balanced and un-balanced) was used. As done with SCFs for individual load cases, the maximum SCF_{total} values are indicated with grey shading.

***Table 4.15** - $SCF_{total,i}$ values for Load scenario 1*

					Load scenario 1 - $SCF_{total,i}$ at Locations:					
Model	θ	β	γ	τ	1	11	2	3	31	4
a5_43				0.30	0.87	0.99	0.25	1.44	0.34	0.75
a5_45	45°	0.51	4.2	0.50	1.17	0.94	0.41	1.32	0.40	0.78
a5_47				0.70	1.46	0.91	0.58	1.23	0.43	0.82
a5_73				0.30	1.00	1.12	0.46	1.47	0.40	0.83
a5_75	45°	0.51	6.9	0.50	1.44	1.13	0.81	1.38	0.66	0.96
a5_77				0.70	1.93	1.11	1.12	1.29	0.93	1.04
a5_123				0.30	1.18	1.36	0.68	1.52	0.78	1.03
a5_125	45°	0.51	12.7	0.50	1.80	1.45	1.20	1.43	1.21	1.25
a5_127				0.70	2.52	1.52	1.76	1.28	1.55	1.42

***Table 4.16** - $SCF_{total,i}$ values for Load scenario 2*

					Load scenario 2 - $SCF_{total,i}$ at Locations:					
Model	θ	β	γ	τ	1	11	2	3	31	4
a5_43				0.30	1.23	0.47	0.10	0.46	1.06	0.42
a5_45	45°	0.51	4.2	0.50	1.43	0.40	0.19	0.41	1.25	0.23
a5_47				0.70	1.56	0.33	0.27	0.42	1.38	0.23
a5_73				0.30	1.21	0.41	0.15	0.50	1.03	0.64
a5_75	45°	0.51	6.9	0.50	1.49	0.44	0.29	0.41	1.28	0.45
a5_77				0.70	1.71	0.39	0.41	0.41	1.51	0.34
a5_123				0.30	1.16	0.40	0.20	0.51	1.07	0.92
a5_125	45°	0.51	12.7	0.50	1.47	0.45	0.35	0.43	1.32	0.74
a5_127				0.70	1.75	0.47	0.52	0.38	1.50	0.63

Presenting this new "total" stress concentration factor wherein the concepts of load combination and the partitioning of stresses are already inherent to the value, allows for a more complete overview and comparison between the different joints and joint locations. Comparing the results in Table 4.15 and Table 4.16 it is seen that the locations of maximum SCF are reduced to two

locations: Locations 1 and 3 for Load scenario 1 and Location 1 for Load scenario 2. A brief examination of the tables also gives a clear indication of the tendencies that can be expected. For example, K-joints in the support region of a bridge span (Load scenario 1) may have larger brace thicknesses and therefore higher τ values due to the higher static (and fatigue) load carried by the brace members. The SCF_{total} values in Table 4.15 remind the engineer that, in terms of the stress relevant to the fatigue design of the structure, it is advantageous to choose joints with $\tau \leq 0.5$.

A more complete synthesis of SCF_{total} values for the entire range of joints studied and a broader range of Load scenarios will be presented in Chapter 6.

4.7 COMPARISON OF SCF RESULTS WITH EXISTING WORK

Data, largely in the form of stress concentration factors, has been generated from the finite element analysis of a parametrically varied set of models. It has been seen that the SCF data, as it was presented in the preceding tables, could be used directly in the determination of hot-spot stresses of welded CHS K-joints with non-dimensional parameters within the range of study. This is a fairly impractical suggestion, however, especially when the inherently iterative nature of the design process is considered. Similar finite element based parametric studies on welded tubular joint SCFs have gone a step further by proposing parametric equations based on regression analyses of the SCF data, whereby the equations are used to find the SCFs of a particular joint geometry and loading. The development of parametric equations is not within the scope of the work presented here. It is, nevertheless, important to situate the present work with respect to this previous work in view of the parametric equations that already exist for, notably, welded CHS K-joints with $\gamma > 12.0$. More specifically, the following questions are posed:

How do the SCF results from the present study compare with the SCF results of the existing finite element database on which the current design specifications[1] are based?

Can the parametric equations adopted to describe the SCF trends in the existing work be extended to the present work?

At this point it must be stated clearly that the comparisons carried out to address these questions concentrate exclusively on the most recent finite element work and resulting parametric equations for welded CHS K-joints. The finite element database was created in a study carried out at TU Delft by Romeijn 1994 and synthesised by Karamanos et al. 1997. In the following figures it will be referred to as “TU Delft”. The FE models used for the TU Delft work were welded CHS K-joints with gap and no eccentricity, except for joints with $\theta = 60°$ and $\beta = 0.6$, where a normalised eccentricity of e / D = 0.17 was introduced in order to avoid overlap.

In light of the numerous other earlier studies that have been carried out on the definition of SCFs for welded CHS K-joint, for example, Kuang et al. 1977, Wordsworth and Smedley 1978, Wordsworth 1981, Marshall and Luyties 1982, Efthymiou and Durkin 1985, Efthymiou 1988, Marshall 1992, it is clear that various other comparisons would be possible. Considering the importance of the TU Delft study in the current design specifications, however, it was decided

1. Design specifications based directly on TU Delft SCF database results are the CIDECT Handbook [Zhao et al. 2001] and IIW Recommendations [IIW 2000]. The specifications are a simplification of the information in Karamanos et al. 1997.

to concentrate on this work. Comparisons between the TU Delft work and the aforementioned, earlier work are made in Romeijn 1994 and Karamanos et al. 1997.

As a first step, it is necessary to understand the equation format used presently in the determination of SCFs for welded CHS K-joints. The format is based on the general form employed in previous design specifications (e.g. IIW 1985, refer to Equation 2.6):

$$SCF_{i,\,Load\ case\ n} = SCF0_{i,\,Load\ case\ n} \cdot \left(\frac{\gamma}{12}\right)^{X1} \cdot \left(\frac{\tau}{0.5}\right)^{X2} \qquad [4.8]$$

where,

$SCF_{i,Load\ case\ n}$: SCF at Location *i* for Load case *n*
$SCF0_{i,Load\ case\ n}$: base SCF for γ= 12.0 and τ = 0.5, at Location *i* for Load case *n*
X1, *X2* : exponents defined on a per joint location and load case basis

Equation 4.8 is composed of two parts: a so-called base SCF, SCF_0, and a power function. The former is a SCF for base values of γ and τ. The base values chosen for the TU Delft database are γ= 12.0 and τ = 0.5. That is, for joints with γ= 12.0 and τ = 0.5 (but varying β and θ) SCF values have been defined at particular joint locations and for specific load cases. The latter is a power function that has the effect of correcting the base SCFs for joints with γ and τ values other than 12.0 and 0.5, respectively. As with the base SCFs, the power function, that is, the exponents *X1* and *X2*, are defined on a per joint location and load case basis.

It has been made clear throughout this chapter that the goal of the present parametric study is to examine the behaviour of joints in the low γ range (γ< 12.0). Nevertheless, to make comparisons between the existing TU Delft database possible, four models were included in the study with parameters that overlap with the previous work: a5_125, a6_125, b5_125 and b6_125, that is, joint models characterised by γ= 12.7 and τ = 0.5. The following section will compare SCF base values from the TU Delft database with those of the present study. This is followed by an evaluation of the power functions whereby SCFs from the present study are compared to the trends predicted by these functions.

4.7.1 Comparison of base SCF values, SCF_0 (γ= 12.0, τ = 0.50)

The comparison of base SCF values is made in Figure 4.14 to Figure 4.18. Each figure compares SCF base values calculated in the present (ICOM) study with SCF base values from the TU Delft FE database. Also included in the figures are the curves proposed in Karamanos et al. 1997 based on the TU Delft FE results (referred to as *Prop. curve* in the figures). Although not explicitly indicated in the figures, it is important to note that the so-called Proposed curves were subsequently adopted by the design specification in very similar or identical form as they are presented here (see Footnote 1). Furthermore, the SCF based comparisons are restricted to the data presented in Karamanos et al. 1997 and therefore do not cover all possible joint locations and load cases.

In Figure 4.14 and Figure 4.15, SCF_0 values due to balanced axial brace loads, F_{ax_br}, at crown locations (Locations 1 and 3) and saddle locations (Locations 2 and 4), respectively, are presented for θ = 45° and 60°, over a range of β values. For this load case, only the TU Delft data points for joints with 60° inclined braces were found in the literature. Based on these figures the following remarks can be made:

- In the left graphic of Figure 4.14 the TU Delft data point at $\beta = 0.6$ corresponds quite well with the ICOM points at similar β values. Contrary to this, the Proposed curves, for $\theta = 45°$ and 60°, are considerably more conservative. It is difficult to speculate on the reason for this conservatism, given the scant amount of information and the missing data points for $\theta = 45°$, although it seems that the Proposed curves were calibrated on data points in the lower β range.
- In the right graphic of Figure 4.14 the TU Delft points for a brace angle of 60° compares well with the corresponding ICOM points. It should be noted that in Karamanos et al. 1997 two conflicting $SCF0_{3,ax\_br}$ values are given for $\theta = 60°$ and $\beta = 0.6$. The value not shown in the graphic corresponds well with the Proposed curve and therefore might explain the conservative positioning of the curves (with respect to the data points that are shown). Furthermore, a discrepancy is seen in the trends from the Proposed curves and the ICOM data: $SCF0_{3,ax\_br}$ values predicted by the Proposed curves increase for a decreasing brace angle, while the ICOM data indicates a slight decrease in the $SCF0$ for the same change in angle. In both cases, however, the respective differences in $SCF0$ values for the different angles is small.

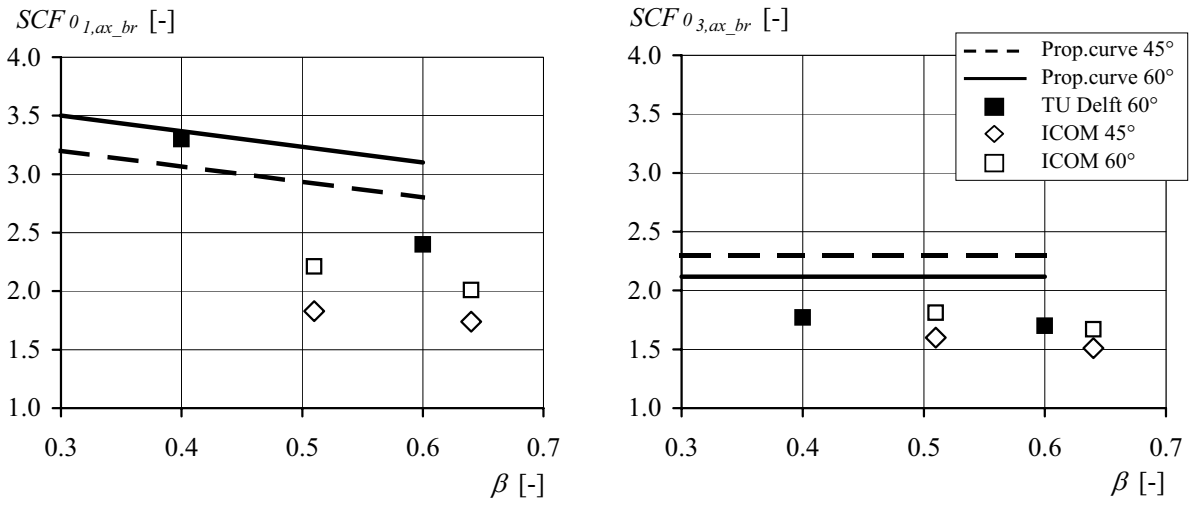

***Figure 4.14** - SCF0 due to balanced axial brace load, chord crown and brace crown locations ($\gamma = 12.0$ and $\tau = 0.5$)*

- The left graphic of Figure 4.15 shows very good correspondence between the two data point sets. A simplification introduced in Karamanos et al. 1997 and also adopted in the design specifications [Zhao et al. 2000, IIW 2000] is made where the $SCF0_{2,ax\_br}$ (and, more generally, the SCF_{2,ax_br}) values at are taken to be equal to $SCF0_{1,ax\_br}$ for balanced axial brace loading. For this reason, the Proposed curves seen in this graphic are the same as in the left graphic of Figure 4.14. The Proposed curves are again conservative compared to the FE data points, in particular, for a brace angle of 45°. The simplification—whereby SCFs at Locations 1 and 2 are equated—is looked at in more detail below.
- In the right graphic of Figure 4.15 it is seen that the proposed curves, as well as the TU Delft data points for $\theta = 60°$ are somewhat unconservative as compared with the values found by ICOM. The $\theta = 45°$ ICOM data points, on the other hand, correspond well with the TU Deft data as well as the Proposed curves.

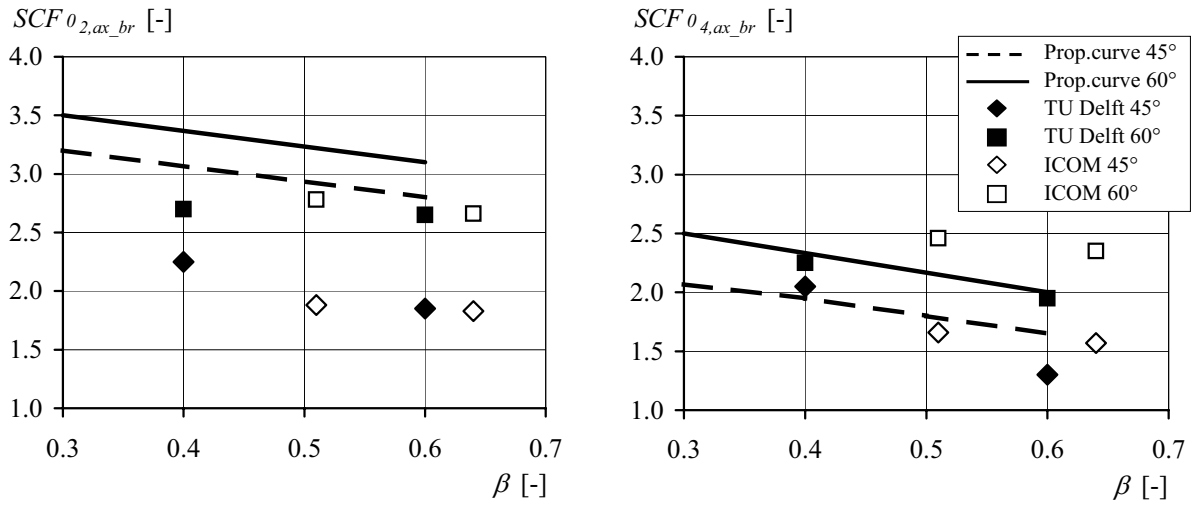

Figure 4.15 - *SCF_0 due to balanced axial brace load, chord saddle and brace saddle locations ($\gamma = 12.0$ and $\tau = 0.5$)*

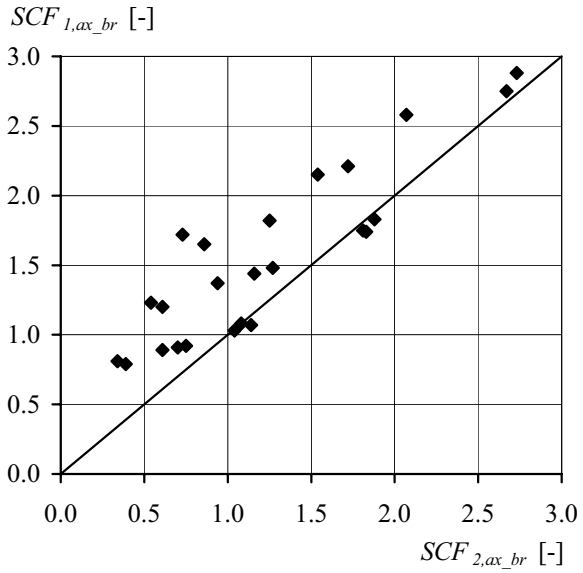

Figure 4.16 - *Comparison between SCF_1 and SCF_2 due to balanced axial brace load*

As already seen above, the assumption that the same SCF values can be used for Locations 1 and 2 in the case of balanced axial brace loads seems overly conservative for the SCFs at Location 2. This was also recognised, to some degree, in Karamanos et al. where it is stated: "This assumption may be conservative for *small* values of brace angle, θ. In fact, the maximum value (of Location 1 and Location 2) from the TU Delft results is used." A comparison between SCFs due to balanced axial brace loading at Location 1 and Location 2 from the present study in Figure 4.16 shows that, in almost all cases, the SCF at Location 2 is lower than that at Location 1, including joints with *large* values of brace angle ($\theta = 60°$). It is understood that the assumption made in Karamanos et al. 1997 was based largely on the need to simplify the SCF calculation process for practising engineers. However, it has also been seen in the present work that there is a need, especially for the bridge applications, to adopt more precise, not overly conservative, definitions of SCF.

In Figure 4.17 SCF_0 values at crown locations (Locations 1 and 3) due to in-plane bending in the brace members are presented for θ = 45° and 60°, over a range of β values. It is recalled that stress concentration factors due to in-plane bending in the braces can be considered negligible at the saddle locations. For the ICOM data points, the maximum SCF_0 between the un-balanced bending moment (M_{ipb1_br}) load case and the balanced bending moment (M_{ipb2_br}) load case (refer to Table 4.5) are shown. The following remarks can be made:

- The left graphic in Figure 4.17 shows fairly good correspondence between points from the two databases, as well as the Proposed curves, with the ICOM $SCF_{0_{1,ipb\_br}}$ for brace angles of 45° and 60° falling in between the values predicted by the Proposed curves.
- In the right graphic in Figure 4.17 both the TU Delft and ICOM data predict higher $SCF_{0_{3,ipb\_br}}$ for joints with brace angles of 45° (as compared with 60°). The ICOM data points, however, show a much smaller influence on this SCF_0 due to the change in brace angle. The Proposed curve for 60° corresponds well with the ICOM data, while the Proposed curve for 45° seems too conservative.

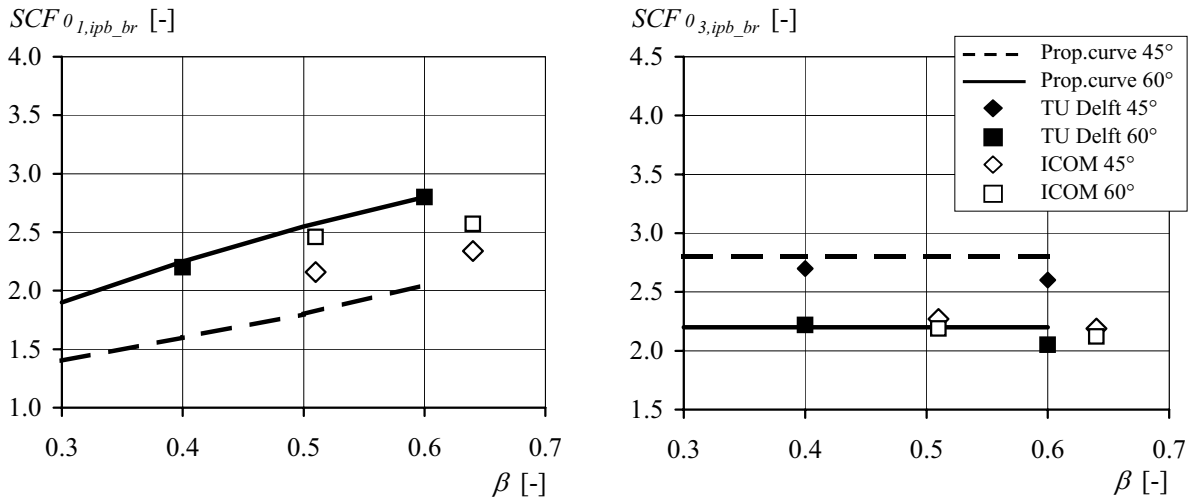

Figure 4.17 - *SCF_0 due to in-plane bending moment in brace, chord and brace crown locations (γ = 12.0 and τ = 0.5)*

Lastly, a comparison of SCF_0 values at the chord crown location due to an axial chord load, F_{ax_ch}, is made. In Figure 4.18 the results from the two databases are, again, similar: the difference caused by a change in brace angle seems to provoke the same response (very little). The $SCF_{0_{1,ax\_ch}}$ values predicted by the Proposed curves are slightly more conservative than the ICOM data.

In general, a good correspondence between TU Delft and ICOM SCF_0 data has been seen. This is especially true when considering that the data was obtained from independent FE studies, employing different tools and procedures (e.g. different finite element analysis programs, a different meshing procedure, etc.) as well as the different approaches used for the construction of the FE models, in particular with respect to the joint eccentricity. Without more detailed information on the TU Delft study (e.g. access to the actual FE models) it is difficult to give precise reasons explaining the differences between the two databases. It is imaginable that part of the difference is due to the weld model used for the joint models and thus it is not surprising

that parametrically identical models of two completely independent studies also resulted in some differences.

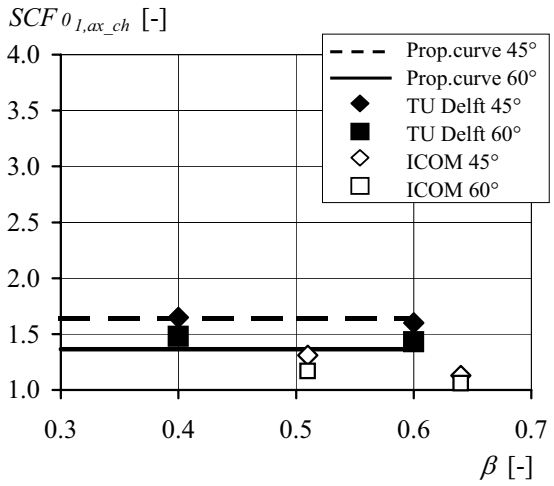

***Figure 4.18** - SCF0 due to axial chord load, chord crown location (γ = 12.0 and τ = 0.5)*

With respect to the Proposed curves, in most of the load cases and joint locations, the Proposed curves predicted higher, that is, more conservative SCF0 values. The most striking case of overprediction occurred at Location 1 for balanced axial brace loading. This is of particular interest for the present study, since Location 1 was the location at which fatigue cracking occurred in the test specimens (as described in Chapter 3). It is recalled that comparisons between measured and calculated hot-spot stresses at Location 1 for the test joints (Figure 3.6) showed that the hot-spot stresses based on existing design specifications gave overly conservative predictions. The design specifications that were used to calculate the hot-spot stresses incorporate curves for SCF prediction that are identical to the Proposed curve in Figure 4.14. Considering the good correspondence that will be seen below between the existing power functions and the present work, it follows that the overprediction of base SCFs in Figure 4.14, and therefore also present in the design specifications, is the underlying reason for the difference between measured and calculated hot-spot stress seen previously.

4.7.2 Validity of existing power functions

In this section, the validity of the power function, the second part of Equation 4.8, used in the determination of SCF values for joints with $\gamma$and τvalues other than 12.0 and 0.5, respectively, is examined. The power functions for different joint locations and load cases were developed using the TU Delft database and for joints with $\gamma \geq$ 12.0. Here it will be determined whether the same functions can be applied to joints with low γvalues, $\gamma \leq$ 12.0.

Three figures with two graphics each are presented for the comparison (Figure 4.19 to Figure 4.21). The three power functions examined in the figures correspond to the power functions adopted by the aforementioned design specifications [Zhao et al. 2000, IIW 2000]. The values of the power function exponents, *X1* and *X2*, are indicated in the figure legends. To isolate the trends predicted by the power functions, SFC values were normalised with respect to SCF0. In Figure 4.19 to Figure 4.21 the normalised SCFs are presented over a range of γ.

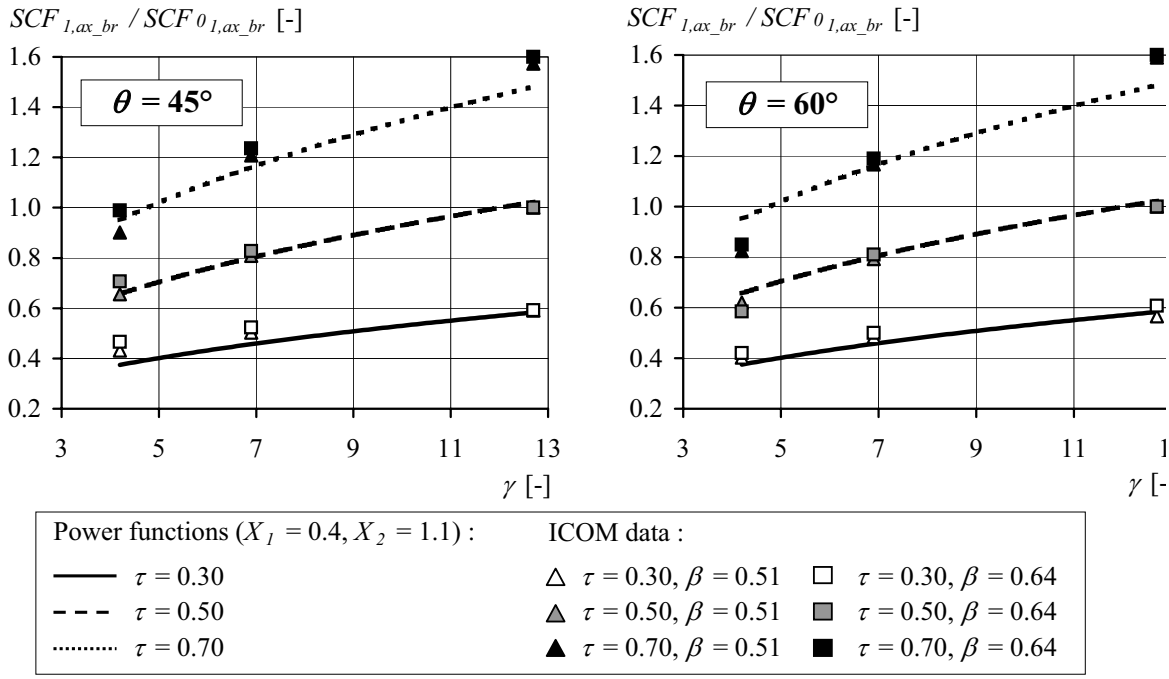

***Figure 4.19** - Comparison between design lines and parametric study results, balanced axial brace load at Location 1*

A very good correspondence is seen between the existing power functions and ICOM data in Figure 4.19, for both values of brace angle. The comparison in Figure 4.20 is also relatively good with the power function slightly under-predicting the normalised SCFs at low gamma values for a brace angle of 45°. The results in Figure 4.19 and Figure 4.20 imply that the correction made by the power functions for γ values greater than 12.0 can also be applied to joints with γ values below 12.0.

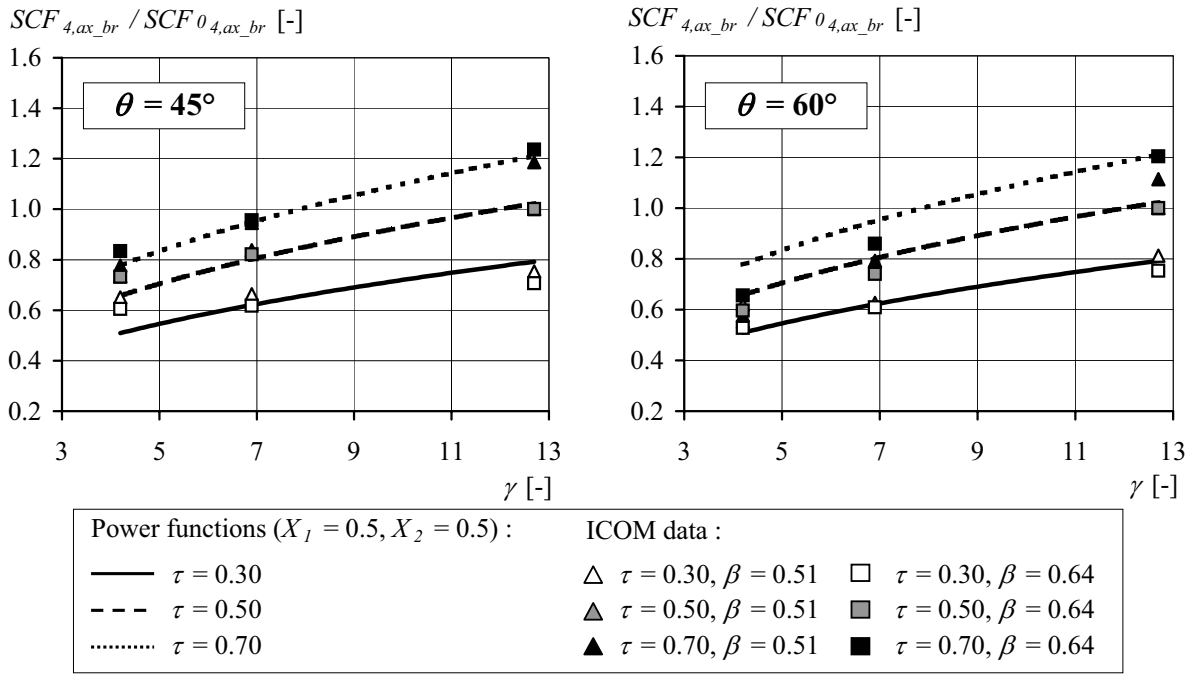

***Figure 4.20** - Comparison between design lines and parametric study results, balanced axial brace load at Location 4*

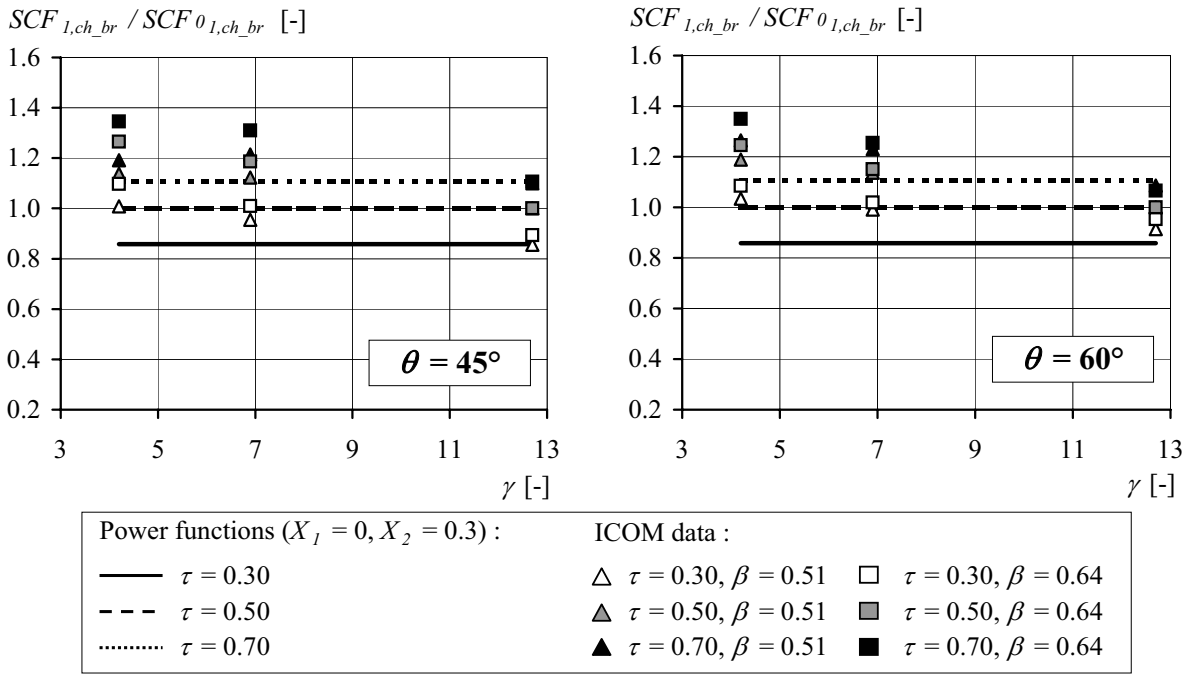

***Figure 4.21** - Comparison between design lines and parametric study results, axial chord load at Location 1*

In Figure 4.21 the power function seems to miss the general trend of the ICOM data. This can be attributed to the influence of γ on the value of the normalised SCF. Looking at the ICOM data, it is clear that as γ increases, the normalised SCF decreases. This trend is not predicted by the power functions, which is reflected in the fact that the power function exponent relevant to γ, *X1*, is taken as zero.

In the calculation of stress concentration factors, the two components of Equation 4.8 imply a strict separation of tasks, whereby the SCF_0 accounts for the effect of the parameters θ and β (for fixed γ and τ parameters) and the power function corrects for effects of varying γ and τ. Stated otherwise, it is assumed that no interaction exists between parameters θ and β and parameters γ and τ other than what is determined for the base model. To test whether this assumption is valid for the ICOM results, a comparison between the two graphs in the same figure (influence θ) and between data points on the same graph, with identical values of τ (influence β) was made. In general, the assumption is supported by the results in Figure 4.19 to Figure 4.21, where only small discrepancies between normalised SCF values due to differing θ and β were seen.

In conclusion, the questions posed at the beginning of Section 4.7 are briefly re-addressed here.

How do the SCF results from the present study compare with the SCF results of the existing finite element database on which the current design specifications are based?

SCF base values, SCF_0, obtained through FE analysis from the present study compare reasonably well with the SCF_0 values from an existing database. Some non-negligible discrepancies were seen, however, between the present SCF_0 values and the Proposed curves. In the event where it is desirable to amalgamate the TU Delft and ICOM SCF databases with the intent of providing coherent equations and design curves for joints with $\gamma < 12.0$ and

$\gamma \geq 12.0$, it will be necessary to address these discrepancies in order to provide a smooth transition between the two bodies of work.

Can the parametric equations adopted to describe the SCF trends from the existing work be the extended to the present work?

Again, a comparison between SCF data from the present study and existing parametric power functions have shown a fairly good correspondence between the two. Based on these results, it is imaginable that, with a few small adjustments, power functions that cover both the models investigated here and from the existing work can be assigned. Nevertheless, the concept of a total stress concentration factor, as introduced in Section 4.6, has been identified as the preferable approach in the definition of hot-spot stresses in CHS K-joints and it is this concept that will be developed further in Chapter 6.

4.8 CONCLUSIONS

A parametric study of a range of FE joint models has been carried out. The parameters investigated in the study are summarised in Table 4.17. The load cases studied are the following: balanced axial brace load, F_{ax_br}, in-plane bending moment in braces, M_{ipb_br}, axial chord load, F_{ax_ch}, in-plane bending chord, M_{ipb_ch}.

***Table 4.17** - Parameters investigated in parametric study*

θ	45°	60°	
β	0.51	0.64	
γ	4.2	6.9	12.7
τ	0.30	0.50	0.70

The following conclusions are made based on the results and observation from the parametric study:

- Examinations of the principal stress distributions at the brace-chord intersection give good indications of the general joint behaviour and the relative effect on that behaviour due to variations in joint parameters.
- Maximum SCFs due to a particular load case are concentrated at certain joint locations:
  - Max. SCFs due to balanced axial brace loads, F_{ax_br}, occur at Locations 1, 11 and 3
  - Max. SCFs due to in-plane bending in the braces, M_{ipb_br}, occur at Locations 1 and 3
  - Max. SCFs due to axial chord loads, F_{ax_ch}, occur at Locations 1 and 31
  - Max. SCFs due to in-plane bending in the chord, M_{ipb_ch}, occur at Locations 1 and 31
- In general, SCF values were found to be relatively low. For brace loads, the SCF values lie mainly between 1.5 and 2.5, while for chord loading the SCF values fall principally between 1.0 and 1.5. The recommended minimum SCF at critical joint locations in design specifications, SCF = 2.0 (except in cases where the SCF can be taken as zero), would be very penalising if applied to the welded CHS K-joints studied here.
- For bridge applications (i.e. where $\gamma < 12.0$), the recommended minimum SCF can be taken as $SCF_{min} = 1.0$ for CHS K-joints when fully penetrated welds are used and the brace-to-chord diameter ratio is $\beta \leq 0.70$.

** The definition of the hot-spot stress (and thus the SCF) is closely related to the choice of fatigue strength ($S_{R,hs}$-N) curve. Since the determination of the SCFs here is also based on the work in Chapter 3, it follows that the SCFs should also be related to the fatigue strength results presented in Chapter 3.*

- For brace load cases, axial force or in-plane bending moment, there is a strong tendency for SCF values to decrease with decreasing γ, especially at locations of maximum SCF. A low γvalue, such as the low γjoints (γ< 12.0) seen in existing bridges, is therefore be a desirable geometric characteristic.
- SCFs and stress distributions due to axial load differ from those due to in-plane bending moments. SCFs from the two load types should be considered separately.
- The use of a new stress concentration factor, SCF_{total}, whereby the concept of load combination and the partitioning of stresses in members is already inherent to the value, facilitates a more complete overview and comparison between different joints and joint locations. SCF_{total} will be developed further in Chapter 6 in order to provide the engineer with a practical design tool.
- Comparisons between results of the present parametric study and a similar, previous study highlight a few non-negligible discrepancies between SCF values found in the two studies. In particular, for SCF values at joint Location 1 due to axial brace loading, where the values found in the present study are considerably lower than values predicted by design curves based on the previous study.

5 EFFECTS OF JOINT SIZE AND SCALE

5.1 INTRODUCTION

The size effect (also known as the scale effect or thickness effect) on the fatigue behaviour of welded structures in general and tubular structures in particular was introduced briefly in Chapter 2, and observed in the fatigue test results described in Chapter 3. It is recalled that, in Chapter 3, the characteristic curves (obtained by statistical regression of the $S_{R,hs}$-N test data) for large and small (thick and thin walled) specimens seemed to indicate a size effect whereby the smaller specimens were characterised by longer fatigue live in comparison with the larger specimens. Subsequently, however, in comparing the characteristic curves of the test specimens to design curves in the specifications, a discrepancy was seen between the two. That is, the design curves did not predict correctly the magnitude of the size effect seen in the test results. In light of this discrepancy and, in light of the fact that the size correction applied presently in the design specifications [Zhao et al. 2000, IIW 2000] has a major influence on the calculated design lives of welded tubular joints, it is of interest to understand better this effect.

Chapter 5 comprises the following sections:

- **Section 5.2** : *Size or scale correction in fatigue*, describes two approaches that have been used in the past to study the size effect—a statistical approach and an analytical approach based on linear elastic fracture mechanics (LEFM);
- **Section 5.3** : *LEFM calculations in welded CHS K-joints*, details the procedure used in an analytical study based on numerical and LEFM methods to investigate the size effect in welded CHS K-joints;
- **Section 5.4** : *Size effect in welded CHS K-joints using analytical approach*, presents and discusses the results of the analytical study;
- **Section 5.5** : *Recommendations,* presents recommendations on the application of the size effect in the design of welded CHS K-joints;
- **Section 5.6** : *Conclusions*.

5.2 SIZE OR SCALE CORRECTION IN FATIGUE

5.2.1 General

To begin, some clarification is needed concerning the terminology used to describe the effect under consideration. In literature three terms are commonly employed: scale effect, thickness effect and size effect. “Scale” effect tends to imply that the joints have been proportionally scaled, which has often been the case in test programs investigating this phenomenon. “Thickness” effect, perhaps the most widely used term, makes reference to wall thickness of the failed member, which is largely seen as the variable with the most significant influence on this phenomenon. Lastly, “size” effect seems to be a more general term, which also encompasses differences in fatigue performance between non-proportionally scaled joints, where the size of the weld or attachment may also affect fatigue behaviour. For the remainder of this chapter the latter term, size effect, will be used, although in some instances specific reference will be made to scale and thickness.

As stated previously, in the majority of experimental investigations on size effect, the specimens were scaled proportionally. In many applications this is a reasonable scenario, where

the entire size of the detail or joint will increase relative to an increase in applied load. In tubular bridges, however, it was seen that along the length of a span the outside diameters of the tubular members are much more likely to remain constant, while the thicknesses of the brace and chord members will be adjusted to account for the changes in stress at different span locations. The bridge application is an example of non-proportional scaling, a scenario where not only the changing wall thickness of the fatigue critical member, but also the relative size of the attachment (brace) and the load ratio may affect the relative fatigue behaviour between joints.

It is recalled that three factors are generally cited, e.g. Marshall 1992, Orjasäter 1995, van Wingerde et al. 1997, Dijkstra and van Straalen 1997, as contributing to the size effect. They are summarised here based on Marshall 1992:

- The statistical size effect refers to the increased probability of having a significant initial flaw with an increase in stressed volume. This effect is well recognised in the design of castings, forgings and machine parts, however, in welded details without profile control, the effect seems to be overwhelmed by the virtual certainty of a severe notch occurring somewhere along the weld toe.
- The metallurgical or technological size effect implies that an increased plate size may result in a coarser grain structure, lower yield strength, higher residual stresses, increased risk of hydrogen cracking during fabrication and a lower notch toughness. However, these contributions to the overall size effect might be expected to saturate once the relevant parameters reach their worst case. As stated in Dijkstra and van Straalen 1997, it is expected that modern steel making will not result in a significant difference in steel quality between smaller and larger elements.
- The geometrical size effect refers to the through-thickness stress gradient that arises at geometrical discontinuities (e.g. notches) and/or due to bending and torsional loads, which can be addressed by stress analysis. Due to the presence of a steeper stress gradient, a grain at the surface of a small specimen will experience a lower strain than a grain at the surface of a thick specimen, for the same stress at the surface [Orjasäter 1995]. A simplified schematic illustrating the geometrical size effect for a welded joint is shown in Figure 5.1 where K_t is the stress concentration factor due to the local notch effects.

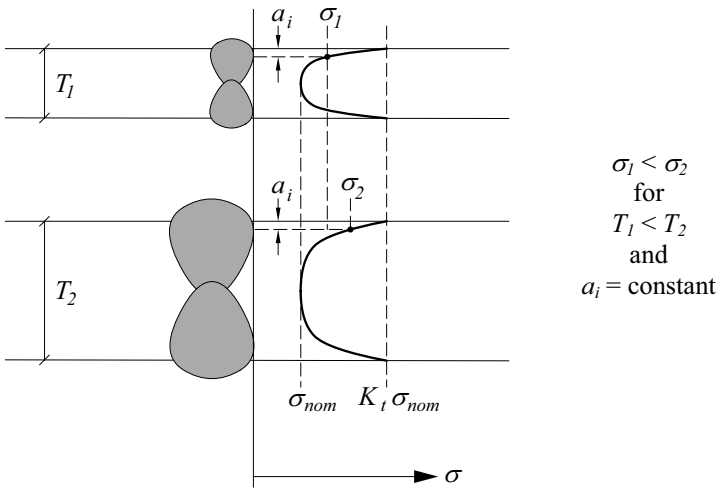

***Figure 5.1** - Simplified schematic showing geometrical size effect for welded butt joint [Berge and Webster 1987]*

As was seen in the brief review in Chapter 2, the size effect is a much studied aspect of welded joint fatigue. A huge push on research into the size effect in the 1980s provided convincing evidence—mostly experimental, but also analytical—of a trend for lower fatigue strength in thicker specimens of, for the most part, the same geometry, for both plate (transverse attachments) and tubular joints[1]. From a practical point of view, the confirmation of the existence of a size effect was reflected in the acceptance of a size correction in various design specifications and codes, e.g. BS 5400 1980, DEn 1984, ECCS 1985, AWS 1986. For tubular joints, the size correction adopted in the most recent design specifications [Zhao et al. 2000, IIW 2000] is one of the most severe corrections (i.e. implies a large reduction in fatigue strength as member thickness is increased), when compared with flat plate joints.

Below, two approaches are described that can be used to quantify the size effect. Section 5.2.2 examines the statistical study carried out to determine the current size correction for tubular joints. Section 5.2.3 describes an analytical study on the size correction carried out for flat plate joints and serves as an introduction to the analytical study on CHS K-joints presented in Section 5.3.

5.2.2 Statistical approach

The following describes and discusses the work [van Wingerde et al. 1997, Wardenier et al. 2002] that resulted in the size correction and the corresponding $S_{R,hs}$-N design curves in the most recent fatigue specifications for welded tubular joints [Zhao et al. 2000, IIW 2000]. The current $S_{R,hs}$-N design curves and design equations have been referred to throughout the present document, particularly in Chapter 3 where comparisons were made between these curves and the results from the test series. Also shown in Chapter 3 were the results of a large database of fatigue test results. It is this database that was used in the determination of the above-mentioned size correction and design curves.

In the determination of the size effect through the statistical analysis of a database of test results it is implied that the resulting design curves and size correction will contain all three influencing factors described in Section 5.2.1—statistical, metallurgical and geometrical size effects. The database of interest here was originally assembled and analysed in order to assess the fatigue design curves in the American Petroleum Institute Design Code [API 1993]. The results of this first study are reported in Dimitrakis and Lawrence 1994 and Dimitrakis et al. 1995. The database included results based on welded tubular joint fatigue test data available at that time. That included data from different types of joints (shapes), different laboratories, different failure locations in the joint, different load conditions, etc.

A subsequent updated version of the database was used in a statistical analysis by van Wingerde et al. 1997. For this study hot-spot stresses were re-evaluated using measured strains, recognised extrapolation procedures and stress-strain ratios. Furthermore, a consistent failure definition was taken where joint failure was taken as N_4: the number of cycles until complete loss of static joint strength. In cases where testing was stopped prior N_4 (for example, the tests described in Chapter 3, which were stopped at N_3, through-thickness cracking), linear extrapolation of the number of cycles was carried out.

1. Some exceptions to this were seen notably for longitudinal attachments (stress parallel to attachment length) where an increase in the thickness of the stressed main plate leads to an *increase* in fatigue life [Smith and Gurney 1986].

In the study by van Wingerde et al. the thickness of the failed member was taken as the most important factor influencing the fatigue behaviour between different joints. This is similar to the size correction first introduced by Gurney [Gurney 1981]. Contrary to Gurney who based the size correction for fatigue strength on the *nominal stress* away from the welded detail, however, van Wingerde et al. employed the hot-spot stress at the weld toe of the tubular joints. By doing this, they assumed that different joint geometries and dimensions can be examined together enabling the development of a single size correction factor for a large range of joints and critical joint locations.

In the manipulation of the database, van Wingerde et al. carried out separate analyses for joints between CHS member and joints between RHS members. For the analysis of welded CHS joints a data set of 173 joints was examined as a whole (T = all thicknesses) and also in sub sets ($T < 16$ mm, $T \geq 16$ mm) where joints were organised according to the wall thickness of the failed member. From this investigation a base $S_{R,hs}$-N design curve for $T = 16$ mm was determined using the characteristic curve at 1.64 s_N of the dependent variable ($logN$) below the mean with a forced slope of $m = 3.0$. The small number of standard deviations (as opposed to the more commonly used 2 s_N in the statistical analysis of test data) was justified by stating that 1.64 s_N corresponds to the calculation of a characteristic curve for an *infinite* number of data points. Along with the characteristic curve, a size correction was established based on a maximum reduction of scatter of the data in the N_4 direction. The following two relationships describe the size effect correction determined by van Wingerde et al.:

$$\frac{S_{R,\,hs,\,T}}{S_{R,\,hs,\,16}} = \left(\frac{16}{T}\right)^{n} \qquad n = 0.06 \cdot \log N_4 \qquad \text{for } 10^3 < N_4 < 5\text{x}10^6 \qquad [5.1]$$

$$\frac{S_{R,\,hs,\,T}}{S_{R,\,hs,\,16}} = \left(\frac{16}{T}\right)^{n} \qquad n = 0.402 \qquad \text{for } 5\text{x}10^6 < N_4 < 10^8 \qquad [5.2]$$

where,

$S_{R,hs,T}$: hot-spot stress range for tube wall thickness, T
$S_{R,hs,16}$: hot-spot stress range for reference tube wall thickness, $T_{ref} = 16$ mm
T : thickness of failed member
n : size effect exponent
N_4 : number of cycles to failure, joint has suffered a complete loss of strength

The right hand side of Equation 5.1 and Equation 5.2 can be recognised as part of Equation 2.4 and Equation 2.5, respectively, in Chapter 3 and is depicted in terms of $S_{R,hs}$-N curves in Figure 2.4. The equations above imply that for a failed member with a wall thickness greater than 16 mm, the fatigue strength of the member is expected to decrease with respect to the fatigue strength of a 16 mm thick member. Between $10^3 < N_4 < 5\text{x}10^6$ the size effect correction exponent, n, is dependent on the number of cycles at failure (N_4) thereby assuming that the size effect tends to be less pronounced for low cycle ranges [van der Vegte et al. 1989, Verheul and Wardenier 1989]. The inclusion of N_4 in the size correction exponent has the effect of rotating the design lines for different wall thicknesses around $N_4 = 1$ cycle. Between $5\text{x}10^6 < N_4 < 10^8$ the size effect correction exponent is taken as a constant value where $0.402 = 0.06 \log(5\text{x}10^6)$.

To provide a visual indication of the size effect correction defined by Equation 5.1 and Equation 5.2, the database in Figure 3.11 is re-plotted in Figure 5.2 in terms of corrected $S_{R,hs}$-N data. That is, using Equation 5.1 and Equation 5.2 the fatigue strengths of the joints in the

database, as well as the test joints from the present study, have each been corrected to represent the fatigue strength of an equivalent 16 mm thick joint. The sizes of the symbols in the figure have been chosen to represent approximately the original thickness of the joint (i.e. the symbol size increases with T). Also included in Figure 5.2 is the $S_{R,hs}$-N design curve obtained by van Wingerde et al. for $T = 16$ mm and subsequently adopted by the current design specifications (Detail Category 114) [Zhao 2000, IIW 2000]. As can be seen in this figure, the design line falls below most of the corrected points.

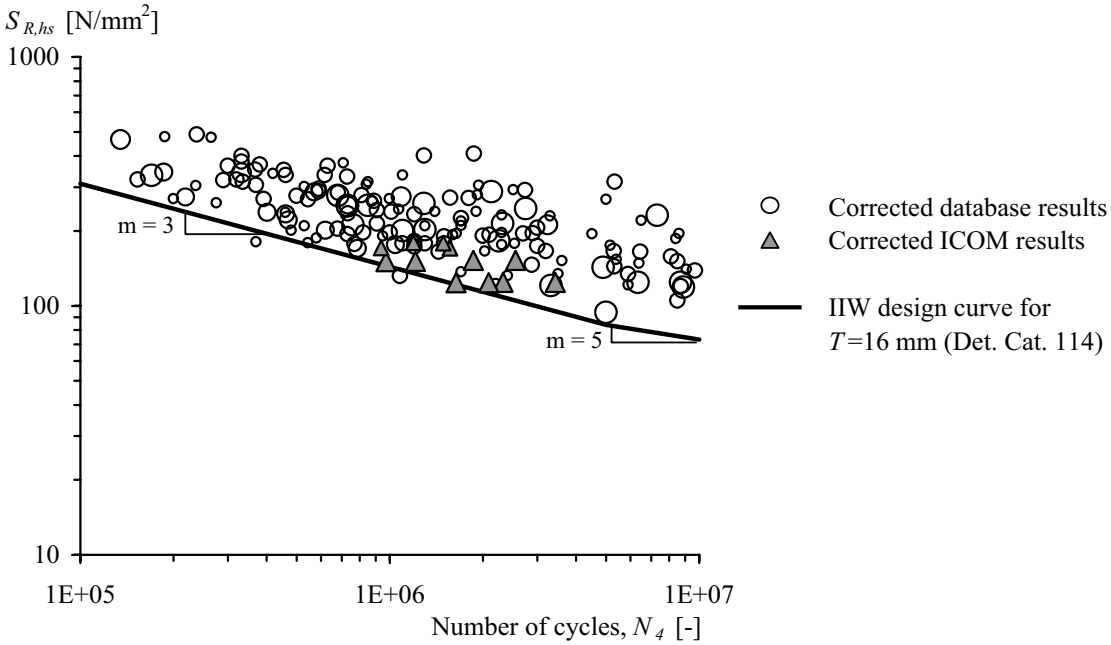

***Figure 5.2** - Base design curve and test results (stress range corrected for size effect) at reference thickness, T = 16 mm*

A comparison of Figure 3.11 and Figure 5.2 does show a reduction in the scatter of the data, thus proving, to some extent, the existence of a size effect dependent on the wall thickness of the failed member. In Schumacher 2003 the influence on the outcome of the range of wall thickness included in the statistical analysis is studied. It is shown that the size effect exponent, n, found using the database under examination is influenced significantly by the scatter in the data. Since a significant part of the scatter is due to the inclusion in the database of several variables such as different types of loading, different joint geometries, etc., and the lack of data for joint thicknesses relevant to bridge applications, the correction factor for the size effect obtained may not be a fair representation of the actual size effect for this specific application. It is therefore suggested that a more realistic correction factor could be found by restricting the range of application of the size correction formula.

5.2.3 Analytical approach

One main study that combined both experimental work and LEFM analysis was carried out by Maddox 1987. This study was concerned with the effect of plate thickness on the fatigue strength of steel plates (with transverse fillet welded attachments) under axial loading. Of particular interest to Maddox were the influences of overall joint geometry and main plate thickness, and for this reason, various combinations of attachment thickness, weld size and main plate thickness were considered in this study.

By investigating the size effect using LEFM methods, only the geometrical size effect (refer to Section 5.2.1) is considered. The geometrical size effect itself can be described as the resultant of three primary characteristics of the detail under examination [Berge and Webster 1987]:

- the magnitude of the stress concentration at the weld toe;
- the gradient of the stress along the plane of crack growth (stress distribution);
- the number of crack growth cycles through the steep stress gradient region, relative to the total number of cycles to failure.

All three characteristics are considered in an analysis of the size effect based on LEFM methods.

The basic joint geometry considered in experimental and theoretical analyses by Maddox is shown in Figure 5.3. As already stated, the detail investigated is an axially loaded plate with a welded non-load-carrying transverse attachment. By studying joints with different combinations of main plate thickness (B) and attachment footprint (L), Maddox was able to confirm the existence of a size effect for **proportionally scaled joints** of this particular detail. His characterisation of the proportional size effect was similar to that determined by Gurney 1981, although slightly less conservative.

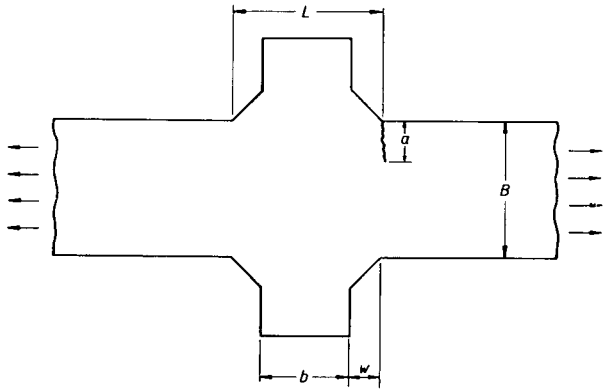

***Figure 5.3** - Detail used by Maddox 1987*

The results of the Maddox study (both experimental and analytical) are shown in Figure 5.4, where the thickness of the main plate is plotted against the relative fatigue strength at $2x10^6$ cycles (the relative fatigue strength is obtained by normalising the fatigue strength of all details at $2x10^6$ cycles with respect to a particular "base" detail—in this case a detail with plate thickness of $B = 13$ mm). In Figure 5.4 it can be seen that a second size effect was also demonstrated: in the case of **non-proportional scaling** (i.e. the size of the attachment footprint remains constant while the thickness of the main plate increases) the fatigue strength will remain approximately constant and *not* decrease with increasing main plate thickness.

The influence of the attachment thickness or, rather, the difference in fatigue strength between proportionally and non-proportionally scaled joints observed by Maddox lead to the suggestion of the alternative correction factor shown in Figure 5.4 (as opposed to the correction that had been proposed by Gurney 1981). A similar result based on statistical analysis of a database of plate detail results, was obtained by de Back et al. 1989, who also suggested that two different size correction factors be used to cover both proportional and non-proportional scaling between joints.

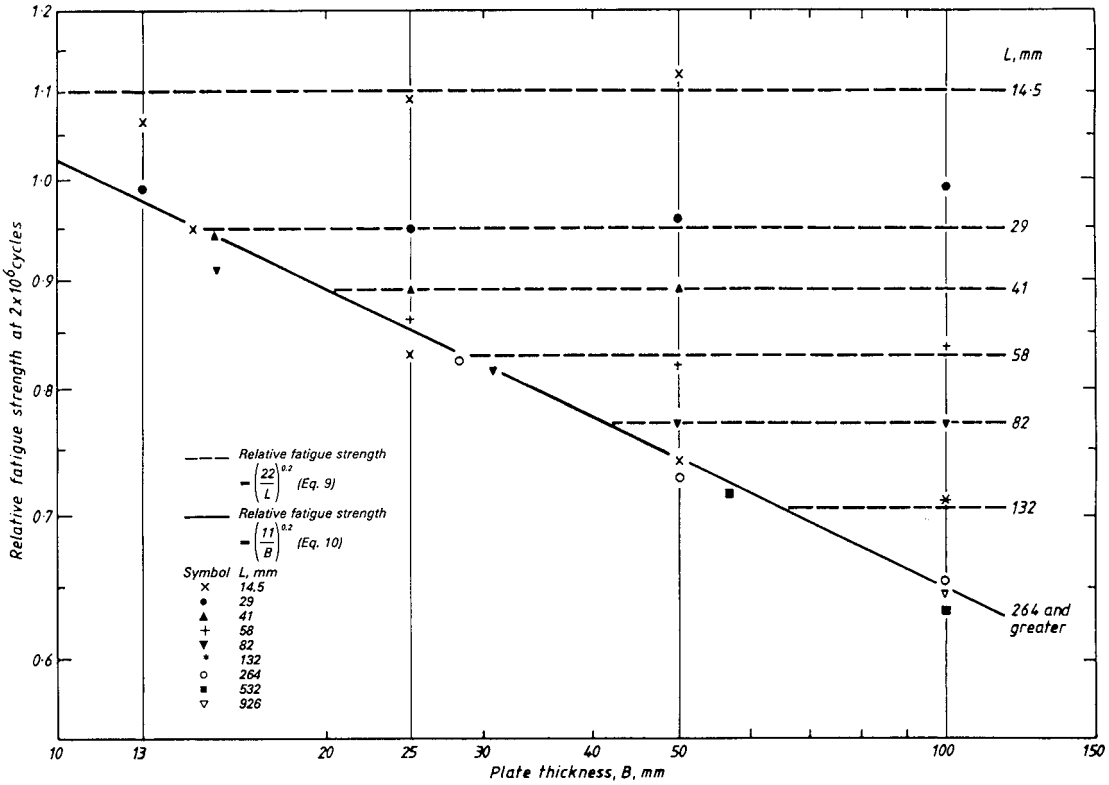

***Figure 5.4** - Results obtained by Maddox [Maddox 1987]*

The work by Maddox has been shown here to demonstrate the feasibility of using an analytical approach based on LEFM methods for investigating the size effect, in particular, in the separation of parameters that are perhaps more difficult to isolate in an experimental study. Based on this latter point, and the fact that welded tubular joint fatigue is a highly parameterised problematic, an analytical approach based on LEFM methods seems like an appropriate tool with which to investigate further the effect in these types of joints. Although numerous other studies, besides that of Maddox, have used the LEFM approach to investigate the size effect in plate details, e.g. Smith and Gurney 1986, Dijkstra et al. 1987, Bell 1987, Bremen 1989, Nussbaumer 1995, few LEFM studies on the size effect have been carried out specifically for tubular joints. This likely stems from the complexity of carrying out a linear elastic fracture mechanic calculations for this type of structural detail.

5.3 LEFM CALCULATIONS IN WELDED CHS K-JOINTS

In this section the method used in the present study to carry out linear elastic fracture mechanics calculations for welded CHS K-joints is described. The method will subsequently be used in Section 5.4 to study the relative fatigue lives, that is, the size effect, between joints with varying parameters (thickness, attachment size, non-dimensional parameters, loading, etc.). A main assumption made is that cracking predominantly occurs at joint Location 1, meaning only calculations of crack growth at Location 1 were carried out.

5.3.1 General

LEFM is a powerful tool for the calculation of the crack propagation part of the fatigue life of welded joints, as long as the crack size remains small compared to the element in which the crack progresses. Assuming a crack subjected to tensile of opening stresses, the crack growth

rate can be expressed as a relationship between the rate or crack propagation *da* / *dN* and the stress intensity factor (SIF) range, ΔK. In the case of stable crack propagation, the most commonly used function to describe this relationship is referred to as the Paris Law [Paris 1960]:

$$\frac{da}{dN} = C\Delta K^m \qquad [5.3]$$

where,

a : crack depth at deepest point in crack
N : number of cycles
ΔK : stress intensity factor range at *a*
C, *m* : material constants

A general way of expressing the stress intensity factor (SIF) range is the following:

$$\Delta K = \Delta\sigma\sqrt{\pi a} \cdot F_c F_f \qquad [5.4]$$

where,

$\Delta\sigma$: stress range due to constant amplitude cyclic loading
F_c : geometry correction factor for local stress gradient at the geometric discontinuity
F_f : correction factor for crack shape and the finite dimensions of the cracked body

In order for the geometry correction factor to (F_c) to be determined, the local stress gradient or, rather, the stress distribution along the anticipated crack path, $\sigma(x)$, must be known. Submodels were developed (refer to Schumacher 2003) in order to simulate the stress distribution throughout the thickness of the joint wall at the location where fatigue cracking is expected, as shown in Figure 5.5.

Figure 5.5 and Figure 5.6 illustrate schematically the crack path and local stress gradient in the form of the stress distribution perpendicular to an anticipated crack path. In Figure 5.6 the location of the assumed initial crack depth (initial defect), a_i, can be seen, as well as the rapid decrease in the stress that occurs as the crack moves away from the surface. As the depth of the crack increases, the stress continues to decrease, but at a gradually reducing rate. At a certain crack depth the decrease in stress becomes linear; this indicates that the crack has propagated out of the region influenced by the weld (geometric discontinuity) and is influenced only by the so-called structural stresses. In a flat plate detail such as that studied by Maddox (Section 5.2.3), the structural stress refers to the nominal stress due to an axial load applied to the main plate. In a tubular joint, the structural stress is a combination of the local shell bending stress, σ_b, and the membrane stress, σ_m, that is, the stress affected by the geometry of the joint, but not affected by the local weld geometry. According to this latter definition and recalling the definition given to the hot-spot stress, σ_{hs} (Section 2.2), it could be expected that the structural stress at the surface (where cracking occurs), σ_t, and the hot-spot stress are one and the same. It will be shown later, however, that this is not the case.

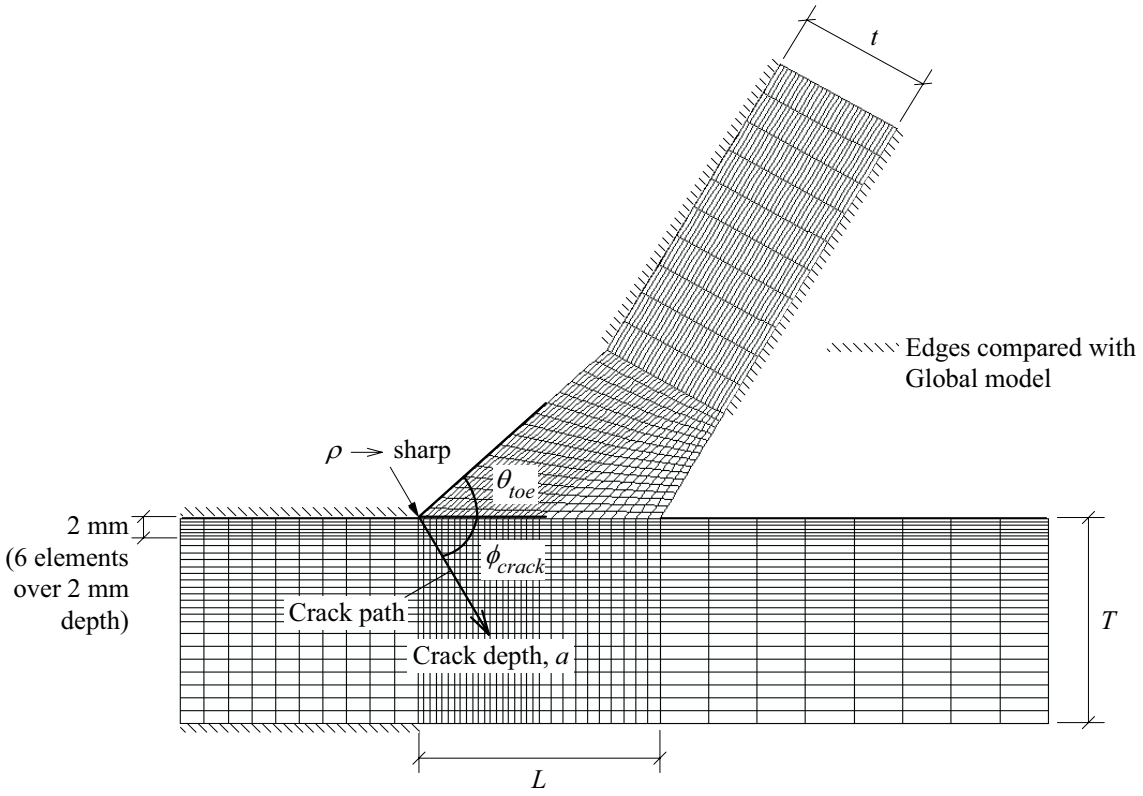

Figure 5.5 - *FEM submodel of local weld geometry and anticipated crack path at Location 1 in CHS K-joint*

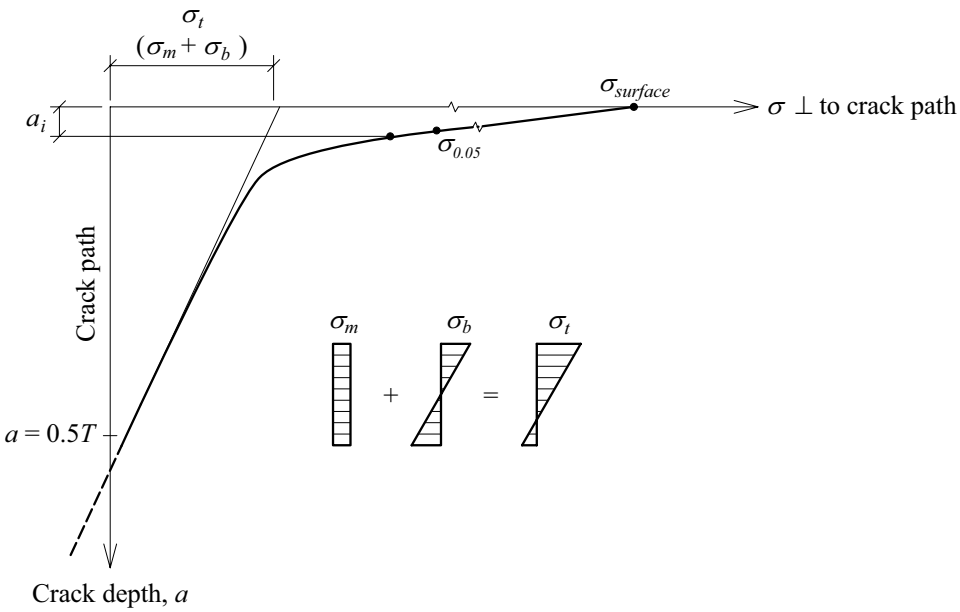

Figure 5.6 - *Stress distribution perpendicular anticipated crack path*

The stress distribution shown in Figure 5.6 is typical of stress distributions in tubular joints, which are characterised by high degrees of bending (DOB). The DOB refers to the linear portion of the stress distribution and can be defined in terms of the following relationship:

$$DOB = \frac{\sigma_b}{\sigma_m + \sigma_b} = \frac{\sigma_b}{\sigma_t} \quad [5.5]$$

where,

DOB : degree of bending
σ_b : shell bending stress
σ_m : membrane stress
σ_t : structural stress at the surface (bending stress + membrane stress)

For Location 1 in a welded CHS K-joint, the DOB is an indicator of the mode of loading, that is, the stress percentages in the brace and chord members. For example, for given joint parameters (β, γ, τ, etc.) at a high percentage of brace stress (of the total affecting the joint) a high DOB is expected, while at 100% chord stress a lower DOB will generally be seen.

5.3.2 Fatigue life calculations

Having determined the stress distribution along the anticipated crack path, it was desirable to carry out fatigue life calculations based on an integration of the relationships presented in Equation 5.3 and Equation 5.4, that is:

$$N = \int_{a_i}^{a_f} \frac{1}{C(\Delta\sigma\sqrt{\pi a} \cdot F_c F_f)} \mathrm{d}a \quad [5.6]$$

where,

N : number of load cycles needed to extend the crack from a_i to a_f
a_i : initial crack depth
a_f : final crack depth
a : crack depth
$\Delta\sigma$: cyclic stress range due to constant amplitude loading
F_c, F_f : correction factors
C, m : material constants

Fatigue life calculations will be used in Section 5.4 to determine relative fatigue strengths at Location 1 of different welded CHS K-joints. A verification of the proposed LEFM approach whereby fatigue life calculations of joint models tested in the laboratory are compared with measured values can be found in Schumacher 2003.

The methodology to determine the stress distribution along the anticipated crack path, $\sigma(x)$, was described briefly above. The correction factor F_f can then be obtained using an approximate calculation procedure developed by Albrecht and Yamada 1977 (described in Schumacher 2003). F_f corrects for the following parameters and characteristics of the cracked body (in comparison with the base case of a central crack in an infinite plate):

- the effects of a free surface;
- the finite width of the cracked body;
- the effects of an elliptical crack front;
- the shape of the crack, given in terms of the ratio between the crack depth (a) and the surface length ($2c$).

Several solutions have been proposed for the calculation of F_f ; the well-known and well-established solution proposed by Newman and Raju 1981 was retained for use here. For this solution, a relationship between crack depth and surface length—(a / T) versus (a / 2c), that is, the crack shape—must be assumed. The crack shape for the present fatigue life calculations was taken from literature (Burns et al. 1987, Dijkstra et al. 1987 and Kam et al. 1994].

5.4 SIZE EFFECT IN WELDED CHS K-JOINTS USING ANALYTICAL APPROACH

5.4.1 Scope of study

For the LEFM procedure that will be used in the analytical investigation of the size effect, it was seen in Section 5.3 that various assumptions were required. The fact that the following investigation will mainly be concerned with comparisons of calculated fatigue strengths, however, means that the assumptions are not critical in the results presented below.

Table 5.1 presents the joint models used in the analytical investigation on the size effect in welded CHS K-joints. It is seen that some of the joints used in the parametric investigation in Chapter 4 are employed again here; it is therefore a joint set with parameters typical to the bridge application (low γvalues). An explanation of the notation used for the joints is given in Section 4.4.2. Joints 1 to 9 represent three sets of proportionally scaled joints, while joints 10 to 18 represent a single set of non-proportionally scaled joints with varying member thicknesses and non-dimensional parameters. Test joints (from Chapter 3) are also included in Table 5.1 for completeness.

Along with the joint dimensions and non-dimensional parameters, Table 5.1 gives the normalised attachment length, L / T, weld angle, θ_{toe}, and weld root radius, ρ, for each joint. It is well-known that the latter two parameters have an influence on the fatigue strength of welded details [Berge and Webster 1987], however, they are kept constant and therefore not investigated in the present study. In Table 5.1, the normalised attachment length, L / T, can be seen to increase with increasing, τ.

In addition to the influence of proportional versus non-proportional scaling, the influence of the loading on the size effect was also examined. Three load cases were examined and they are shown in Table 5.2. Only axial loading was considered, which corresponds to the following stress scenarios in the members: 100% stress in the chord, 50% stress in the chord and 50% stress in the brace, 100% stress in the brace. Although it is unlikely that 100% load in either the chord or the brace will occur, the load cases have been chosen to represent the entire range of possible axial load scenarios.

Fatigue life calculations within the scope of an analytical investigation into the size effect have been carried out on a range of joint models. In the present section, the results of these calculations are presented and discussed. Most of the results will be presented in terms of the *relative fatigue strength*. It is recalled that this value refers to the stress (nominal stress, hot-spot stress or other) affecting the location of fatigue cracking, which would be required to obtain a fatigue life of 2×10^6 cycles, relative to the stress at the same location in a reference joint. As already seen in Figure 5.2 and Figure 5.4, the relative fatigue strength plotted against, for example, the thickness of the failed member, can give indications of the magnitude of the size effect between joints or details of differing thickness.

***Table 5.1** - Geometries and parameters of models used for size effect study*

		Model	D	T	d	t	θ	β	γ	τ	θ_{toe}	L/T	ρ
			[mm]				[-]					[-]	
Test		S31	168.3	12.5	88.9	8	60°	0.53	6.7	0.64	43°	1.12	0
		S21	273	20	139.7	12.5	60°	0.51	6.8	0.63	43°	1.03	0
Proportional scaling	1.	b5_73a	275	20	141	6	60°	0.51	6.9	0.30	50°	0.45	0
	2.	b5_73	508	37	260	11	60°	0.51	6.9	0.30	50°	0.45	0
	3.	b5_73b	824	60	422	18	60°	0.51	6.9	0.30	50°	0.45	0
	4.	b5_75a	275	20	141	10	60°	0.51	6.9	0.50	50°	0.76	0
	5.	b5_75	508	37	260	18.5	60°	0.51	6.9	0.50	50°	0.76	0
	6.	b5_75b	824	60	422	30	60°	0.51	6.9	0.50	50°	0.76	0
	7.	b5_77a	275	20	141	14	60°	0.51	6.9	0.70	50°	1.06	0
	8.	b5_77	508	37	260	26	60°	0.51	6.9	0.70	50°	1.06	0
	9.	b5_77b	824	60	422	42	60°	0.51	6.9	0.70	50°	1.06	0
Non-proportional scaling	10.	b5_43	508	60	260	18	60°	0.51	4.2	0.30	50°	0.45	0
	11.	b5_45	508	60	260	30	60°	0.51	4.2	0.50	50°	0.76	0
	12.	b5_47	508	60	260	42	60°	0.51	4.2	0.70	50°	1.06	0
	13.	b5_73	508	37	260	11	60°	0.51	6.9	0.30	50°	0.45	0
	14.	b5_75	508	37	260	18.5	60°	0.51	6.9	0.50	50°	0.76	0
	15.	b5_77	508	37	260	26	60°	0.51	6.9	0.70	50°	1.06	0
	16.	b5_123	508	20	260	6	60°	0.51	12.7	0.30	50°	0.45	0
	17.	b5_125	508	20	260	10	60°	0.51	12.7	0.50	50°	0.76	0
	18.	b5_127	508	20	260	14	60°	0.51	12.7	0.70	50°	1.06	0

***Table 5.2** - Load cases considered in size effect study*

Load case	Schematic	Designation	
Axial chord		σ_{ax_ch}	100% chord stress
Combined axial	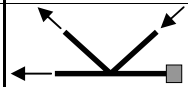	$\sigma_{ax\_ch} = \sigma_{ax\_br}$	50% chord stress, 50% brace stress
Balanced axial brace		σ_{ax_br}	100% brace stress

For the load cases considered, the results are divided into two main parts: an investigation into the size effect between proportionally scaled joints and an investigation into the size effect between non-proportionally scaled joints. It is recalled that the analytical study presented herein was only carried out for Location 1 of welded CHS K-joints. Fatigue life calculations were carried out for initial crack depths a_i = 0.2 mm and 0.4 mm; as similar trends (in terms of the

size effect) were seen for the two values, the results below are from calculations taking a_i = 0.2 mm. The crack growth constants were taken to be C = 2.0x10-13 and m = 3.0 according to Gurney 1979, the standard values for C-Mn steels.

5.4.2 Proportional scaling

The following results deal with models 1 to 9 in Figure 5.1. The same trends were seen between the three proportionally scaled joint sets (models 1-2-3, 4-5-6, 7-8-9) that is, every dimension has been proportionally scaled with the exception of θ_{toe} and ρ. For clarity, only results from a single set (e.g. b5_75a, b5_75, b5_75b, referred to as set b5_75) are shown in the following figures. Since it is the trends that are of primary interest, relative values are presented i.e. the results have been taken relative to one joint and one load case: b5_75a under 100% chord loading.

In Figure 5.7 the relative fatigue strengths of set b5_75 are compared in terms of nominal stress, σ_{nom}, and hot-spot stress, σ_{hs}. It is recalled that most of the work carried out on non-tubular, that is, welded plate joints has employed relative fatigue strength definitions based on nominal stress. Here, nominal stress refers to the axial stress in the loaded members (chord or brace), away from the joint. The left graph in Figure 5.7 indicates that between 100% stress in the chord and 100% stress in the brace, a large difference (approximately 35-40%) in the relative fatigue strength can occur. This is not surprising, since the nominal stress, by definition, ignores the stress concentrations caused by the different types of loading (all chord, or all brace, i.e. low DOB or high DOB).

These stress concentrations are taken into account, to some degree, by the hot-spot stress. In the right graph of Figure 5.7, where the relative fatigue strength based on hot-spot stress has been plotted, it can be seen that the difference in fatigue strength between the different load cases is significantly reduced (but not entirely eliminated).

In the case of proportional scaling and assuming a constant initial defect size, a_i, it is mainly the difference in main plate (or tube) thickness that will cause a difference in fatigue strength. In Figure 5.7 the size effect is shown in terms of the chord wall thickness. That is, for the same load case, the size effect is reflected in the decrease in relative fatigue strength with an exponential increase in the chord thickness (the member through which the crack propagates) of a proportionally scaled set of joints. A size effect exponent, n, can be found to describe this decrease, whereby:

$$\text{Relative fatigue strength} = \left(\frac{\text{Reference } T}{T \text{ considered}}\right)^n$$

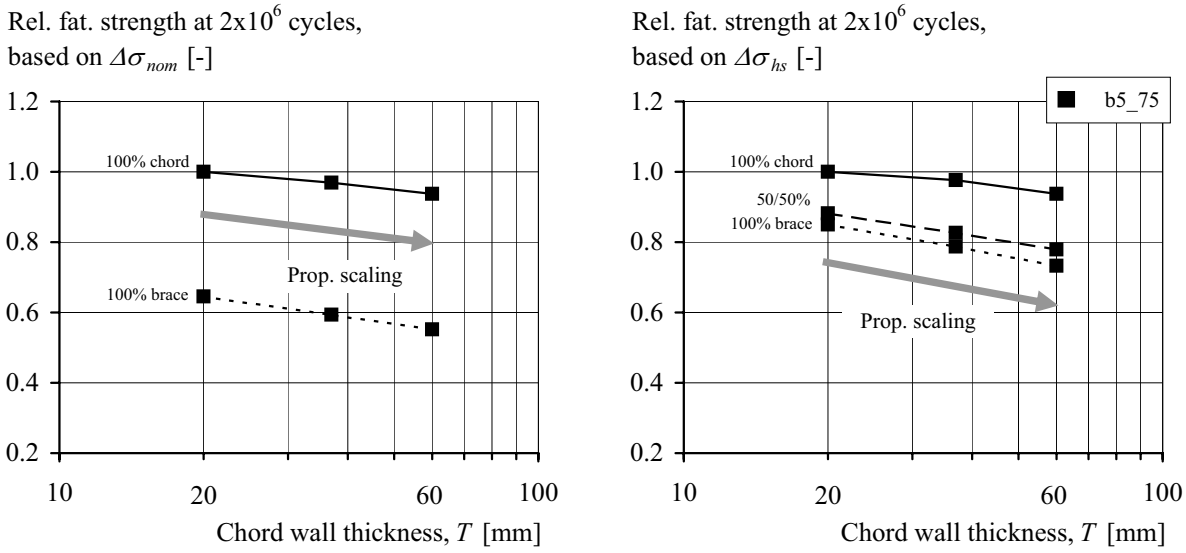

***Figure 5.7** - Calculated relative fatigue strength at 2x10^6 cycles based on nominal stress, $\Delta\sigma_{nom}$ (left) and hot-spot stress, $\Delta\sigma_{hs}$ (right)*

Size effect exponents have been calculated using both nominal stress and hot-spot stress based relative fatigue strength results, for an increase in chord wall thickness from 20 mm to 60 mm. They are shown for all three, proportionally scaled model sets (b5_73, b5_75, b5_77), and are presented in Table 5.3 and Table 5.4.

***Table 5.3** - Calculated size effect exponent, n, for proportional scaling, using $\Delta\sigma_{nom}$*

For an increase T = 20 mm to T = 60 mm

	100% chord stress		100% brace stress	
	n	SCF	*n*	SCF
b5_73	0.061	1.16	0.150	1.07
b5_75	0.059	1.33	0.143	1.75
b5_77	0.061	1.44	0.124	2.58

***Table 5.4** - Calculated size effect exponent, n, for proportional scaling, using $\Delta\sigma_{hs}$*

For an increase T = 20 mm to T = 60 mm

	100% chord stress		50%/50% ch/br		100% brace stress	
	n	SCF	*n*	SCF*	*n*	SCF
b5_73	0.060	1.16	0.122	1.12	0.140	1.07
b5_75	0.059	1.33	0.112	1.54	0.136	1.75
b5_77	0.056	1.44	0.110	2.01	0.128	2.58

* $SCF = 0.5 \cdot SCF_{1,ax\_br} + 0.5 \cdot SCF_{1,ax\_ch}$

Regarding Table 5.3 and Table 5.4, the following remarks can be made:

- The size effect exponent caused by the 100% chord stress load case is very small. This is likely due to the combination of a small stress concentration and a small stress gradient through the wall thickness due to a low DOB. This observation has been made by others,

e.g. Orjasäter 1995, who have investigated the relationship between the size effect exponent, *n*, and the stress concentration in a welded joint (at the weld toe). In general, it has been shown that *n* tends to decrease with a decreasing stress concentration. Care must be taken when making this assertion, however, since it is based on the assumption of an unchanged stress gradient. The case may also arise where the SCF is small, but there is nevertheless a certain size effect due to the gradient caused by a high DOB (this can be seen for joint b5_73 at 100% brace loading).

- When the brace is loaded (and as a result the DOB at the anticipated crack path increases, DOB > 0.5) it is seen that a more significant size effect exponent is found. Although still considerably lower than the values proposed by van Wingerde et al. 1997 ($n = 0.378$ at $N = 2\text{x}10^6$ cycles), the values for 50% brace / 50% chord loading and 100% brace loading correspond well with other similar studies (e.g. Dijkstra et al. 1987 who carried out finite element based LEFM calculations on a T-butt geometry and Lee and Bowness 2002 who carried out LEFM calculations on tubular joints using T-butt solutions).

Returning to Figure 5.7, a marked reduction in the difference in relative fatigue strengths occurred upon application of the hot-spot stress (as opposed to the nominal stress). But even a relative fatigue strength based on hot-spot stress cannot account entirely for the difference caused by the different load cases (as seen in the 15 to 20% difference in relative fatigue strengths for the different load cases at the same chord thickness). Furthermore, contrary to what is normally expected between low DOB (100% chord load) and high DOB (100% brace load) stress distributions—a higher stress gradient is generally considered more favourable in terms of fatigue life calculations—it is seen in Figure 5.7 that the 100% chord load case yields a higher relative fatigue strength value.

This phenomenon can be explained when considering the *structural stress* along the anticipated crack path. The structural stress, σ_t, was defined above as a combination of the local shell bending stress, σ_b, and membrane stresses, σ_m, that is, the stress affected by the geometry of the joint, but not affected by the local weld notch (refer to Figure 5.6). As was stated above, according to this latter definition and recalling the definition used for the hot-spot stress, it might be expected that the structural stress at the surface (where the crack initiates) and the hot-spot stress are one and the same. However, an examination in the models studied here, under different cases of loading, has shown that this is not the case.

The difference in hot-spot stress and structural stress or, rather, the effect of this difference on the relative fatigue strength can be explained by considering Figure 5.8. In this figure, the stress intensity factor is shown as a function of the crack depth for three different load cases. For each load case, the joint has been loaded to the same level of *hot-spot stress* at Location 1. Two major observations are made concerning Figure 5.8:

- For 100% brace stress, the SIF range decreases less rapidly in the first crucial distance of propagation (typically $a / T < 0.1$), which implies a crack that will propagate faster and thus contribute to a lower fatigue strength.

- Although in all three load cases the joint was loaded to the same hot-spot stress at the weld toe, the SIF ranges near the surface differ significantly.

This latter point is related, albeit indirectly, to the structural stress, which, at the location of crack initiation can be substantially different from the hot-spot stress as it is defined here (i.e. a

value extrapolated to the weld toe, along the joint surface, from a region outside the influence of local weld effects).

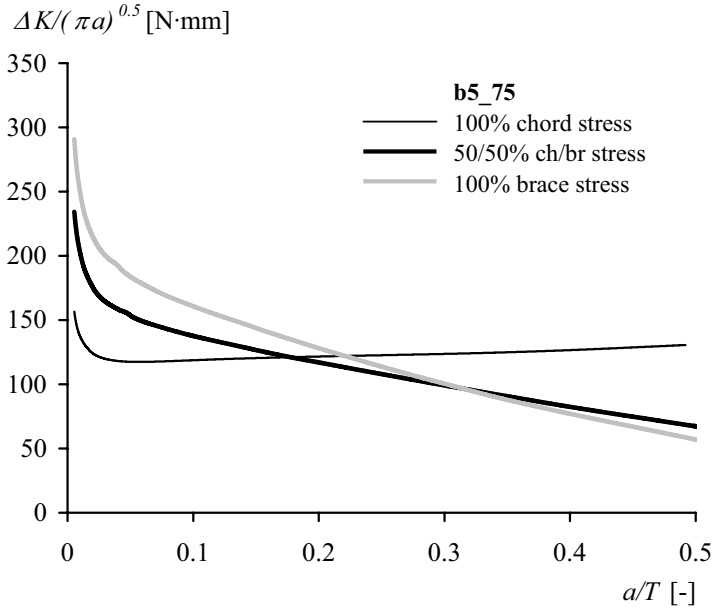

***Figure 5.8** - Stress intensity factor for joint b5_75 subjected to three types of loading, σ_{hs} = 150 N /mm^2*

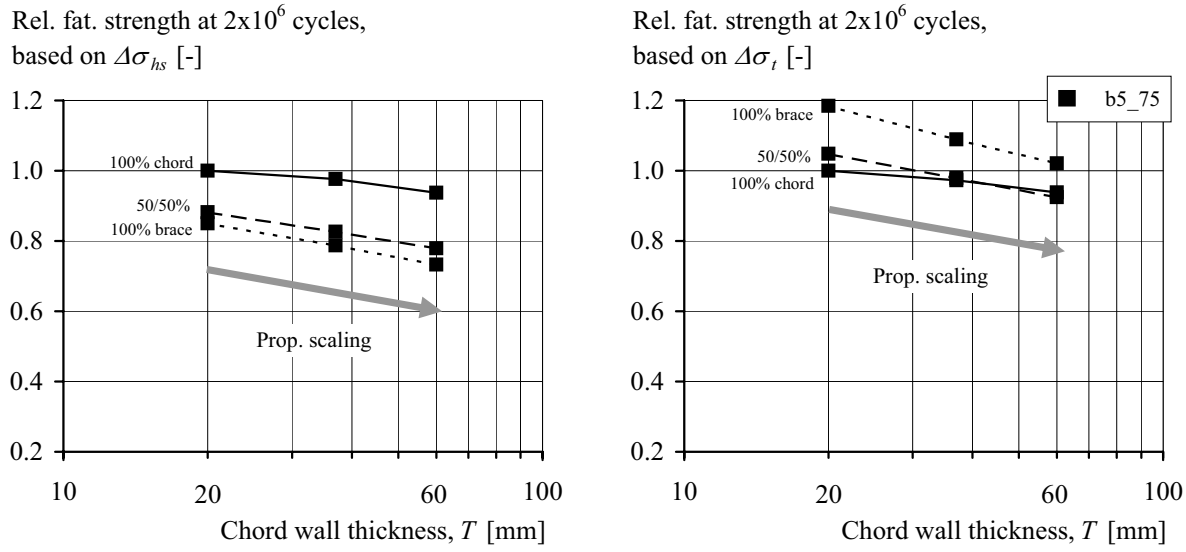

***Figure 5.9** - Calculated relative fatigue strength at 2x10^6 cycles based on hot-spot stress, σ_{nom} (left) and structural stress, σ_t (right)*

In light of this discrepancy between hot-spot stress and structural stress, it might by conjectured that calculation of the relative fatigue strength based on the structural stress (instead of the hot-spot stress) might, in fact, reduce even more (or even eliminate entirely) the differences between load cases seen in Figure 5.7. To test this hypothesis, Figure 5.9 compares the graph of relative fatigue strengths based on hot-spot stress seen above (Figure 5.7) with a graph for which the relative fatigue strengths have been calculated based on σ_t. While the differences between the lines for the different load cases are slightly smaller than for the hot-spot stress case, the

structural stress cannot account entirely for the overall effect caused by the loading. This is disappointing, but not surprising, since it too (like the hot-spot stress) is a single value, at a single location, which does not include the notion of the stress gradient through the thickness of the chord. Furthermore, both the structural stress and the hot-spot stress are values calculated on the *surface* of the joint (chord) and, therefore, are values that would be more logically associated with crack initiation than crack propagation.

Nevertheless, it is interesting to note that the definition of relative fatigue strength based on structural stress does lead to a more intuitive result between the different load cases. That is, the joints subjected to 100% brace stress (a higher DOB) display a higher relative fatigue life than the joints subjected to 100% chord stress (a lower DOB).

5.4.3 Non-proportional scaling

Non-proportional scaling can be interpreted in two ways. On one hand, when non-proportional scaling occurs and the main plate (or tube) thickness remains constant, in this case, virtually each dimension can vary with respect to the others and the stress concentration factor will differ between joints and cause a difference in fatigue strength. This includes the case, for example, of two joints with the same chord thickness, but different brace-to-chord thickness ratios (τ), however, it may also include joints with the same chord thickness, but different chord slenderness values (γ) or brace-to-chord diameter values (β). On the other hand, non-proportional scaling can also imply a situation where the main plate (or tube) thickness varies (as well as other dimensions). In this latter case, the size effect is the result of many different factors.

Figure 5.10 illustrates the effects of non-proportional scaling in terms of the non-dimensional parameter τ. Relative fatigue strengths from models 10-11-12, 13-14-15 and 16,17,18 from Table 5.1 are shown (calculated based hot-spot stress). Values have been taken relative to the fatigue strength of model b5_75 under 100% brace loading.

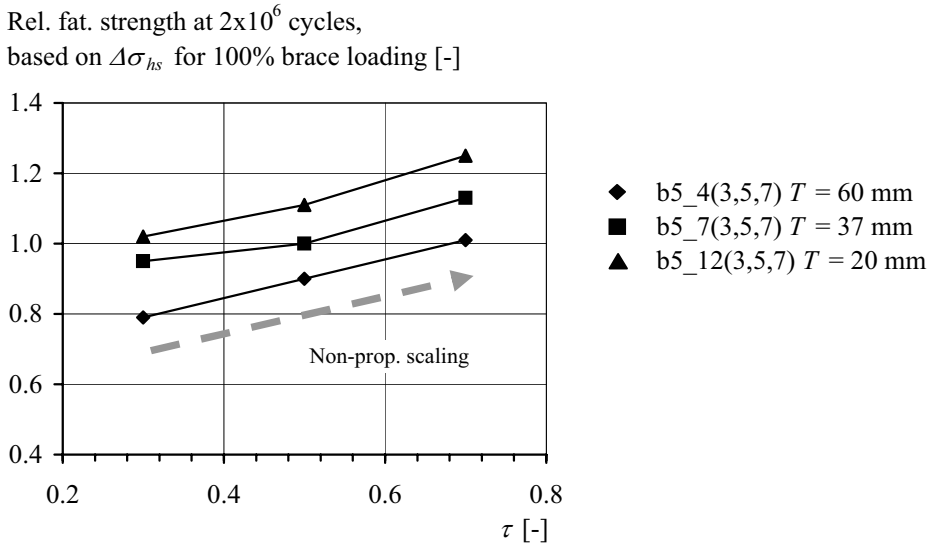

***Figure 5.10** - Influence of τ on relative fatigue strength in terms of chord thickness (left) and in terms of τ (right)*

Most notable in Figure 5.10 is the *increase* in relative fatigue strength with an increase in τ. This increase is interesting, because it seems to contradict the assumption made by van Wingerde et

al. 1997 that the hot-spot stress is, in fact, able to account for the differences between non-proportionally scaled joints (thus their concentration on the thickness, *T*, as the main size effect parameter). As already alluded to above, this is not surprising, since the hot-spot stress—a 2-dimensional surface stress—is being used to quantify a 3-dimensional phenomenon.

As for the size effect relationship found earlier for proportionally scaled joints, a similar relationship could be established based on the non-dimensional joint parameter, τ, for example:

$$\text{Relative fatigue strength} = \left(\frac{\text{Reference } \tau}{\tau \text{ considered}}\right)^{n'}$$

Exponents for non-proportional scaling, *n'*, for all three load cases are given in Table 5.5. The negative exponent indicates an increase in the relative fatigue strength over the range of τ considered (0.3-0.7). Although the magnitude of the two exponents n and n' (Table 5.4 and Table 5.5) are not directly comparable (since they are not applied to the same base) it is significant that different contributing factors to the overall size effect (proportional and non-proportional scaling) can influence the fatigue strength of several joints in a completely different manner.

Table 5.5 - *Calculated size effect exponent, n', for non-proportional scaling, using* $\Delta\sigma_{hs}$

For an increase τ = 0.3 to τ = 0.7	100% chord stress	50%/50% ch/br	100% brace stress
	n'	n'	n'
T = 20 mm	-0.098	-0.235	-0.240
T = 37 mm	-0.094	-0.142	-0.205
T = 60 mm	-0.093	-0.169	-0.290

In fact, from the results of the fatigue life calculations carried out on *all* joint models listed in Table 5.1 and for the three load cases illustrated in Table 5.2, other trends, involving different parameters, can be seen.

To obtain an idea of what this means in more general terms, relative fatigue strengths from models 10 to 18 as well as the test joint model are plotted in Figure 5.11. The calculated values include fatigue strengths due to all three load cases; in this case, all results have been taken relative to the joint b5_125 (T = 20 mm) subjected to a 50/50% brace/chord loading. Also shown in the figure are design lines representing size correction factors of $n = 0.378$ [van Wingerde et al. 1997] and $n = 0.25$ [Gurney 1979] also adjusted to the fatigue strength of joint b5_125. It is noted that relative fatigue strengths are plotted against the thickness of the fatigue critical member, i.e. the chord.

When considered as a whole, the results in Figure 5.11 are telling: any semblance of a size effect seen previously has been largely over-ridden by scatter due to the combination of numerous joint parameters (thickness, loading, τ, γ), each with its own effect on the fatigue strength of the joints. Although there appears to be an effect of increased scatter with an increase in the thickness of the critical member, this is more likely due to the fact that the non-dimensional joint parameters are not evenly represented at all values of wall thickness.

On the other hand, when only the results from the 50/50% and 100% brace load cases are considered (solid data points) the same magnitude of size effect as seen earlier (n = 0.12-0.15,

where *n* is in reference to the failed wall thickness) can be imagined. Ignoring the 100% chord load data is perhaps a more reasonable representation of the results, since in reality (for example, in a truss girder), a certain percentage of load will always be present in the brace members (typically implying a DOB of 0.5 or higher).

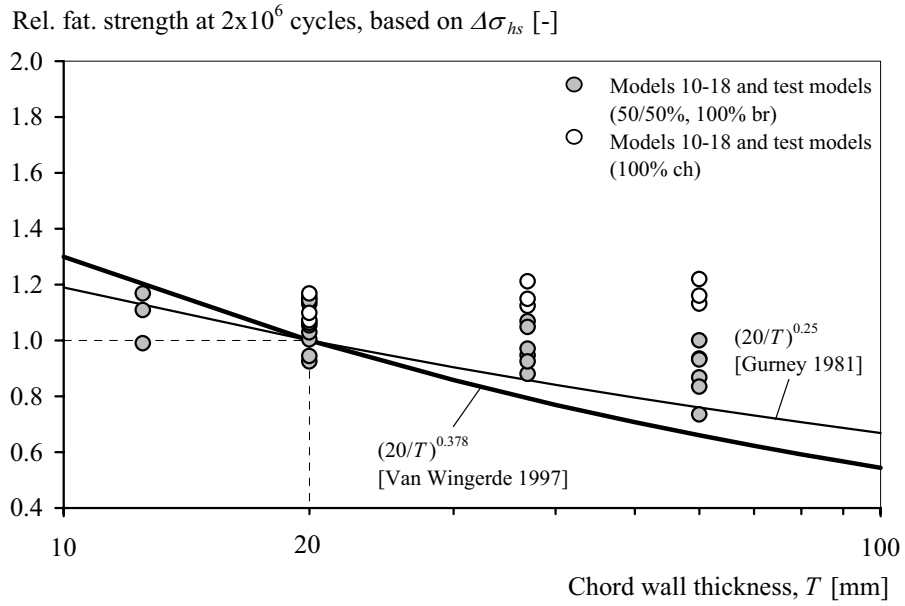

***Figure 5.11** - Calculated relative fatigue strength at 2x10^6 cycles based on hot-spot stress, σ_{hs}*

To complicate matters, it is recalled that the joint model set used in the present analytical investigation of size effect in welded CHS K-joints is considerably simplified. Simplification was necessary to isolate certain parameters of interest and to study their influence on the size effect, however, in order to propose a broadly applicable correction factor, *all* influencing parameters must be taken into account. Many of the parameters that influence the size effect (but that are not taken into account by the analytical investigation) have already been mentioned above; others have not been discussed explicitly, but are well-documented in the literature, they include:

- other joint parameters (e.g. θ, β, γ> 12.0), other joint failure locations, joint types, other load types and combination (notably, bending moment load, not studied above);
- the effect of crack initiation, the effect of load shedding (at greater crack depths);
- the effect of weld angle (θ_{toe}) and a constant (or variable) notch root radius (ρ);
- the effect of residual stresses, post weld heat treatment and weld improvement.

5.4.4 Final remarks

The analytical study on size effect that was presented in this chapter is the first of its kind carried out specifically for welded tubular joints. Although various trends were demonstrated and quantified, the problem nevertheless remains extremely parameterised and sensitive to small differences, making it difficult, at this stage, to suggest a single (or several) comprehensive correction factor to describe the size effect phenomenon. Of the results that have been seen, however, two points seem particularly relevant to the application of welded CHS joints in bridges:

- Low stress concentration factors seem to contribute to a lower size effect for joints of different thickness. Considering the results from Chapter 4—where it was found that the SCFs for K-joints with non-dimensional parameters typical to bridges are relatively low—this could be an advantageous characteristic in terms of this effect.
- A large degree of scatter due to a large range of parameters included in size effect data can result in a conservative size effect correction factor. Ideally, the size effect needs to be addressed within the framework of the specific application within which it will be used, e.g. bridges, offshore, cranes.

Obviously, the latter is a proposal that requires more work whereby a systematic approach—both experimental and analytical—is taken and whereby a realistic and justified solution can be reached, resulting in more economical designs. The groundwork for this work has been started here: for example, results from the analytical study can be used to design an experimental program for which the most relevant parameters (or parameter combinations) are tested and whereby a clearer insight into the effect of certain parameters on the size effect can be obtained.

Nevertheless, a recommendation for the bridge application that is based on our current knowledge is given in the next section.

5.5 RECOMMENDATIONS

It is worth noting that for none of the results presented in this chapter—statistical nor analytical—did it seem justified to apply a size correction factor greater than the factor proposed by Gurney (n = 0.25) [Gurney 1979]. In fact, in numerous instances, it was even deemed reasonable to deduce a size effect correction significantly inferior to that of Gurney.

Based on this reason and using the results obtained in Chapter 3, the following $S_{R,hs}$-N design curves are recommended for use in combination with the determination of SCF values presented in Chapter 4. These curves can be expressed as:

$$\log(S_{R,hs}) = \frac{1}{3}(12.010 - \log(N_4)) + \left(0.25 \cdot \log\left(\frac{20}{T}\right)\right) \quad \text{for } 10^3 < N_4 < 5\text{x}10^6 \qquad [5.7]$$

$$\log(S_{R,hs}) = \frac{1}{5}(15.551 - \log(N_4)) + \left(0.25 \cdot \log\left(\frac{20}{T}\right)\right) \quad \text{for } 5\text{x}10^6 < N_4 < 10^8 \qquad [5.8]$$

where,

$S_{R,hs}$: hot-spot stress range
N_4 : number of cycles to failure, joint has suffered a complete loss of strength
T : thickness of failed member, *for 12.5 mm $\leq T \leq$ 60 mm*

The design curves described by Equation 5.7 and Equation 5.8 are shown in Figure 5.12. A reference curve characterised by $S_{R,hs}$ = 80 N/mm^2 at 2x10^6 cycles, that is, a Detail Category 80, is taken for T_{ref} = 20 mm. This value accounts for the standard set of design curves found in fatigue specifications (e.g. SIA 263 2003, Eurocode 3 2002) and is the closest detail category to fall below the test results obtained in Chapter 3. Furthermore, it is important to notice that, between 20 mm (the reference thickness) and 12.5 mm, the fatigue resistance *increases* with *decreasing* member thickness.

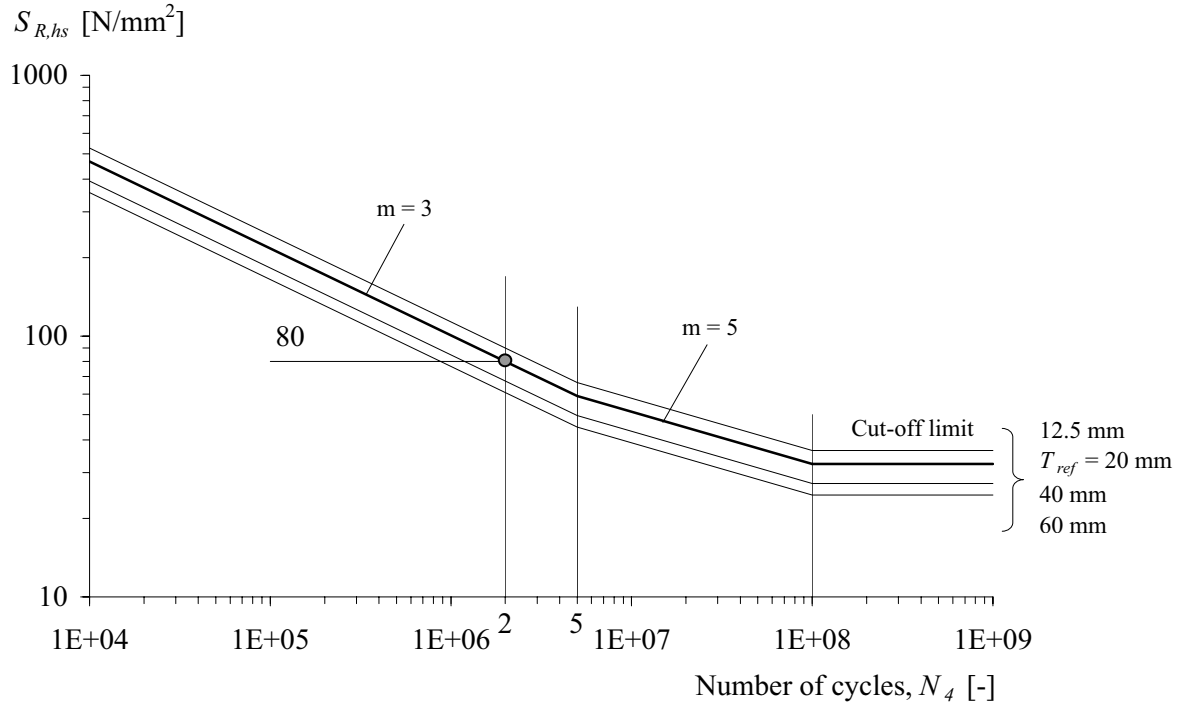

Figure 5.12 - *Recommended $S_{R,hs}$-N design curves for welded CHS joints*

5.6 CONCLUSIONS

The so-called size effect has been examined, using both a statistical and an analytical approach. The statistical approach was based on the regression of a large database of welded CHS joint fatigue test results. The analytical approach was carried out using a validated LEFM fatigue life calculation procedure. The following main conclusions can be drawn from the work presented in this chapter:

Statistical approach

- In a statistical approach to the size effect, using as input a large database of welded CHS joint fatigue test results, a regression analysis shows a reduction in the fatigue strength dependent on the wall thickness of the failed member.
- The inclusion of many different parameters in this database, the related large degree of scatter in the data and the lack of data for joint thicknesses relevant to bridge applications make it questionable whether the correction factor for the size effect, *n*, obtained previously from this database, is a fair representation of the actual size effect phenomenon, in particular for bridge applications.

Analytical approach

- Comparisons between proportionally scaled CHS joints show that an increase in chord wall thickness (the member through which the crack propagates) results in a decrease in the calculated relative fatigue strength of the joint. It is seen that the magnitude of the size effect is influenced by the loading applied to the joint (degree of bending) and the magnitude of the stress concentration at the location of cracking.
- In terms of non-proportional scaling the relative fatigue strength between joints is influenced by non-dimensional parameters such as $\tau(t / T)$.

- Based on current knowledge, the use of a EN1993-1-9 [Eurocode 3 2002] fatigue class 80 (for a reference case of $T = 20$ mm) is recommended, in conjunction with a size effect exponent $n = 0.25$ for the bridge application.

6 DESIGN GRAPHS AND EXAMPLES

6.1 INTRODUCTION

The results, analysis and discussion presented in the previous chapters make it clear that there are many factors influencing the fatigue behaviour of welded CHS joints—it is a complex problem. Nevertheless, a designer needs guidelines that, on one hand, do not completely bury the complexity of the problem, while, on the other hand, provide the information with which economical structures can be safely and intuitively designed.

This chapter will build on a concept introduced earlier (Section 4.6), that is, the total stress concentration factor, SCF_{total}, where it is recalled that the SCF_{total} was presented previously for two load scenarios in a continuous bridge span. Chapter 6 is composed of the following sections:

- **Section 6.2** : *Total joint SCF, SCF_{total}*, describes a graphical approach to the calculation of SCF_{total} for a complete range of load scenarios;
- **Section 6.3** : *Presentation of SCF_{total} envelopes*, presents SCF_{total} envelopes for the joints examined in the present study;
- **Section 6.4** : *Worked design example*, presents a brief example demonstrating the application of the SCF_{total} to the design of actual welded CHS K-joints;
- **Section 6.5** : *Conclusions*.

6.2 TOTAL JOINT SCF, SCF_{total}

6.2.1 SCF_{total} for range of load scenarios

In Chapter 4, Equation 4.7, the definition for SCF_{total} at a particular location in the joint, Location *i*, was given as:

$$SCF_{total,i} = \frac{\Delta\sigma_{hs,i}}{\Delta\sigma_{total\ nom}} \qquad [6.1]$$

that is,

$$SCF_{total,i} = \frac{\Delta\sigma_{hs,i}}{\Delta\sigma_{nom\_br} + \Delta\sigma_{nom\_ch}} \qquad [6.2]$$

where,

$SCF_{total,i}$: total SCF at joint Location *i* due to combined loading
$\Delta\sigma_{hs,i}$: hot-spot stress range at joint Location *i*
$\Delta\sigma_{total\ nom}$: total nominal stress range affecting the joint
$\Delta\sigma_{nom\_br}$: total nominal stress range in the tension brace
$\Delta\sigma_{nom\_ch}$: total nominal stress range in the chord

For the full development of Equation 6.1 and Equation 6.2 the reader is referred to Section 4.6. It is recalled that the denominator in Equation 6.2 implies a scalar superposition of member stress ranges; the fact that the stresses act in different directions is accounted for by individual SCFs. In order to demonstrate the concept of a SCF_{total} for a complete load scenario range, the same stress partitioning in the members is taken as was used in Section 4.6. It is recalled that

this partitioning in the members reflects the ratio of stresses due to axial load and in-plane bending in the brace and chord members recommended in the current design specifications [Zhao et al. 2000, IIW 2000]. For the case in Section 4.6 the total nominal stress range in the braces, $\Delta\sigma_{nom\_br}$, consists of 75% axial stress ($\Delta\sigma_{ax\_br}$) and 25% in-plane bending moment stress ($\Delta\sigma_{ipb\_br}$), while the total nominal stress range in the chord, $\Delta\sigma_{nom\_ch}$, consists of 65% axial stress ($\Delta\sigma_{ax\_ch}$) and 35% in-plane bending moment stress ($\Delta\sigma_{ipb\_ch}$). It is important to note, however, that this particular partitioning of stresses is only a choice made for demonstration purposes. As will be shown in the next section, Section 6.3, it is entirely possible that different partitioning schemes be used. This will not, however, alter the basic ideas presented here.

The SCF_{total} values in Section 4.6 were presented for two load scenarios. Each load scenario was defined by a combination of two stress components that make up the total nominal stress range, $\Delta\sigma_{total\ nom}$ ($\Delta\sigma_{total\ nom} = \Delta\sigma_{nom\_br} + \Delta\sigma_{nom\_ch}$). For example, it was seen that in Load scenario 1, 80% of $\Delta\sigma_{total\ nom}$ affecting the joint was due to the tension brace load, while the other 20% was due to the chord load.

It is, of course, likely that many other combinations of brace and chord stress will arise along a typical bridge span and it is therefore desirable to find a method of presenting the total stress concentration factor for a range of brace stress (or chord stress) percentages.

In Figure 6.1 and Figure 6.2, values of SCF_{total} have been calculated for two of the K-joint models studied in Chapter 4, b5_43 and b5_127. The SCF_{total} has been calculated for the six most critical (in terms of hot-spot stress) joint locations over a range of brace stress percentages, from 0% (implying that only the chord is loaded) to 100% (implying that only the braces are loaded).

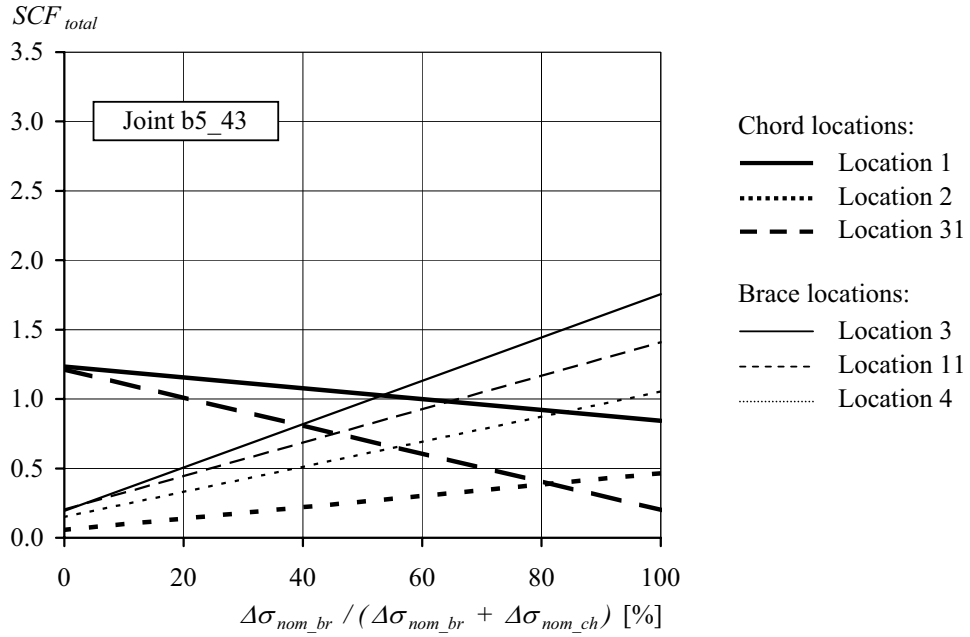

***Figure 6.1** - SCF_{total} calculated for Model b5_43 over range of brace stress percentages*

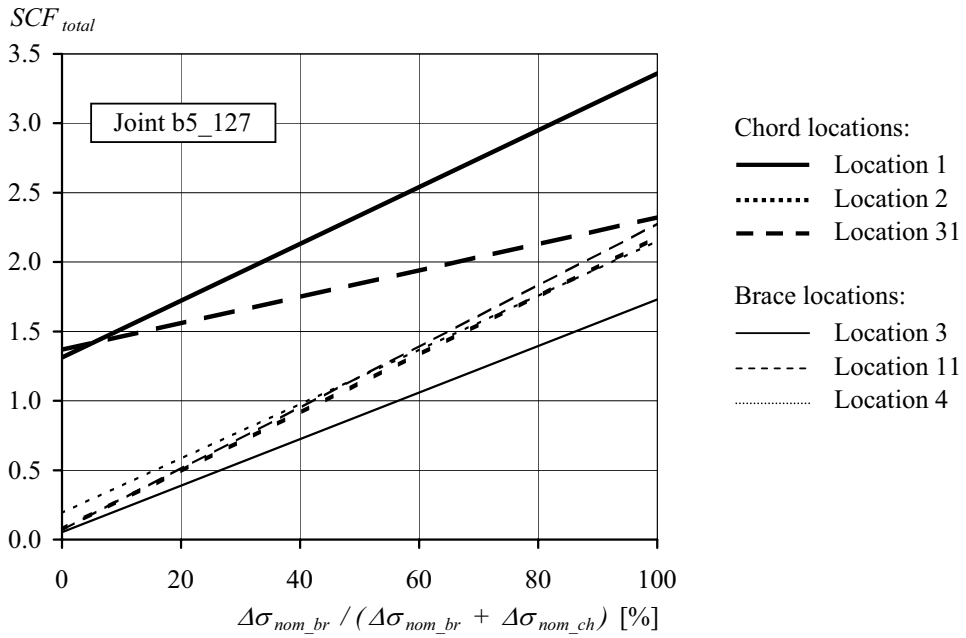

Figure 6.2 - *SCF_{total} calculated for Model b5_127 over range of brace stress percentages*

The SCF_{total} lines in Figure 6.1 and Figure 6.2 show that, depending on the joint and the location in the joint, the total stress concentration can either decrease from a maximum at 0% brace stress to a minimum at 100% brace or vice versa; as expected, the SCF_{total} for brace locations is almost or equal to zero at 0% brace stress. The two joints that were chosen to illustrate the concept of a SCF_{total} over a range of stress percentages are representative of the trends that will be seen later in the chapter. From a design point of view, the figures give a clear indication of what locations on the joint are characterised by the highest SCF_{total} values and thus the highest hot-spot stress ranges, $\Delta\sigma_{hs}$, for a particular brace stress percentage. In fact, for joints b5_43 and b5_127, there exist clearly definable boundaries of maximum SCF_{total}, whereby the information necessary for design, for those particular joints, can be reduced to a maximum SCF_{total} envelope, consisting of either a single line or a two intersecting lines as seen in Figure 6.3. SCF_{total} envelopes will be presented for a range of joints in Section 6.3. It should be noted that, although indicated in Figure 6.3 for clarity, subsequent presentation of the SCF_{total} envelopes will no longer specify the precise crack locations (1, 11, 2, 3, etc.), rather only the maximum values of SCF_{total} in the brace and chord will be given.

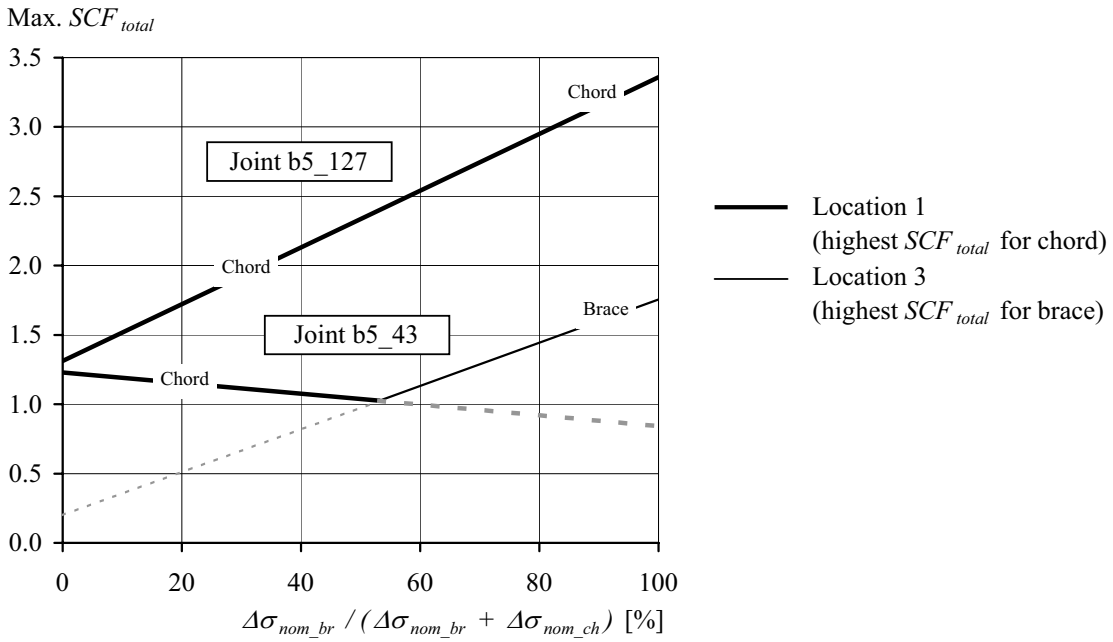

***Figure 6.3** - Maximum SCF_{total} envelopes for b5_43 and b5_127*

6.2.2 Partial inclusion of size correction

In Figure 6.3 it can be seen that, for some joints, the maximum SCF_{total} is either in the chord or in the brace depending on the percentage of brace stress affecting the joint. For these joints, (assuming the size effect is accounted for using the method in the current design specification, in the sense that the size correction depends on the wall thickness of the critical member) the hot-spot stresses in both the brace and chord must be verified separately, against their respective $S_{R,hs}$-N resistance curves: $S_{R,hs,t}$ -N for the brace and $S_{R,hs,T}$ -N for the chord.

A more practical solution is envisaged wherein the ratio of the size effect corrections for the brace and the chord is integrated in the SCF_{total} and the verification of hot-spot stress is subsequently carried out with reference to a single $S_{R,hs}$-N curve for both the brace and the chord. This so-called partial integration of the size effect can be explained by recalling the following relationship quantifying the size effect correction for the brace (Equation 6.3) and chord (Equation 6.4):

$$\frac{S_{R,\,hs,\,t}}{S_{R,\,hs,\,16}} = \left(\frac{20}{t}\right)^{n} \qquad [6.3]$$

$$\frac{S_{R,\,hs,\,T}}{S_{R,\,hs,\,16}} = \left(\frac{20}{T}\right)^{n} \qquad [6.4]$$

where,

$S_{R,hs,t}$: hot-spot stress range in *brace*
$S_{R,hs,T}$: hot-spot stress range in *chord*
$S_{R,hs,16}$: hot-spot stress range with wall thickness of failed member = 20 mm
t : thickness of failed brace member
T : thickness of failed chord member
n : size effect exponent, taken as n = 0.25 (see recommendation in Section 5.5)

Dividing Equation 6.3 by Equation 6.4 it is seen that the ratio of hot-spot stress in the brace to the hot-spot stress in the chord can be related to the joint wall thickness parameter, τ:

$$\frac{S_{R,\,hs,\,t}}{S_{R,\,hs,\,T}} = \left(\frac{T}{t}\right)^n = \left(\frac{1}{\tau}\right)^n \qquad [6.5]$$

$$S_{R,\,hs,\,t} = \tau^{-n} \cdot S_{R,hs,\,T} \qquad [6.6]$$

Remembering that in the design of a joint using the $S_{R,hs}$-N curve approach the following inequality must be respected:

$$\Delta\sigma_{hs\ (brace)} \leq S_{R,\,hs,\,t} \quad \text{(at the same number of cycles)} \qquad [6.7]$$

and recalling in Equation 4.7 that,

$$\Delta\sigma_{hs,\,i} = SCF_{total,\,i} \cdot \Delta\sigma_{total\ nom} \qquad [6.8]$$

it can be concluded that,

$$\tau^n \cdot SCF_{total\ (brace)} \cdot \Delta\sigma_{total\ nom} \leq S_{R,hs,\,T} \qquad [6.9]$$

where,

$\Delta\sigma_{hs\ (brace)}$	: design hot-spot stress range at critical *brace* location
τ	: brace-chord thickness ratio (t / T)
$SCF_{total\ (brace)}$	: SCF at brace location due to combined loading
$\Delta\sigma_{total\ nom}$	: total nominal stress range affecting the joint

The relationship in Equation 6.9 implies that the SCF_{total} for the brace locations, when combined with a relative size effect correction (τ^n) can be compared directly to the SCF_{total} for the chord locations, since the subsequent verification of hot-spot stresses will be carried out with reference to the same $S_{R,hs}$-N curve, namely $S_{R,hs,T}$-N.

The effect of Equation 6.9 on SCF_{total} values for brace locations is illustrated in Figure 6.4 for joint models b5_43 and b5_127. Logically, no size effect is seen for joint b5_127 since the chord location is critical at all percentages of brace stress. For joint b5_43, however, a significant shift in the brace envelope is seen. With the size effect partially taken into account, it is possible to calculate the hot-spot stress at a single location (either on the chord or on the brace) for comparison with a single $S_{R,hs}$-N design curve ($S_{R,hs,T}$-N).

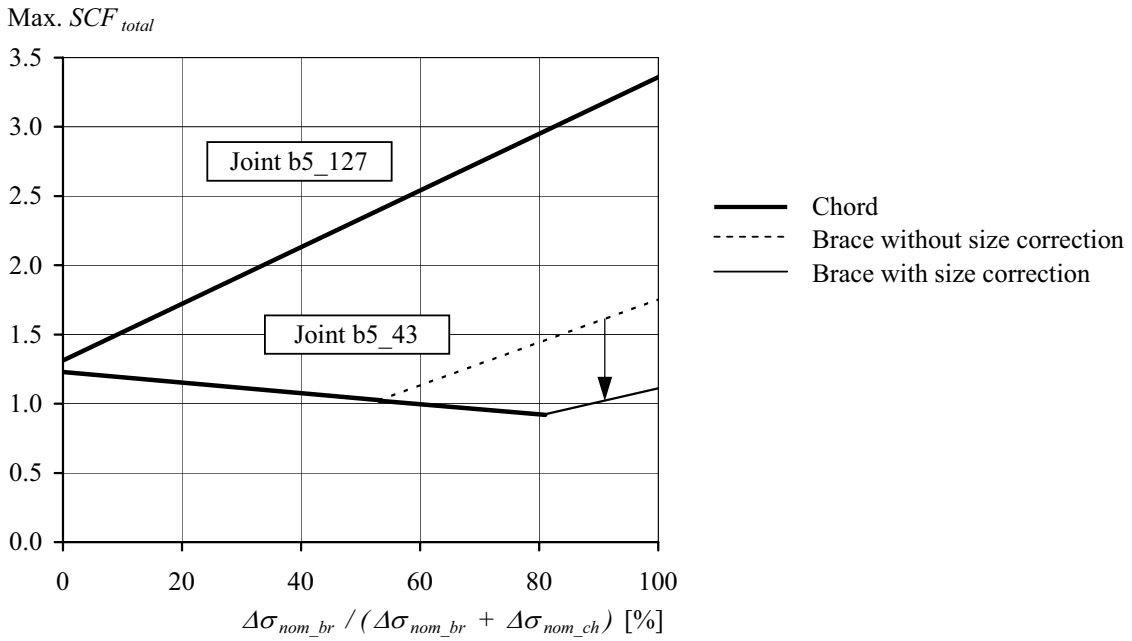

***Figure 6.4** - SCF_{total} envelops for joint models b5_43 and b5_127, effect of partial integration of size effect on brace SCF_{total} values in brace*

6.3 PRESENTATION OF SCF_{total} ENVELOPES

The SCF_{total} envelopes for a range of joint models are presented in Figure 6.5 to Figure 6.10. The SCF_{total} values are based on the SCF values for different load cases and joint locations from the parametric study presented in Chapter 4 ($\gamma \leq 12.0$) and from existing recommendations ($\gamma > 12.0$). Table 6.1 summarises the different parameter values treated in each figure. Each graph in the figures represents a particular combination of β and γ (γ= 4.0, 8.0, 12.0, 18.0, 24.0, 30.0); each figure presents SCF_{total} values for a particular brace angle, θ (θ= 45°, 60°) and stress partitioning in the members (e.g. the ratio of stresses due to axial load and in-plane bending in the brace and chord members). Due to the small effect of β on the SCF_{total}, the maximum value of SCF_{total} is given for a range of β ($0.50 \leq \beta \leq 0.70$).

***Table 6.1** - Parameter values and stress partitions covered in Figure 6.5 to Figure 6.10*

				Stress partition in members, [%]		
θ	β	γ	τ	Brace	Chord	Figure
[°]	[-]	[-]	[-]	$\%\Delta\sigma_{ax\_br}$ / $\%\Delta\sigma_{ipb\_br}$	$\%\Delta\sigma_{ax\_ch}$ / $\%\Delta\sigma_{ipb\_ch}$	
45	0.50 - 0.70	4.0 - 30.0	0.30 - 0.70	75 / 25	65 / 35	6.5
60	0.50 - 0.70	4.0 - 30.0	0.30 - 0.70	75 / 25	65 / 35	6.6
45	0.50 - 0.70	4.0 - 30.0	0.30 - 0.70	100 / 0	100 / 0	6.7
60	0.50 - 0.70	4.0 - 30.0	0.30 - 0.70	100 / 0	100 / 0	6.8
45	0.50 - 0.70	4.0 - 30.0	0.30 - 0.70	0 / 100	0 / 100	6.9
60	0.50 - 0.70	4.0 - 30.0	0.30 - 0.70	0 / 100	0 / 100	6.10

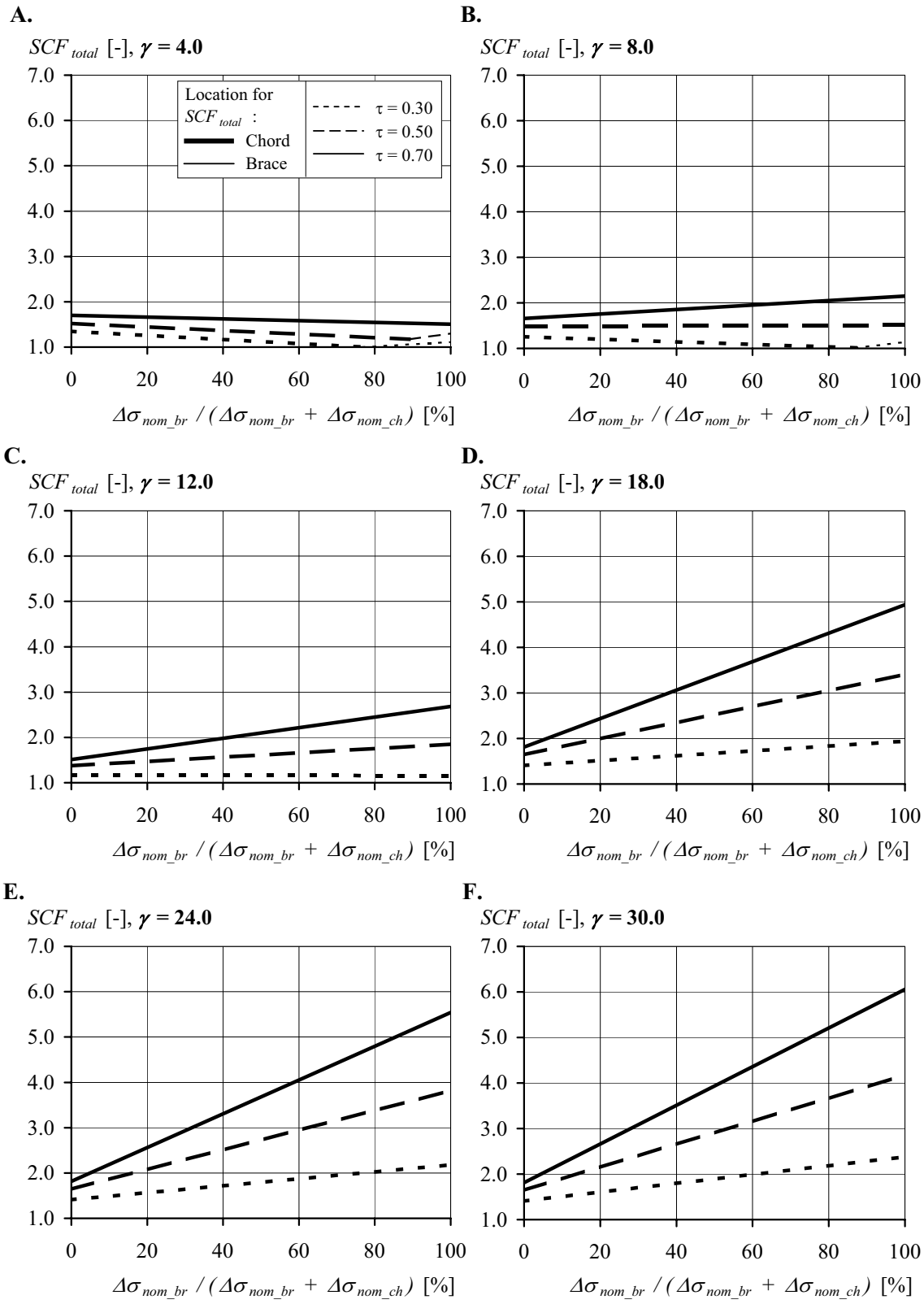

N.B. Graphs A., B. and C. from Schumacher 2003, graphs D., E. and F. from IIW 2000.

***Figure 6.5** - SCF_{total} : β =0.50-0.70, θ = **45°**, stress partition 75/25% (brace) 65/35% (chord)*

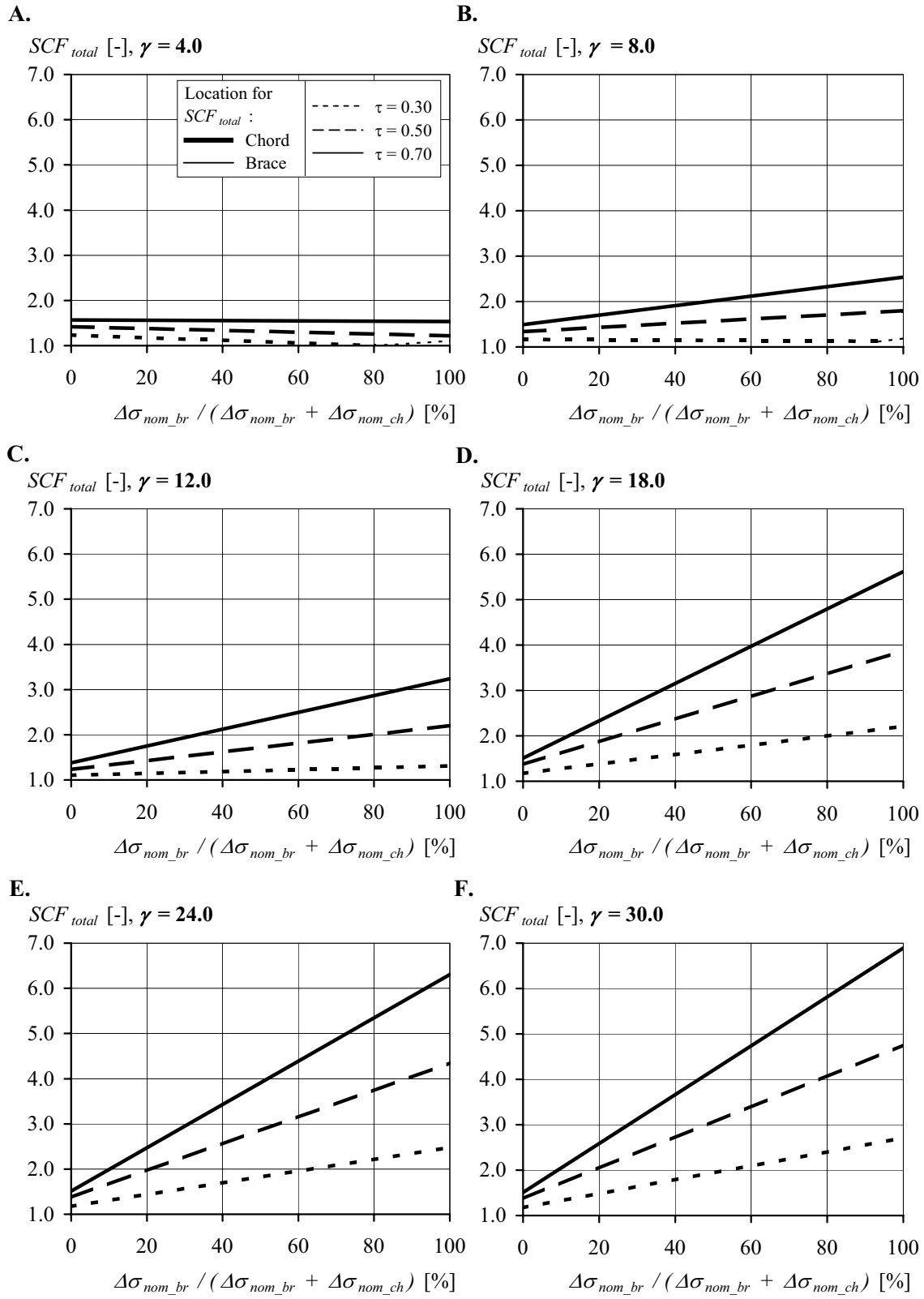

N.B. Graphs A., B. and C. from Schumacher 2003, graphs D., E. and F. from IIW 2000.

***Figure 6.6** - SCF_{total} : β =0.50-0.70, θ = **60°**, stress partition 75/25% (brace) 65/35% (chord)*

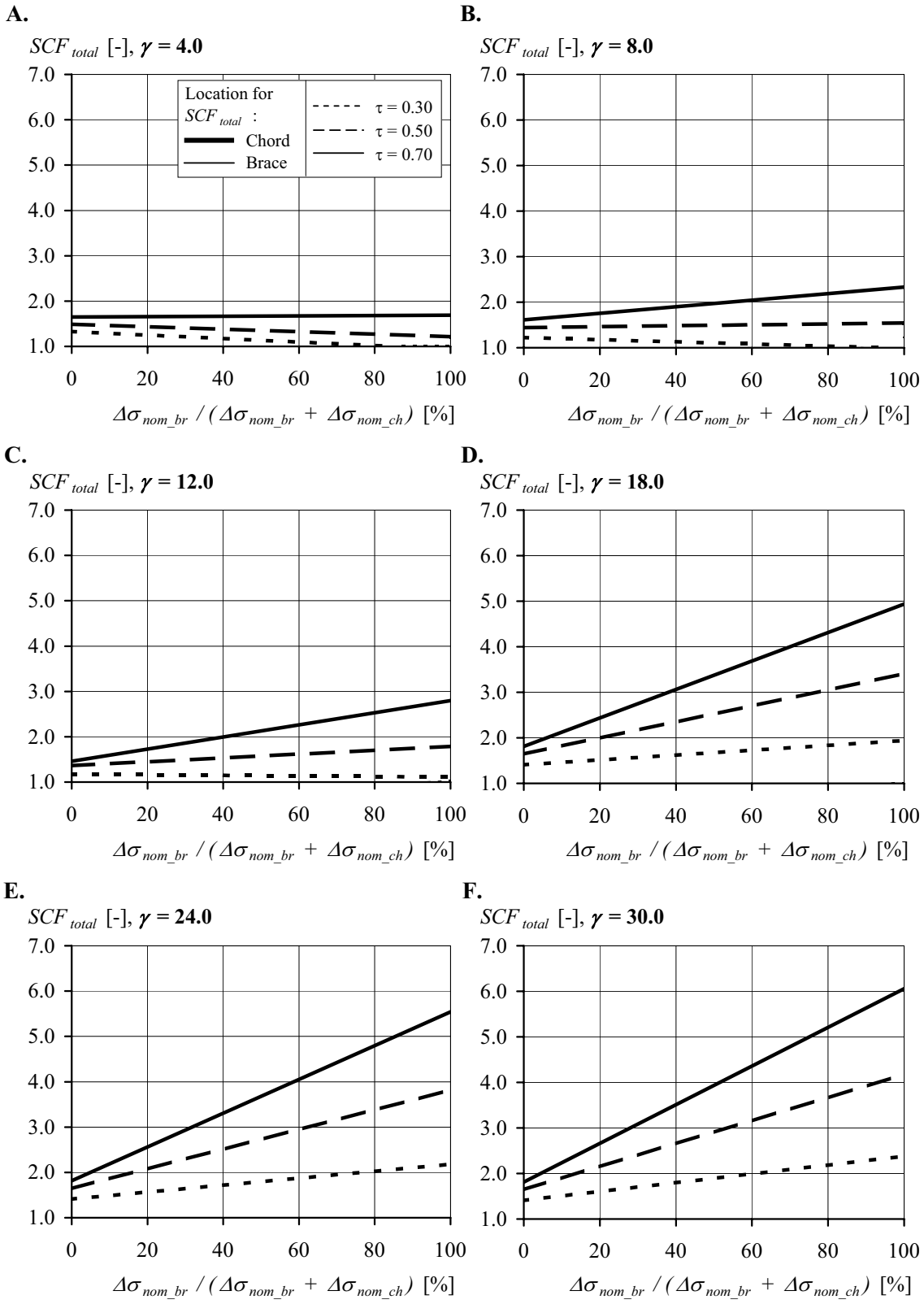

N.B. Graphs A., B. and C. from Schumacher 2003, graphs D., E. and F. from IIW 2000.

***Figure 6.7** - SCF_{total} : β =0.50-0.70, θ = **45°**, stress partition 100/0% (brace) 100/0% (chord)*

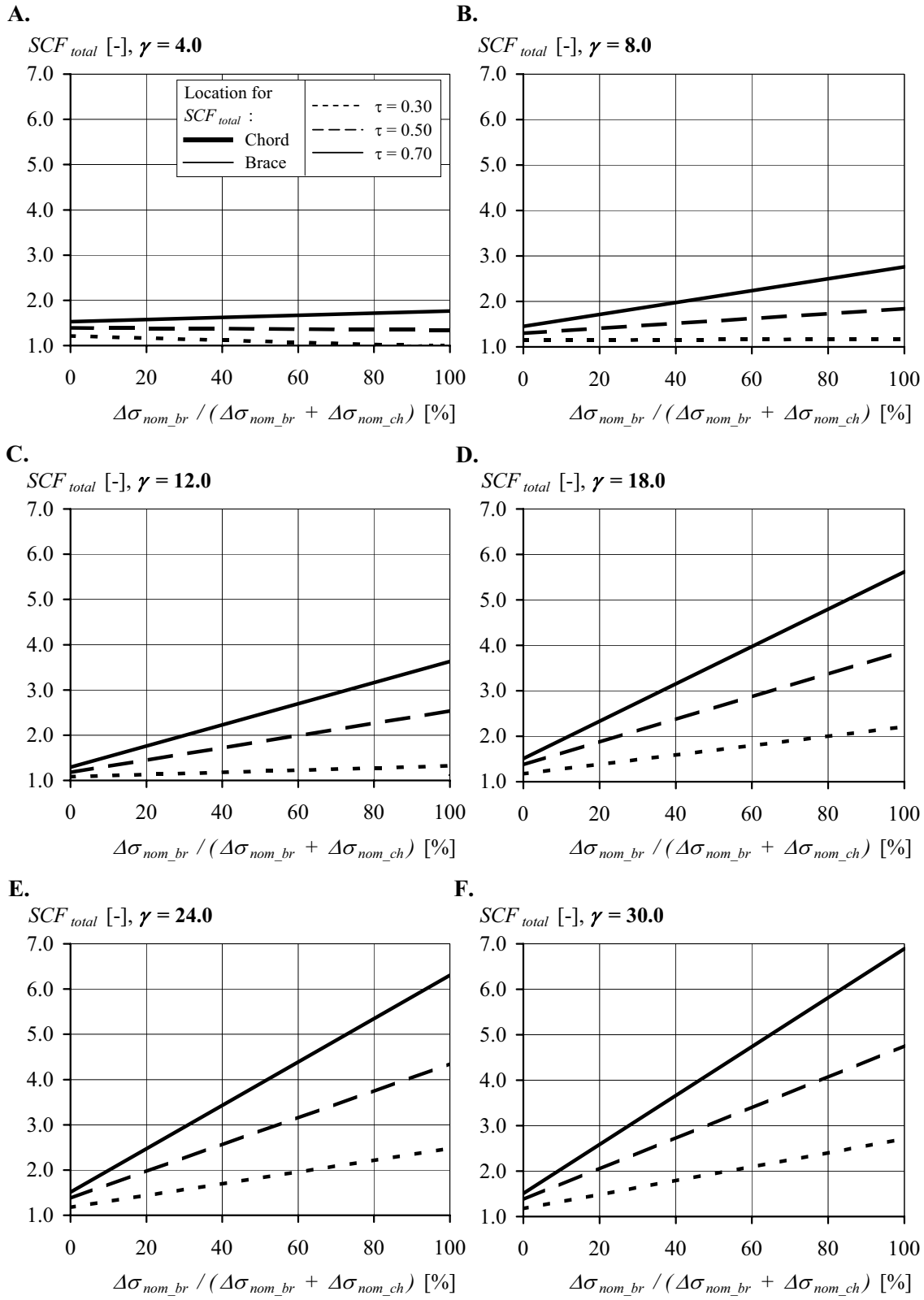

N.B. Graphs A., B. and C. from Schumacher 2003, graphs D., E. and F. from IIW 2000.

Figure 6.8 *- SCF_{total} : β =0.50-0.70, θ = **60°**, stress partition 100/0% (brace) 100/0% (chord)*

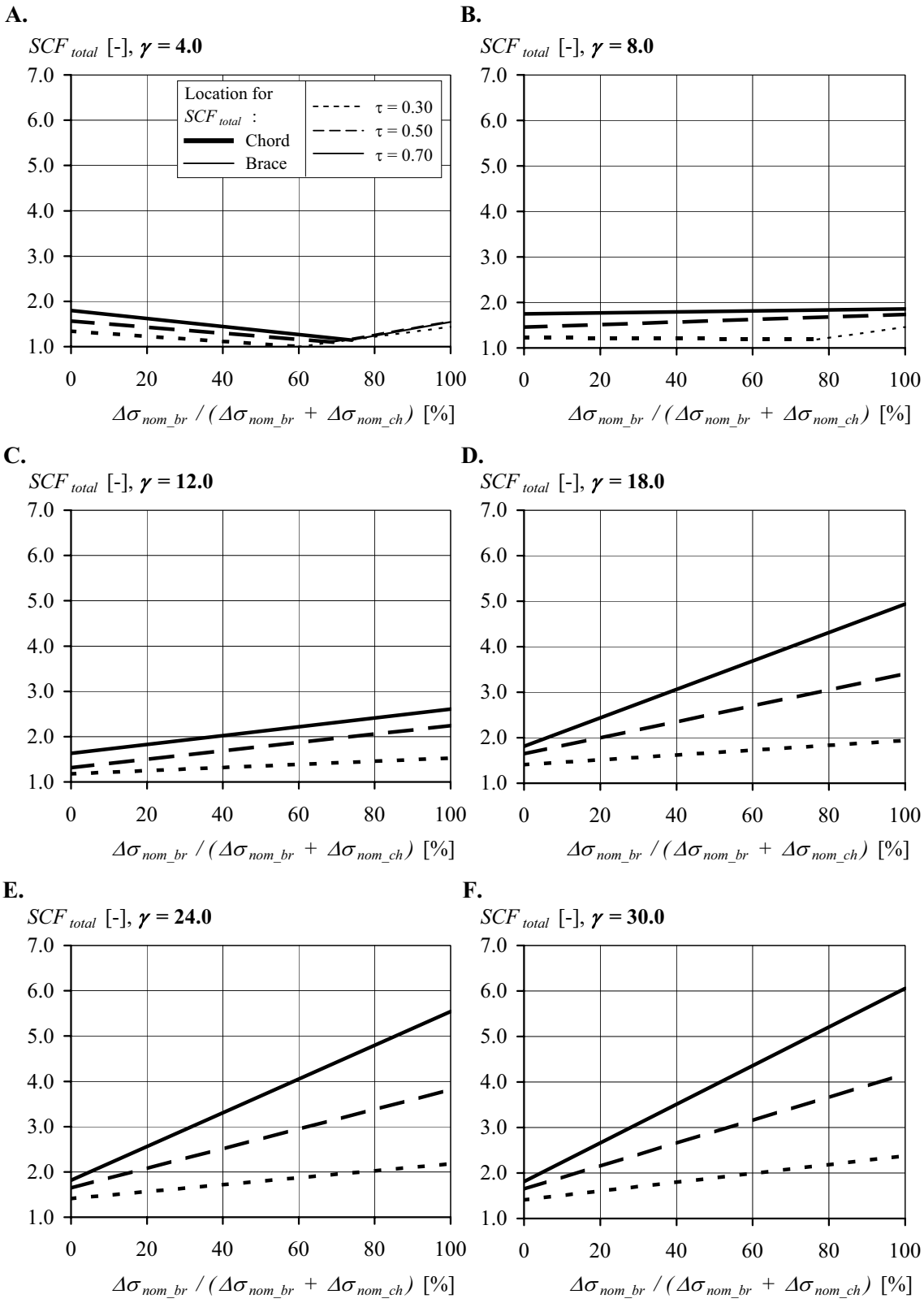

N.B. Graphs A., B. and C. from Schumacher 2003, graphs D., E. and F. from IIW 2000.

***Figure 6.9** - SCF_{total} : β =0.50-0.70, θ = **45°**, stress partition 0/100% (brace) 0/100% (chord)*

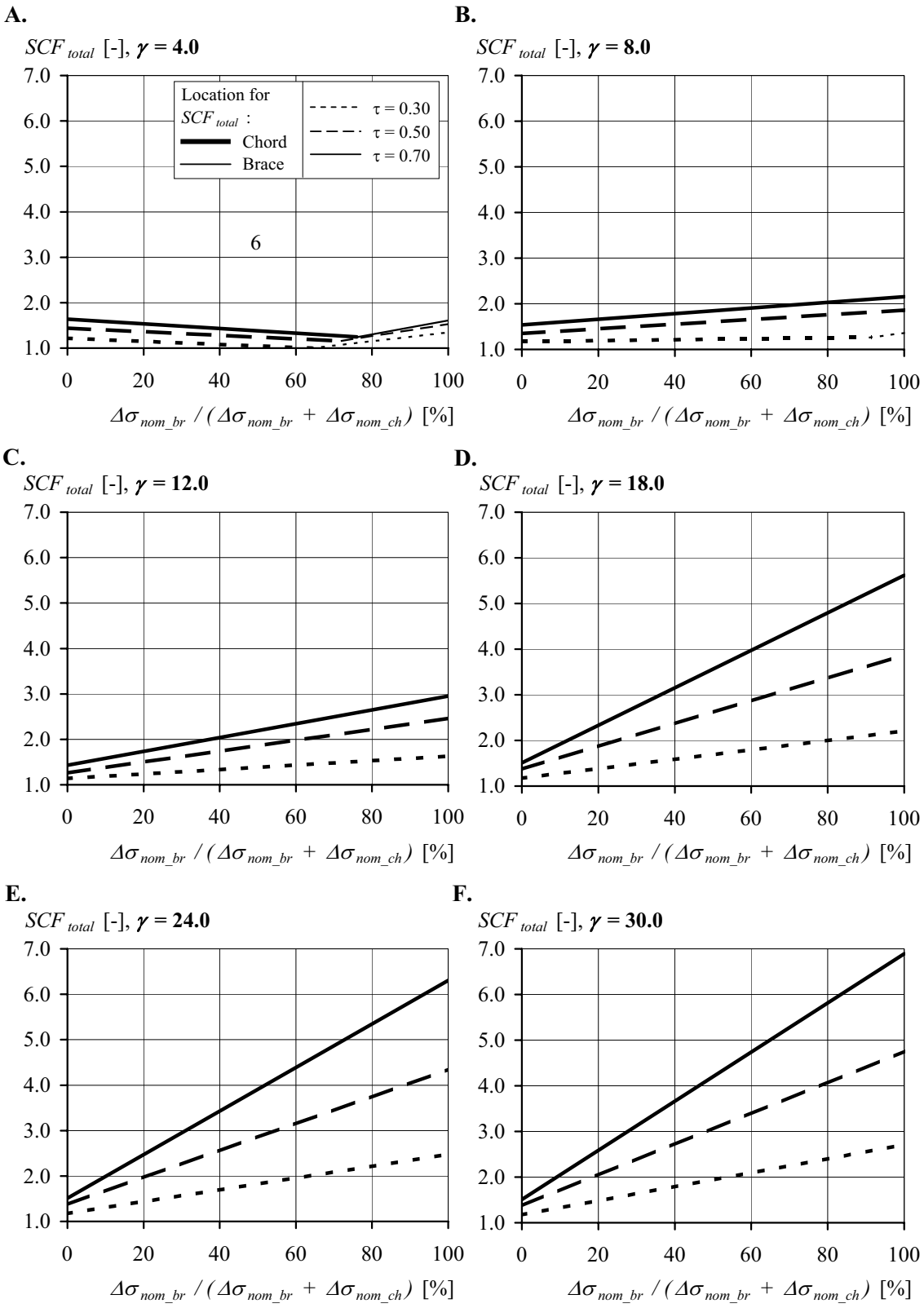

N.B. Graphs A., B. and C. from Schumacher 2003, graphs D., E. and F. from IIW 2000.

***Figure 6.10** - SCF_{total} : β =0.50-0.70, θ = **60°**, stress partition 0/100% (brace) 0/100% (chord)*

The following observations and comments with respect to, for example, Figure 6.5 and Figure 6.6 can be made:

- The effect of different parameters on the SCF_{total} is clear: increases in γ and τ increase the SCF_{total} values. Furthermore, an increase in τ has the effect of concentrating the location of the maximum SCF_{total} in the chord. Contrary to this, it is seen that θ has relatively little influence on the SCF_{total} envelopes.
- For none of the envelopes in Figure 6.5 and Figure 6.6 does the SCF_{total} fall below a value of 1.0. In reality a SCF_{total} value of less then 1.0 is possible and can be due to a combination of two factors: the choice of the particular member stress partitioning scheme and the low SCF values caused by in-plane bending moments, $SCF_{ipb\_br} < 1.0$. Since an $SCF < 1.0$ seems counter-intuitive when included within the context of design lines or tables, however, a minimum value of 1.0 has been used here.

6.4 WORKED DESIGN EXAMPLE

To illustrate the practical application of the SCF_{total} concept, a design example is given. The fatigue design procedure is summarised in table format (Table 6.2). For each design example ("Preliminary design" and "Real design") two joints are examined: a joint in the vicinity of the bridge support and a joint in the vicinity of the mid-span. It is recalled that in the fatigue design of a bridge truss comprising a series of K-joints that, due to a moving load, *each* brace per joint will likely be subjected to a tensile load (stress) range. For this reason, a single K-joint requires a two step design verification, whereby each brace and the corresponding chord branch (the length of chord adjacent to the brace in question) must be verified (in each case it is assumed that the opposite brace is subjected to a corresponding balanced compression load). The **mid-span joint** in the "**Preliminary design**" example is used to explain the various design steps (step numbers are given in Table 6.2):

Step 1 : Member dimensions and loads

Chord and brace dimensions have been determined based on the static design of the bridge. The K-joint is characterised by two identical braces. The bridge is loaded based on the fatigue load models specified in the Swiss construction design code "Actions on structures" [SIA 160 1989]. A structural analysis is carried out assuming a continuous chord and pin-ended braces (refer to Section 4.2); magnification factors (according to Zhao et al. 2000 and IIW 2000) are applied to the resulting member stresses to account for additional secondary bending moments in both the braces and the chord; this results in a total nominal stress range for each member, $\Delta\sigma_{nom}$. Since the bending moment in the braces and chord has been accounted for through magnification factors of 1.3 and 1.5, respectively, this implies a stress partitioning in the brace of 75% / 25% (that is, 75% of the nominal stress in the brace is due to an axial force, while 25% is due to an in-plane bending moment) and a stress partitioning in the chord of 65% / 35% (that is, 65% of the nominal stress in the chord is due to an axial force, while 35% is due to an in-plane bending moment).

***Table 6.2** - Recalculation of CHS bridge joints using SCF_{total}*

Step		Preliminary design				Real design*			
		support		mid-span		support		mid-span	
		br.	ch.	br.	ch.	br.	ch.	br.	ch.
1.	d, D [mm]	267	508	267	508	267	508	267	508
	t, T [mm]	25	40	11	25	25	50	11	50
	A [cm^2]	190	588	88.5	379	190	719	88.5	719
	ΔN [kN]	498	599	328	956	498	599	328	956
	Magnification factor [-]	1.3	1.5	1.3	1.5	1.3	1.5	1.3	1.5
	$\Delta\sigma_{nom}$ [N/mm^2]	34	15	48	38	34	13	48	20
2.	θ	60		60		60		60	
	β	0.53		0.53		0.53		0.53	
	γ	6.4		10.2		5.1		5.1	
	τ	0.63		0.44		0.50		0.22	
	e / D	0.20		0.10		0.20		0.10	
3.	% Brace stress	69		56		73		71	
	$\Delta\sigma_{total\ nom}$ [N/mm^2]	49		86		47		68	
	SCF_{total}	1.8		1.5		1.4		1.0	
	Critical location	chord		chord		chord		chord	
	$\Delta\sigma_{hs}$ [N/mm^2]	89		129		65		70	
4.	Damage corr. factor	0.83		0.83		0.83		0.83	
	$\Delta\sigma_{e,hs}$ [N/mm^2]	**74**		**107**		**54**		**58**	
	$S_{Rc,hs}$ for T = 20 mm	80		80		80		80	
	$S_{Rc,hs}$ for $T = T_{chord}$	**67**		**76**		**64**		**64**	
	Part. safety factor, γ_{fat}	0.9		0.7		1.2		1.1	

* Actual dimensions used for bridge.

Step 2 : Non-dimensional joint parameters

The non-dimensional parameters of the joint are obtained. To note is the low γvalue (γ< 12.0) and the presence of an eccentricity—both characteristics are included in the SCF_{total} concept.

Step 3 : Calculation of hot-spot stress range

The percentage of brace stress of the total nominal stress affecting the joint is obtained in the following manner:

$$\text{Percentage brace stress} = \frac{\Delta\sigma_{nom\_br}}{\Delta\sigma_{nom\_br} + \Delta\sigma_{nom\_ch}} \cdot 100 = \frac{48}{48 + 38} \cdot 100 = 56\%$$

The total nominal stress affecting the joint, $\Delta\sigma_{total\ nom}$, is calculated through a summation of the total nominal brace stress, $\Delta\sigma_{nom\_br}$, and the total nominal chord stress, $\Delta\sigma_{nom\_ch}$. SCF_{total} is obtained from a linear interpolation of γ values found in Figure 6.6B and C (refer to Table 6.1). For a γ value between 8.0 and 12.0, and a percentage of brace stress of 56%, it is immediately

clear that the critical fatigue location is in the chord. Interpolating to get the value for γ = 10.2 and τ = 0.44, one finds SCF_{total} = 1.5. The hot-spot stress range is found in the following simple operation:

$$\Delta\sigma_{hs} = SCF_{total} \cdot \Delta\sigma_{total\ nom} = 1.5 \cdot 86 = 129\ \text{N/mm}^2$$

As explained in Section 6.2.2, the SCF_{total} accounts for the relative size effect between braces and chord and, therefore, only one value of hot-spot stress must be calculated and verified.

Step 4 : Verification

The hot-spot stress range is adjusted using a fatigue damage correction factor (according to SIA 161 1990). The correction factor takes into account the difference between the cumulative damage effect of realistic traffic and that of the fatigue load in the code. The resulting equivalent hot-spot stress range, $\Delta\sigma_{e,hs}$, can now be compared to the appropriate $S_{R,hs}$-N design curve at $2x10^6$ cycles.

It is reiterated that the definition of the hot-spot stress is closely related to the choice of the $S_{R,hs}$-N design curve. The SCF_{total} developed herein are based on SCF and hot-spot stress values obtained in laboratory testing. For these tests a certain fatigue strength curve for K-joints with chord wall thicknesses of 20 mm was obtained. This curve will be used as a basis for design here ($S_{Rc,hs}$ for T = 20 mm, 80 N / mm^2 at $2x10^6$ cycles refer to Figure 6.11).

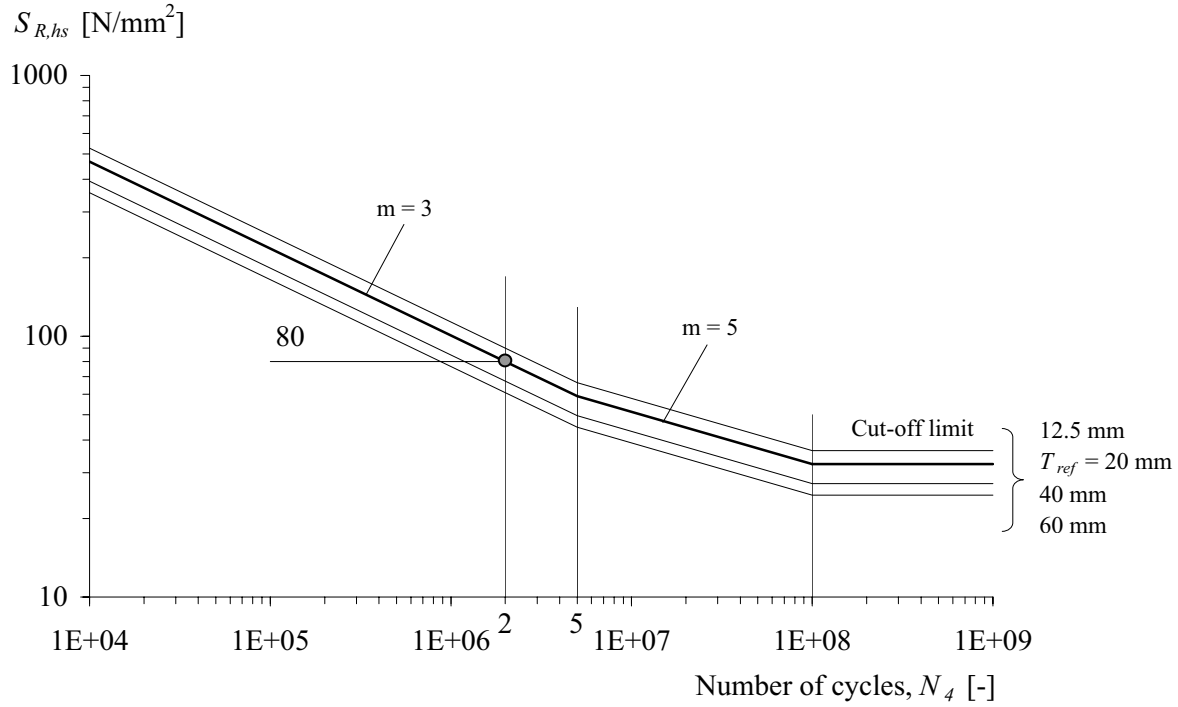

***Figure 6.11** - Recommended $S_{R,hs}$-N design curves for welded CHS joints*

Since the critical fatigue location is on the chord, the base $S_{R,hs}$-N design curve is adjusted for a thickness of T = 25 mm. The ratio between the equivalent hot-spot stress range, $\Delta\sigma_{e,hs}$, and the fatigue strength corrected for plate thickness at $2x10^6$ cycles, $S_{rc,hs}$, gives a partial safety factor, γ_{fat}. Assuming the joint to be a fail-safe joint with periodic inspection and maintenance,

a partial safety factor of 1.1 must be ensured [SIA 161 1990]. In Table 6.2 it is seen that the partial safety factor at the chord location is not satisfied.

Having failed the fatigue verification, an appropriate adjustment to the K-joint is sought. An obvious approach involves a decrease in stresses affecting the joint. This can be achieved in several ways, for example, an increase in the diameter of the brace and/or the chord, or an increase in the wall thickness of the brace and/or the chord. A change in the diameter is an impractical suggestion, since it is likely the diameters of both the brace and chord are constant along the bridge length (a change in one joint would thus require a change over the entire length). A rapid inspection of Figure 6.6B and C suggests that a decrease in SCF_{total} is possible through a reduction in τ, γ and, depending on the value of τ, the percentage of brace stress. A decrease in τ and γ occurs when the chord thickness, T, is increased. As seen in Table 6.2, it is exactly this solution that has been chosen in the actual bridge design ("Real design"). An increase in T for the joints at both support and mid-span (in fact, the engineer opted for a constant chord wall thickness along the entire bridge span for the actual bridge structure) results in a decrease in τ and γ, and the total nominal chord stress range. Furthermore, although a decrease in the chord stress can have the effect of increasing SCF_{total}, in this case, changes in the other parameters were large enough to decrease the SCF_{total}. The partial safety factors calculated for the "Real design" example indicate a combination of joint dimensions and loading that satisfy the fatigue verification ($\gamma_{fat} \geq 1.1$).

6.5 CONCLUSIONS

The concept of a total stress concentration factor, SCF_{total}—wherein the influence of load combination and the partitioning of stresses are already inherent to the value—has been demonstrated for a range of CHS bridge K-joints. The following conclusions can be drawn:

Concept

- SCF_{total} values at critical joint locations can be represented as a linear relationship over a complete load (or stress) scenario range, from 100% load in the chord to 100% load in the braces. This representation shows that SCF_{total} values relevant in design, that is, maximum SCF_{total} values, occur at mostly only one or two locations in the joints studied here.
- A partial inclusion of the size effect in the SCF_{total} envelopes has been demonstrated. A relative size effect between the brace and the chord (related to the τ joint parameter) can be taken into account in SCF_{total}, whereby the subsequent verification of hot-spot stress (calculated based on the SCF_{total} envelopes) is carried out with reference to a single $S_{R,hs}$-N curve for both the brace and the chord.

Design method

- SCF_{total} envelopes for the range of welded CHS K-joints illustrate clearly the effect of different parameters on the SCF_{total}: increases in γ and τ increase the SCF_{total} values. Furthermore, an increase in τ has the effect of concentrating the location of the maximum SCF_{total} in the chord.
- The chord-to-brace diameter ratio, b, has a relatively small influence on SCF_{total}. Values of SCF_{total} can therefore be given such that they cover a range, $0.50 \leq \beta \leq 0.70$.

- The demonstration of the SCF_{total} concept within the framework of a design example illustrates the feasibility and relative simplicity of its use in a welded CHS bridge K-joint design process.

7 SUMMARY, CONCLUSIONS AND RECOMMENDATIONS

7.1 SUMMARY

Circular hollow section (CHS) members are being used in modern bridge applications. In numerous examples the CHS members have been cut and welded together directly to form the main load-carrying trusses of steel-concrete composite bridges. The welded connection between brace and chord members form an intersection characterised by variable stiffness, a non-uniform stress distribution and complex three-dimensional behaviour, all of which can be unfavourable when the joint is subjected to fatigue loading. To date, research on the fatigue of welded tubular joints has been driven primarily by the offshore petroleum industry. The design specifications based on this research seem overly conservative when used to design bridges. The main objective of this study was to investigate two specific aspects of welded CHS bridge joint fatigue design: the determination of joint stresses at critical fatigue locations and the so-called size or scale effect on the fatigue resistance of these joints.

Sixteen large-scale welded CHS K-joints were tested by the Steel Structures Laboratory (ICOM) at the Swiss Federal Institute of Technology in Lausanne (EPFL). The joints were tested as part of a truss structure to ensure realistic load and boundary conditions. The parameters studied were member dimensions, fabrication methods (fully penetrated welds with or without backing rings) and weld improvement (needle peening). This experimental work provided data on the static strain (stress) response of the truss members and the joints. In all joints the measured hot-spot stresses at locations of fatigue cracking were found to be lower than the hot-spot stresses calculated using current design specifications. $S_{R,hs}$-N results were obtained for evaluation of the joint fatigue resistance. Differences between the fatigue resistances of joints of different size were seen.

A finite element model was developed that represents accurately the geometry of the test joints, in particular, the weld shape and volume at the brace-chord intersection. For comparisons with experimental data the solid element model was fixed to a simplified representation of the remainder of the test truss comprising beam elements. It was seen that the calculated elastic behaviour of the solid element joint model can be used to predict the strain response of the test joints, including tests joints with backing rings (refer to [Schumacher 2003]) and joints with different dimensions. The finite element model of the test joints was standardised (using a specific gap size definition and a widely accepted weld model) to ensure uniformity in the models created subsequently for the parametric study. Also required for the parametric study was a K-joint model that can be loaded with individual load cases, as opposed to the combined load condition in a truss structure. To do this it was shown that a solid K-joint model loaded in isolation, using simplified boundary conditions, can be used to closely reproduce the previously validated truss joint behaviour.

Common bridge parameters, in particular, joints with low chord slenderness, $\gamma(D / 2T)$, that are not covered by design specifications, were studied using a set of 36 finite element models. The main joint parameters investigated were: θ, $\beta\,(d / D)$, $\gamma(D / 2\mathrm{T})$ and $\tau\,(t / T)$. Five load cases were applied per model and the response of the joints was evaluated at several locations around the brace-chord intersection. The results of the parametric study are given in a database of stress concentration factors that can be used in the determination of fatigue design stresses. A comparison was made between finite element model results obtained in the present study and values from similar studies on which current design specifications are based.

The results of the parametric study alone are not enough to explain the difference in the fatigue resistance of welded tubular joints subjected to the same stress, but of different size or scale. A submodeling technique, using the finite element joint models of the parametric study as a basis, was developed in order to simulate the stress distribution through the thickness of the joint wall at the location where fatigue cracking could be expected. The stress distributions were subsequently used in linear elastic fracture mechanics calculations for the determination of the fatigue strengths of the joints. The comparison of calculated fatigue strengths provided indications on the size effect between joints, as influenced by different member thicknesses, geometries and different load cases.

The desire to provide the engineer with a simple, coherent approach to the design of welded CHS K-joints for bridges has led to a modified calculation method. Based on the results of this study, the method synthesises graphically the most relevant parameters for the determination of welded CHS K-joint hot-spot stresses.

7.2 CONCLUSIONS

Progress has been made towards understanding the fatigue behaviour of welded CHS bridge joints. In Section 1.2 a list of objectives was given for the work presented herein. Below, several of the most significant conclusions from the work are presented on a per chapter basis. The conclusions with direct practical application are not given here, but have been re-grouped in Section 7.3 Recommendations.

Chapter 2 – Welded CHS joint fatigue

1. The hot-spot stress method is the only current method for the fatigue design of tubular joints that is both scientifically acceptable and practical for use by design engineers.

Chapter 3 – Experimental investigation

2. The laboratory fatigue tests of large-scale welded CHS K-joint trusses reveal hot-spot stresses measured at the location of fatigue cracking that are lower than stresses calculated using design specifications, supporting the notion that the specifications are too conservative. Furthermore, results have shown that one of the most fatigue susceptible locations in welded CHS K-joints is at the weld toe, in the gap region of the chord (Location 1). Cracking progresses at an angle through the thickness of the chord wall as well as along the brace-chord weld; crack propagation is stable even after through-cracking of the chord wall has occurred.

3. $S_{R,hs}$-N test results from eight test joints with 20 mm failed chord members indicate lower fatigue strengths when compared with corresponding $S_{R,hs}$-N design curves. This implies that, although the hot-spot stresses may be lower than what is currently calculated (Conclusion 2), the fatigue strength curves corresponding to these stresses are also lower. Furthermore, a comparison between the fatigue strength of (nominally) proportionally scaled welded CHS K-joints seems to support the general view that larger joints, with thicker members, can exhibit lower fatigue strength.

4. The use of a backing ring to ensure full weld penetration does not affect the fatigue resistance of the joints in comparison to joints with fully penetrated welds without backing rings, since failure of the joints is dictated by cracking from the weld toe at the joint surface.

5. Weld improvement (needle peening) applied to a critical location in the joint will delay fatigue cracking at that location. In the tests presented herein, the delay translates into at least a factor of three in fatigue life, which corresponds to a 60% increase in the fatigue strength of the joints. Care must be taken, however, when weld improving tubular joints at a specific location, since the critical location can shift as a result of this procedure and cracking can occur at other locations in the joint.

Chapter 4 – Numerical study

6. Using a validated finite element model, SCFs have been calculated for a range of CHS K-joint geometries, dimensions and load cases. These values can be used directly in the determination of hot-spot stresses for the design of welded CHS bridge K-joints.

7. In general, SCF values were found to be relatively low. For brace loads, the SCF values lie mainly between 1.5 and 2.5, while for chord loading the SCF values fall principally between 1.0 and 1.5.

8. Particularly relevant to the CHS truss bridge application, it has been seen that for brace load cases—axial force or in-plane bending moment—there is a strong tendency for SCF values to decrease with decreasing $\gamma (D / 2T)$, especially at locations of maximum SCF. A low γ value, such as the low γ joints ($\gamma < 12.0$) seen in existing bridges, is therefore a desirable geometric characteristic—a recommendation that should be reflected in the design specifications.

9. The parametric study has also included a range of joints covered by the finite element work on which the current design specifications are based. A comparison of the stress concentration factors obtained from the two studies shows a substantial difference in the predicted SCFs in the chord gap region (Location 1) for balanced axial brace loading, specifically, the predicted SCFs from the present study are lower than those predicted by the design specifications. As balanced axial brace loading is a predominant load case, the difference in predictions has significant consequences and explains the overly-conservative values seen previously in the design of CHS bridge trusses and in comparisons with test results.

Chapter 5 – Effects of joint size and scale

10. In a statistical approach to the size effect—defined as a term that encompasses differences in fatigue performance between both proportionally and non-proportionally scaled joints—using as input a large database of welded CHS joint fatigue test results, a regression analysis shows a reduction in the fatigue strength dependent on the wall thickness of the failed member. However, the inclusion of many different parameters in this database, the related large degree of scatter in the data and the lack of data for joint thicknesses relevant to bridge applications make it questionable whether the correction factor for the size effect obtained from this database (e.g. $n = 0.378$ at 2×10^6 cycles, refer to Equation 5.1 and Equation 5.2), is a fair representation of the actual size effect phenomenon, in particular for bridge applications.

11. In an analytical approach it is seen that the magnitude of the size effect is influenced by the loading applied to the joint and the magnitude of the stress concentration at the location of cracking. Low stress concentrations seem to contribute to a lower size effect for joints of different thickness.

12. A large degree of scatter due to a large number and range of parameters included in the size effect can result in a very conservative size effect correction factor. To improve upon this, the size effect should to be addressed within the framework of the specific application within which it will be used, e.g. bridges, offshore, cranes.

13. For none of the results presented in Chapter 5—statistical nor analytical—does it seem justified to apply a size correction factor greater than the factor proposed by Gurney 1979 (e.g. $n = 0.25$). In fact, in numerous instances, it was even deemed reasonable to deduce a size effect correction significantly inferior to that of Gurney.

Chapter 6 – Design graphs and examples

14. A graphical synthesis of the results from this study provides a simplified yet coherent method for the design of welded CHS K-joints. The proposed concept of a total stress concentration factor and corresponding graphs give realistic fatigue design stresses that will aid in the design of CHS trusses in steel and composite bridge construction.

7.3 RECOMMENDATIONS

The following summarises recommendations for the design of welded CHS K-joints in bridges that have been drawn from the work presented in this report:

- The engineer is referred to Appendix A, which contains several examples of recently constructed bridges, in order to obtain some feeling for the dimensions, type of joints, etc. common to bridges with welded CHS joints. Appendix B contains information about detailing of the joints.

- The hot-spot stress method is the only current method for the fatigue design of tubular joints that is both scientifically acceptable and practical for use by design engineers.

- One of the most fatigue susceptible locations in welded CHS K-joints is at the weld toe, in the gap region of the chord (Location 1).

- The relevant hot-spot stress range for fatigue design can be found using the design method presented in Chapter 6. Also included in this chapter is a design example. For low γ values, typically $\gamma \leq 12.0$, the proposed method gives lower stress concentration factors and hot-spot stresses than current specifications. The range of parameters presented in the design graphs in Chapter 6 cover most practical bridge applications.

- The recommended minimum SCF at critical joint locations in current design specifications, SCF = 2.0 (except in cases where the SCF can be taken as zero), is very penalising if applied to welded CHS *bridge* K-joints. When $\gamma \leq 12.0$, the recommended minimum SCF can be taken as SCF = 1.0 for CHS K-joints when fully penetrated welds are used and the brace-to-chord diameter ratio is $\beta \leq 0.70$.

- The hot-spot stress ranges given in this report must be applied to a fatigue strength curve characterised by $S_{R,hs} = 80$ N/mm^2 at 2x10^{6}cycles, that is, a Detail Category 80, for a reference thickness $T_{ref} = 20$ mm. The size correction factor exponent shall be taken as $n = 0.25$ (this is a conservative assumption).

- When the fatigue verification is not satisfied, the design graphs presented in Chapter 6 provide a tool which helps to quickly see the influence of the various joint parameters on the stress concentration and, thus, to make the appropriate modifications to the design (i.e. joint

dimensions, parameters, etc.). Furthermore, depending on the case at hand, the possibility of using weld improvement methods in order to improve the fatigue resistance of the joint could be considered. Appendix B, §10.3.3, gives information on the benefits to using various weld improvement methods, as well as the procedures required in the application and verification of these methods.

- It is highly recommended to design joints with fully penetrated welds. In order to ensure good penetration, the inclusion of backing rings is recommended (see Appendix B).

8 REFERENCES

Albrecht, P. and Yamada, K. 1977. **Rapid calculation of stress intensity factors**. J. Struct. Div., ASCE 103, No. ST 2, pp. 377-389.

API (American Petroleum Institute) 1993. **Recommended practice or planning, designing and constructing fixed offshore platforms**. API RP2A-LRFD, Washington D.C., USA.

AWS (American Welding Society) 2000. **ANSI/AWS D1.1-2000 Structural Welding Code-Steel**. American Welding Society, Inc., Miami, USA.

de Back, J., van Delft, D.R.V., Noordhoek, C. 1989. **The effect of plate thickness on the fatigue life of welded tubular joints and flat specimens**. Proceeding: Eighth International Conference on Offshore Mechanics and Aritic Engineering – Vol. III, ASME, The Hague, The Netherlands.

Baregg Info 2000. **3'186 t schwer, 249 Tage lang**. Baudepartement des Kantons Aargau, Info 4 Spezial, Aarau, Switzerland.

Beale, L. and Toprac,A.A. 1967. **Analysis of in-plane T, Y and K welded tubular connections**. Welding Research Council Bulletin 125.

Bell, R. 1987. **Stress intensity factors for weld toe cracks in welded T plate joints**. CANMET Project No. 708803, Carleton University, Ottawa, Canada.

Berge, S. and Webster, S.E. 1987. **The size effect on the fatigue behaviour of welded joints**. Paper PS 8, 3rd International ECSC Offshore Conference on Steel in Marine Structures, Delft, The Netherlands.

Bremen, U. 1989. **Amélioration du comportement à la fatigue d'assemblages soudès: étude et modelisation de l'effet de contraintes résiduelles**. PhD. Thesis 787, Ecole Polytechnique Féderale de Lausanne, Switzerland.

BS 5400 1980. **Steel, concrete and composite bridges, Part 10: Code of practice for fatigue**. British Standards Institution.

BS 7608 1993. **Code of practice for: Fatigue design and assessment of steel structures**. British Standards Institution.

Burns, D.J., Lambert, S.B., Mohaupt, U.H. 1987. **Crack growth behaviour and fracture mechanics approach**. Paper PS 6, 3rd International ECSC Offshore Conference on Steel in Marine Structures, Delft, The Netherlands.

Dauner, H.-G. 1997. **Stahlverbundbrücken im Aufwind**. Schweizer Ingenieur und Architekt, SIA, No. 26, pp. 10-16, Zürich, Switzerland.

Dauner, H.-G., Décorges, G., Oribasi, A., Wéry, D. 1998. **The Lully Viaduct, a composite bridge with steel tube truss**. Journal of Constructional Steel Research, Vol. 46, No. 1-3, Paper No. 55, Elsevier Science Ltd., Oxford, U.K.

DEn (Department of Energy) 1984. **Offshore installations: guidance on design and construction**. Third edition, UK Department of Energy, Her Majesty's Stationary Office, London, U.K.

Detandt, H. and Couchard, I. 2003. **The Hammerbrücke Viaduct, Belgium**. Structural Engineering International, Vol. 13 No. 1 pp. 16-18.

Dijkstra, O.D., Snijder, H.H., Overbeeke, J.L., Wildschut, H. 1987. **Prediction of fatigue crack growth for welded joints using stress intensity factors determined by FEM calculations**. Paper TS 52, 3rd International ECSC Offshore Conference on Steel in Marine Structures, Delft, The Netherlands.

Dijkstra, O.D. and van Straalen, I.J.J. 1997. **Fracture mechanics and fatigue of welded structures**. WRC Proceedings IIW.

Dimitrakis, S.D. and Lawrence, F.V. 1994. **The effect of Weldment sieze and sea water exposure on the fatigue life of welded tubular joints**. OMAE, Vol. III, Materials Engineering, ASME.

Dimitrakis, S.D., Lawrence, F.V., Mohr, W.C. 1995. ***S-N* curves for welded tubular joints**. OMAE, Vol. III, Materials Engineering, ASME.

DNV RP-203 2001. **Fatigue Strength Analysis of Offshore Structures.** Det Norske Veritas.

Dubois, V. 1994. **Fatigue de détails soudés traités sous sollicitations d'amplitude variable**. PhD Thesis 1260, Ecole Polytechnique Féderale de Lausanne, Switzerland.

ECCS (European Convention for Constructional Steelwork) 1985. **Recommendations for the Fatigue Design of Steel Structures**. Technical Committee 6 - Fatigue, First Edition.

Efthymiou, M. and Durkin, S. 1985. **Stress Concentrations in T/Y and Gap/Overlap K-joints**. Behavior of Offshore Structures, pp. 429-440, Delft, The Netherlands.

Efthymiou, M. 1988. **Development of SCF formulae and generalized functions for use in fatigue analysis**. OTJ, Surrey, U.K.

Eurocode 3 (prEN 1993-1-9) 2002. **Design of steel structures, Part 1.9: Fatigue strength of steel structures**. CEN, Brussels, May 2002.

Eurocode 3 2003. **Design of steel structures, Part 1.9: Fatigue strength of steel structures**. CEN, Brussels, 2003.

Gurney, T.R. 1979. **The influence of thickness on the fatigue strength of welded joints**. 2nd International Conference on the Behaviour of Offshore Structures, Vol. 1, Paper 41, pp. 523-534. BHRA Fluid Engineering, Cranfield, Bedford, England.

Gurney, T.R. 1981. **Some comments on fatigue design rules for offshore structures**. 2nd International Symposium on Integrity of Offshore Structures, pp. 219-234. Applied Science Publishers, Barking, Essex, England.

Haagensen, P.J. and Maddox, S.J. 2001. **IIW Recommendations on Post Weld Improvement of Steel and Aluminium Structures**. IIW Commission XIII, XIII-1815-00.

Herion, S. 1994. **Räumliche K-Knoten aus Rechteck-Hohlprofilen**. Ph.D. Thesis, University of Karlsruhe, Germany.

Herion, S. and Puthli, R.S. 1998. **Fatigue design and secondary bending moments in RHS K-joints with gap**. 8th International Symposium on Tubular Structures, Singapore.

Hibbitt, Karlsson, & Sorenson, Inc. (HKS) 2000. **ABAQUS / Standard Version 6.0.1 (computer software)**. Hibbitt, Karlsson, &Sorenson, Inc., Pawtucket, Rhode Island, U.S.A.

Hirt, M.A. 1971. **Fatigue behaviour of rolled and welded beams**. PhD. Dissertation, Lehigh University, Bethlehem, Pennsylvania, U.S.A.

IIW (International Institute of Welding) 1985. **Recommended fatigue design procedure for hollow section joints. Part 1 – hot spot stress method for nodal joints**. IIW Sub commission XV-E, Doc. XV-582-85.

IIW (International Institute of Welding) 1996. **Fatigue design of welded joints and components**. Author: A. Hobbacher, XIII-1539-96/XV-845-96.

IIW (International Institute of Welding) 2003. **Fatigue design of welded joints and components**. Author: A. Hobbacher, XIII-1965-03/XV-1127-03.

IIW (International Institute of Welding) 2000. **Fatigue design procedure for welded hollow section joints**. X.-L. Zhao & J.A. Packer (eds.), Doc. XIII-1804-99, XV-1035-99, Cambridge: Abington.

Kam, J.C.P., Dover W.D., Ma, C.N. 1994. **The prediction of crack shape development for in-service cracks in offshore welded tubular joints**. Elsevier Science, Marine Structures 8.

Karamanos, S.A., Romeijn, A., Wardenier, J. 1997. **Stress concentrations and joint flexibility effects in multi-planar welded tubular connections for fatigue design**. Stevin Report 6-98-05, CIDECT Report 7R-17/98, Delft University of Technology, The Netherlands.

Kellogg, M.W. 1956. **Design of piping systems**. Second Edition, John Wiley.

Kinra, R.K. and Marshall, P.W. 1979. **Fatigue analysis of the Cognac platform**. Offshore Technology Conference, Paper OTC 3378, Houston, Texas.

de Koning, C.H.M., Wardenier, J., Dutta, D. 1992. **Fatigue behaviour of multiplanar welded hollow section joints and reinforcement measures for repair**. TNO-Bouw Report No. BI-92-0005 / 21.4.6394.

Kuang, J.G., Potvin, A.B., Leick, R.D. 1975. **Stress concentration in tubular joints**. Offshore Technology Conference, Paper OTC 2205, Houston, Texas.

Kuang, J.G., Potvin, A.B., Leick, R.D., Kahlich, J.L. 1977. **Stress concentration in tubular joints**. J.Soc. Petroleum Engineers.

Kuhlmann, U., Günther, H.-P., Rainer, S., Häderle, M.-U., Stubba, G. 2002. **Zur Anwendung geschweisster Hohlprofilknoten im Brückenbau**. Stahlbau, Vol., No., pp., Ernst & Sohn, Berlin.

Lee, M.M.K. and Bowness, D. 2002. **Estimation of stress intensity factor solutions for weld toe cracks in offshore tubular joints.** International Journal of Fatigue 24 (2002), pp. 361-375.

Maddox, S.J. 1970. **Fracture mechanics applied to fatigue of welded structures**. Welding Institute conference on fatigue of welded structures, Brighton.

Maddox, S.J. 1987. **The effect of plate thickness on the fatigue strength of fillet welded joints**. The Welding Institute, Abington Publishing, Cambridge, U.K.

Maddox, S.J. 1991. **Fatigue strength of welded structures**. Abington Publishing, Cambridge, U.K.

Marshall, P.W. and Graff, W.J. 1976. **Limit state design of tubular connections**. Behavior of Offshore Structures, BOSS, Trondheim, Norway.

Marshall, P.W. and Luyties, W.H. 1982. **Allowable stresses for fatigue design**. Behavior of Offshore Structures, BOSS, Boston, Ma, USA.

Marshall, P.W. 1992. **Design of welded tubular connections, basis and use of AWS code provisions**. Elsevier, Amsterdam, The Netherlands.

Microsoft 2000. **Microsoft Excel**. Microsoft Corporation, One Microsoft Way, Redmond, WA, U.S.A.

Newman, J.C. and Raju, I.S. 1981. **An empirical stress-intensity factor equation for the surface crack**. Engineering Fract. Mech., Vol. 15, No 1-2, pp. 185-192.

Niemi, E. 1992. **Recommendations concerning stress determination for fatigue analysis of welded components**. IIW Doc. XIII-1458-92 XV-797.

Noordhoek, C. and de Back, J. (Eds.) 1987. **Steel in marine structures**. 3rd International ECSC Offshore Conference on Steel in Marine Structures, Delft, The Netherlands.

Nussbaumer, A. 1995. **Application de la méchanique de la rupture: étude de l'effet d'échelle dans les joints soudés soumis à la fatigue**. Constr. Métallique, No. 3.

Orjasäter, O. 1995. **Effect of plate thickness on fatigue welded components**. IIW-JWG XIII-XV-118-93.

Packer, J.A., Wardenier, J., Kurobane, Y., Dutta, D., Yeomans, N.F. 1992. **Design guide for rectangular hollow section (RHS) joints under predominantly static loading**. CIDECT, Comité International Pour le Développement et L'étude de la Construction Tubulaire, Serial No. 3, Köln: TUV-Verlag Rheinland, Germany.

Packer, J.A. and Henderson, J.E. 1992. **Design guide for hollow structural section connections**. Canadian Institute of Steel Construction.

Panjeh Shahi, E. 1994. **Stress and strain concentration factors of welded multiplanar joints between square hollow sections**. Doctoral Thesis, Delft University of Technology, Delft University Press, The Netherlands.

Paris, P.C 1960. **The growth of cracks due to variations in load**. PhD. Dissertation, Lehigh University, Bethlehem, Pennsylvania, U.S.A..

Romeijn, A., Puthli, R.S., de Koning, C.H.M., Wardenier, J. 1992. **Stress and strain concentration factors of multiplanar joints made of circular hollow sections**. 2nd International Offshore and Polar Engineering Conference, San Francisco, U.S.A.

Romeijn, A. 1994. **Stress and strain concentration factors of welded multiplanar tubular joints**. Doctoral Thesis, Delft University of Technology, Delft University Press, The Netherlands.

Romeijn, A., Karamanos, S.A., Wardenier, J. 1997. **Effects of joint flexibility on the fatigue design of welded tubular lattice structures**. 7th International Offshore and Polar Engineering Conference, Honolulu, U.S.A.

Rondal, J., Würker, K.G., Dutta, D., Wardenier, J, Yeomans, N. 1991. **Structural stability of hollow sections**. CIDECT, Comité International Pour le Développement et L'étude de la Construction Tubulaire, Serial No. 2, Köln: TUV-Verlag Rheinland, Germany.

Schlaich, J. and Schober, H. 1999. **Rohrknoten aus stahlguss**. Stahlbau, Vol. 68, No. 8, pp. 652-665, Ernst & Sohn, Berlin, Germany.

Schumacher, A. and Bays, P. 2002. **Viaduc de Lully: Mesures lors des essais de charges (in French)**. Mandate Report N° IC 676-1, ICOM - Steel Structures Laboratory, Ecole Polytechnique Fédérale de Lausanne (EPFL), Switzerland.

Schumacher, A. and Blanc, A. 1999. **Stress measurements and fatigue analysis of the new bridge at Aarwangen**. ICOM - Steel structures laboratory, Publication No 386, Ecole Polytechnique Fédérale de Lausanne (EPFL), Switzerland.

Schumacher, A. and Edder, P. 2001a. **The Dättwill Bridge: Stress Measurements During a Load Test (in French)**. Mandate Report N° IC 697-1, ICOM - Steel Structures Laboratory, Ecole Polytechnique Fédérale de Lausanne (EPFL), Switzerland.

Schumacher, A. 2003. **Fatigue behaviour of welded circular hollow section joints in bridges**. PhD Thesis 2727, Ecole Polytechnique Féderale de Lausanne, Switzerland.

SDRC 1999. **I-DEAS (R)**. Structural dynamics research coorporation (SDRC), 2000 Eastman Drive, Milford, OH, U.S.A.

SIA 160 (Swiss Society of Engineers and Architects) 1989. **Actions on Structures**. Swiss Society of Engineers and Architects, Zurich, Switzerland.

SIA 161 (Swiss Society of Engineers and Architects) 1990. **Constructions métalliques**. Société suisse des ingénieurs et des architectes, Zurich, Switzerland.

SIA 263 (Swiss Society of Engineers and Architects) 2003. **Construction en acier**. Société suisse des ingénieurs et des architectes, Zurich, Switzerland.

Smith, I.F.C. and Gurney, T.R. 1986. **Changes in the fatigue life of plates with attachments due to geometrical effects**. The Welding Institute, Research / Development.

Stahlbau Nachrichten 2002. **Als Stahlverbundkonstruktion errichtet - Neubau der Talbrücke Korntal-Münchingen**. Deutscher Stahlbau-Verband DSTV, 1/2002, pp. 17-19, Verlagsgruppe Wiederspahn, Wiesbaden, Germany.

van der Vegte, G.J., de Back, J., Wardenier, J. 1989. **Low cycle fatigue of welded structures – Analysis of low cycle fatigue tests on tubular T- and X-joints**. Stevin report 25.6.89.11/A1, CIDECT report 7H-89/2-E, Delft University of Technology, The Netherlands.

van Wingerde, A.M. 1992. **The fatigue behavior of T- and X-joints made of square hollow sections**. Heron, Volume 37, No. 2.

van Wingerde, A.M., van Delft, D.R.V., Wardenier, J., Packer, J.A. 1997. **Scale Effects on the Fatigue Behaviour of Tubular Structures**. WRC Proceedings IIW.

Verheul, A. and Wardenier, J. 1989. **The low cycles fatigue behaviour of axially-loaded T-joints between rectangular hollow sections**. CIDECT Report 7H-89/1-E, Stevin Report25.6.89.22/A1, Delft, The Netherlands.

Virlogeux, M., Bouchon, E., Berthellemy, J. and Resplendino, J. 1997. **The Antrenas Tubular Arch Bridge, France**. Struct. Engineering International, Vol. 7 No. 2 pp. 107-109.

Wardenier, J. 1982. **Hollow section joints**. Deflt University Press, The Netherlands.

Wardenier, J., Kurobane, Y., Packer, J.A., Dutta, D., Yeomans, N.F. 1991. **Design guide for circular hollow section (CHS) joints under predominantly static loading**. CIDECT, Comité International Pour le Développement et L'étude de la Construction Tubulaire, Serial No. 1, Köln: TUV-Verlag Rheinland, Germany.

Wardenier, J., van Wingerde, A.M., Packer, J.A., Yeomans, N.F. 2002. **Recommended hot-spot stress design for fatigue assessment of hollow sections joints**. Les 60 Ans du Professeur Manfred A. Hirt, Eds. Crisinel, Lebet, Nussbaumer, Laboratoire de la construction métallique (ICOM), Ecole Polytechnique Fédérale de Lausanne (EPFL), Switzerland.

Wordsworth A.C. and Smedley, G.P. 1978. **Stress concentrations at unstiffened tubular joints**. European Offshore Steels Research Seminar, Proceedings, Paper 31, Cambridge, U.K.

Wordsworth, A.C. 1981. **Stress concentration factors at K and KT tubular joints**. Fatigue of offshore structural steels, Conference Proceedings, pp. 59-69.

Zhao, X.L., Herion, S., Packer, J.A., Puthli, R.S., Sedlacek, G., Wardenier, J., Weynand, K., van Wingerde, A.M., Yeomans, N.F. 2000. **Design guide for circular and rectangular hollow section welded joints under fatigue loading**. CIDECT, Comité International Pour le Développement et L'étude de la Construction Tubulaire, Serial No. 8, Köln: TUV-Verlag Rheinland, Germany.

9 APPENDIX A: EXAMPLES OF ROAD AND RAILWAY BRIDGES

9.1 INTRODUCTION

The goal of this annex is to present the reader with some examples of tubular bridges by providing general information and a review of the design options chosen.

Each bridge is presented in the format of a data sheet containing pictures and available general information about the bridge (location, span, etc...) as well as particularities in the design and method of bridge construction.

Table 9.1 *- Summary of tubular bridge examples*

Section	Name	Location	Year	Bridge type
§9.2	Lully viaduct	The Canton of Fribourg, Switzerland	1997	two tubular space trusses
§9.3	Aarwangen bridge	The Canton of Bern, Switzerland	1997	two planar tubular trusses
§9.4	Dättwil bridge	The Canton of Argovie, Switzerland	2001	single tubular space truss
§9.5	Antrenas bridge	Marvejols, Lozère, France	1994	arch bridge
§9.6	Woodlands water crossing	Texas, USA	1994	multiple planar tubular trusses
§9.7	Hammerbrücke viaduct	Belgium, between Brussels and German border	1999	single tubular space truss

9.2 LULLY VIADUCT

.

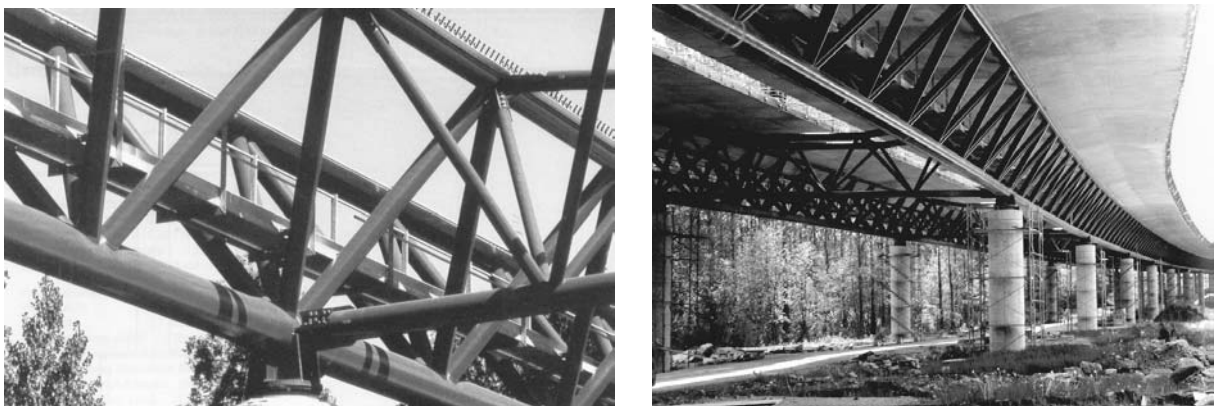

***Figure 9.1** - Lully Viaduct under construction (left) and near completion (right)*

Owner: The Canton of Fribourg, Switzerland

Structural designer: Dauner Ingénieurs Conseils

Contractor: Zwahlen & Mayr SA

Year of construction : 1997

Location: Highway A1, Lausanne - Bern, Switzerland

Length (total, spans): 970 m, 42.75 m

Width: 2 x 13.25 m

Bridge type: beam bridge with two tubular space trusses, each supporting a separate 2-lane concrete deck

Joints: type KK, $\theta = 60°$, $\phi = 69°$

Tube characteristics: CHS 267 x 11 - 25 (brace), CHS 508 x 25 - 50 (chord)

Non-dimensional parameters: $\beta = 0.53$, $\gamma = 5.08 - 10.16$, $\tau = 0.44 - 0.50$

Total Price: 33 million CHF

Particularities:

The innovative design of the Lully viaduct offers a light, transparent structure made of a triangular cross-section fabricated entirely from unstiffened circular tubes. The result is a twin space truss, with a typical span of 42.75 m. Each transversal triangular cross-section is 2.9 m high and 4.0 m wide, and is supported by a single slender pier. The largest tube diameter and thickness are over 500 mm and nearly 70 mm respectively. Welded overlapping K-joints and KK-joints form the brace-to-chord connections along the top and bottom chords, respectively. The deck slab is connected directly to the top chord with uniformly distributed welded shear connectors.

Method of construction: by crane

Commentary:

Geometric calculations, precision cutting and edge preparation of the tubes were necessary for performing the full penetration welds [Dauner et al. 1998]. The "heart and soul" of this bridge

lay in the facilities for cutting the brace edges. The fabrication would not have been possible without this equipement which cuts tubes lengthwise and prepares contact and welding surfaces. The brace member edges were cut to fit the outer contour of the chord members using computer guided cutting technology. Due to the bevels (ranging between 30° and 45° at the edges) and backing rings, full penetration could be ensured.

References: [Dauner 1997, Dauner et al. 1998].

9.3 AARWANGEN BRIDGE

.

Figure 9.2 - *Aarwangen bridge under construction (left) and completed (right)*

Figure 9.3 - *Aarwangen bridge: pedestrian bridge (left) and an intermediate support (right)*

Owner: The Canton of Bern, Switzerland

Structural designer: Hartenbach & Wenger AG

Contractor: Senn AG

Year of construction: 1997

Location: Main road Langenthal - Niederbipp, Switzerland

Length (total, spans): 96 m, 2 x 48 m

Width: (pedestrian separated) 7 m

Bridge type: beam bridge with two planar tubular trusses, tubular bracing and cross beams

Joints: type K, $\theta = 45°$

Tube characteristics: CHS 194 x 20 - 28 (brace), CHS 406 x 36 - 50 (chord), Grade S355 steel

Non-dimensional parameters: $\beta = 0.48$, $\gamma = 4.06 - 5.64$, $\tau = 0.40 - 0.78$

Total Price: 3.5 million CHF

Particularities:

This bridge, on a heavely-travelled cantonal road in Aarwangen, Switzerland, was errected in 1997 to replace an existing bridge. Next to it is an old railway truss bridge. The new bridge needed to be modern yet, at the same time, aesthetically compatible with the adjacent railway bridge. A solution using two parallel planar CHS trusses was chosen. The prefabricated deck is

attached to the truss by groups of shear stud connectors. A pedestrian bridge is attached to the main road bridge.

Method of construction: on the river bank, floated into place

Commentary:

Advantages: Fabrication was very quick due to the use of a prefabricated deck. The top truss chord is a CHS section, on which two vertical plates and a horizontal plate are welded. This provides the deck with a flat resting surface.

Disadvantages: The tubes were cut without the use of computer guided cutting technology. Therefore, the bevels were 45° around the entire brace edge and full penetration around the enitre brace-to-chord joint could not be ensured.

References: [Schumacher and Blanc 1999]

9.4 DÄTTWIL BRIDGE

***Figure 9.4** - Dättwil bridge under construction (left) and completed (right)*

***Figure 9.5** - Dättwil bridge: intermediate support (left) and typical KK-joint (right)*

Owner: The Canton of Argovie, Switzerland

Structural designer: Dauner Ingénieurs Conseils

Contractor: Zwahlen & Mayr SA

Year of construction: 2001

Location: Highway A1, Bern - Zurich, Switzerland

Length (total, of spans): 204 m, 26 m + 4 x 38 m + 26 m

Width: 13.25 m

Bridge type: beam bridge with one tubular space truss supporting a 2-lane concrete deck

Joints: type KK, $\theta = 60°$, $\phi = 69°$

Tube characteristics: CHS 267 x 11-25 (brace), CHS 508 x 50 (chord)

Non-dimensional parameters: $\beta = 0.53$, $\gamma = 5.08$, $\tau = 0.22\text{-}0.50$

Total Price: 11 million CHF

Particularities:

The Dättwil bridge is very similar to the Lully Viaduct. The tubular space truss is also triangular in the transverse direction. Due to this configuration, no cross frame or torsion reinforcement is

necessary. Torsion support for the truss is provided at the piers. For this project, a stipulation requiring construction of the bridge to be completed within 8 months lead to the choice of a welded CHS truss with a prefabricated concrete deck. Considerable construction time could be saved since the truss was assembled and fabricated prior to arriving on site.

Method of construction: by crane

Commentary:

Advantages: Fabrication was very quick due to the use of a prefabricated deck. The CHS top chord was supplied with welded "wings", which were subsequently welded to plates embedded in the prefabbricated deck.

Disadvantages: Detailing of the chord to deck connection caused some problems.

References: [Baregg Info 2000, Schumacher and Edder, P. 2001a, Stahlbau Nachrichten 2002].

9.5 ANTRENAS BRIDGE

Figure 9.6 - *The Antrenas tubular arch bridge*

Owner: The Government of France

Structural designer: Service d'étude technique des routes et autoroutes (SETRA)

Contractors: Etablissements J. Richard Ducros, GTM Construction

Year of construction: 1994

Location: Marvejols, Lozère, France (part of the Highway A75)

Length: 86 m, principal span: 56 m

Width: 11 m

Bridge type: arch bridge

Joints: type KK

Tube characteristics: CHS 508 x 16 (braces), CHS 1200 x 32(steel arch)

Non-dimensional parameters: $\beta = 0.42$, $\gamma = 18.75$, $\tau = 0.50$

Total Price: unknown

Particularities:

A polygonal arch was selected which allows the loads to be ideally balanced, especially at the arch ends. The arch has an opening of 56 m and a mean radius of about 60 m. The steel arch has a circular cross section, 1.2 m in diameter and 32 mm thick. Since the arch terminates near the traffic lanes, the lower sections have been filled with concrete to improve impact resistance from vehicles. The deck is a prestressed concrete slab with two longitudinal ribs directly supported by the steel struts that join the arch to the deck. The struts direct the loads to the central tubular arch. Viewed longitudinally, the CHS steel struts form a triangular tubular truss. Straight arch segments were designed between successive KK-joints. All joints between the arch segements were butt-welded. However, welding was difficult because cylinders of different sizes had to be joined, and the angles between the welded parts were often very acute.

Method of construction: assembled, in its entirety, on temporary supports placed under the nodes of the truss

Commentary:

Advantages: Visible at a great distance, this aestethic and innovative bridge provides a distinct landmark for the entrance to the region of Causses.

Disadvantages: In regards to the fatigue design, difficulties were encountered in the butt welding of the joints due to the acute angles encountered and the differences in tube sizes.

References: [Virlogeux et al. 1997].

9.6 WOODLANDS WATERWAY CROSSING

***Figure 9.7** - Woodlands Waterway Crossing*

Owner: Texas Department of Transportation

Structural designer: HNTB, Houston

Contractors: Trinity Industries, Houston, Texas

Year of construction: 1994

Location: Texas, USA (precise location not known)

Length: 16.78 m

Width: 15.09 m

Bridge type: muliple beam bridge with planar tubular trusses

Joints: type N

Tube characteristics: CHS 150 x 7.1 (braces), CHS 200 x 12.7 (bottom chord), RHS 200 x 250 x 12.7 (top chord), Grade 50 (ASTM A847) steel

Non-dimensional parameters: $\beta = 0.75$, $\gamma = 8.00$, $\tau = 0.56$

Total Price: $1 million US

Particularities: The lateral bracing of the bottom chords is not continuous (in fact, it occurs between adjacent truss pairs only).

Method of construction: by crane

9.7 HAMMERBRÜCKE VIADUCT


***Figure 9.8** - Hammerbrücke Viaduct, overview*

Owner: Belgian National Railways, Brussels

Structural designer: TUC RAIL, Brussels

Contractor: A.M. Duchene, Delens, Belgium

Year of construction: 1999

Location: High-speed railway, between Brussels and German border, Belgium

Length: 2 x 100 m

Width: 9 m

Bridge type: beam bridge with a single tubular space truss

Joints: type KK

Tube characteristics: RHS

Non-dimensional parameters: Not known

Total Price: 12 million CHF

Particularities:

This bridge was built to replace an old viaduct, which had suffered serverely from partial demolition during the wars of the last century.

The lower chord and the diagonals consist of welded box elements. The upper chords of the truss are open profiles, which are completely encased in the concrete deck slab. To facilitate the erection of the steel structure, both the lower chord member upper flange and the upper member lower flange were oriented perpendicularly to the sloping plane of the diagonal. The upper slab was cast on the steel structure, supported by the final bearings.

Method of construction: transportation of steel parts by rail, erection of steel structure by cranes on piers, abutments and two temporary supports

Commentary:

Advantages: The lower chord member is not exposed to thermal radiation, when the sun is at its zenith, thus having lower thermal gradients in the structure.

Commentary: [Detandt et al. 2003].

10 APPENDIX B: DETAILING AND FABRICATION RECOMMENDATIONS

10.1 INTRODUCTION

The detailing and fabrication recommendations in the following Appendix are based on a review of various applicable standards and guidelines pertaining to the design of tubular structures under static and fatigue loads. This Appendix is intended to provide a summary of the information contained in these sources. For further information, it is recommended that the various sources be consulted directly. Additional recommendations based on recently built bridges and the recent testing experiences of ICOM are also contained herein as noted.

10.2 DETAILING

10.2.1 Tube Wall-to-Tube Wall Butt Welds

Figure 10.1 shows an example of a tube wall-to-tube wall butt weld detail with an interior thickness transition. It is a matter of some debate as to whether the inclusion of the backing ring (shown in the figure) is necessary. In most current standards, the exclusion of the backing ring results in a reduction in the fatigue detail category [Eurocode 3 2003, SIA 263 2003, BS 7608 1993]. In some of these standards [i.e. Eurocode 3 2003] this penalty may be reduced or eliminated if the engineer can show through appropriate nondestructive testing that a full penetration weld has been successfully achieved. Recent experience at ICOM has shown, however, that such testing is not guaranteed to detect lack of penetration in these weld details. It is therefore on the engineer's confidence and discussions with the welders that the decision about the need for a backing ring to ensure successful fully penetrated welds should be based.

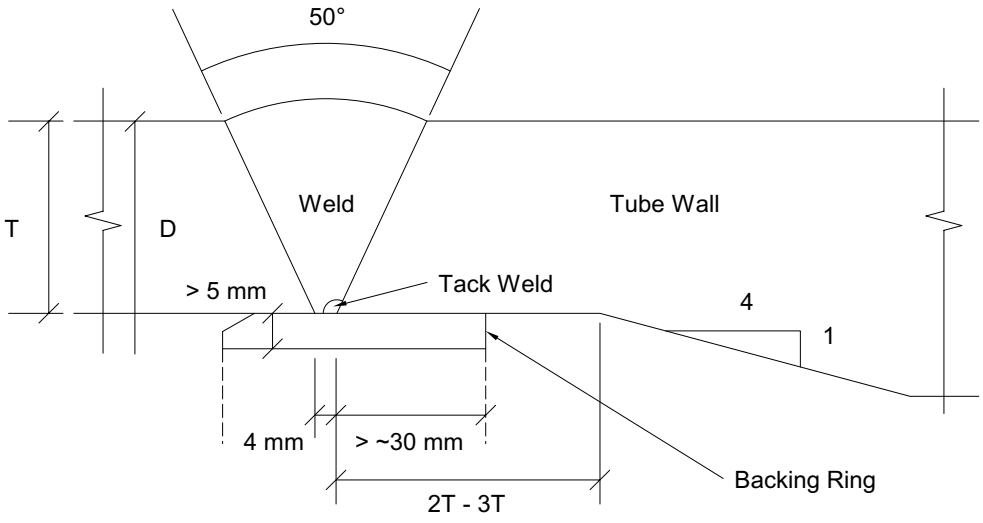

***Figure 10.1** - Tube wall-to-tube wall butt weld detail with thickness change on the inside.*

In general, the backing ring has been included in recent tubular bridge construction projects in Switzerland [Dauner 1998]. Along with the higher detail category, it is also felt that the backing ring increases the ease of welding, thus increasing the probability of the weld being satisfactory in all other respects. For these reasons, the use of a backing ring is recommended for tube wall-to-tube wall butt weld connections.

According to [DNV RP-C203 2001], at locations where tube wall-to-tube wall butt welds are accompanied by a thickness transition, the risk of root cracking can be reduced if the thickness change is made via a change in the outside, rather than the inside tube diameter (normally of the thicker tube). This can be explained by the reduced tension on the inside surface associated with the exterior thickness transition. Although less of an issue for offshore structures, aesthetic considerations may make such a detail undesirable for highly visible bridge structures.

10.2.2 Single and Double K-Joints

Figure 10.2 and 10.3 show typical single and double K-joints. As shown in Figure 10.2, welded K-joints can be further subdivided into fully overlapping, partially overlapping or gap joints. The tests conducted to date at ICOM have focused on gap joints. Although fully and partially overlapping K-joints are known to have higher static strengths, gap joints have the advantage of being easier to fabricate from the point of view of end preparation, construction tolerance and ease of inspection / nondestructive testing (NDT) [Wardenier et al. 1991].

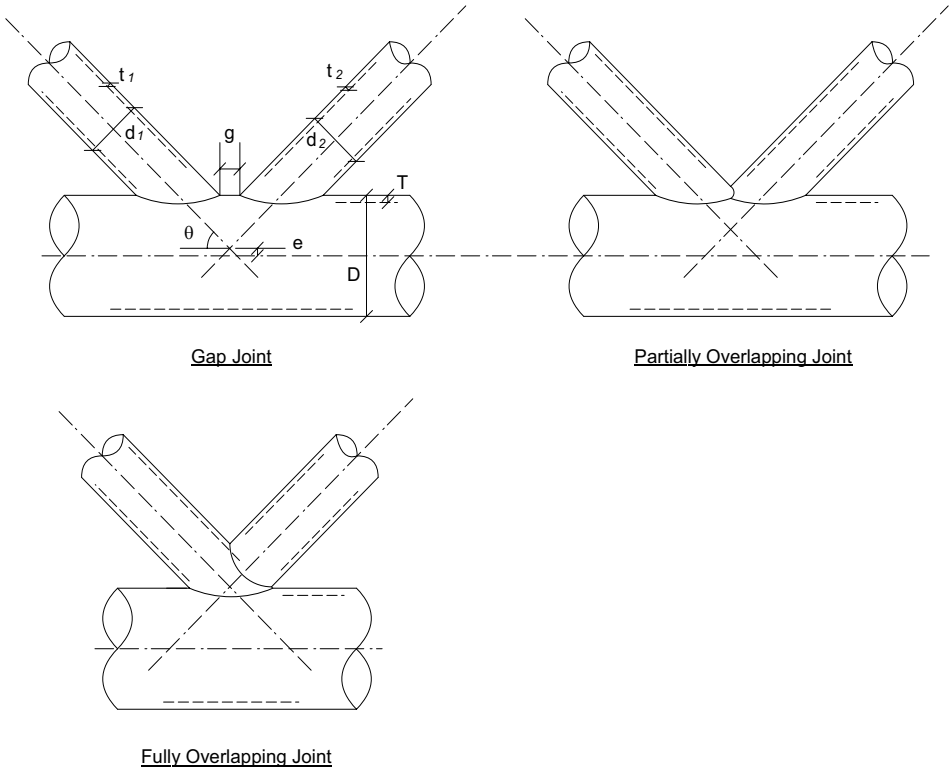

***Figure 10.2** - Different welded K-joint types.*

In order to carry out the static design of tubular K-joints using conventional design rules [see Wardenier et al., 1991], it is required that: $-0.55 < e/d_o < 0.25$. This requirement ensures that the bending moments due to joint eccentricity may be ignored for static design. Other geometric limitations for static design according to [Wardenier et al. 1991] include: $0.2 < \beta < 1.0$, $\gamma < 25$, and $30° < \theta < 90°$ (see Section 2.2 of the main report for definitions of the various geometric parameters). Depending on which standard is used for fatigue design, various additional geometric limitations may apply, and should be followed where appropriate.

Figure 10.3 - *Example of a double K-joint with instrumentation (Dättwil).*

Regarding the welding of gap-type tubular K-joints, the following additional recommendations apply:

- It is recommended that the gap, g, between the outer walls of the diagonals be no less than $t_1 + t_2$. This limitation is intended to ensure that there is no overlapping of the diagonal welds [Wardenier et al. 1991].
- The weld between the diagonal and the chord of a K-joint should always extend around the entire circumference of the diagonal and have a static strength equal to or greater than that of the diagonal (in tension and in compression). Full penetration welds should always be used for fatigue sensitive tubular joints.
- Figure 10.4 shows the starting and stopping sequence for the weld between the diagonal and chord recommended by [IIW 2000]. This sequence is intended to ensure that the welds are continuous through the zones where peak hot spot stresses are most likely to occur, thus reducing the risk that a fatigue strength limiting defect will occur within one of these zones.
- In the test program presented herein and in recent tubular bridge construction projects in Switzerland [Dauner 1998], backing rings have been used for the K-joints. It is a conclusion of this work that these backing rings have no beneficial effect on fatigue life, provided that proper full penetration welds are successfully executed. Regardless, backing rings are recommended as they are known to increase the ease of welding, and thus the probability of a satisfactory weld. Furthermore, recent tests at ICOM have shown that modern nondestructive testing (NDT) methods cannot be guaranteed to detect lack of penetration at the roots of tubular joints.

- A minimum diagonal angle, θ, of 30° is recommended for reasons of weldability [Marshall 1992]. Regardless, for large or unusually complex projects, the construction of a mock-up to ensure weldability may be warranted.
- Although [Wardenier et al. 1991] allow diagonal to chord diameter (β) ratios up to 1.0, it is recognized that full penetration welds can be achieved with much less effort if the diameter of the diagonal is significantly less than that of the chord, i.e. $\beta \leq 0.7$.

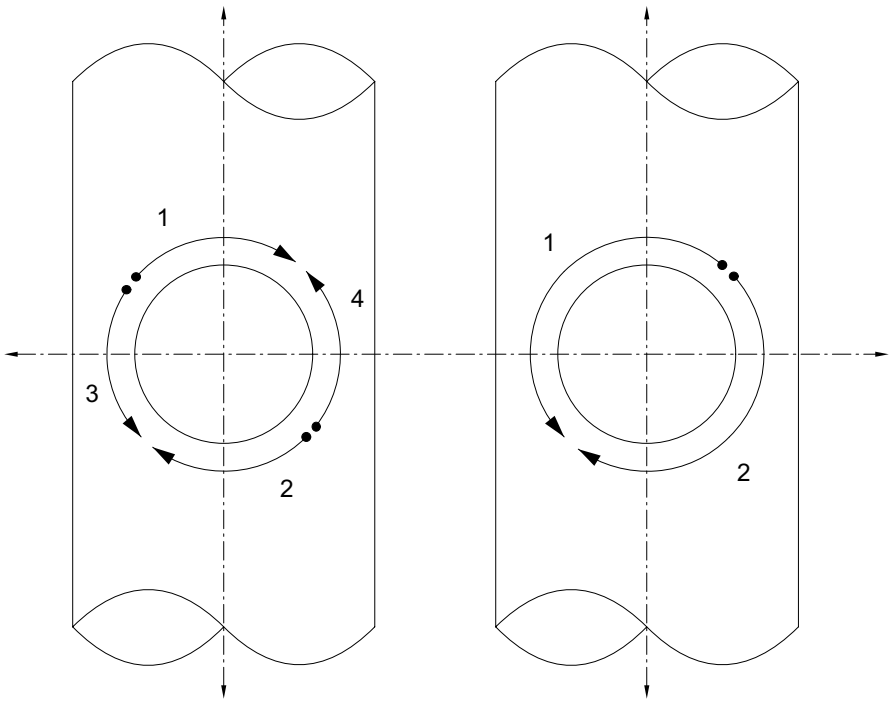

Figure 10.4 *- Welding sequence.*

10.3 FABRICATION

10.3.1 Tube End Cutting

Figure 10.5 shows tubular bridge diagonal (brace) ends prepared with computer guided cutting technology. Such technology, which has only become available in recent years, has done much to aide in the rise in popularity of tubular bridge structures. Prior to this, a paper template and manual cutting procedure was used as described in [Marshall 1992]. Such methods may still be the most economical for small, one-time projects. Regardless of the cutting method used, end cutting must be planned and executed in such a way as to ensure that full penetration welds can be achieved around the full circumference of the diagonal.

Figure 10.5 - *End preparation of diagonal members with backing rings in place.*

10.3.2 Pre-assembly and Assembly Sequence

Little is given in the various standards and recommendations in terms of direction regarding the pre-assembly and assembly sequence for tubular bridge structures. [Schumacher 2003] describes the cutting and welding procedures used for the test specimens discussed herein. [Dauner 1998] briefly discusses the procedures adopted for the Lully Viaduct. From this, and further discussion with the fabricator of the Lully Viaduct, the following can be ascertained: Essentially, following the end preparation of the diagonal elements, the pieces for a predetermined length of the bridge are fit together in a frame in the shop. This frame should be adjustable so that the proper bridge camber and curvature in plan may be ensured. The size of bridge section fabricated in the shop is generally driven by transportation limits (weight, size) and the limitations of the on-site assembly equipment. Once the pieces are fit together, they are then tack welded in place. Following this step, final welding of each joint is executed. On site erection methods will vary depending on the nature of the project and the site conditions. In the case of Lully, the steel bridge structure was installed from the ground level. Once entire spans were in place, forming and pouring of the concrete slab could proceed.

Tubular truss structures being relatively flexible (compared with conventional steel bridge forms such as deep I- or box girders for example), the welds are not highly restrained. Regardless, as with most welded structures, it should be considered in both the design and fabrication of tubular truss structures that the welds may induce:

- unwanted deformations (possibly resulting in the structure not meeting predefined tolerances)
- self equilibrating forces in the members

This is most likely to be the case when larger welds are made such as tube wall-to-tube wall butt welds in the chord members.

10.3.3 Weld Improvement

Various steel codes and recommendations are starting to acknowledge the beneficial effects of weld improvement on fatigue life [IIW 2003, Haagensen and Maddox 2001, DNV RP-C203 2001, BS 7608 1993]. The improvements in fatigue life (or strength) permitted in these codes can be summarized as follows:

- For Burr grinding and TIG dressing, various IIW recommendations [IIW 2003, Haagensen and Maddox 2001] permit at least a 1.3 times improvement in fatigue strength (~2.2 times improvement in fatigue life) for details in Fatigue Class 90 or less and for welded details with hotspot stresses less than 100 MPa.
- For needle and hammer peening, the same IIW recommendations indicate that the Fatigue Class becomes 125 for any properly treated detail with an untreated Fatigue Class of 90 or less, provided the maximum nominal compressive stress in the applied load spectrum is not greater than $0.25f_y$ (this corresponds to at least a 1.4 times improvement in fatigue strength). When using this increase, it is recommended that the applied stress range be taken as equal to the calculated stress range, $\Delta\sigma$, if R is less than 0, and equal to the maximum applied stress, σ_{max}, if R is greater than zero and the entire stress range is positive.
- [DNV RP-C203 2001] allows an improvement in fatigue life of 2.0 times (~1.26 times improvement in fatigue strength) for weld profiling, burr grinding and TIG dressing. Hammer peening results in an improvement in fatigue life of 4.0 times (~1.59 times improvement in fatigue strength), however hammer peening is not recommended on joints of members for which failure will result in substantial consequences.
- [BS 7608 1993] allows an improvement in fatigue strength of 1.3 times (~2.2 times improvement in fatigue life) for grinding. For other methods, this standard recommends confirmation by testing.

[Haagensen and Maddox 2001] provide detailed recommendations for carrying out some of the more common post weld treatment procedures. For needle peening (the treatment method used on the Series S4 specimens), these recommendations can be summarized as follows:

- A standard needle gun of the type used for removing slag and scale will generally be suitable. The ends of the needles should be rounded. Although not done for the Series S4 specimens, [Haagensen and Maddox 2001] indicate that it may be useful to modify the chuck to align the needles in a rectangular pattern rather than a round one. The peening tool used for the Series S4 tests had 15 x 3 mm diameter needles and was operated at an air pressure of 6 bars.
- Treatment should occur in four passes at a peening speed not greater than 800 mm/min.
- It is recommended that the tool be held perpendicular to the surface to be treated (i.e. ~45° to the plate surface when treating the toe of a normal fillet weld). It is not necessary for the operator to exert excessive force.

In addition to the above recommendations, the following steps should be taken to ensure the high quality and the effectiveness of the treament:

- Clear indication should be made on the fabrication plans of the areas to be treated (see example in Figure 10.6).

- Peening tool operators should be obliged to undergo a training program. This program should include a demonstration of the recommended procedure described above, exhibition of correctly and incorrectly treated surfaces, and practice peening on at least 1 m of weld.
- After treatment, a visual inspection for the characteristic indentations typical to needle peened details should be carried out with a low power (5-10x) magnifying glass. According to [Haagensen and Maddox 2001], staining of the surface with toolmaker's blue prior to treatment may make it easier to detect untreated areas.

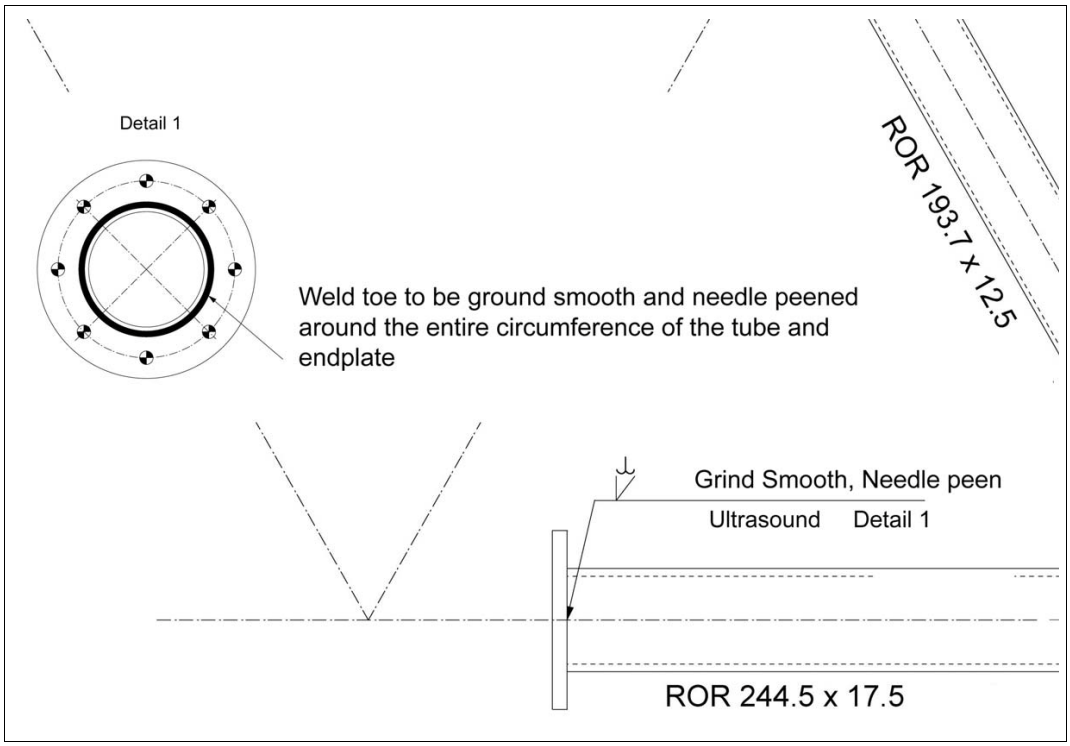

***Figure 10.6** - Indication of weld improvement on drawings.*

Finally, it should be noted that great care should be taken when determining the area to be treated. The IIW allowances for improvement in fatigue life do not consider the possible shift in the critical crack location that was observed in the tests conducted at ICOM when only the critical crack initiation site was treated. For this reason, when applying weld improvements to tubular joints, it is recommended that the entire joint be treated, and that appropriate measures be taken to ensure that full penetration welds are achieved so that the risk of weld root cracking is minimized.